INTERFACIAL TENSION AND PHASE BEHAVIOUR OF NITROGEN AND HYDROCARBON VAPOUR-LIQUID SYSTEMS

Thesis submitted in accordance with
the requirements of the
University of Liverpool
for the degree of
Doctor in Philosophy

by

Jamal Fahmi Shweikeh

July 1996

UNIVERSITY OF LIVERPOOL

ABSTRACT

Doctor in Philosophy

"INTERFACIAL TENSION AND PHASE BEHAVIOUR OF NITROGEN AND HYDROCARBON VAPOUR-LIQUID SYSTEMS"

by Jamal Fahmi Shweikeh

In this work the interfacial tension and phase behaviour of nitrogen and hydrocarbon vapour-liquid systems have been investigated. A specially designed high pressure rig has been used to measure the interfacial tension (IFT), equilibrium phase densities and phase compositions of selected model hydrocarbon systems and stocktank oil. The main aim has been to study the bulk and interfacial thermodynamic behaviour of these systems and improve the understanding of the miscibility process of nitrogen gas and light hydrocarbon gases in hydrocarbon liquids. Model systems of pure, binary, ternary, quaternary and multicomponent hydrocarbons, as well as a stocktank oil sample, have been examined as a function of pressure up to 35 MPa and temperatures up to 363 K. Compressed nitrogen gas, and mixtures of nitrogen with methane and ethane gases, were introduced into the examined systems to maintain the pressure. Pure liquid hydrocarbons have also been examined as a function of temperature up to 363 K at saturation vapour pressures.

A significant amount of new experimental data has been obtained for these systems. The IFT, phase densities and compositions for these systems represent measurements not previously available in the literature. The data obtained have been fitted to simple polynomial functions for interpolation.

In this work scaled particle theory has been used to develop expression for computing surface and interfacial tension. The calculated values from these two expressions have been compared with the experimental data and good comparisons have been demonstrated, particularly for the pure and binary systems. However, for the mixed systems examined the comparisons were not as good.

The experimental data have been compared with correlations used to calculate IFT, ST, vapour liquid equilibrium (VLE) and phase densities. The parachor-dependent correlations for evaluating IFT underestimate the experimental data with large deviations. However, the Macleod-Sugden expression and corresponding states correlation for ST calculation for the pure liquids examined give good agreement with experimental data.

The extended corresponding states approach (EXCS) and the Peng-Robinson equation of state (PR EOS) have been compared with the experimental data for phase densities and phase compositions. These comparisons have shown good agreement for most of the systems. The predictions are most accurate at well below the critical point. The EXCS is in very good agreement with experimental data for pure liquids and gases. The predicted values of Henry's Law constant (K_H) from the scaled particle theory applied to the bubble point curves for the solubility of N_2 and CH_4 in the hydrocarbons have shown good agreement with experimental data for most of the systems studied.

The experimental results obtained in this thesis give an important source of data relevant to oil reservoir phenomena and many industrial chemical operations involving interfacial and phase behaviour processes.

ACKNOWLEDGEMENTS

I would like to express my gratitude to my supervisors, Dr. John Satherley and Professor David J. Schiffrin for their guidance and academic support. I would like to acknowledge the cooperation of Dr. John Satherley and his continued support, help and fruitful discussions throughout this work. His broad scientific and technical knowledge, innovation and enthusiasm for work have helped in stimulating the working atmosphere. I gratefully appreciate the help of the technical and administrative support staff. Special thanks are due to Mr. Jack Dutton in the mechanical workshop for his machining work, Mr. Charles P. Clavering in the electronics workshop for his excellent cooperation and for checking the electronic instruments, Mr. Bert Chappell for his glassblowing service and Mr. Steve Apter in the analysis micro-laboratory.

I gratefully acknowledge financial support from the British Council for funding my tuition fees and from Professor David Schiffrin and Dr. John Satherley for providing my maintenance expenses.

Very special thanks are due to my wife and children for their patience and support in all aspects. I would also like to thank my family and friends back home especially my mother, brothers and sisters for their moral support and encouragement.

CONTENTS

LIST OF SYMBOLS AND ABBREVIATIONS

A	Surface area or density meter constant
A_c	Cross sectional area of spherical cavity
B	Density meter calibration constant
EXCS	Extended corresponding states model
α	Molecular polarizability
β_T	Isothermal compressibility coefficient
β	Universal critical exponent for IFT
c	Spring constant in oscillator
CH	Cyclohexane
n-C_1	Or nC_1: methane
n-C_5	Or nC_5: n-pentane
n-C_6	Or nC_6: n-hexane
n-C_7	Or nC_7: n-heptane
n-C_8	Or nC_8: n-octane.
nC_5+nC_6	nC_5/nC_6
c_i	Interactive energy coefficient, where c_{dis}, c_{dip} and c_{ind} are the dispersion energy constant, the dipole-dipole energy constant and the inductive energy constant respectively
CSC	Corresponding states correlation
γ	Surface tension and interfacial tension
γ_o	Scale factor for IFT
ϵ/k	Energy parameter (energy well depth) in the Lennard-Jones model
ϵ_i	Interactive energy, where the subscript i is *dis, dip* and *ind* which stand for the energy of dispersion, dipole and induced dipole respectively
f	Fugacity
f	Natural frequency of oscillation
F	Force on horizontal plane in a pendant drop at equilibrium
τ	Period of oscillation
$G_{L,v}$	Molar Gibbs free energy in the liquid (subscript L) or vapour phase

	(subscript v)
G_c	Molar Gibbs free energy of cavity formation
G_i	Molar Gibbs free energy of interaction
g	Gravitational constant
H	Molar enthalpy
IFT	Interfacial tension
j,Λ	Partition functions per molecule for the translational and internal degrees of freedom
k	Boltzman constant
k_{ij}	Peng-Robinson parameter (binary parameters)
K_H	Henry's law constant
m	Number of components or mass of a hollow body (an oscillater)
M	Molecular weight
μ	Dipole moment or chemical potential or universal critical exponent for IFT
N_A	Avogadro's number
N	Number of molecules
P	Pressure or parachor (for component parachor: P_i), or a horizontal plane inside a pendant drop
P_c	Critical pressure
P_r	Reduced pressure
P_{vp}	Vapour pressure
P_M	Pressure for mixture determined from mixing rule
P_e	Excess pressure in the Young-Laplace equation
PR	Peng-Robinson EOS (equation of state)
ρ	Number density (N/V)
$\rho_{L,v}$	Phase density (liquid or vapour phase density), kg m^{-1}
r	Radius of cavity
R	Universal gas constant
R	Ratio of hard sphere diameters σ_2/σ_1
R_1,R_2	External and internal radii of curvature
SPT	Scaled particle theory

ST	Surface tension
σ	Hard-sphere diameter
σ_M	Pseudo-solute or solvent hard-sphere diameter
S	Molar entropy
T	Absolute temperature or an abbreviation for Toluene
T_c	Critical temperature
T_r	Reduced temperature
T_{br}	Reduced boiling temperature
T_M	Absolute temperature for mixture determined from mixing rule
U	Molar internal energy
V,v	Molar volume
V_c	Critical volume
VLE	Vapour-liquid equilibrium
y	Reduced density
ω	Acentric factor
ϕ	Angle between the tangent and the X axis in pendant drop
x	Mole fraction (composition) of liquid phase
x'	Mole fraction (composition) of vapour phase
X	cross sectional radius at a horizontal plane in a pendant drop

1. INTRODUCTION

This thesis is concerned with the measurement and interpretation of interfacial and bulk thermodynamic properties in nitrogen-hydrocarbon systems. Experimental measurements on interfacial tension (IFT), phase density and phase composition have been carried out on these systems using a specially designed high pressure rig. IFT was determined using the method of the digital image processing on pendant drops.[1] The measurements were made in the coexistence region up to a maximum of 35 MPa or up to the critical pressure of the system at constant temperature of 313.15 K. Measurements were also made on three pure hydrocarbons as a function of temperature against their vapour pressures up to 363.15 K.

The systems studied include pure n-alkanes and mixtures of: binary (n-alkane+isomer), ternary (n-alkane+aromatic+cycloalkane), quaternary (four n-alkanes) and stocktank oil samples pressurised with N_2, N_2+CH_4, $N_2+CH_4+C_2H_6$, and $CH_4+C_2H_6$. The measurements provide a fundamental source of experimental data on the properties of these hydrocarbon systems to serve as the basis for a better understanding of the behaviour of these fluids, and on the effect of pressure, temperature, and composition on the IFT in such fluids. The utilisation of these experimental data enables assessment of predictive theories such as the parachor-dependent correlations, corresponding states correlations (CSC), and scaled particle theory (SPT) for IFT prediction, and the Peng-Robinson equation of state (PR EOS) for equilibrium phase properties.

Phase-equilibrium thermodynamics is a subject of fundamental importance and is of particular interest in many operations in the manufacture of chemical products involving phase contacting process such as: high pressure hydrogenation, high pressure-catalytic synthesis, phase-reactors, supercritical extraction, extraction, adsorption, absorption, distillation, leaching and others. It is also of particular importance in the oilfield and natural gas operations, where reservoir fluids exist in two or more phases.

An understanding of these processes is based on the physical chemistry of phase-equilibria. Thermophysical and thermochemical bulk and interfacial properties are essential for process design and production of such process operations. The development of efficient industrial processes and economical methods in production and recovery could substantially save the consumption of raw materials and natural resources. Improving process efficiency and developing economical methods for improved recovery of petroleum reservoir fluids could assist in increasing both usable reserves and the supply of energy.

In a typical chemical plant or an oil refinery separation operations form between 40-80% of the total plant investment.[2] Equilibrium physical property data are essential for reservoir simulation to manage oil recovery, but also in many production and refining[3] processes. To illustrate the need for accurate IFT data in a fractured oil reservoir with a typical block height of ~3 m, if the interfacial tension was estimated to be 1 mNm^{-1}, instead of 0.5 mNm^{-1}, a drop of ultimate drainage recovery performance of ~27% would be expected.[4]

N_2, CO_2, and light hydrocarbons (e.g. CH_4), in addition to their use in various applications in the chemical process industry, have been used as a high pressure gas drive[5] for miscible displacement of petroleum reservoir recovery. Flooding reservoirs with CO_2 has been used in the U.S.A. with promising results[6] and current research is focused on the mechanism of its displacement and interfacial properties.[7] There also has been some studies on light hydrocarbons miscibility processes.[5, 6]

Recently, phase-equilibrium and interfacial property studies of (N_2 + n-alkane) have become increasingly of practical importance.[8] For example, phase equilibrium data in nitrogen systems are necessary for the design of low-temperature rectification units, e.g. for the separation of coal gasification products. Also in fluid extraction, pure nitrogen or nitrogen mixtures are used as extracting agents of low solvent power but high selectivity.[9]

Nitrogen has been used in oilfield operations for gas cycling, gas lift and reservoir pressure maintenance.[8] In recent years, the use of nitrogen as a gas drive for improved oil and gas recovery has become attractive for high-pressure reservoirs.[8] Nitrogen displacement of reservoir oil has been shown as a promising technique for improved oil recovery in the North Sea.[10] However, although promising from a technical point of view, economic consideration may preclude its use. A few successful pilot floods have been carried out. A multiple contact process has been proposed[10], leading finally to a supercritical single phase fluid at high pressures. In spite of this, there have been very few studies on the interfacial physical chemistry of multicomponent nitrogen-hydrocarbons systems. The miscibility of nitrogen in crude oil is complex and not well understood. Establishing a strong fundamental basis of its phase behaviour at high pressures is essential for better understanding of the miscibility phenomenon. Thus, there is a practical as well as a fundamental thermodynamic and theoretical interest in studying these systems.

There is a lack of data in the literature for such thermophysical properties, particularly for mixtures. For many fluids the properties are estimated or predicted from empirical correlations. Often the empirical correlations are useful but limited to the range on which they are based. Use outside this range can lead to significant errors. The range is usually dictated by available experimental data. For example, the Antoine equation provides a useful method for obtaining the vapour pressure and boiling temperature of liquids in the range between the triple point temperature and a reduced temperature (T_r)<0.85. It fails near the critical temperature.[11]

In general, the stronger the theoretical basis, the more reliable the correlation. The thermophysical or thermochemical properties of every substance involved in a process depend directly on the nature of its molecules. This can be expressed in terms of molecular size, shape, charge distribution, polarity, forces of attraction and repulsion between molecules etc.. For example the equation of van der Waals, the Virial equation and other equations of state tie the deviations from the ideal-gas law to the nature of the molecules quantitatively.[11] The more that is known about the fluid molecular behaviour the better the prediction of its properties. The

interfacial properties are difficult to measure or to predict, particularly for mixtures, since the composition of the surface is not the same as that of the bulk. A fundamental physical treatment of the molecular behaviour at the interface in relation to the bulk phases is needed, in order to develop improved theories based on physical principles.[12]

Interfacial tension (IFT) and phase density are important properties for various fluid systems. IFT has a particular significance in the petroleum industry for oil recovery, production and refining. This property is essential for predicting the performance of the reservoir through determining the capillary pressure and forces, the relative permeabilities of the oil and gas phases, the residual oil saturation after drainage by gas, and thus the displacement efficiency. Several studies[13,14,15] have been made on the influence of IFT on the flow rate of gas-oil in porous media. It has an important role in controlling two-phase flow behaviour, which in turn is a function of transport properties, and thus on oil recovery, particularly at low values of IFT near the critical point. Thus an accurate estimation of IFT is required for modelling oil reservoir processes. For gas-condensate systems relative permeability curves are enhanced when the IFT is low.[13] Near the critical region, IFT is the dominant fluid property which determines these curves.[16] In this region IFT is very low and approaches zero. There is a practical need to improve on the understanding, in this region, of the conditions which influence the IFT.

Vapour-liquid equilibrium data at high pressures for hydrocarbon systems are needed for direct industrial applications. In the oil industry, such data are essential for oil reservoir fluid simulation for predicting thermophysical and thermochemical properties such as IFT, phase densities, viscosities, molecular weights and for providing parameters in mixing rules. And since reservoir oils are formed from multicomponent mixtures therefore P, T, x, x' (pressure, temperature and phase composition) data are of practical interest for all types of hydrocarbon mixtures, including n-alkanes, isomers, aromatics, naphthenes etc. with gases N_2, CO_2, H_2S, CH_4, C_2H_6.

Several fluid phase equilibria research studies at high pressures and temperatures, have been reported for vapour-liquid hydrocarbon systems. For example, Krichevsky and Gamburg[17] (1942) measured P, T, x' data for N_2-Benzene, while Michels et al.[18] (1950) and Akers[19] (1954) obtained experimental P, T, x, x' for N_2-nC_7 and ammonia-H_2-N_2 systems respectively, up to 80 MPa. Sage and Lacey[20] (1950) made vapour-liquid equilibrium (VLE) measurements on some N_2-light hydrocarbon binary systems. Reamer and Sage[21] (1963) measured the VLE for the binary mixture CO_2 in n-decane. Alwani and Schneider[22] (1969), Lentz[23] (1969), Engels and Schneider[24] (1979) measured P, V, T data for binary mixtures of liquid hydrocarbons and aromatics with water at high pressures, but their measurements did not include x and x'. Peter et al.[25] (1970) measured the phase composition between 373 to 453 K up to 90 MPa, for three N_2-hydrocarbon binary systems. They reached the critical point under these conditions. Legret et al.[26] (1981) measured the phase VLE data, using a static cell method for the N_2-nC_7 system up to 100 MPa and temperatures between 233 and 433 K. Wisotzki and Schneider[27] (1985) made an experimental VLE study on the binary systems N_2-ethane and N_2-n-pentane, using an optical high pressure-cell, up to 200 MPa between 88 to 313 K.

Metcalfe and Raby[28] (1986) conducted an experimental VLE for N_2-rich gas condensate system (Anschutz Ranch East reservoir fluids) using a variable volume windowed PVT-cell. They used the experimental data to tune and develop the parameters of the Redlich-Kwong (RK) equation of state (EOS) used in reservoir simulation models. Llave and Chung[8] (1988), using a specially designed-flow switching technique apparatus, made experimental VLE measurements on N_2-hydrocarbon binary, ternary and quaternary systems up to 35.85 MPa, from 305.4 to 373.2 K. Darwish et al.[29] (1994) and Park et al.[30] (1995) measured the solubility of methane and carbon monoxide in three aromatic hydrocarbons from 323 to 433 K up to 23.3 MPa using a static equilibrium cell. They analyzed the results with the Soave-Redlich-Kwong (SRK) and Peng-Robinson (PR) EOS's and calculated the Henry's Law constants from the Krichevsky-Kasarnovsky equation.

As can be seen from the above review on VLE studies, most of research has been carried out on binary systems and very few on mixed systems. There is, therefore, a need for further experimentation to determine VLE in multicomponent systems and further assessment of predictive EOS.

Up to date the majority of experiments on IFT behaviour of hydrocarbon systems have been restricted to the analysis of pure hydrocarbons at low pressure and moderate temperatures, and of some binary mixtures over limited ranges of pressure and temperature. Most of the extended predictive correlations for mixtures, such as the parachor-dependent correlations[31], have relied on pure systems correlations which have been tested on experimental results of pure components, mainly straight-chain hydrocarbons. There is a lack of experimental data for multicomponent mixtures. In general, experimental results for systems as a function of pressure and temperature are scarce. The following is a brief literature review in this area.

Jasper[32] (1972) measured the surface tension of a large number of pure liquids as a function of temperature up to approximately the boiling point. Vargaftik[33] (1975) has compiled selected values of surface tension and other physical properties, for pure components as a function of temperature. Some of these values are experimental but many are predicted. Timmermans[34] (1950, 1965) gives physical properties, including surface tension and density, for pure components mainly at ambient and low temperatures and pressures. Critical Tables[35] (1928) provide various thermophysical properties for pure components at low temperatures.

Weinaug and Katz[2, 3], (W-K) (1943) measured the surface tension of methane-n-propane binary liquid mixtures in equilibrium with vapour, using the capillary-rise and drop-volume methods, over the temperature range 258-363 K and the pressure range 0.276-10.34 MPa. He developed an extension of the Macleod-Sugden relation[36] (M-S) (1923) and Fowler's concept[37] (1937) for mixtures based on the experimental data from the binary systems. He also measured the surface tension of nitrogen in n-heptane and in n-butane at three values of pressures up to 6.895 MPa

and temperatures up to 360 K. From these measurements he calculated the parachors for nitrogen dissolved in n-heptane and in n-butane from the extended parachor relation and found that the nitrogen parachor value varies in the two systems. Thus this approach was not satisfactory.

Stegemeier[38] (1959) measured the IFT for the binary systems of CO_2-n-butane and CO_2-n-propane. Hough and Stegemeier[39] (1961), based on these results and on the scaling theory, concluded that the value of the exponent (n) in the W-K model should be 3.66, instead of 4.

Simon et al.[40] (1978) conducted an experiment to measure the IFT and phase behaviour properties of CO_2-reservoir oil systems at high pressures. Their results for the equilibrium phase composition were uncertain due to existence of asphalt materials in the oil samples. They found that their predictions of IFT using the W-K model had large deviations from experimental values. Firoozabadi et al.[4] (1988) measured the surface tension of a crude cut-nitrogen and reservoir crude-gas systems at high pressures, using the pendant drop method, for the purpose of determining the parachor of the cuts. They found that the calculated parachors gave reasonable predictions of surface tension for the measured gas-condensate systems but for systems containing residues (asphalt materials) the obtained parachor values were not suffice and further experiments on surface tension would be needed.

Recently, research in this area has been concentrated on measuring the IFT, viscosity and phase density of gas-oil fluid systems, and comparing predictive correlations with experimental results. Hsu et al.[5,6] (1985), Nagarajan and Robinson[7] (1986), and Gasem et al.[41] (1989) measured the IFT, equilibrium phase density and composition for CO_2 in n-butane, in n-decane and in n-tetradecane binary systems respectively. They used a pendant drop-PVT cell experimental facility, and made the measurements at 320 K, 344 K and 378 K at pressures up to the critical point.

Danesh et al.[42] (1990) made IFT, phase density and composition measurements on a gas-condensate reservoir fluid using the liquid-gas meniscus

thickness method. Huygens et al.[43] (1993) measured low IFT (0.045-9.45 mNm^{-1}), using a pendant drop-digitizing technique, and phase densities for nitrogen-low volatile oil systems consisting of methane/n-butane/n-tetradecane at conditions similar to those in North-Sea oil reservoirs. They made the measurements at pressures between 30 MPa-40MPa and a constant temperature of 373 K. They found large deviations in comparing the results with parachor-dependent correlations. Tang et al.[44] (1993), measured the IFT, using a pendant drop digital image processing technique, phase density and composition for four nitrogen-hydrocarbon binary systems: n-pentane, n-hexane, n-heptane, n-octane. Their measurement were made at constant temperature of 313.15 K and pressures up to 40 MPa. Their results were consistent and in good agreement with literature values at low pressures.

Fawcett[31] (1994) measured low IFT using a laser light scattering technique (LLS), and phase properties for a six-component gas-condensate model, the results were compared with parachor-dependent predictive correlations, which was found to give significant deviations from experimental results. Dorshow[45] (1995), using a surface LLS technique, measured the IFT and oil viscosity at high pressures for gas-oil systems from Prudhoe Bay fluids.

It can be concluded from the above review on IFT measurements that most reported research has been restricted to pure and binary systems and very few studies on multicomponent systems over wide ranges of pressure and temperature have been reported. There is a need for further experimentation to cover mixtures, from various families of compounds, over full ranges of pressure and temperature, to investigate the effect of VLE on IFT and assess further predictive theories.

In industry the standard methods of IFT and equilibrium phase property prediction rely mainly on empirical or semi-empirical relations. The parachor-dependent methods such as the Macleod-Sugden (M-S) for pure component systems, the Weinaug and Katz (W-K), its modified version the Hough and Stegemeier (H-S) and the Lee-Chien[46] (L-C) (1984), for mixed hydrocarbon systems, are widely used for the prediction of IFT under reservoir conditions. These correlations and similar

ones (chapter 2) are, however, empirically based on a limited range of experimental results. Although they might be expected to give accurate predictions over their range of applicability, they give poor predictions on many occasions[31]. The W-K correlation is commonly used because of its simplicity and because the M-S relation, from which it was extended, has been tested widely with pure component data.

Several authors have attempted to modify the W-K correlation with more complex mixing rules for multicomponent fluids, or with a parameter which varies between the density difference between oil and gas phases (chapter 2). The Lee and Chien[46] (1984) correlation, of similar form to the W-K, is based on critical scaling theory, and although it is widely used, it can produce large deviations where the critical properties of the fluid mixture are uncertain. Broseta and Ragil[47] (1995) proposed to express the parachor in terms of critical amplitudes and the acentric factor. Although the results are promising so far it has only been tested on a few pure components.

Ali[16] (1994), in a review of the Parachor-dependent correlations, attributes one of the reasons for the poor performance of the parachor correlations to the presence of isomers, naphthenic and aromatic compounds in the C_{7+} fractions, which influence the estimation of parachor values. The main reason, for this poor performance, is that these correlations are empirical and a more comprehensive correlation or theory describing this property, based on a physical understanding, is needed. This conclusion matches with the findings of Anderko[12] (1990) that the future progress and better predictions of the vapour-liquid interface of complex mixtures will come from the development, based on physical ideas, of molecular behaviour and concepts of statistical mechanics, rather than on empirical fit to collected data.

The other physically based theoretical models such as the gradient theory[48] (1981) and the principle of two-scale-factor-universality[49] (1991) based on scaling theory, have not been developed sufficiently for complex mixtures. In addition, the calculations involved in using these theories require a large amount of time and a

large number of adjustable parameters. Determining the later requires an extensive experimental data-base which is presently lacking.

For the prediction of fluid phase equilibria a few equations of state (EOS) can be used. The Peng-Robinson (PR EOS), Redlich-Kwong (RK) and the Soave-Redlich Kwong (SRK) are widely used in the oil industry[50] for reservoir fluids phase equilibria and prediction of physical properties. Chapter 2 (section 2.2) describes these EOS's, and the PR EOS will be used to predict the VLE, for the systems examined in this study. The results of the calculation are compared with experimental data in chapter 6.

Chapter 2, section 2.1 and 2.3, provide a comprehensive review of the IFT and ST predictive correlations. Section 2.1 covers the parachor-dependent correlations, which are commonly used in industry, and section 2.3 describes the corresponding states correlation (CSC) for surface tension prediction, which applies mainly to pure systems.

One of the targets in this work was to utilise the experimental results to assess available predictive thermodynamically based theories such as the scaled particle theory (SPT). Reiss et al.[51] (1959) introduced the theory based on statistical mechanics of dense fluids by relating the intermolecular properties of hard sphere fluids to their macroscopic thermodynamic properties.

An attempt to extend the Reiss's-SPT relation for surface tension (ST) to temperatures above ambient has been made. Further, an expression, based on one-fluid theory and SPT has been developed to calculate IFT in two-phase mixed systems. Chapter 3, reviews SPT and gives the derivation of the above two expressions.

A comparison between the solubility-experimental results and predicted values from Henry's law constant-SPT expression was made. The IFT and ST proposed expressions were tested, and compared with the experimental results, giving good

trend of prediction particularly for the pure and binary systems. These are discussed in chapter 6.

In chapter 4, a detailed description of the rig, the experimental apparatus and the measuring technique is given, together with the experimental procedure and rig operation techniques. The results of all the experimental and analytical work will be presented in chapter 5. In chapter 6, the experimental results are discussed. Chapter 6 also presents the comparison of the measured results with the PR EOS, the prediction of Henrys' Law constant (K_H) from an SPT expression and the prediction of IFT and ST from the parachor-dependent and corresponding states correlations. The results of the IFT prediction from the expressions outlined in chapter 3 are also discussed. The final chapter (7) contains the conclusion and an outline of further research in this field.

A list of symbols and abbreviations is given in the front of the thesis. Tables of the experimental results can be found in the appendix at the end.

2. REVIEW OF VAPOUR-LIQUID EQUILIBRIUM AND INTERFACIAL TENSION CORRELATIONS

In this chapter a review of the correlations which are used to predict fluid properties is given. Section 2.1 discusses the various forms of the parachor correlations for IFT and ST prediction, their origin and brief history of their development, and their significance and use in industry. Section 2.2 deals with the Peng-Robinson equation of state, a widely used equation for calculating physical properties and fluid phase equilibria in the oil industry. Section 2.3 describes the corresponding states correlations for ST prediction and its range of applicability. These three correlations were used for comparison with the experimental results obtained in this study (chapter 6).

2.1 Prediction of IFT By The Parachor Approximation

2.1.1 IFT Correlations Using Parachors

Macleod[36] (1923) found that the IFT is proportional to the density difference between a liquid and its vapour to a forth power for a wide temperature range. Sugden[52] (1924) expressed the proportionality constant in terms of the parachor, a property characteristic of each pure component:

$$P = \frac{\gamma^{1/4} M}{(\rho_L - \rho_v)} \qquad (2.1)$$

where P is the parachor, γ is the surface tension, M is the molecular weight of the compound and ρ_L and ρ_v are the densities of the liquid and vapour phases in equilibrium. It was found that the parachor could be estimated from the molecular structure. A parachor contribution could be assigned to each type of atom or group of atoms in molecules. The molecular parachor could be determined by summing the contributions from each group in the molecule. Quayle[53] (1953) gives an extensive

review of methods for determining the parachor and list values for a large number of compounds.

Weinaug and Katz[2, 3] (W-K) (1943) extended the above parachor approximation to mixtures by using a linear mole fraction additive mixing rule :

$$\gamma^{1/4} = \sum^{n} P_i \left[x_i . \frac{\rho_L}{M_L} - x_i^{v} . \frac{\rho_v}{M_v} \right] \qquad (2.2)$$

where x_i and x_i^v are the mole fractions of the $i^{th.}$ component in the liquid and vapour phase respectively, and M_L and M_v are the molecular weights of the liquid and vapour phases calculated from simple mole fraction mixing rule in each phase.

2.1.2 Parachor Correlations

Eq.(2.2) and similar ones are used widely in the oil and chemical industries. A series of attempts have been made to improve the prediction capabilities by correlating the parachor estimated from the measurement of basic physical properties[16] of various hydrocarbon systems.

Fowler[37] (1937) investigated the dependence of the Macleod-Sugden equation (Eq.(2.1)) close to the critical point using an expansion of a general equation of state and expressing the parachor in terms of critical parameters but with little progress.

Lennard-Jones and Corner[54] (1940) derived an equation for the parachor based on statistical thermodynamics using a lattice model for the liquid : P = (const.) $\varepsilon^{1/4}$ $\sigma^{5/2}$, where ε and σ are the pair potential parameters given in the Lennard-Jones model. This predicts the parachor within 3 to 4% of experimental values for a range of compounds.[55]

Baker and Swerdloff[56] (1955) used an expression relating the parachor to the molecular weight of hydrocarbons, M, such that: P = 40 + 2.38 M. Nokay[57] (1959) proposed a correlation for values of the parachor in terms of the specific gravity.

Hough and Stegmeier[39] (H-S) (1961) used an exponent value for the surface tension in Eq.(2.2) of (1/3.66), instead of (1/4), which was derived from critical scaling results for propane and butane. Lee and Chien[46] (L-C) (1984) introduced a correlation based on critical scaling theory for calculating the mixture parachor. They took the pseudocritical properties of the mixture and then used a corresponding states equation to calculate the parachor.

Fanchi[58] (1985 and 1990) used regression analysis to develop a relationship between the parachor and the critical properties of the fluid. Parachor correlations related to the molecular weight of the hydrocarbon systems were also derived: $P = 10 + 2.92$ (M/g mol^{-1}) for paraffins + CO_2 + N_2 and $P = 69.9 + 2.3$ (M/g mol^{-1}) for hydrocarbon mixtures. Firoozabadi et al.[4] (1988) found a quadratic relation as a function of molecular weight for crude cuts and a linear one for n-alkanes from experimental data. A similar relation but with different coefficients was proposed by Ahmed[59] (1989) for hydrocarbon mixtures.

Satherley and Schiffrin[60] (1992) suggested that the molecular parachor for a liquid far from the critical temperature is really only a function of molecular properties encompassed in the hard sphere diameter : $P = 2.841 \times 10^{19}\ T^{1/4}\ f(y)\ (\sigma^3/\sigma^{1/2})$, where T is the temperature, f(y) is a function of the number density, y [= $(\pi\sigma^3 N_A)/6V$], where N_A is Avogadro's number, V is the molar volume and σ is the hard sphere diameter of the liquid.

Broseta and Ragil[47] (1995) applied critical scaling theory to relate the parachors of pure compounds to their critical parameters. They used the parachor exponent in the W-K approximation, defined earlier, of 11/3 ($\sim$3.667): $P = (0.85 - 0.19\ \omega)\ T_c^{12/11} / p_c^{9/11}$, where ω is the Pitzer acentric factor[1] and T_c and p_c are the

---

[1] The ω factor proposed by Pitzer, represents the acentricity or nonsphericity of a molecule. It is used as a parameter to estimate the complexity or deviation of simple-fluid behaviour. For monatomic gases it is zero. For CH_4 is very small. It increases with higher molecular weight hydrocarbons and with polarity.

critical temperature and pressure respectively. However, the expression needs further testing with experimental data for its applicability.

Huygens et al.[43] (1993) measured low IFT values (0.045-9.45 mNm^{-1}) for nitrogen-low volatile oil systems using pendant drop-digitizing technique at conditions that are typical for North-Sea oil reservoirs. These measurements were made at four characteristic compositions as a function of pressure in the pressure range of 30 to 40MPa at a constant temperature of 373.15 K. They found that at near-critical conditions, the system behaves in accordance with critical scaling theories and the IFT can be described as a power law-function of the density difference. They compared the obtained IFT values with parachor-dependent methods (W-K, L-C and H-S). They found large deviations and therefore they concluded that, under the measurements conditions, these predictive methods are not satisfactory for estimating the IFT.

Fawcett[31] (1994) evaluated IFT correlations and parachors to predict low interfacial tensions in condensate systems. A six component gas-condensate model and a rich reservoir gas-condensate were used. The experimental low IFT values were compared with the (W-K) approximation [Eq.(2.2)], the (L-C) correlation and the (H-S) correlation values. It was concluded that all these correlations were in error, with the highest percentage error for the W-K model, of more than ~70%. For the L-C correlation a dependence on the systems was found. Improved H-S parachor values were also derived as a function of molecular weight. This approach gave smaller deviations for some systems: $P = 2.448\,M + 81.2$ for a crude cut and $P = 3.148\,M + 12.18$ for n-alkanes.

Ali[16] (1994) used the Katz-Firoozabadi[61] (1978) and Whitson (1984) data, on a generalized set of physical properties for petroleum fractions C_6 to C_{45}, to derive a parachor correlation in terms of the molecular weight of the cut or single carbon number fraction in relation to the group boiling point. Ali[16] (1994) presented a review of the above methods, including the correlation derived, and others to predict parachors of (nC_7+) fractions and pseudocomponents. A comparison of these

methods including the W-K, L-C, H-S correlations as an IFT prediction models was made. Experimental IFT values between 0.0583 to 4.1 mNm^{-1} for eight different reservoir oil fluid mixtures with CO_2 and N_2 were used for the comparison and it was concluded that all the correlations could predict the results to no better than a mean absolute deviation of around 20% and many to no better than 40 %.

This clearly shows that the parachor approach is very limited in its predictive capabilities. The approach is an empirical concept based on accumulated experimental data fitted to evaluate the correlation. As mentioned in the above review, several attempts have been made to adjust the parachor values and improve on the correlation according to specific system needs but with only limited success. The predictions from various proposed correlations always showed a large deviation from experimental results. Although this concept is outmoded in physical chemistry, it continues to be widely used in the oil industry, and consequently remains the benchmark for assessing improved techniques. A more reliable fundamental approach is needed which is based on physical understanding rather than on empirical fitting of data. In the next chapter, the scaled particle theory (SPT), which is a molecularly based theory will be described. The theory will be developed, and a proposed expression for IFT prediction will be introduced.

2.2 Peng - Robinson Equation of State

The Peng-Robinson equation of state (PR EOS) is an analytical cubic equation of state with two constants. It is an algebraic relation between pressure, temperature and molar volume. It is cubic in volume and if expanded would contain volume terms raised to powers up to a third. It can represent both liquid and vapour behaviour of nonpolar molecules[11] over quite substantial ranges of both temperature and pressure and is relatively simple from a computational point of view, comparing favourably with other types of EOS's which are non-cubic. There are four well known cubic EOS's: van der Waals, Redlich-Kwong (RK), Soave, and Peng-Robinson (PR). The two EOS's which are commonly used in the oil industry are PR

and RK.[50] The PR EOS particularly is widely used for reservoir fluid simulation, for vapour-liquid equilibria (VLE) predictions, construction of phase diagrams and calculation of physical properties of phase density and phase composition at variable temperatures and pressures of hydrocarbon mixtures.

The PR equation is based on an equation of state of the van der Waals form taking into account the temperature dependence of the molecular attraction term, a(T):

$$P = \frac{RT}{v-b} - \frac{a(T)}{v\,(v+b) + b\,(v-b)} \qquad (2.3)$$

where : $b = 0.0778\ (RT_c/p_c)$

$a(T) = a(T_c)\ \dot{\alpha}(T_R,\omega)$

$a(T_c) = 0.45724\ \ (R^2T_c^{\,2}/p_c)$

ω = acentric factor (see footnote for definition in previous section)

$T_R = T/T_c$.

$\dot{\alpha} = [1 + \beta(1-T_R^{\,1/2})]^2$

$\beta = 0.37464 + 1.54226\ \omega - 0.26992\ \omega^2$

where $\dot{\alpha}$ is a function of reduced temperature and acentric factor, which represents a kind of molecular shape[62]. The equation uses the conventional mixing rules for mixtures that are quadratic in the mole fractions :

$$b_M = \sum_{i=1}^{m} \sum_{j=1}^{m} x_i\, x_j\, b_{ij} \qquad (2.4)$$

where the subscripts M is for the mixture, m for the number of components, i and

$$a_M(T) = \sum_{i=1}^{m} \sum_{j=1}^{m} x_i x_j a_{ij}(T) \tag{2.5}$$

$$b_{ij} = \frac{1}{2} (b_{ii} + b_{jj}) (1 - c_{ij}) \tag{2.6}$$

$$a_{ij}(T) = [a_{ii}(T) a_{jj}(T)]^{\frac{1}{2}} (1 - k_{ij}) \tag{2.7}$$

j are for the pure components (from 1 to m). The mole fractions x_i and x_j can be either for the liquid or the vapour. k_{ij} is called the Peng-Robinson parameter (or binary interaction coefficient), which is assumed to be independent of pressure and temperature, and is small in value. It reflects interaction between molecules and tends to zero for an ideal solution. For a binary mixture the absolute values of c_{ij} (= c_{12}) and k_{ij} (= k_{12}) are small compared to unity. k_{12} has different values for each binary pair. For a nonpolar mixture it is common to set $c_{12} = 0$ and to fit the equation to binary vapour-liquid equilibrium composition data to obtain k_{12} for the mixture.

According to Prausnitz et al.[2] the Peng-Robinson equation of state generally shows good agreement with experimental results for both the bubble point and dew point curves but shows poor agreement in the critical region, and the calculated two-phase region is often found to be larger than that given by experiment.

In this study, a computer package NIST Thermophysical Properties of Hydrocarbon Mixtures Database implementing the Peng-Robinson Equation of State[63] and the Extended Corresponding States Correlation, was used to compute the phase compositions and phase densities respectively, for various systems at equilibrium conditions. These have been compared with the experimental results (chapter 6). The NIST package was used with default parameters throughout the computations.

2.3 Surface Tension from Corresponding States Correlation

The Law of corresponding states, proposed by van der Waals in (1873), asserts the generalisation that equilibrium properties which depend on intermolecular forces are related to the critical properties in a universal way.[11] According to the corresponding states (CS) theory if the pressure, volume and temperature are related to the corresponding critical properties the function relating reduced pressure ($P_r = P/P_c$) to reduced volume ($V_r = V/V_c$) becomes the same for all substances. The CS theory, used extensively for establishing correlations of PVT data, has been extended to include other fluid properties.[11]

Van der Waals[64] (1894) suggested that the dimensionless group ($\gamma/P_c^{2/3}\ T_c^{1/3}$) can be correlated with ($1-T_r$). Brock and Bird[65] (1955) developed this suggestion for nonpolar liquids and proposed that:

$$\frac{\gamma}{P_c^{2/3}\ T_c^{1/3}} = (0.132\alpha_c - 0.279)\ (1 - T_r)^{11/9} \qquad (2.8)$$

where α_c is the Riedel parameter at the critical point and is evaluated from $d(\ln P_{vp})/d(\ln T_r)$ where P_{vp} is the vapour pressure.

Miller[66] (1963) related α_c to the reduced boiling temperature (T_{br}) and P_c:

$$\alpha_c = 0.9076\ [1 + \frac{T_{br}\ \ln(P_c\ /\ 1.01325)}{1 - T_{br}}] \qquad (2.9)$$

By inserting Eq.(2.9) in Eq.(2.8) it can be shown that:

$$\gamma = P_c^{2/3}\ T_c^{1/3}\ Q\ (1 - T_r)^{11/9} \qquad (2.10)$$

where:

$$Q = 0.1196\ [1 + \frac{T_{br}\ \ln(P_c\ /\ 1.01325)}{1 - T_{br}}] - 0.279 \qquad (2.11)$$

Reid et al.[11] mentioned that the accuracy for this relation is similar to that for

the Macleod-Sugden relation[36] discussed earlier. This relation is, however, not applicable to compounds exhibiting strong hydrogen-bonding (water, alcohols, acids) and to quantum liquids (hydrogen, helium, neon).

The above relation [Eq.(2.10)] can be applied to mixtures but since the composition of the surface is not the same as that of the bulk, the critical constants of the mixture representing the surface are uncertain. However, a simple mole fraction mixing rule can be used to estimate p_{cM}, T_{cM} and Q_M, where the subscript M is for the mixture. The accuracy is of the same order as that obtained from the parachor relation for mixtures [Eq.(2.2)]. However, the CSC relation has an advantage in that only the system compositions are required for evaluation of surface tension. Murad[67], Rice and Teja[68] estimated the surface tension for pure liquid and binary hydrocarbon systems including n-alkanes, isomers and cycloalkanes using a corresponding states correlation (CSC). In their calculations they included a shape factor and the assumption of a linear variation of acentric factor with the dimensional group. Good agreement was found with experimental data for many of the examined fluids particularly the pure systems.

In this work, Eqs.(2.10) has been used to calculate the surface tension for pure liquids as a function of temperature and the results have been compared with experimental values over the measured range of temperature (chapter 6).

3. SCALED PARTICLE THEORY

Scaled particle theory (SPT) links intermolecular parameters of fluids with their bulk thermodynamic properties. Reiss et al.[51] introduced the theory based on a statistical mechanical treatment of dense fluids relating the dimensions of hard sphere fluids to their macroscopic thermodynamic properties. They used and evaluated the properties of the exact radial distribution function which yields an approximate expression for the reversible work required to introduce a hard sphere into a dense fluid containing spherical particle by using distance scaling as a coupling procedure. They derived[51] an expression for the reversible work of cavity formation, G_c, as an asymptotic expansion including constant terms which are functions of the density, pressure, temperature, hard sphere diameter of the fluid and the radius of a sphere which excludes the centres of the solvent molecules. Pierotti[69] used this expression in terms of reduced number density, y, as:

$$G_c = RT\left\{-\ln(1-y)+\left[\frac{3y}{1-y}\right]R+\left[\frac{3y}{1-y}+4.5\left[\frac{y}{1-y}\right]^2\right]R^2+\left[\frac{yp}{\rho kT}\right]R^3\right\} \quad (3.1)$$

where y is the reduced number density $= (\pi.\rho.\sigma^3_1)/6$, σ_1 and σ_2 are the molecular diameters for solvent and solute respectively, ρ is the number density and R is σ_2/σ_1.

3.1 Prediction of the Solubility of Gases in Liquids using SPT

3.1.1 Solubility in Pure Solvents

The chemical potential of a solute in a liquid solvent can be expressed as[69]:

$$\mu = -U_2 + PV_2 + RT \ln\left[\frac{\Lambda_2^3}{j_2}\right] + RT \ln\left[\frac{N}{V}\right] \qquad (3.2)$$

where U_2 is the molar internal energy of the solute in the solution, P is the hydrostatic pressure, V_2 is the partial molar volume of the solute, V/Λ_2^3 and j_2 are the partition functions per molecule for the translational and internal degrees of freedom of the solute, and N is the number of solute molecules in the volume, V, of the solution.

Based on the above expression for the chemical potential, Pierotti[69] extended the SPT and used it for determining Henry's law constant for solutes in very dilute solutions.

The theory considers the process of introducing the solute molecule into the solvent in two steps: in the first step, a cavity is made in the solvent to accommodate the solute molecule for which the required reversible work of cavity formation (or partial molecular Gibbs free energy) is G_c. In the second step, the solute molecule interacts with the surrounding solvent according to some potential law for which the reversible work of interaction (partial molecular Gibbs free energy) is G_i.

G_i was approximated[69] assuming it is equal to the partial molar enthalpy of interaction, which is approximately equal to E_i. E_i is the sum of the interaction energies (ϵ_i) of a mole of solute molecules with the solvent averaged over the configurations of the solvent. This also implied that the effect of the molar entropy is negligible compared to E_i and that at low pressure, the PV term is also negligible. Then E_i ($\approx G_i$) was evaluated by integrating the interaction energy as a function of radius [$\epsilon_i(r)$], assuming the radial distribution function to be unity outside the solute radius and an uniformly distributed solvent. The interaction energy term, $\epsilon_i(r)$, was that proposed by F. London[70], and it included all interaction of a polarizable polar solute with a polarizable polar solvent. The final expression for G_i is given by:

$$G_i = RT \left[- \frac{16}{3} \epsilon_{dis} \left[\frac{1}{kT} \right] - 8(\epsilon_{ind} + \epsilon_{dip}) \left[\frac{1}{kT} \right] \right] \qquad (3.3)$$

where the subscripts *dis*, *dip* and *ind* stand for the energy of dispersion, dipole and induced dipole respectively. k is the Boltzman constant.

Using Lennard-Jones energy parameters and assuming a hard sphere model the interaction energy coefficient, c_i, for dispersion, dipole and induced dipole molecular energies can be calculated from:[69]

$$c_{dis} = 4\ \epsilon_{12}\ \sigma_{12}^6 = 4\ \sqrt{\epsilon_1 \epsilon_2}\ \left[\frac{\sigma_1 + \sigma_2}{2}\right]^6 \tag{3.4}$$

$$c_{dip} = \frac{2}{3}\ (\mu_1 \mu_2)^2\ \left[\frac{1}{kT}\right] \tag{3.5}$$

$$c_{ind} = \mu_1^2\ \alpha_2 + \mu_2^2\ \alpha_1 \tag{3.6}$$

where c_{dis}, c_{dip} and c_{ind} are the dispersion (or London) energy constant, the dipole-dipole energy constant and the inductive energy constant respectively. α_1 and α_2, μ_1 and μ_2 are the polarizabilities and dipole moments of the solvent and solute respectively. ϵ_1 and ϵ_2 are the potential energy parameter (energy well depth) in the Lennard-Jones model for the solvent and solute respectively. σ_{12} is an effective molecular diameter for the solvent and solute=$[(\sigma_1+\sigma_2)/2]$ and it is defined as the distance at which the dispersion and repulsive interactions are equal in magnitude.

For solutions of non-polar solute and solvent molecules only the dispersion energy coefficient, c_{dis}, needs be considered in the evaluation of G_i in Eq.(3.3) since the terms c_{ind} and c_{dip} vanish.

In deriving the Henry's law constant (K_H) expression using the above chemical potential expression [Eq.(3.2)], it was assumed that the molecular interactions in the gas phase are negligible i.e. the reversible work ($G_c + G_i$) in the gas phase is negligible, and in the solution (liquid phase) is equal to ($-U_2 + PV_2$). Also for very dilute solutions $N/V = x/V_2$, where x is the solute mole fraction, and the solute fugacity, $f_2 = K_H x$. Based on these assumptions G_c, G_i, x/V_2, and f_2 were

substituted in the appropriate terms of Eq.(3.2) forming two equations, one for the chemical potential of the solute in the gas phase and another one in the solution. These two equations were equated since the solute was at equilibrium. After arranging the various terms, the Henry's law constant was calculated as:

$$\ln K_H = \frac{G_c}{RT} + \frac{G_i}{RT} + \ln\left[\frac{RT}{V_1}\right] \qquad (3.7)$$

where K_H is Henry's Law constant (Pa), G_c is the partial molar Gibbs free energy of cavity formation ($Jmol^{-1}$), G_i is the partial molar Gibbs free energy of interaction ($Jmol^{-1}$), T is the absolute temperature (K), V_1 is the molar volume of the solvent (m^3mol^{-1}) and R is the universal gas constant ($JK^{-1}mol^{-1}$).

By inserting the above expressions of G_c and G_i in terms of the reduced number density and molecular parameters Eq.(3.7) was then expressed as:

$$\ln K_H = \ln\left[\frac{RT}{V_1}\right] - \left[\frac{16}{3}\epsilon_{dis}\left[\frac{1}{kT}\right]\right] - \left[8(\epsilon_{ind}+\epsilon_{dip})\left[\frac{1}{kT}\right]\right] - \ln(1-y) + \left[\frac{3y}{1-y}\right]R + \left[\frac{3y}{1-y} + 4.5\left[\frac{y}{1-y}\right]^2\right]R^2 + \left[\frac{yp}{\rho kT}\right]R^3 \qquad (3.8)$$

where the value of G_i is the second and third terms in the right hand side (R.H.S.) of Eq.(3.8) and G_c is the sum of the fourth to the seventh terms on the R.H.S. of the equation. The reduced number density, y, R and k are as defined above. $\epsilon_i=(\pi.\rho.c_i/6\sigma_{12}^3)$ where ρ, c_i and σ_{12} are as defined in the previous section. P is the pressure. The number density, ρ, can be calculated from:

$$\rho = \frac{(solvent\ density)\times N_A}{(solvent\ molecular\ weight)} \qquad (3.9)$$

where N_A is Avogadro's number.

The chemical potentials of the solute in the liquid and gas phases are equal. In obtaining the G_i expression the theory assumes that there are no entropic contributions to the interaction energy, i.e. it assumes that all changes in entropy which result from the dissolution of a gas in a solvent are given by the energy of cavity formation. The theory also assumes a potential function for describing solute-solvent intermolecular forces in terms of a Lennard-Jones (6-12) pairwise additive potential. It uses theoretical results for hard sphere systems, i.e. no attractive forces, as a starting point. Thus all molecules are rigid and the internal molecular degrees of freedom (rotation and vibration) are not affected by the solution process.

3.1.2 Solubility in Mixtures

Eq.(3.1) applies for the introduction of a gas solute into a pure solvent. Pierotti[69] derived the following equation for calculating the reversible work of introducing a hard sphere solute into a fluid mixture containing *m* components treated as hard spheres:

$$G_c = -RT \left\{ \ln(1-y_3) - \left[\frac{3y_2}{1-y_3}\right]\sigma_s - \left[\frac{3y_1}{1-y_3} + 4.5\left[\frac{y_2}{1-y_3}\right]^2\right]\sigma_s^2 \right\} - \left[\frac{\pi}{6} N_A \rho \sigma_s^3\right] \quad (3.10)$$

where σ_s is the molecular diameter of the solute molecule. The reduced number density, y_l, and the number density for each component, ρ_j, are given by:

$$y_l = \frac{\pi}{6} \sum_{j=1}^{j=m} \rho_j \sigma_j^l \quad (3.11)$$

where x_j and M_j are the mole fraction and molecular weight of the j^{th} component

$$\rho_j = x_j \left[\frac{(total\ density\ of\ solvents) \times N_A}{\sum_{j=1}^{m} x_j M_j} \right] \qquad (3.12)$$

respectively.

The contribution from the energy of interaction is now given by:

$$G_i = -\frac{32}{9} \pi R \sum_{j=1}^{m} \rho_j \epsilon_{sj} \sigma_{sj}^3 - \frac{4}{3} \pi N_A \left[\sum_{j=1}^{m} \frac{\rho_j \mu_j^2 \alpha_s}{\sigma_{sj}^3} + \sum_{j=1}^{m} \frac{\rho_j \mu_s^2 \alpha_j}{\sigma_{sj}^3} \right]$$
$$- \frac{8}{9} \frac{N_A}{kT} \pi \left[\sum_{j}^{m} \frac{\rho_j \mu_j^2 \mu_s^2}{\sigma_{sj}^3} \right] \qquad (3.13)$$

where all the symbols in the equation are as defined in the previous section. The subscripts s and j are for solute and the components of the mixture respectively. ϵ_{sj} and σ_{sj} are the mixed pair potential parameters for the solute and the j^{th} component. $\epsilon_{sj} = \sum_j (\epsilon_s \epsilon_j)^{1/2}$.

Only the first term on the R.H.S. of this equation needs be considered for nonpolar solute and nonpolar solvents interaction since the values of their dipole moments are zero, whereas the first term and part of the second term should be considered if either of the solute or the solvent is polar. If both the solute and solvents molecules are dipolar then all terms in the equation should be used.

The Henry's Law constant for the case of a mixed solvent is given by:

$$\ln K_H = \frac{G_c}{RT} + \frac{G_i}{RT} + \ln \left(RT \sum_{j=1}^{m} \rho_j \right) \qquad (3.14)$$

where G_c and G_i are given by Eq.(3.10) and Eq.(3.13) respectively.

This above equation has been used in the present work to compare experimental results with calculated values of K_H for the examined systems.

3.2 Applications of SPT

SPT has been used in many applications of solution studies of various systems[69] including:[71] determination of surface tensions and solubilities[91,69], solubilities in fused salts[72] and liquid metals[73], electrolytic solutions[74], mixtures of hard spheres[75], correlating transfer properties between solvents[76], hydrophobic interaction[77], microemulsions[78], liquid crystals[79], evaluation of the pair correlation function[80], and relating ionization kinetics and thermodynamics to molecular properties.[81] The theory has been used for the evaluation of thermodynamic functions in solutions such as enthalpies, standard free energy of solution, entropy and heat capacity (e.g. Morel-Desrosiers and Pierre Morel[82], Nasehzadeh and Abraham[83], Leyendekkers[84]), solubilities, micellization and hydrophobic interaction (e.g. Geblewicz and Schiffrin[85], Sen[74], Nandi and Basumallick[86]). In most of these applications, the SPT has given satisfactory results and very good match with experimental data. However, many authors found that the theory is sensitive to the solvent or solute hard sphere diameter chosen. Therefore care has to be taken regarding the possible uncertainty in the results if the hard sphere diameter of the molecules are not known with certainty.

Gibbons[87] investigated the theory by using hard non-spherical particles of mixtures having the same shape but different sizes and calculated the values of the

second and third virial coefficients, which compared well with the actual values.

Wilhelm and Battino[88] used SPT theory to determine the solubility, Gibbs free energy, enthalpy and entropy of solution of various gases in polar and non-polar liquids at ambient to low temperatures at atmospheric pressure. They used the theory to determine the Lennard-Jones (6-12) pair potential parameters for the solvents and heats of vaporization.[89] Their calculated values were in good agreement with experimental results. Gas solubility data were also used with the theory to determine the dependence of the effective hard sphere diameter, σ_1, for various liquids at atmospheric pressure on temperature, by expressing l_1, the linear coefficient of expansion of the effective hard sphere diameter, as $l_1=(\sigma_1)^{-1}(d\sigma_1/dT)$, where $d\sigma_1/dT$ is its temperature coefficient. Using this approach, it was found that for highly polarizable molecules the results contradicts with literature values and the approach generally showed an uncertainty of $\pm$ 30%.

Using the theory, Schulze and Prausnitz[90] determined the Henry's Law constant for the solubilities of gases in water at temperatures up to 573.15 K. They found that the constant is sensitive to the characteristic molecular size parameter. Therefore, using experimental solubility data, they correlated the size parameter within the framework of the SPT as a function of temperature up to 573.15 K for the K_H prediction as $\sigma_{12}=[(\sigma_1+\sigma_2)/2]F(T)$ where $F(T/K)=16280(K/T)^2-141.75(K/T)+1.2978$. At 273.15 K, F=0.997 at 573.15 K, F=1.10. They found that the calculated values of K_H using this approach gave good agreement with experimental results.

As can be seen from the above review, the SPT has been used in various applications for predicting solute and solvent properties. The theory is based on simple assumptions, discussed earlier, that do not fully cover the properties of real systems. Thus it provides a useful basis for correlating phase-equilibrium data and thermodynamic functions for simple fluids. However, in many occasions it has been applied satisfactorily to real fluid systems by e.g. adjustment of the molecular parameters and evaluation of the interactive energy contributions in highly polar systems.

3.3 Prediction of Surface Tension from SPT

Reiss et al.[51] developed an approximate relation for calculating the surface tension (ST) of pure liquids using SPT by considering the gas phase to be a hard non-interacting wall. The value of surface tension was derived from the expression of the reversible work of cavity formation and the surface area of the cavity:

$$\gamma = \frac{[\ \sigma\ R\ T\ (2\ +\ y)\ ]}{4V\ (1\ -\ y)^2}\ -\ \frac{p\sigma}{2} \qquad \textbf{(3.15)}$$

where R, y, V, T and σ have the same meanings as defined before. The pressure term ($p\sigma/2$) is negligible at ambient pressure.

Using this relation, Mayer[91] calculated the hard sphere molecular diameter, σ, and the isothermal compressibility, β_T, of a large number of pure liquids using literature values of the surface tension. The diameters obtained decreased at high temperatures, and increased with surface tension. The compressibilities were calculated from the molecular diameters using the expression:

$$\beta_T = \frac{\sigma\ (2\ -\ 3y\ +\ y^3)}{4\ (1\ +\ 2y)^2} \qquad \textbf{(3.16)}$$

Although agreement with experimental values was good for both the ST and the isothermal compressibility the calculations were performed only at temperatures close to ambient and well below the critical temperature (T_c).

3.4 Development of SPT for ST and IFT Prediction

3.4.1 Surface Tension Prediction

Mayer[91] and other authors (e.g. Ref.88 and 89) tested Eq.(3.15) for the prediction of ST for pure liquids over small ranges of temperature close to ambient and good predictions were obtained. In this work Eq.(3.15) has been tested over a much larger ranges of temperatures up to 363.15 K for three liquids: n-pentane, isopentane and n-hexane. The values calculated from this relation [Eq.(3.15)] were found to have rather good agreement with the measured ST values at ambient temperatures. However, at higher temperatures it was found that this equation over estimates the ST with significant deviations (chapter 6).

It appears that Eq.(3.15) applies best to liquids for temperatures very much less than the critical temperature, where the vapour phase density is negligible. Further, this equation and that for G_c [Eq.(3.1)] from which it is derived takes no account of attractive interaction energies.

To improve the prediction and its applicability over a wider range of temperature, a first step would be to include an interactive energy term in the relation along similar lines as suggested by Pierotti[69] for the calculation of Henry's Law constant.

From the Gibbs relation, the surface tension is given by:[92]

$$\gamma = \left[\frac{\partial G}{\partial A}\right]_{T,P,n} \tag{3.17}$$

where G is the molar Gibbs free energy, A is the surface area and in the present case will be equal to the surface area, A_c, of the spherical cavity opened up in the liquid.

Let $G=G_c+G_i$, where G_c and G_i are the contributions to the free energy from the cavity and interaction terms respectively and defined in Eqs.(3.1) and (3.3).

Now,
$$\left[\frac{\partial G}{\partial A}\right]_{T,P,n} = \left[\frac{\partial G_c}{\partial A_c}\right]_{T,P,n} + \left[\frac{\partial G_i}{\partial A_c}\right]_{T,P,n} \tag{3.18}$$

$$A_c = 4\pi r^2 = 4\pi\sigma_{12}^2 \tag{3.19}$$

where $(\partial G_c/\partial A_c)$ is given by Eq.(3.15).

It remains only to calculate $(\partial G_i/\partial A_c)$. G_i is given by Eq.(3.3). In the present case only the dispersion term is considered since the molecules investigated have no dipole moment.

Inserting the value of $\epsilon_{dis}=(\pi.\rho.c_{dis}/6\sigma_{12}^3)$ in Eq.(3.3) and substituting for c_{dis} [Eq.(3.4)], Eq.(3.3) reduces to:

$$G_i = \frac{-32}{9}\ \pi\ R\ \rho\ \epsilon\ \sigma^3 \tag{3.20}$$

If the solute and/or solvent are strongly polar then the other terms of Eq.(3.3)

should also be considered when evaluating G_i.

Taking the derivative of G_i in the above equation with respect to A_c [Eq.(3.19)] gives:

$$\frac{dG_i}{d(4\pi\sigma^2)} = -\frac{4}{3}\,\rho\,\epsilon\,R\,\sigma \qquad (3.21)$$

Therefore, combining Eqs.(3.15) and (3.21) gives the final expression for the surface tension:

$$\gamma = \frac{\sigma R}{V}\left[\frac{T\,(2 + y)}{4(1 - y)^2} - \frac{4\,\epsilon}{3}\right] \qquad (3.22)$$

This equation has been used to calculate the ST of pure liquids as a function of temperature and the results have been compared with the experimental values over the examined range of temperature (chapter 6).

3.4.2 Interfacial Tension Prediction

The above treatment for ST prediction takes no account of the presence of a second phase. In the case of a liquid/vapour system at ambient conditions where the vapour density is very much less than that of the liquid this is a reasonable approximation and the effect of the vapour phase can be ignored as shown by the results in chapter 6. However, for liquid/liquid systems or liquid/vapour systems at high pressure both phases must be considered in any treatment to calculate the interfacial tension. In these cases the presence of the second phase has a substantial effect on the surface free energy.

Since SPT gives a simple way of computing the surface tension from the work of cavity formation it seems appropriate to attempt an extension to the interfacial case. However, two problems arise. 1) SPT treats cavity formation in a single phase. Therefore the above treatment of surface tension which arises from the work of cavity formation cannot be readily extended to the interfacial case. A different approach must be followed. To overcome this problem SPT will be used to compute the free energy of each phase, treated independently, at each (T,P). The properties of each phase will be computed taking account only of the mole fraction of components in the other phase. 2) Multicomponent two phase systems have components partitioned between phases. This means that in terms of SPT a cavity in a mixed solvent must be opened up, and further, the 'solute' molecule to fill the empty cavity can no longer be just a single molecule. Pierotti[69] gives a method of introducing a solute molecule into a mixed solvent as described above for Henry's Law calculations but not for mixed solutes. To deal with this problem of mixed solutes and solvents the one-fluid approximation[2] will be utilised. This theory proposes simple mixing rules, based on the mole fraction of components, for converting a phase containing a mixture of molecules to a phase composed of a single pseudo component with appropriate molecular properties, σ_M and ϵ_M, where M represents the values of the pseudo component. This means that at different (T,P) the fluid will have different molecular properties depending on the mole fraction of components.

Let G_L equal the sum of the cavity and interaction terms, as described in section 3.1.2, for the liquid phase and let G_v equal the sum of the cavity and

interactions terms for the vapour phase. The interfacial tension is then given by:

$$\gamma = \frac{G_L - G_v}{A} \qquad \textbf{(3.23)}$$

where A is the total interfacial surface area. Both G_L and G_v can be calculated from SPT but the value of A is not known. Eq.(3.23) can be expressed as:

$$\gamma = \frac{N^L}{A}\frac{G^L}{N_A} - \frac{N^v}{A}\frac{G^v}{N_A} \qquad \textbf{(3.24)}$$

where N^L and N^v are the total number of molecules in each phase respectively and N_A is Avogadro's number. Recognising that $N^L = \rho^L \sigma^L A$, where ρ^L is the number density in the liquid phase and σ^L is the molecular diameter of the molecules comprising the liquid phase components and similarly for the vapour phase Eq.(3.24) can be rewritten as:

$$\gamma = \rho^L \sigma_M^L \frac{G^L}{N_A} - \rho^v \sigma_M^v \frac{G^v}{N_A} \qquad \textbf{(3.25)}$$

where the subscript M represents the parameter for the pseudo component in that phase. Before Eq.(3.25) can be used to calculate the interfacial tension using SPT an effective diameter, σ_M, and energy parameter, ϵ_M, used to calculate the G_i terms, must be determined from the one-fluid approximation. The effective molecular diameter for each phase is given by the mixing rule:[2]

$$\sigma_M^3 = \sum_i^m \sum_j^m \left[\frac{\sigma_i + \sigma_j}{2}\right]^3 x_i\, x_j \qquad \textbf{(3.26)}$$

where σ_i and x_i are the molecular diameter and mole fraction of component i in the phase under consideration, and the energy parameter, ϵ_M, is given by:

where ϵ_i is the energy parameter of component i. By utilising Eq.(3.26) and (3.27)

$$\varepsilon_m \sigma_x^3 = \sum_i^m \sum_j^m \left(\varepsilon_i + \varepsilon_j \right)^{\frac{1}{2}} \left[\frac{\sigma_i + \sigma_j}{2} \right]^3 x_i x_j \qquad (3.27)$$

all the terms in Eq.(3.25) are available either from experimental information or can be calculated from SPT.

The determination of G_c, for each phase in a binary system consisting of one solute and one solvent is given by Eq.(3.1) where the pseudo molecular diameter in the liquid phase is given by $\sigma_M^{Lv} = [(\sigma_M^L + \sigma_M^v)/2]$. The value of G_i can be determined from Eq.(3.13), for each phase. Thus for a nonpolar binary system:

$$G_i^v = -\frac{32}{9} \pi R \sum_{j=1}^{m=2} \rho_j \epsilon_{sj} \sigma_M^{v\,3} \qquad (3.28)$$

$$G_i^L = -\frac{32}{9} \pi R \sum_{j=1}^{m=2} \rho_j \epsilon_{sj} \sigma_M^{Lv\,3} \qquad (3.29)$$

The number density and reduced number density in each phase can be calculated using the phase density, the pseudo molecular diameter in each phase, σ_M, and the phase composition from:

$$\rho^{L,v} = \frac{(phase\ density) \times N_A}{\sum_{i=1}^{m=2} x_i M_i} \qquad (3.30)$$

$$y = \frac{\pi}{6} \rho^{L,v} \sigma_M^{L,v\,3} \qquad (3.31)$$

For multicomponent systems, Pierotti's approach[69] for mixed solvents [Eq.(3.10)] was used to evaluate G_c, and using the concept of one-fluid theory for estimating the pseudo-solute diameter, $\sigma_s = \sigma_M$, from Eq.(3.26). Thus for multicomponent systems the value of G_c for the liquid phase is determined from

Eq.(3.32), and for the vapour phase from Eq.(3.10). The calculated value of σ_M for the vapour phase is the pseudo solute molecular diameter, σ_s, in the liquid phase and visa versa. G_i is determined from Eq.(3.33) for each phase for nonpolar solute-polar solvent/s systems, and from Eq.(3.34) for nonpolar systems:

$$G_c^L = -RT \left\{ \ln(1-y_3) - \left[\frac{6y_2}{1-y_3}\right]\sigma_s - \left[\frac{6y_1}{1-y_3} + 9\left[\frac{y_2}{1-y_3}\right]^2\right]\sigma_s^2 \right\} - \left[\frac{\pi}{3} N_A\, p\, \sigma_s^3\right] \quad (3.32)$$

$$G_i^{L,v} = -\frac{32}{9}\,\pi\, R \sum_{j=1}^{m} \rho_j\, \epsilon_{sj}\, \sigma_M^{Lv\ 3} - \frac{4}{3}\,\pi\, N_A \sum_{j=1}^{m} \frac{\rho_j\, \mu_j^2\, \alpha_s}{\sigma_M^{Lv\ 3}} \quad (3.33)$$

$$G_i^{L,v} = -\frac{32}{9}\,\pi\, R \sum_{j=1}^{m} \rho_j\, \epsilon_{sj}\, \sigma_M^{Lv\ 3} \quad (3.34)$$

The number density and reduced number density in each phase, are given by:

$$\rho^{L,v} = \frac{(phase\ density) \times N_A}{\sum_{i=1}^{m} x_i\, M_i} \quad (3.35)$$

$$y_i = \frac{\pi}{6}.\rho^{L,v}.\left[\frac{\sigma_M^L + \sigma_M^v}{2}\right]^i \quad (3.36)$$

In this work, Eq.(3.25) has been used to calculate the IFT of mixed systems as a function of pressure and constant temperature using the experimental values of phase compositions and densities. The results have been compared with the

experimental values of IFT over the examined range of pressure (chapter 6).

4. EXPERIMENTAL

4.1 Introduction

The measurements of interfacial and bulk fluid thermodynamic properties of hydrocarbons at elevated pressures and temperatures were carried out in a specially designed high pressure rig. Both pure and mixed hydrocarbon model systems were examined as well as stocktank oil. The interfacial tensions (IFT's), equilibrium phase densities and phase compositions in the coexistence region were measured as a function of pressure up to 40 MPa. The measurements were made isothermally at a constant temperature of 313.15 K. In some systems the critical region was accessible within this temperature and pressure. Compressed nitrogen, methane, ethane or mixtures of these were used to maintain the pressure. Measurement were also made on three pure hydrocarbons at elevated temperatures against their vapour pressures, up to 363 K.

These systems are miscible or partially miscible under elevated pressures, and thus need a special technique to enable the IFT to be measured at thermodynamic equilibrium inside the pressure vessel. The other available measuring techniques described in the literature for IFT studies at high pressures are generally only suitable for the study of immiscible fluids. The experimental rig employed in this work, provides a convenient environment for these systems to reach thermodynamic equilibrium and to perform the measurements as required. It consists

of an IFT cell, a fluid phase circulating pump, a gas chromatograph unit for the composition measurements and a density meter for phase density measurements. All of these units are connected in a closed loop of high pressure tubing valves and fittings [Fig. 4.1]. All the experiments have been made in the closed system. A significant advantage of this experimental rig is that all the measurements, IFT, phase composition and density, can be made on the same system at the same time. This obviates the need to make up identical system compositions in separate measuring apparatus. The type of measurements, however, are still complicated and require considerable effort and care in order to obtain reliable results. Therefore, to carry out these experiments experimental procedures, such as equipment operation techniques and fluid manipulation, were followed carefully.

The experimental technique utilises digital image processing on pendant drops[1] to determine the IFT. The rig was designed with specifications to meet the required demand for an adequate mechanism to form pendant drops, an optical pathway through the pressure cell, an optimum way of equilibrating all the liquid or gas phases at the same temperature and pressure inside the rig, an efficient method for stirring the fluids inside and a technique for measuring simultaneously bulk fluid equilibrium properties with minimum errors. The optical technique, using digital image processing on pendant drops[1], together with the adequate mechanism for forming pendant drops made the measuring method particularly well suited for high pressure studies. The method[93] was capable of measuring low IFT's down to the ultralow region where the two phases approach complete miscibility and the drop size is less than 1 mm in diameter.

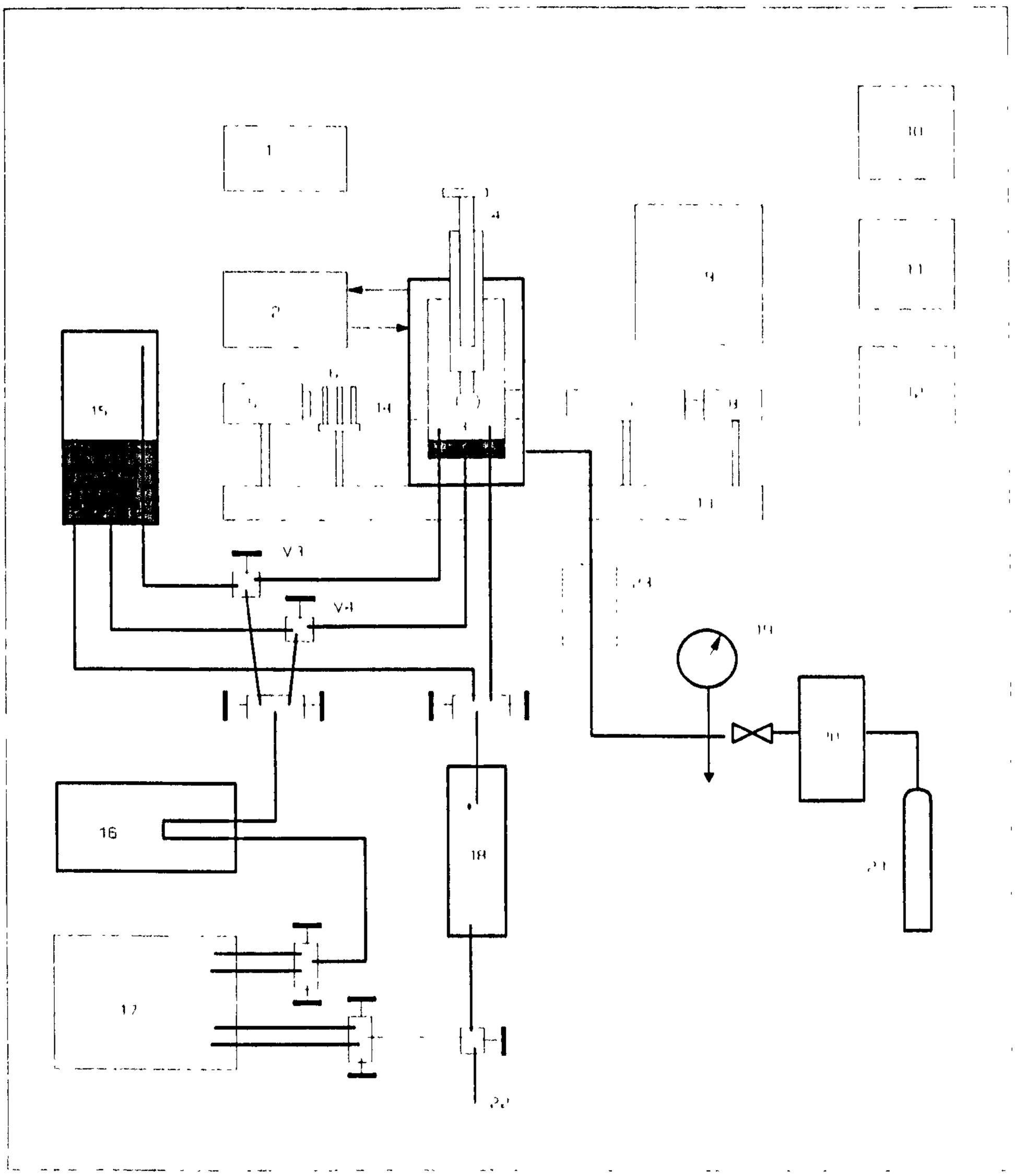

Figure 4.1 Schematic diagram of the high pressure rig. 1. Digital multimeter for temperature readout from platinum resistance thermometer, 2. Grant thermostating bath, 3. Interfacial tension cell, 4. Pendant drop syringe, 5. Projector light source, 6. Diffuser, green light filter and iris, 7. Carl Zeiss photomacrographic zoom lens, 8. Sony CCD video camera, 9. Gemini GM924 Galaxy 3 microcomputer with digitizer board, 10. Epson MX-80 printer, 11. Epson HI-80 plotter and 12. Panasonic WV5360 9" video monitor, 13. Anti-vibration table, 14. Window assembly, 15. Reservoir cell, 16. Anton Paar DMA 512 high pressure density cell, 17. Unicam GC and Valco high pressure valves, 18. Ruska Magnetic circulating pump, 19. Budenburg 70 MPa standard test pressure gauge graduated in 0.5 MPa intervals, 20. Gas compressor, 21. Nitrogen gas cylinder, 22. To drain. 23. Pressure transducer. The dashed lines represent electrical connections and the thick lines represent the high pressure system and tubing.

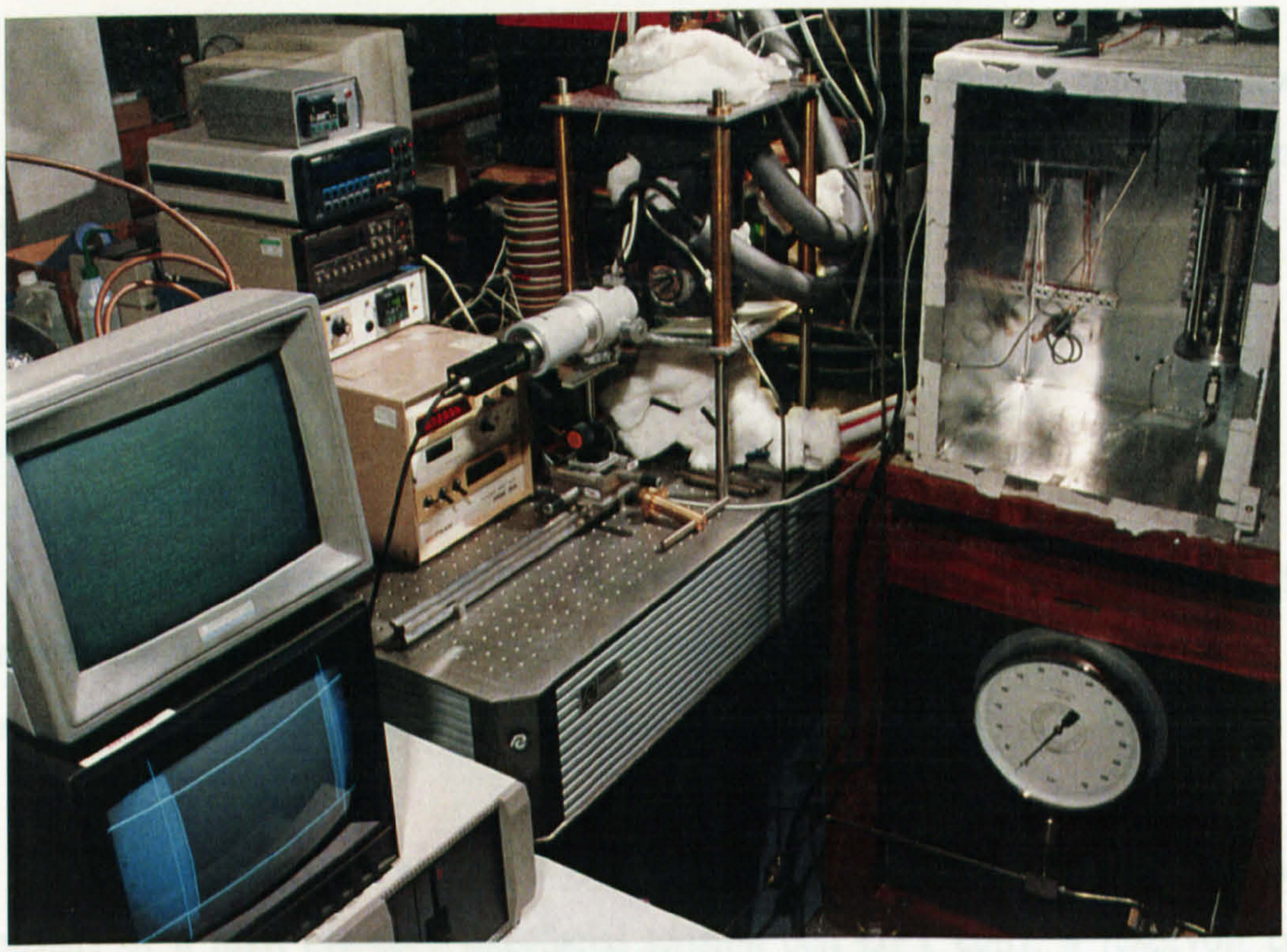

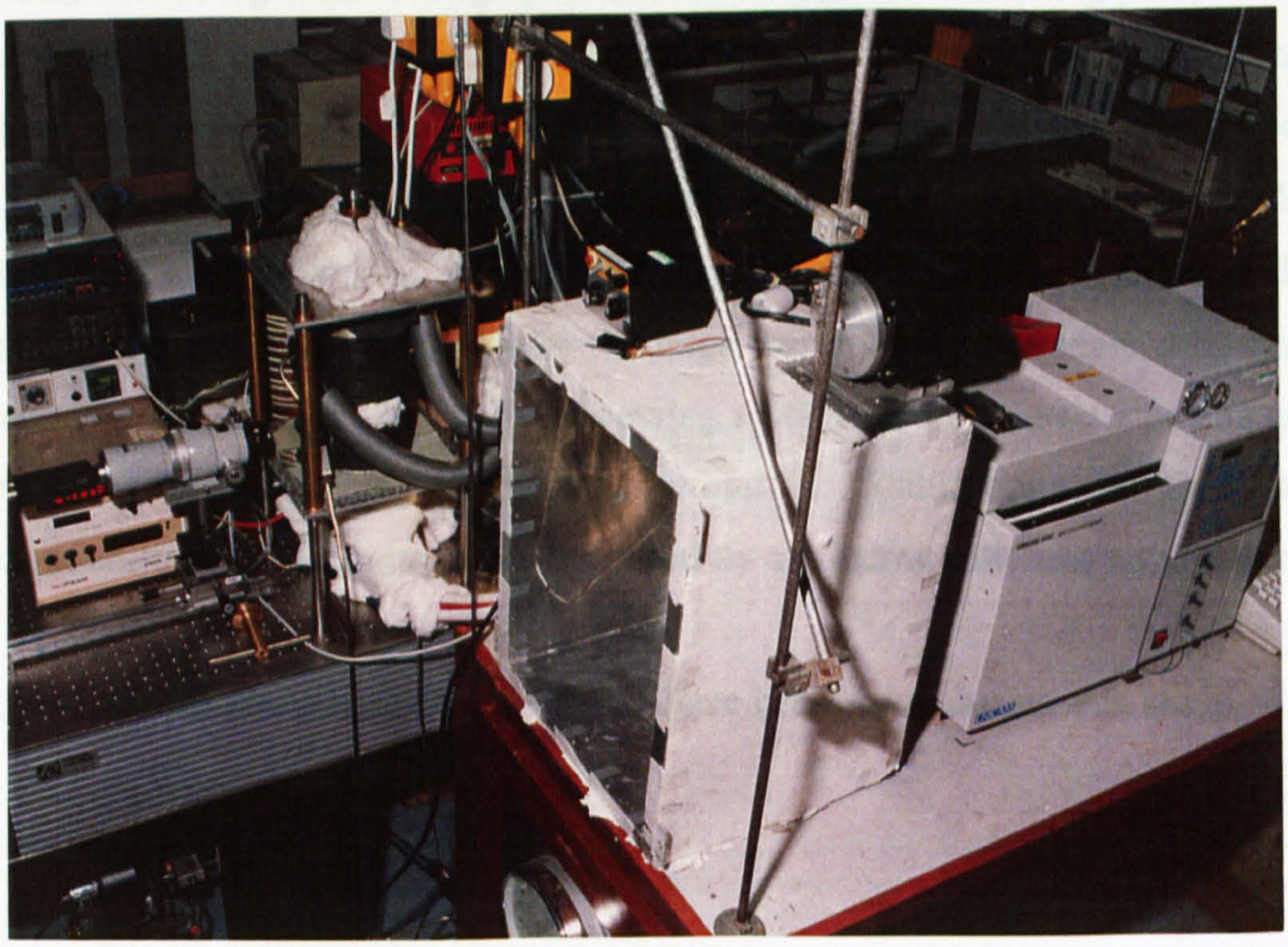

PLATES 4.1 and 4.2 Showing the high pressure rig with main equipment and instruments including the IFT cell, the magnetic pump and the GC used for experimentation.

In this chapter a description of the rig, the experimental apparatus and the measuring technique will be given together with the experimental procedure and rig operation techniques.

4.2 The Experimental Rig

The rig has been developed over the past few years and recently significant improvements have been carried out on it. The main design features have been described by Satherley et al.[94,95] and also by Tang et al.[44].

Fig. 4.1 shows a schematic diagram of the high pressure equipment used. It consists of a high pressure interfacial tension cell (IFT cell), a reservoir cell, a density meter, a gas chromatography unit and a magnetic circulating pump. The IFT cell [Fig. 4.2] enables the measurement of IFT to values as low as 0.001 mNm^{-1} within the pressure range 0.1 - 40 MPa and temperatures between ambient and 353 K. At low pressures the rig can be operated at higher temperatures, up to 393 K. Both inert and flammable gases can be used in the cell. A computerised digital image processor is used to acquire the edge coordinates of pendant drop profiles (section 4.3). The rig and image processing system is mounted on a pneumatically supported optical table to minimise vibration. Stabilisation of the ambient temperature in the laboratory was achieved by a window split unit air conditioner.

Recent equipment improvements have been made during this study. It was

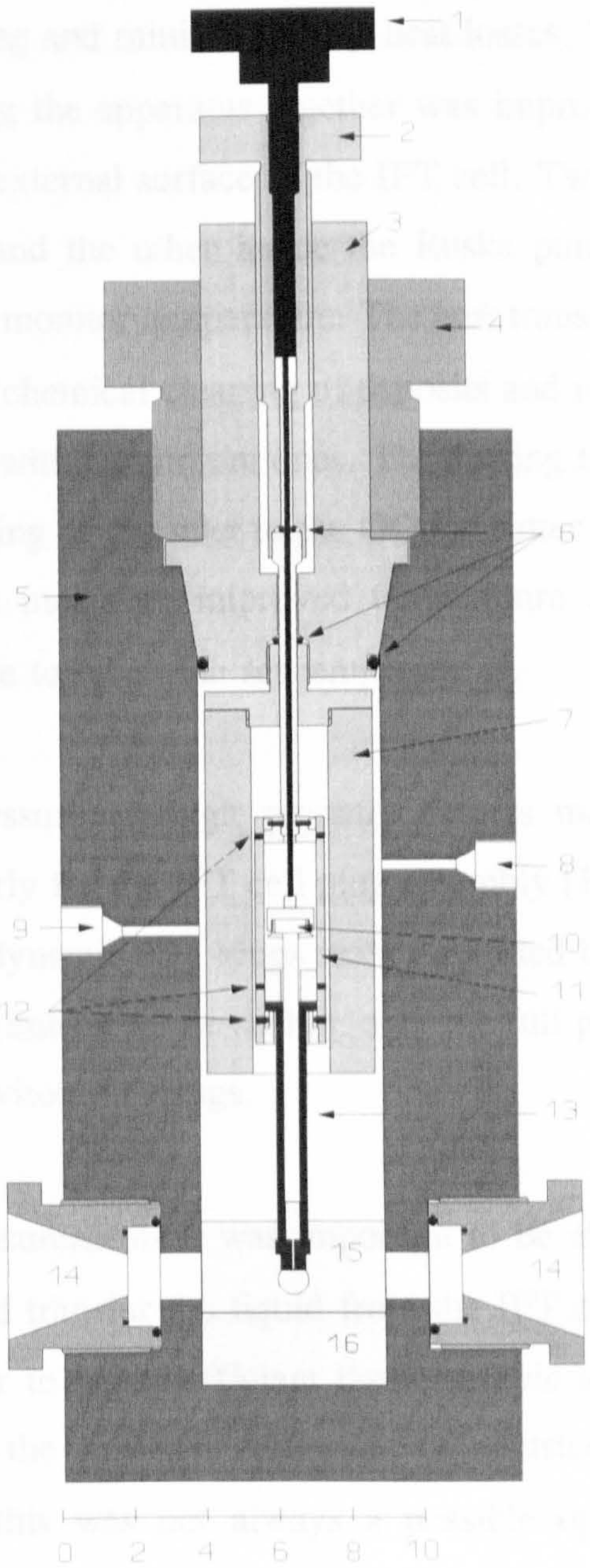

Figure 4.2 Diagram of high pressure interfacial tension cell. External dimensions of pressure vessel body: 292 mm long x 127 mm O.D.. Internal dimensions: 200 mm x 50.8 mm I.D.. Internal volume = 405.4 cm^3. 1. Syringe plunger manipulator., 2. Syringe barrel manipulator, 3. Closure plug, 4. Closure head, 5. Pressure vessel body, 6. Dynamic Viton 'O'-ring seals, 7. Spacer to reduce internal volume, 8. High pressure gas port, 9. Thermocouple port, 10. Syringe plunger, 11. Syringe mounting assembly, 12. Locking screws, 13. Syringe barrel, 14. Window assembly, 15. Organic liquid phase, 16. Aqueous liquid phase.

essential in carrying out the experiments to maintain a steady equilibrium temperature by preventing and minimising any heat losses. The lagging around the valves and tubing linking the apparatus together was improved, particularly at the inlet of the GC and the external surface of the IFT cell. Two thermometers, one at the GC sampling inlet and the other inside the Ruska pump oven housing, were installed to continuously monitor temperature. The heat transfer in the IFT cell water jacket was improved by chemical cleaning of deposits and replacing copper fittings to the aluminium jacket with aluminium ones. The heating tape and insulation were extended around the tubing of the inlet to the GC for better temperature control. In carrying out the above measures improved temperature stability was obtained. Further, it took less time to reach the set temperatures.

To maintain pressure all high pressure fittings must seal correctly. The sealing system particularly for the IFT cell plug assembly [Fig. 4.2], was improved by using a set of viton dynamic 'O' -rings seals supported by PTFE back up rings. The PTFE back up ring enhanced the sealing over the full pressure range by giving addition support to the viton 'O'-rings.

During IFT measurements it was important to be able to change the liquid level in the IFT cell and transfer the liquid from the IFT cell to the reservoir cell, and visa versa, in order to have sufficient liquid sample to form a pendant drop. Although the height of the reservoir cell could be adjusted to maintain the liquid level in the IFT cell this was not always a possible option especially at high pressures. This may be due to that the height of the reservoir cell was not enough to overcome the capillary pressure in the tubing. Another option was to use the pump to transfer the liquid from the IFT cell. However, the existing valve arrangement did not allow this. By inverting the connecting valve V4 [Fig. 4.1] between the reservoir and the IFT cell the liquid in the IFT cell could be pumped into the reservoir cell when required.

To cover the low pressure range of measurements for pure components at elevated temperatures against their vapour pressures, a differential pressure

transducer type PDCR 120/35WL-Druck Ltd. ($\Delta P = 0.35$ MPa) was connected to the inlet line of the IFT cell to measure the vapour pressure. The transducer was driven by a 10 V D.C. (direct current) input voltage and the output voltage was read from a digital voltmeter which displayed the readings in millivolts. The pressure could then be converted into MPa from a calibration equation. A correction for atmospheric pressure was made.

Another improvement which has been made is concerned with the size of the measuring capillary. At high pressures near the critical region, the values of the phase densities became close to each other and forming a pendant drop becomes difficult. To overcome this difficulty and to extend the measurements of IFT to the low region near the critical point a small capillary tip diameter of (0.61 mm) was employed.

4.3 The IFT Cell and Measurement Technique

4.3.1 The High Pressure IFT Cell

The IFT cell [Fig. 4.2] was designed to measure IFT's in fluids with miscibility at high pressures. A full description of the cell design is given by Satherley et al..[94] However, a brief description of the cell is given below.

The cell was designed for a maximum working pressure of 40 MPa at a maximum operation temperature of 423 K, however, the maximum safe working pressure at this temperature was 51 MPa. The cell was made from 321 stainless steel which has adequate tensile strength. It has an outside diameter of 127 mm and an internal diameter of 50.8 mm [Fig. 4.2], with a surrounding jacket for temperature control using thermostating fluid. The two diametrically positioned window assemblies were designed utilising viton 'O'-ring seals and pyrex glass optical flats 25.4 mm diameter × 9.14 mm each, which gave an optical pathway through the lower part of the cell of 11 mm diameter. The cell had an internal moveable syringe,

for pendant drops formation, controlled externally. The syringe was mounted on the end of two threaded concentric rods passing through the centre of the closure plug, with dynamic viton 'O'-ring seals. The outer rod moves the whole syringe with 30 mm of travel and the inner one controls the plunger position with 20 mm of travel.

One of the main advantages of the cell is that it enables the measurement of the interfacial tension between fluid phases in equilibrium inside a pressure vessel at high pressure. The optical technique using digital image processing on pendant drops[1] was ideally suited for extending the measurements to the ultralow region of interfacial tension, where the two phases approach complete miscibility and the drop size is less than 1 mm in diameter. In order to form a droplet for IFT measurements, after equilibrium conditions have been established in the cell the moveable syringe is lowered until its capillary tip is immersed in the liquid phase. A sample of the liquid is sucked up and then the syringe is returned to the gas phase. A pendant drop can then be formed by extruding the liquid inside the syringe by lowering the plunger with the aid of its screw. The drop can be easily viewed through the cell windows.

4.3.2 IFT Measurement by Digital Image Processing Technique

In this section the principles of the method will be discussed. The applications and the IFT measurement technique will be described later in section 4.3.3.

The method is based on relating the boundary tension to the geometrical dimensions of the drop using the inflexion plane method. Girault et al.[1] and Satherley et al.[93] described the method in detail and how it is used to calculate the interfacial tension.

Generally, all the methods proposed in the past rely on the different ways in which the value of the IFT is extracted from the coordinates of the drop.[97,93] In

analyzing the geometrical dimensions of a pendant drop for the purpose of IFT measurement, the required information to determine the IFT is contained in the shape assumed by the drop. The way in which this problem is tackled depends on the method of the measurement of the physical dimensions of the drop[96,97]. The main limitation for the use of the pendant (or sessile) drop technique with previous conventional methods, is in the very slow and laborious acquisition of the drop coordinates and the long times taken in the calculation and processing the image. However, recent advances in digital image processing has opened up the possibility for real time acquisition of a large number of x, y coordinates of axisymmetric shapes with associated fast processing and averaging over many video frames. This technique makes direct use of the Laplace-Young equation of capillarity.

Fig. 4.3 shows a pendant drop profile at equilibrium. To relate the boundary tension to the coordinates of the drop profile the mechanical equilibrium balance of forces on the drop at a horizontal plane P inside the drop has to be analyzed. The volume of the liquid in the drop underneath a horizontal plane at equilibrium is calculated from the balance of forces on the plane by considering the excess pressure due to curvature of the drop:

$$F_1 + F_3 = F_{2y} \qquad (4.1)$$

where F_1 is the apparent weight of the volume of the drop under the plane, F_3 is the vertical component of the excess pressure due to the curvature of the interface and F_{2y} is the vertical projection of the boundary tension which acts parallel to the interface at the plane considered. The excess pressure, P_e, is given by the Young-Laplace equation:

$$P_e = \frac{2\gamma}{r} \qquad (4.2)$$

where r is the radius of curvature and γ is the surface tension. From Eq.(4.2) the Laplace equation for any axisymmetric geometry is given by:

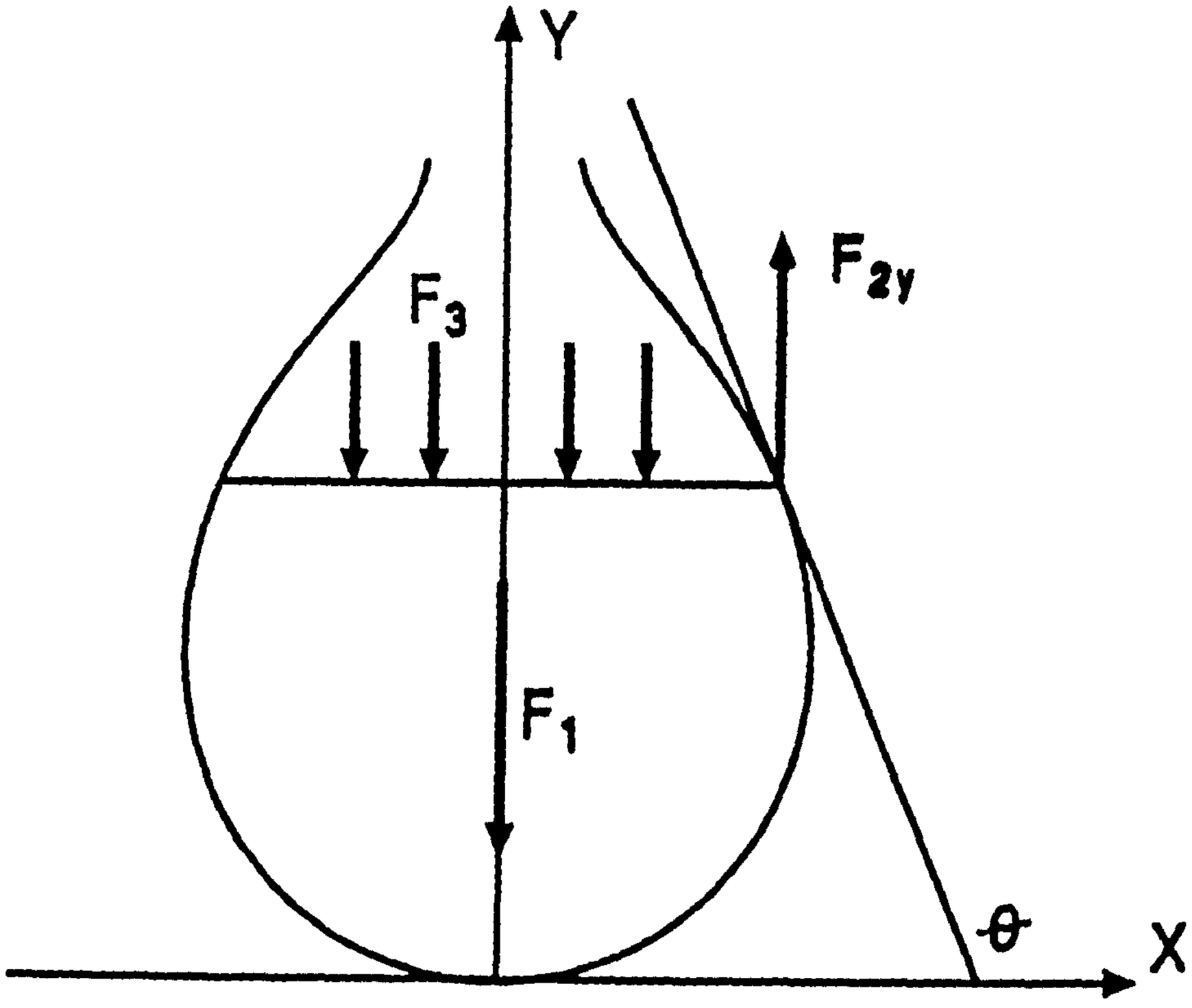

Figure 4.3. Showing a pendant drop profile and the equilibrium forces at a chosen horizontal plane.

$$P_e = \gamma \left(\frac{1}{R_1} + \frac{1}{R_2}\right) \qquad (4.3)$$

This is the fundamental equation of capillarity, where P_e is the excess pressure, R_1 and R_2 are the external and internal radii of curvature respectively. Inserting the values of the balance of forces F_1, F_{2y} and F_3 in Eq.(4.1), the following relationship is obtained:

$$V\Delta\rho g + \gamma\left(\frac{1}{R_1} + \frac{1}{R_2}\right)\pi X^2 = 2\pi X\gamma\sin\phi \qquad (4.4)$$

where V is the volume of the drop under the plane, $\Delta\rho$ is the difference in phase densities, X is the cross-sectional radius at the plane P located at a distance Y from the apex taken as the origin, g is the gravitational constant and ϕ is the angle between the tangent and the X axis [Fig. 4.3]. The method which had been used in this work, i.e. the inflexion plane, reduces Eq.(4.4) to a simple form for a change of curvature of the profile of a hanging drop. At the inflexion plane $1/R_1$ is equal to zero from the geometrical definition of R_2, and from Eq.(4.4) the interfacial tension is then given by:

$$\gamma = \frac{V\Delta\rho g}{\pi X_{infl}\sin\phi} = \frac{V\Delta\rho g R_{infl}}{\pi X_{infl}^2} \qquad (4.5)$$

4.3.3 The Interfacial Tension Measurement Technique

A computerised digital image processor was used to acquire the edge coordinates of the pendant drop profiles. The processor calculates the parameters X_{infl}, ϕ_{infl} and V in the above equation using a microcomputer according to the equation:

$$\gamma \,/\, Nm^{-1} = \frac{\gamma\ (Nm^{-3}.pixel^2)}{scale\ factor^2} \qquad (4.6)$$

where pixels are the picture elements of the video image and the scale factor is the

number of pixels per mm.

Girault et al.[1] has given a comprehensive description of the digitizing technique and calibration. The scaling factor for the number of pixels/mm ratio must be determined by calibration. To determine this ratio stainless steel rods of known dimensions were used. Different widths of objects were needed for different lens magnifications. Three sizes of rods were used for different magnifications of lenses. The objects used were uniform in cross section such as syringe needles for high magnification and engineer's depth gauges for low magnification. The diameter of the objects were measured with a digital calliper to $\pm$ 0.01 mm accuracy. During calibration it was essential to maintain the image in sharp focus and unique alignment of tessovar, object and light source set. The image of the object of known dimension (stainless steel rod) was displayed on the monitor screen, digitized and then transferred via programmed data transfer to the microcomputer for processing. A program computes the number of pixels represented by the total width of the object.

The technique required the use of a special lens with high magnification and a long working distance to accurately enlarge the drops for video analysis. A Carl Zeiss Tessovar photomacrographic zoom lens was used which had a rotating nosepiece with 4 objective lens (0.25x, 0.5x, 1x, and 2x). In addition to the zoom feature, object magnifications in the range 0.4x to 12.8x could be obtained. An optical amplifier gave a further 4x magnification. A Sony AVC-3250CE television camera was used with this zoom lens. The lens and the camera were mounted on an optical metal rail in line with the IFT cell window for focusing the drops. Drops as small as 0.4 mm in diameter could be magnified to fill the monitor screen size using the 4x enhancement. Optical distortion was minimal from the centre of the picture to the edge. A light source, diffuser, monochromatic green filter and iris diaphragm were placed [Fig. 4.1] on the opposite side of the pressure cell and also mounted on an optical rail for ease of alignment and movement.

A microcomputer [Gemini GM924 Galaxy 3] fitted with a 1 Mbyte 64180

CPU board running at 12 MHz and operating under CP/M 80 was used for data acquisition and calculations. The memory above 64 kbytes was available as a RAM drive and as an interlink medium storage location for the ASCII drop profile coordinates. A 20 Mbyte hard disc was used to store the data acquisitions along with relevant information about the physical conditions at the time of the data acquisition, i.e. temperature, pressure, density, scale factor and direction of drop. A maximum of 417 video frames could be stored in the RAM drive with each frame containing the ASCII coordinates of one drop profile, 2296 bytes. The digitizer eliminates all data which are not part of the drop edge. The time between frame acquisitions can also be altered under software control from the maximum acquisition rate of every second video frame, to any desired time.

The automatic generation of a large number of coordinate points makes the use of the pendant drop method feasible since the shape of the drop in the region of the inflexion plane can be fitted to a sufficiently accurate polynomial. The method combined very short computational time with high accuracy. An estimated overall accuracy of the IFT measured values was within $\pm$ 0.05 mNm^{-1}, $\pm$ 0.005 mNm^{-1}, and $\pm$ 0.0005 mNm^{-1} for IFT ranges: $>$ 5, 0.1-5 and $<$ 0.01 mNm^{-1} respectively.

The IFT was computed from these coordinates by a curve fitting procedure using Eq.(4.6) given the density difference between phases as input. Typically, 20 video frames were recorded in one acquisition and this was repeated three or four times until consistent results were obtained. The large amount of digital data available made this calculation reliable and simple.

4.4 The Circulating Pump

An essential condition in performing these experiments was to maintain the liquid and gases phases at equilibrium. This was achieved by mixing the initial liquid and gas components using a circulating pump [Fig. 4.1]. This pump was also used for transferring the fluids from one part of the rig to another as desired. The

circulating pump is a magnetic type manufactured by Ruska Instrument Corp., U.S.A model 2330 - 802. It was designed for use at high pressures up to 82.8 MPa, and temperatures up to 450 K, with a flow rate capacity of 10^{-4} m^3min^{-1}. The inside of the pump has four gravity operated check valves in a high pressure tube with a check valve at each end of a magnetic internal piston where its movement follows a second outer cylindrical magnet controlled by a variable speed small electric motor. The outer cylindrical magnet is connected by a flexible cable to the circumference of an axially rotating disk. Rotation results in the outer magnetic cylinder being raised and lowered, thus moving the internal magnetic piston and maintaining a steady circulating rate of either the liquid or gas phase. The pump is mounted vertically in a thermostatically controlled oven.

To maintain steady and reliable results the internal components of the pump were always kept clean from any possible deposition or contamination which may remain from previous experiments, particularly when using multicomponent stocktank oil systems. Experience showed that any remaining traces of substances such as water, emulsifiers, alcohol or various other organic impurities previously examined can lead to unreliable results. In some instances, this can lead to an increase in the time for the phases to reach equilibrium. Generally, petroleum ether or n-pentane were used as solvents for cleaning the rig. Care was taken in selecting the cleaning solvent after an experimental run. For example, it was found that using alcohol or acetone for flushing the rig after experimentation with a stocktank oil or an organic mixture caused waxy deposits. This also lead to contamination of the column in the gas chromatograph and therefore to unreliable analytical results. Similar behaviour was observed in the density measurements. Such contaminants in the system, particularly deposits of small waxy particulates, may cause erosion or damage to the piston check valve packing seals and affect the circulating performance of the pump, and were therefore avoided. If the pump was operated at excessive pumping rates, dislocation of the piston assembly occurred caused by circulating viscous fluids. An optimum pump speed was required to maintain homogeneous mixing of the system. During experimentation it was found that if the pump was operated at moderate speeds ($\sim$20% of the motor full speed range) then

good efficiency of circulation of the gas and liquid phases was obtained.

4.5 Density Meter

4.5.1 Method

The density was measured using an Anton Paar DMA 512 high pressure density cell connected to an Anton Paar DMA 55 digital density meter (Anton Paar Ltd.). These instruments simplify the accurate determination of the density of liquids and gases by reducing the procedure to the electronic measurement of measuring the frequency of oscillation of a hollow oscillator. It operates on the principle of change in its natural frequency when filled with liquid or the gas. The mass, and thus, the density of the liquid or gas changes this natural frequency due to the gross mass change of the oscillator caused by the introduction of the liquid or gas. The oscillator in the high pressure cell consists of a hollow tube made of stainless steel which is electronically excited in an undamped fashion. The direction of the oscillation is perpendicular to the plane of the U-shaped sample tube. The frequency of the oscillator is only influenced by the fraction of the volume of fluid which is actually in the vibrating part of the sample tube. It is essential that the sample tube (the oscillator) is kept completely filled during measurement. The oscillator may be considered as a hollow body of mass m and volume v which is suspended from a spring having a spring constant c. The density of the sample, ρ, which fills the system can be determined from the natural frequency, f, of this oscillating system and thus from its period, τ, using the following relations:

$$f = \frac{1}{2\pi} \times \sqrt{\frac{c}{\rho . v + m}} \qquad (4.7)$$

$$\tau = 2\pi \times \sqrt{\frac{\rho \times v + m}{c}} \qquad (4.8)$$

Taking the square of both sides of Eq.(4.8) gives:

$$\tau^2 = \rho \left(\frac{4\pi^2 v}{c}\right) + \left(\frac{4\pi^2 m}{c}\right) \qquad \textbf{(4.9)}$$

Then let:

$$A = \frac{4\pi^2 v}{c} \quad ; \quad B = \frac{4\pi^2 m}{c} \qquad \textbf{(4.10)}$$

Which gives:

$$\rho = \frac{1}{A}\left(\tau^2 - B\right) \qquad \textbf{(4.11)}$$

A and B are not easy to measure directly since they contain the volume of sample taking part in the vibration and the elasticity of the vibrator. However, they can be determined from two calibration measurements on two samples of known densities (e.g. nitrogen and water or air and water) at the same temperature and pressure as the unknown density. A and B are then given by:

$$A = \frac{\tau_1^2 - \tau_2^2}{\rho_1 - \rho_2} \quad ; \quad B = \tau_1^2 - A\rho_1 \qquad \textbf{(4.12)}$$

The density of the sample is calculated by the built-in microcomputer according to Eq.(4.11) and displayed digitally.

The sample can either be injected into the sample tube or it can flow continuously through it. The essential requirement is that the fluid in the U-tube is homogeneous. If gas bubbles in a liquid phase or liquid droplets in a gas phase form in the tube then the instrument readings become erratic. Care was taken during the measuring procedure to avoid possible entrapped air or vapour bubbles. The sample tube was thoroughly cleaned of any insoluble substances or contamination remaining from previous measurements. A basic requirement for accurate measurement was good temperature control of the sample in the oscillator, since the constants A and B are temperature dependent. This is due to the temperature dependence of the sample cell's modulus of elasticity, and to its thermal coefficient of expansion. The manufacturer recommends a temperature stability of $\pm$ 0.01 K. A water bath with

a thermostatic accuracy of ± 0.005 K was used to maintain the temperature (section 4.7). The overall measuring error of the density was within ± 0.05 kg m^{-3}.

4.5.2 Calibration

The density meter was calibrated to determine the A and B constants by determining the oscillator's internal spring constant and the volume of the tube by using fluids of known densities as a function of both pressure and temperature. It was calibrated with triply distilled degassed water and with helium and nitrogen at a temperature of 313.15 ± 0.01 K and as a function of pressure up to 40 MPa. The temperature of the sample tube was controlled to better than ± 0.01 K to avoid thermal drift. The temperature was measured using a platinum resistance thermometer (2 or 4 wires with seamless 316 st. st. sheaths, manufactured to IEC 751:1983 by TC Ltd., U.K.) inserted into the centre of the U-tube assembly. Table 1 shows the values obtained for the constants A and B at elevated pressures at 313.15 K. These constants have been used throughout the experiments.

To cover the low pressure range of measurements with pure components at elevated temperatures against their vapour pressures, a calibration was also carried out using nitrogen and water as a function of temperature up to 363.15 K. During calibration the vapour pressures were determined by converting the output potential from the differential pressure transducer, as a function of temperature, into units of bar and adjusting for atmospheric pressure (section 4.2). The calibration was performed first using pure nitrogen followed by triply distilled water. The measurements were made by raising the temperature of the fluid in the rig and of the density meter at approximate temperature intervals of 10 K, from about 302 K and up to 363 K. When using nitrogen gas as the calibrating fluid, the pressure of nitrogen was gradually increased at each isothermal temperature run, and the data were recorded for the elevated values of pressure from 0.1 MPa and up to about 0.45 MPa at about 15 intervals of pressure. For each measured interval the period and the transducer output were recorded. The rig was allowed to reach thermal equilibrium at each temperature after introducing the compressed gas. When water

was used for calibration, the rig was cleaned, evacuated and the water was then introduced into the IFT cell. It was circulated by the pump for a very short period and then allowed to settle to make sure that the water sample was free of bubbles, and completely filling the sample tube in the density meter. The IFT cell was then closed, evacuated to remove remaining air in the system. Nitrogen was used to pressurise the water in the sample tube. Since nitrogen diffusion through the water in the small bore high pressure tubing is very slow particularly at low pressures the periods could be obtained within a short time over the desired pressure and temperature range. The presence of any nitrogen in the water could be detected in the GC analysis. The previous procedure for nitrogen calibration was followed for the water calibration.

The measured periods of oscillation, τ, for nitrogen and water for all the temperatures [Tables 2 to 7] were plotted against their pressures as shown in Figs. 4.4 and 4.5. A straight line was obtained for each temperature. The values of the slopes and the intercept values with the period, τ, axis were plotted against their corresponding temperatures [Figs. 4.6 and 4.7] and from the two equations representing the slopes and intercepts for each fluid a general equation for nitrogen and another for water was obtained as a function of pressure and temperature:

$$\tau_2 \,/s = (-1.4\times 10^{-6}\, T/K + 4.9569\times10^{-4}\,)\, P/MPa + 0.001183\, T/K + 5.4763 \qquad \textbf{(4.13)}$$

$$\tau_1 \,/s = (\, 4.119\times10^{-8}\, T/K + 1.7199\times10^{-5}\,)\, P/MPa + 0.0010894\, T/K + 5.87303 \qquad \textbf{(4.14)}$$

Eq.(4.13) is for nitrogen and Eq.(4.14) is for water. To determine the values of the constants A and B in Eq.(4.12) for each fluid at any desired temperature and pressure their reference densities were used, ρ_1 and ρ_2, together with the measured values (from the above equations) of the periods, τ_1 and τ_2. The data obtained from this procedure gave an estimated accuracy for a measured density of about $\pm$ 0.08 kg m^{-3}. The water density literature values were obtained from NBS/NRS steam tables-computer package[98], and from the IUPAC International Thermodynamic Tables-computer package (Imperial College)[99] for nitrogen and helium. The vapour

pressure values for the pure systems studied (n-hexane, n-pentane and isopentane) which were required to determine A and B at different temperatures above the boiling point and up to 363 K were obtained from Vargaftik.[33]

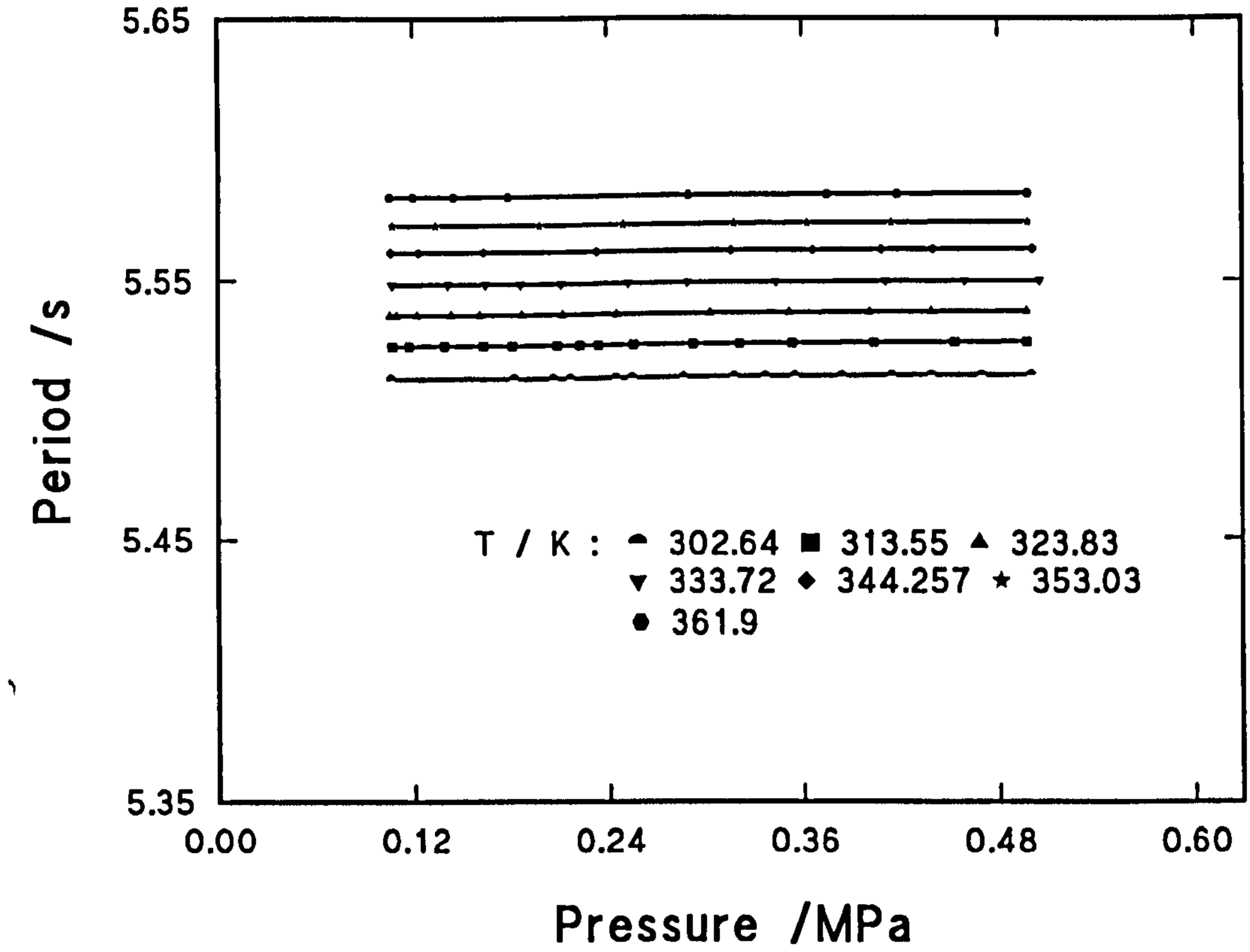

Figure 4.4. Density meter calibration using pure nitrogen: plots of periods versus pressures as a function of temperature.

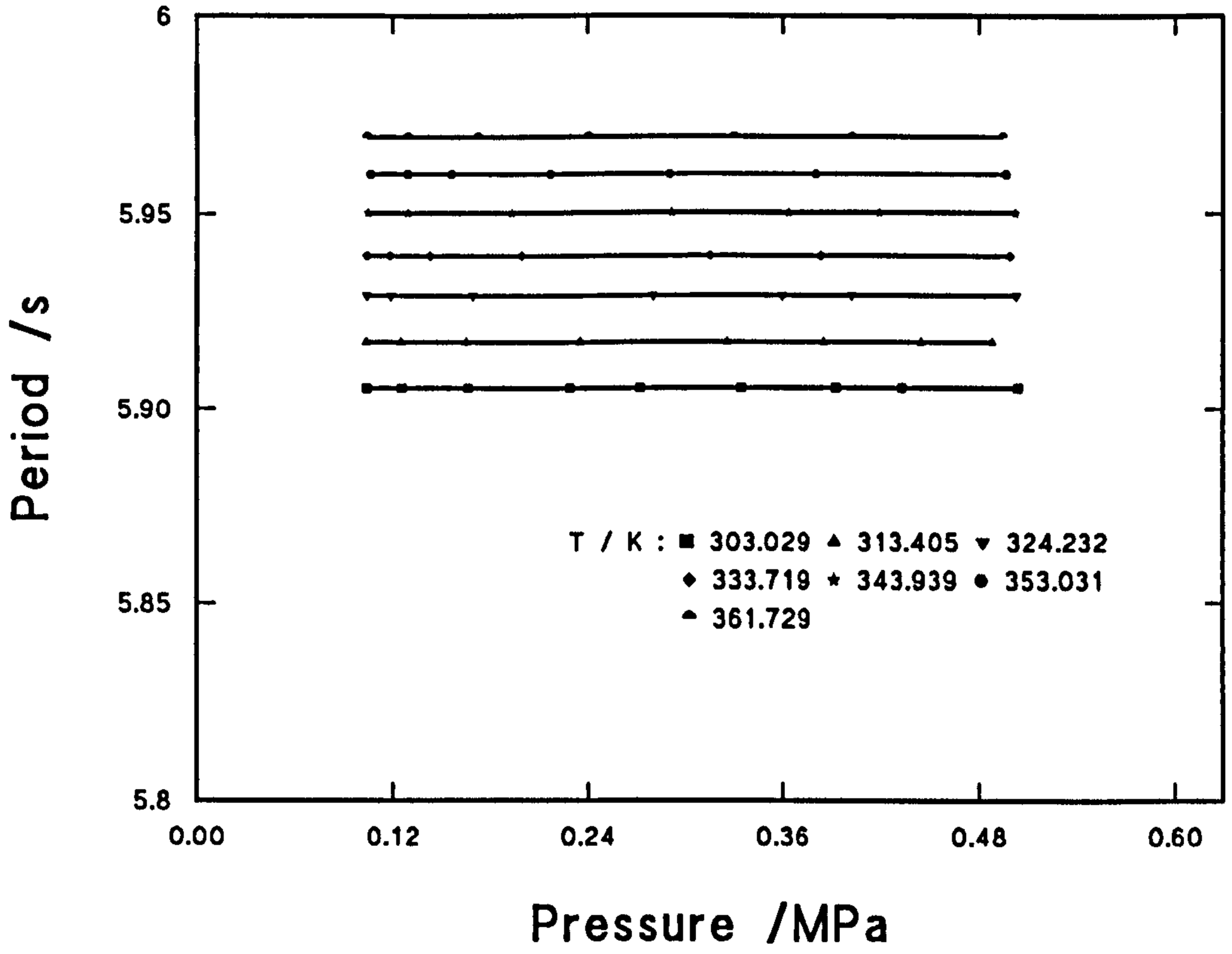

Figure 4.5. Density meter calibration with triply distilled water: plots of periods versus pressures as a function of temperature.

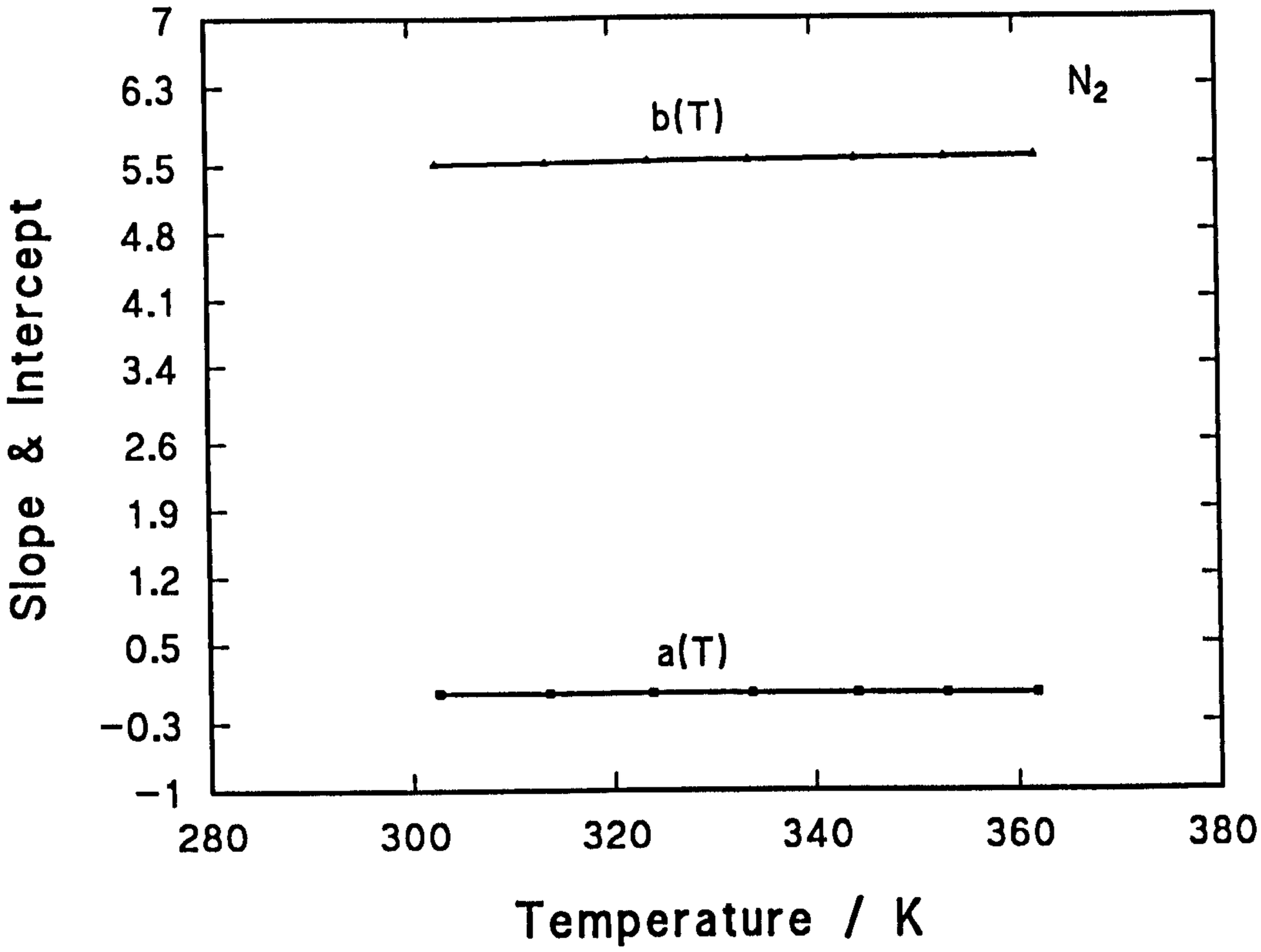

Figure 4.6. Density meter calibration with pure nitrogen: Slopes and intercepts with periods versus temperatures.

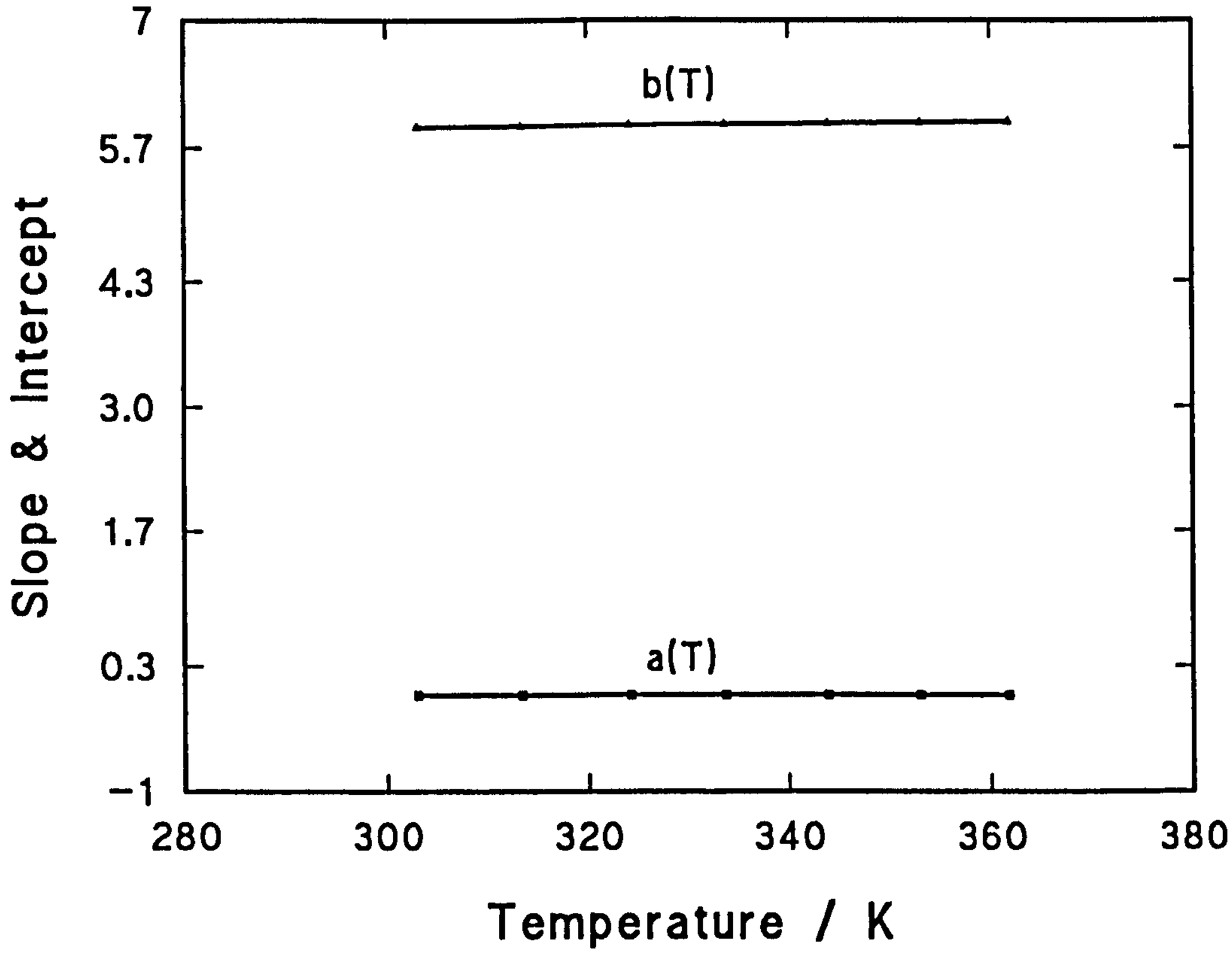

Figure 4.7. Density meter calibration with triply distilled water: Slopes and intercepts with periods versus temperatures.

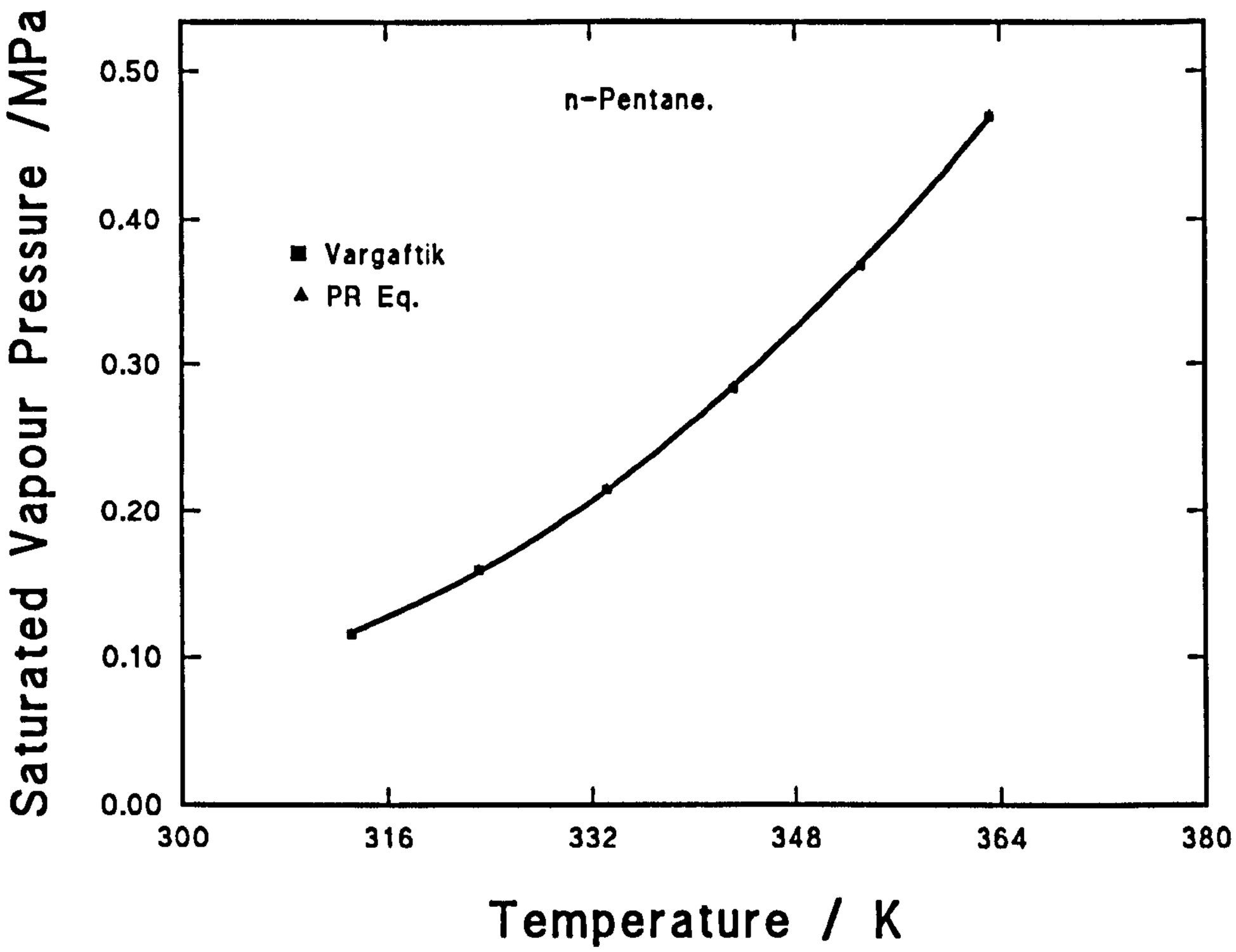

Figure 4.8. Saturated vapour pressures of n-pentane as a function of temperature.

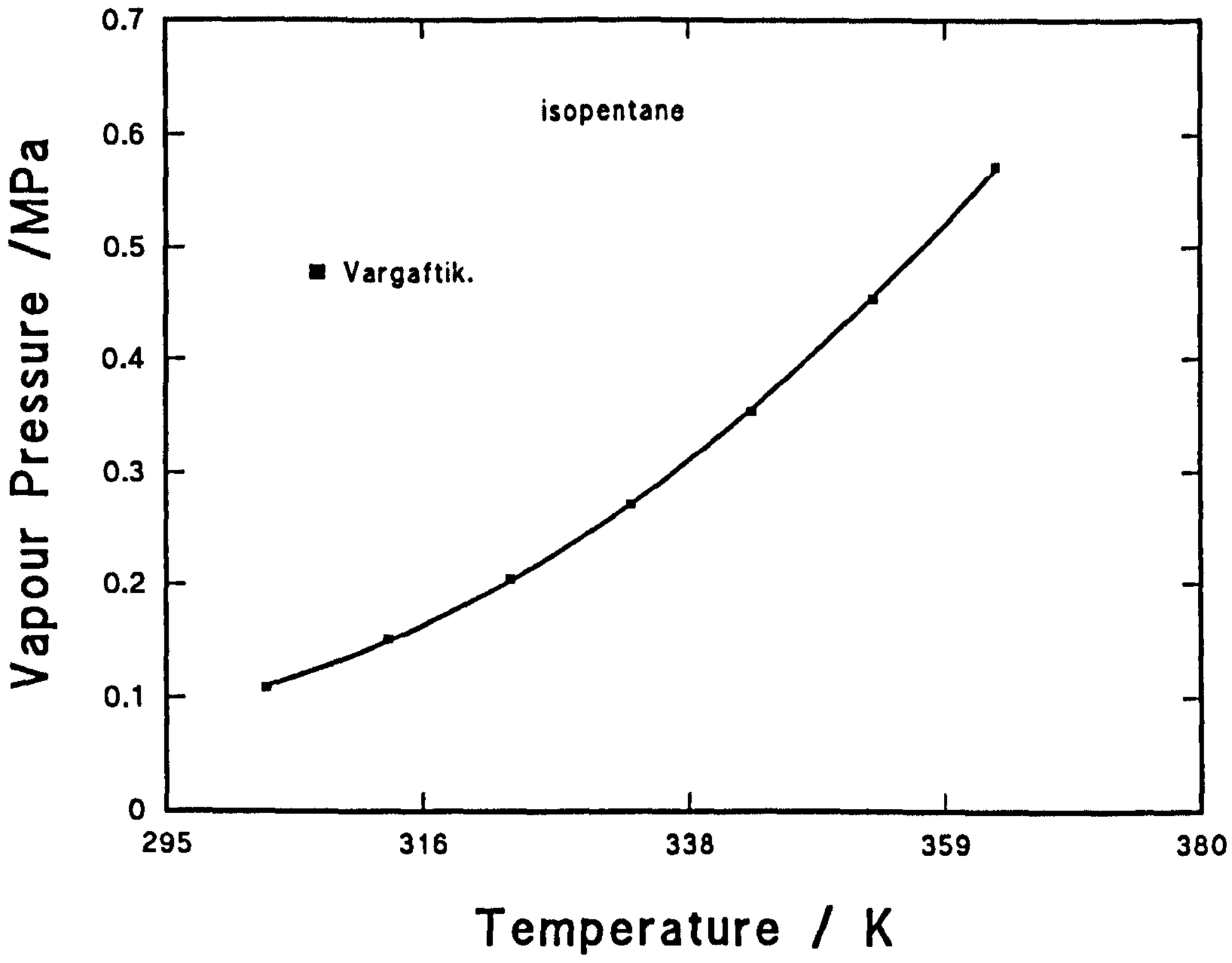

Figure 4.9. Saturated vapour pressures of isopentane as a function of temperature.

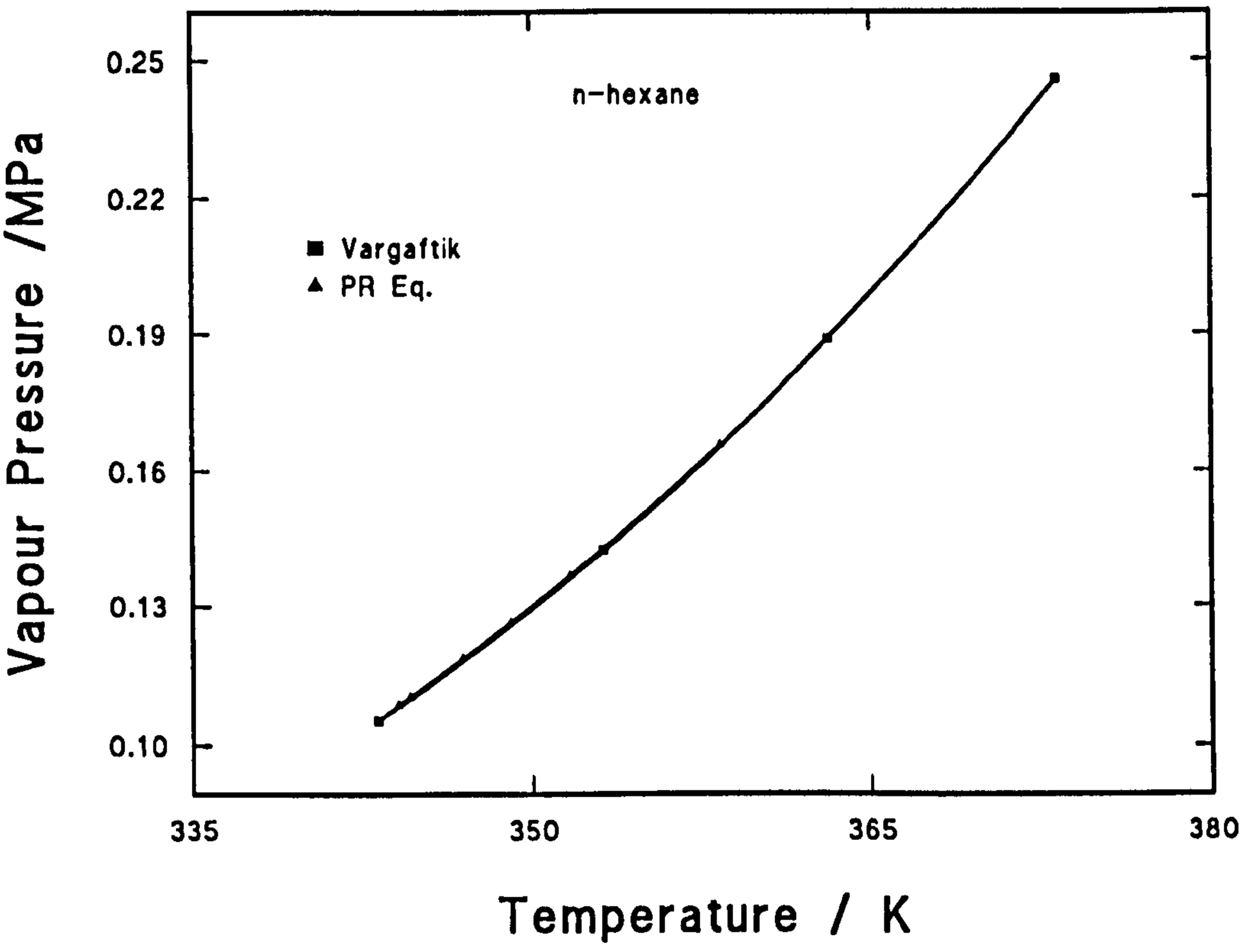

Figure 4.10. Saturated vapour pressures of n-hexane as a function of temperature.

These vapour pressure values were in excellent agreement with these values predicted from the Extended Corresponding States Correlation (EXCS)[100] [Figs. 4.8, 4.9 and 4.10], therefore they were used for determining A and B.

4.6 Gas Chromatograph

4.6.1 Description

The gas chromatograph (GC) [Fig. 4.1] used for composition analysis was a UNICAM 4600 series, (UNICAM Analytical systems) specially designed for sample handling from high pressure systems by utilising two high pressure Valco valves. The composition of liquid and gas phases can be determined for hydrocarbons up to n-decane including hydrocarbon gases and nitrogen. The GC includes a sample injector, detector and column oven, each with an independent temperature control. A three-ramp temperature programmer with automatic cooling and a set of special functions including time and date recording, a cooling sequence and automatic start-up, temperature setting, carrier and reference gas pressure gauges were all provided in a control display key-board. A computing integrator PU4815 (Philips Scientific) was connected to the GC which had the required functions and programmes to initiate sampling and storing analytical data.

The column oven temperature and the detector oven temperature were set at 443.15 K during measurements. The injector oven temperature was variably set between 313.15 to 453.15 K according to the boiling point of component. The chromatographic column was made of stainless steel with an outside diameter 1/8" and a total length of 5 m, it was filled with Chromosorb P as an absorbent (mesh size 60-80). The analysis channel was complete with thermal conductivity (TC) detector and TC amplifier, with output in mV. The detector was a sealed unit which contained four closely matched filaments mounted in four cells in the detector body. Carrier and reference gases enter the body via the inlet couplings and exit via the

outlet pipes. The sensitivity of the system was a function of the difference in temperature between the filaments and the detector body. A two level temperature switch was available on the TC amplifier to control the filament temperatures: low (513.15 K) and high (553.15 K). The temperature switch (sensitivity) was set at low during the analysis and the backoff (base-line) was kept at 1000 mV.

Helium was used as the carrier and reference gases, and was supplied to the instrument from a cylinder via a molecular sieve to remove any moisture or trace impurities. A compressed air cylinder connected to the actuators of the Valco valves supplied air for pneumatic control. The pressure on both the helium and air supply was maintained at 0.4 MPa. One of the Valco valves [Fig. 4.1] was used throughout the experiments. It had an injection volume of 0.5 μl and was operated automatically by its pneumatic actuator once a run or an injection command was initiated by the computing integrator.

A small bubble flowmeter was used in conjunction with the built in stopwatch facility on the instrument front panel keyboard to measure the flow rate of helium through the detector. The helium flow rates for the carrier gas and the reference gas were adjusted by small needle valves. The carrier and reference gas pressure flow rates were measured and set at the appropriate values for the operating conditions. The pressure of the carrier gas was maintained between 0.14 - 0.18 MPa, with a flow rate of 11.2 - 16.2 ml min^{-1} according to the column oven temperature range (313.15 - 453.15 K). The pressure of the reference gas was kept at ~0.1 MPa, with a flow rate of 27.9 ml min^{-1}.

4.6.2 Calibration

When a sample is injected into the sample loop of the high pressure valves in the GC, it is essential that it is analytically transferred to the column oven, where it is heated and evaporated. When a component of the sample comes off the column a sharp peak is recorded by the integrator [Fig. 4.11]. The sharp peak arises from the difference between the thermal conductivity of the reference gas and the sample.

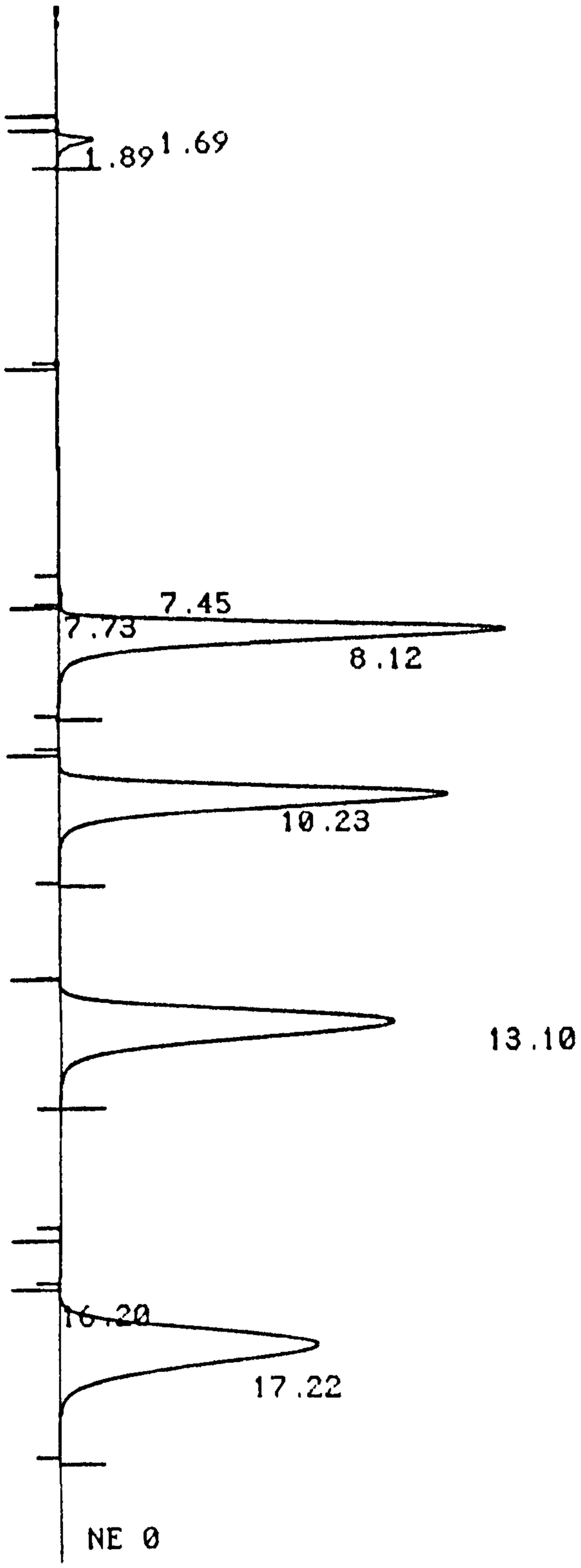

Figure 4.11. Typical GC analysis showing sharp peaks. Each peak represents an area response for each component in a mixture.

The most volatile component comes off the column first since it has the lowest boiling point. For example, methane comes off before n-pentane and n-pentane comes off before cyclohexane. Each component has a specific retention time under defined operating conditions. The area under a peak is called the area response and is proportional to the number of moles of that component present in the sample volume. But the GC cannot directly determine the number of moles. The later must be found by calibration. By using a pure component or a mixture of known composition, the number of moles of each component injected into the column can be calculated from the known volume, temperature and pressure of the sample loop. The area response divided by the number of moles of injected component gives a molar response factor (MRF). Unlike the area response this quantity is a characteristic of a component under a specified operating conditions. An area response of a component divided by that component's MRF equals the number of moles of that component. For a mixture of specified components but unknown amounts the area responses, divided by the respective MRF quantities enables the mole fractions of components in the mixture to be determined.

When calibrating the GC [Fig. 4.1] with different gaseous components or mixtures the rig, after being cleaned, was closed and evacuated. The gases were then pumped into the rig using the compressor. When calibrating with liquid hydrocarbon components, an appropriate amount of the liquid was poured into the pressure cell to make sure that liquid filled the tubing and reached the GC. The cell was then closed and evacuated for a short period to remove remaining air. The circulating pump was operated briefly to ensure filling of the system throughout. Nitrogen was then used as the pressurising medium on the surface of the liquid. Since nitrogen diffusion through the liquid in the small bore high pressure tubing is slow the results of area response and density could be obtained within a short period over a desired pressure range. The presence of any nitrogen in the liquid could be detected in the GC analysis. The results obtained are plotted as shown in Fig. 4.12. Since gases are more compressible than liquids the number of moles of a component approximately doubles with increase in pressure over the examined pressure range (up to 35 MPa), [Fig. 4.13]. For liquids, due to their low compressibility, an appreciable rise in

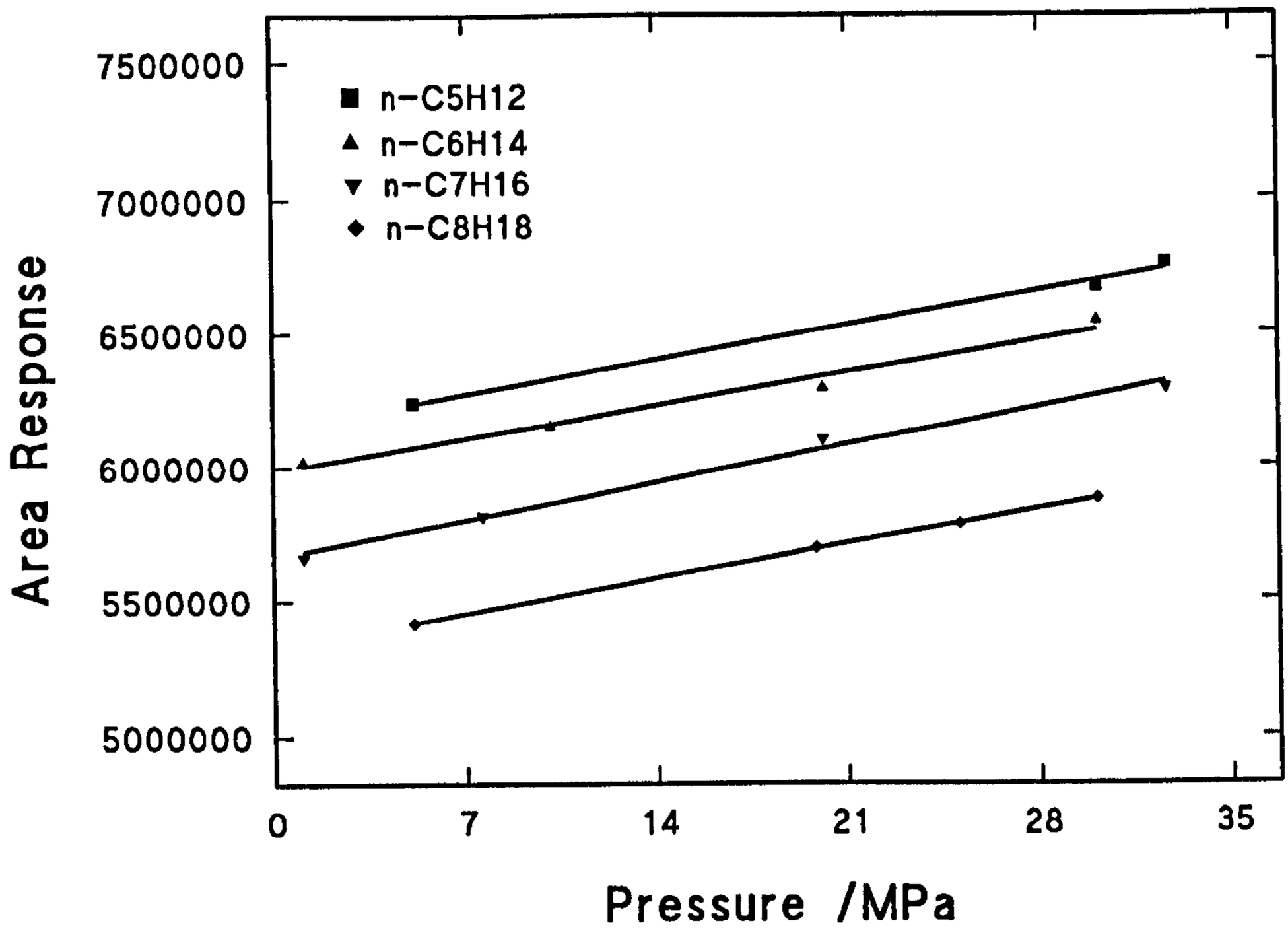

Figure 4.12. Area response obtained from GC calibration for various components at 313.15 K.

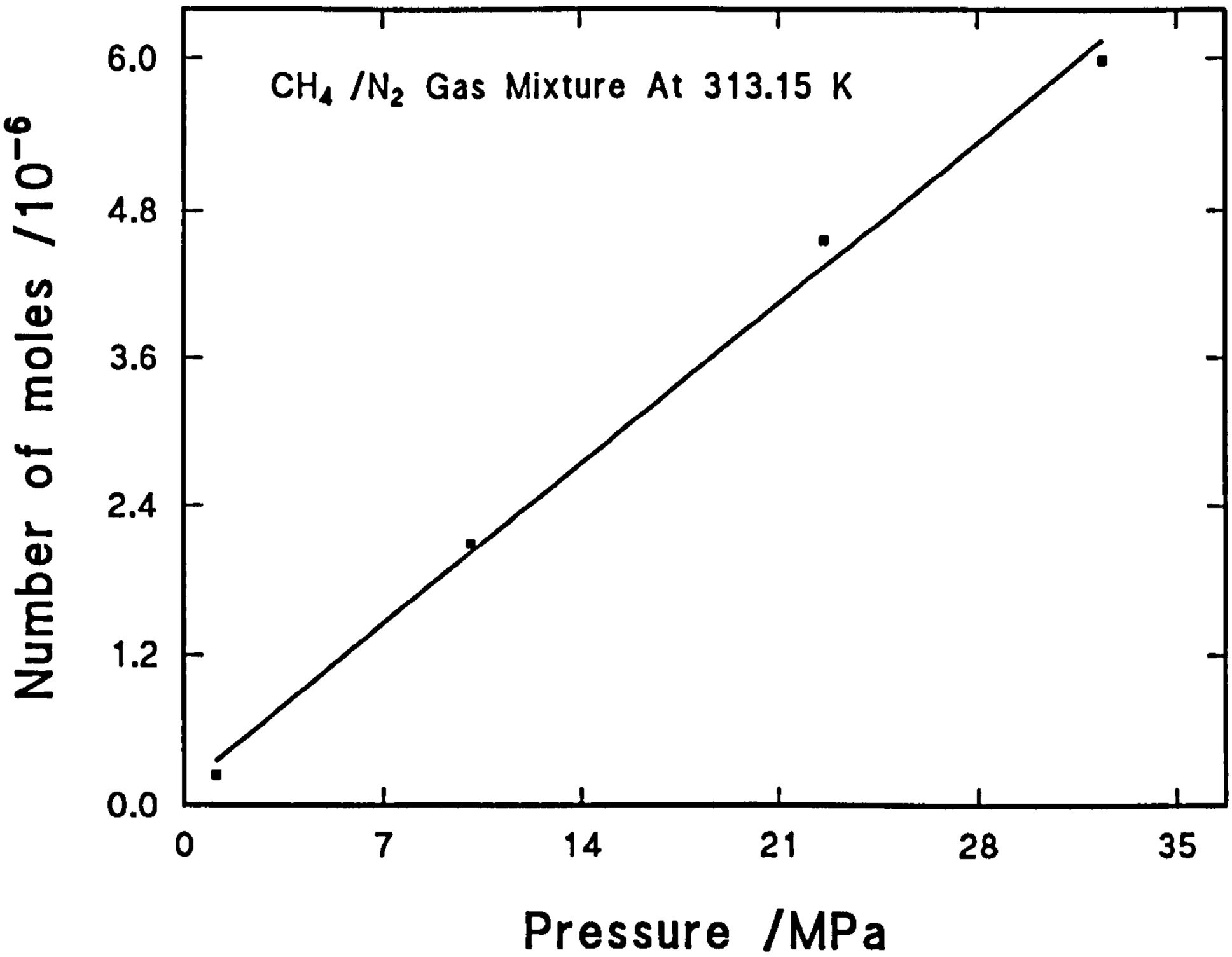

Figure 4.13. GC calibration: number of moles as a function of pressure for methane/nitrogen mixture at 313.15 K.

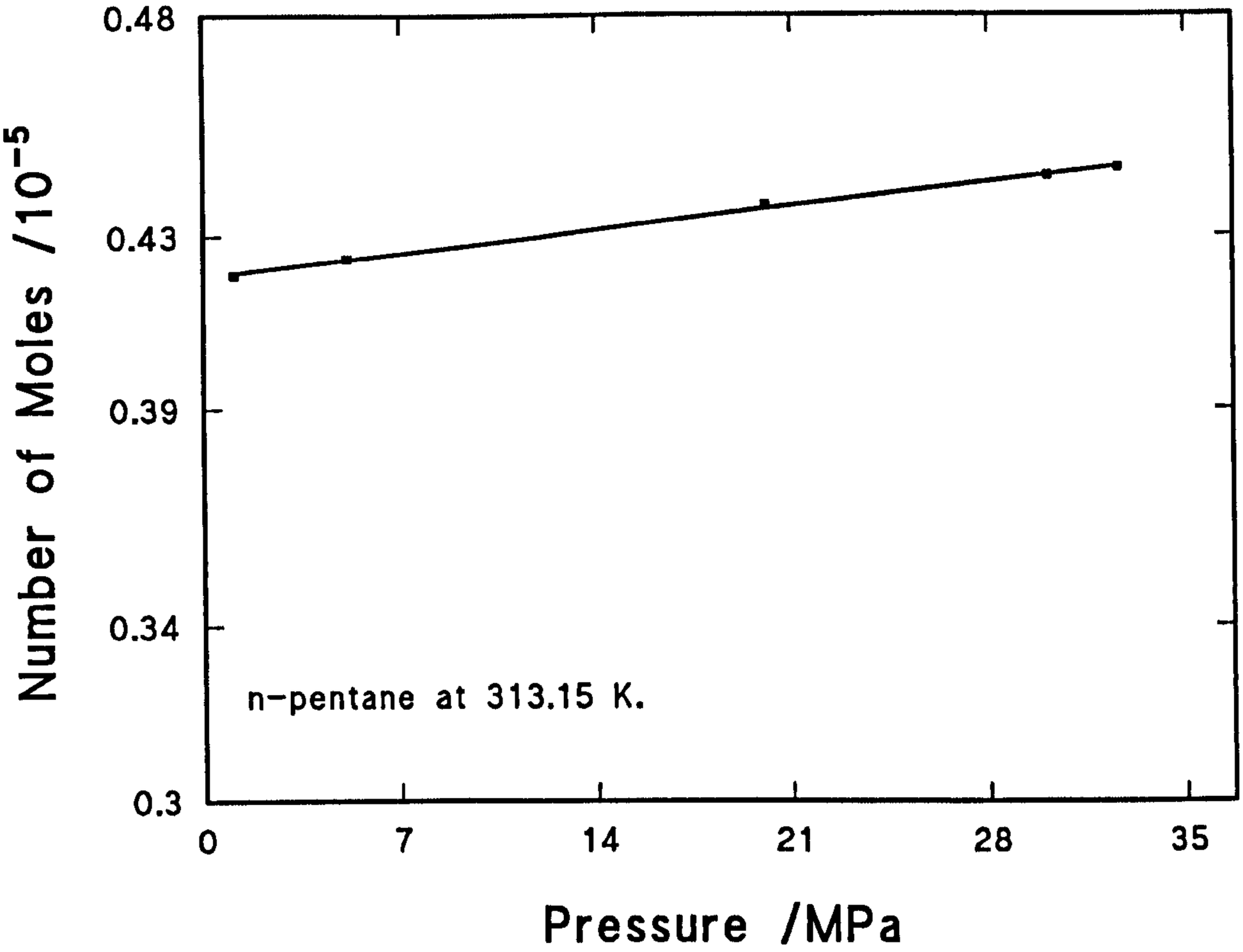

Figure 4.14. GC calibration: number of moles for n-pentane as a function of pressure at 313.15 K.

pressure causes only a small change in number of moles [Fig. 4.14].

The number of moles of a component was determined from its measured density, ρ, its injected volume i.e. 0.5 μl and its molecular weight, M:

$$Number\ of\ moles = \frac{Mass}{M} = \frac{(0.5 \times 10^{-9} \times 10^{-6}) \times \rho}{M} \qquad (4.15)$$

As mentioned above, for an MRF to be valid, it must be determined at the same GC operating conditions as that of the experiment. For example, if the calibration was made for a sample mixture at a GC inlet temperature of 313.15 K, a column oven temperature of 333.15 K, a carrier gas flow rate of 16.2 ml min^{-1} and reference gas flow rate of 27.9 ml min^{-1} then the experiment should be made in exactly the same conditions.

If a multicomponent mixture is to be analyzed a difficulty may arise in separating the components in the column and the results can be unreliable. A trial can be made on running samples to find the adequate set of GC condition depending on the boiling points of the individual components in the mixture. As an example, a mixture of n-pentane, isopentane, methane and nitrogen was analyzed most adequately with a GC column temperature of 333.15 K (but not at 313.15 K) and the mixture of n-pentane, cyclohexane, toluene and nitrogen was analyzed at 453.15 K.

Determination of the MRF for various components, as shown in Figs. 4.15 to 4.17, indicates that the MRF values are almost constant at different pressures, and are a characteristic quantity for each component and for a given set of conditions of the GC. In initial experiments, it was found that the MRF number was not pressure dependent. Consequently, in the remaining calibrations the MRF number was determined at low pressures. Table 8 shows the MRF values obtained for the different components at specified GC conditions. Using these values the number of moles of a component in a sample was obtained from dividing its area response by its MRF value. The mole fractions were determined by normalising the number of

moles for each component.

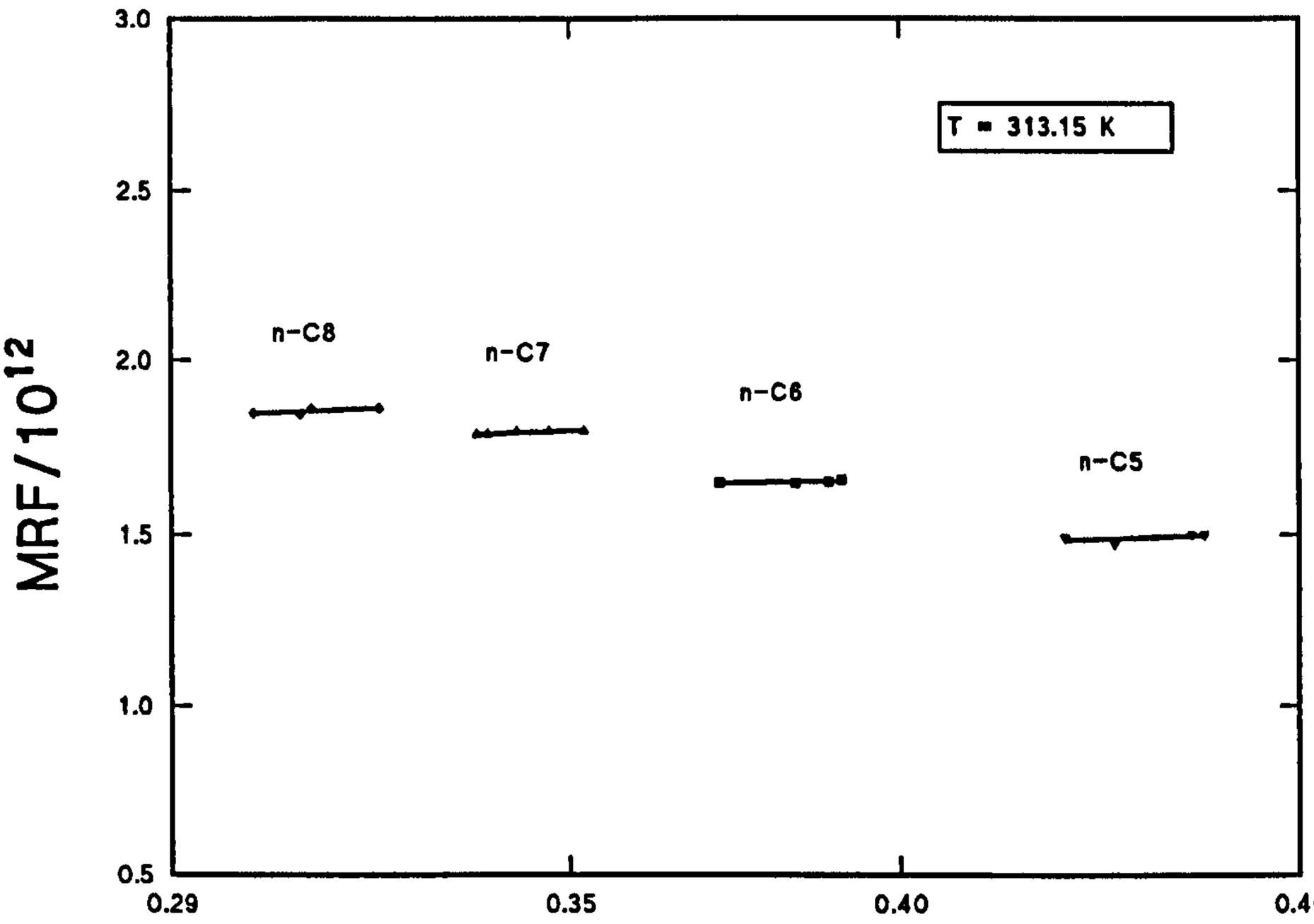

Figure 4.15. GC calibration: MRF values for each component are almost constant with number of moles rise.

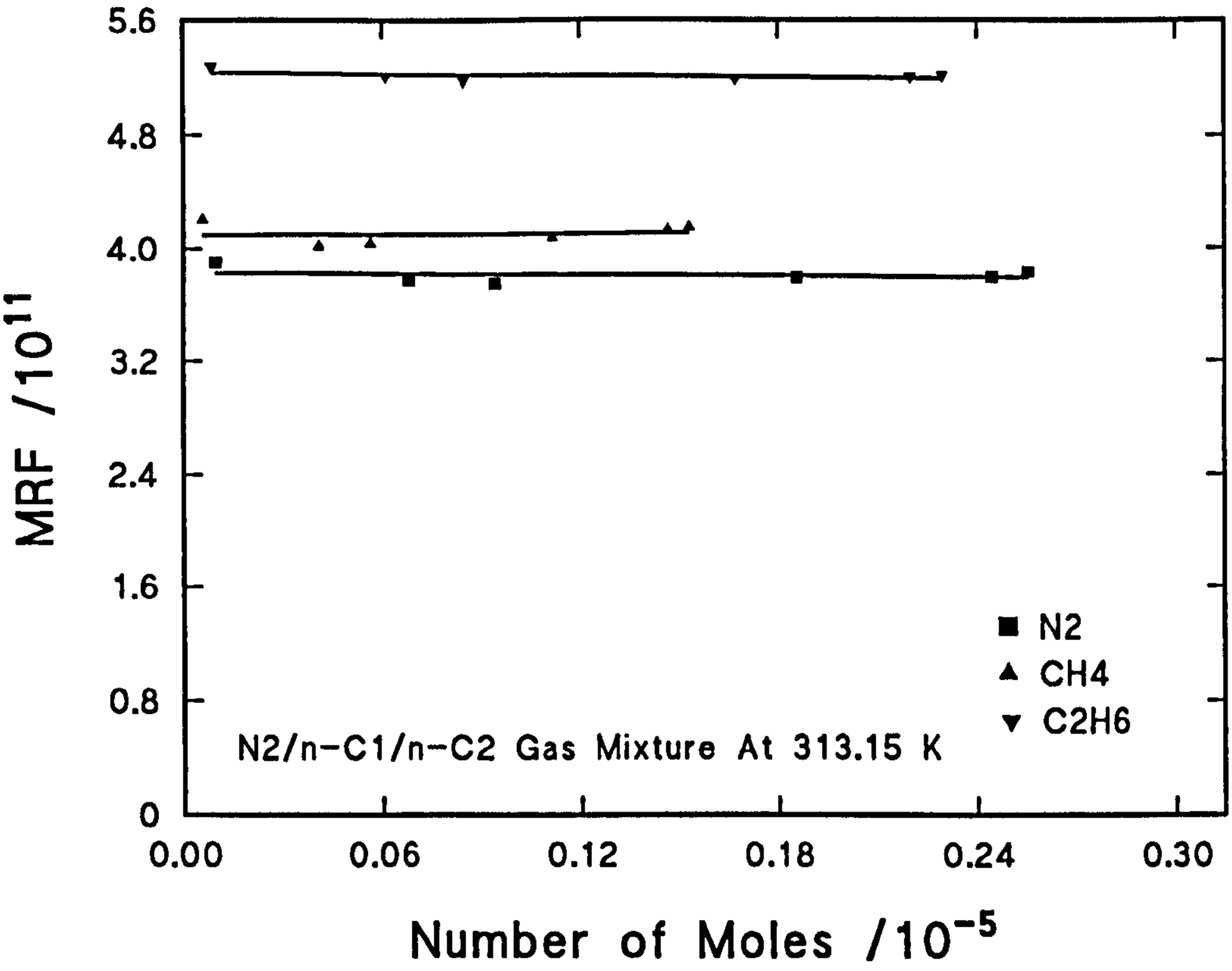

Figure 4.16. GC calibration: MRF values for each component are almost constant with number of moles rise.

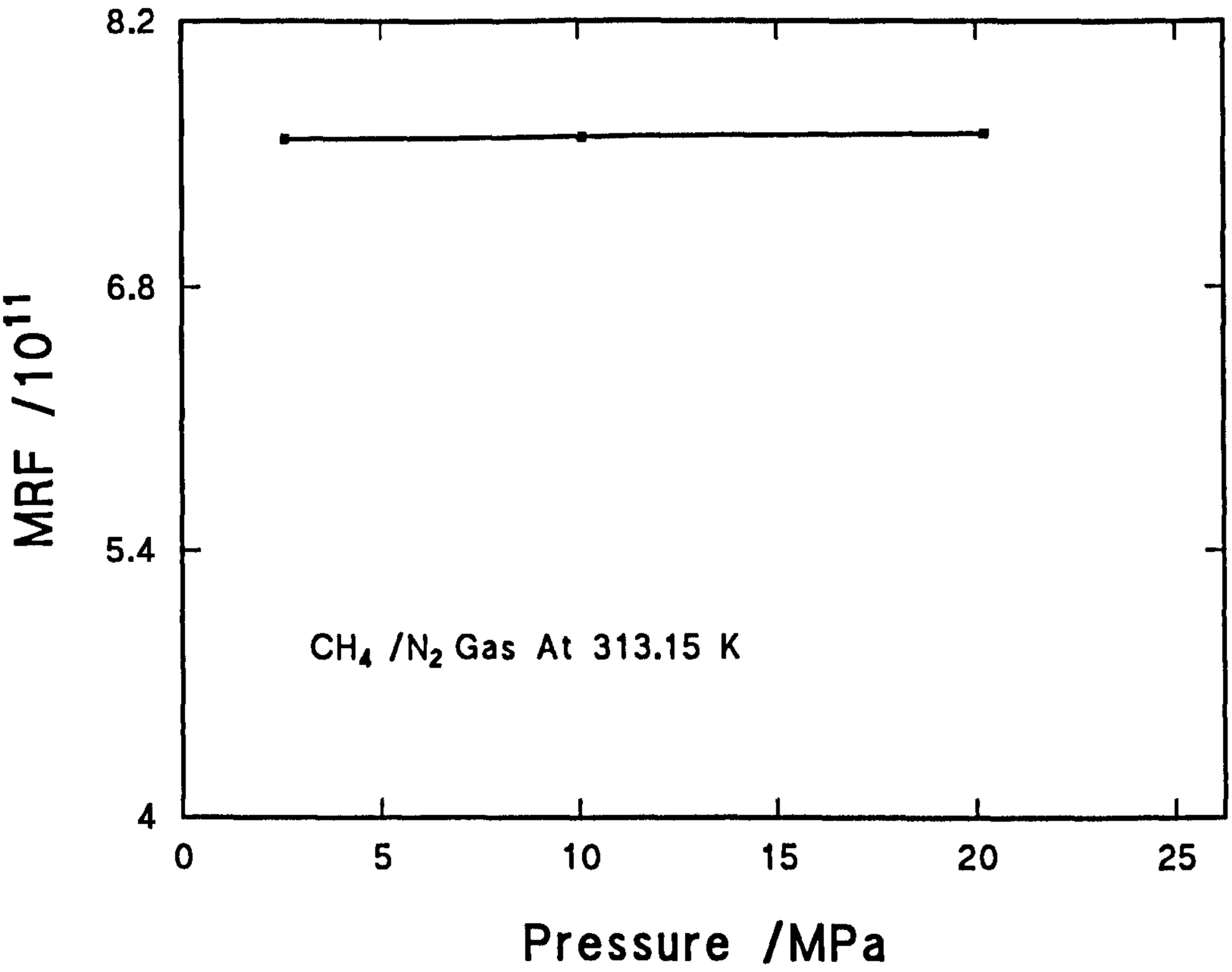

Figure 4.17. GC calibration after conditioning the Valco injection valve. MRF values are almost constant with pressure rise.

4.7 Pressure and Temperature Control

The pressure was generated with a reciprocating action gas compressor (Stansted Fluid Power Ltd.) which has a capacity of 350 MPa. Bottled nitrogen or hydrocarbon gas mixtures were connected to the gas inlet of the rig and the gases were admitted through a constant pressure gas regulator set at ~3 MPa and then compressed to the desired pressure with the gas compressor. The pressure was measured and monitored by a Budenberg Standard Test Gauge, located at the gas inlet [Fig. 4.3], which has a range of scale 0.1 - 70 MPa with 0.5 MPa divisions. The gauge was supplied calibrated against a dead weight pressure balance. The stability of the pressure readings was within ± 0.05 MPa. For low pressure measurements, up to 0.45 MPa, a differential pressure transducer was used (section 4.2 and 4.5.2).

The temperature of the IFT cell was controlled by means of a water jacket. Water at the desired temperature was supplied to the cell jacket and thermostated by a water bath (Grant Ltd.). The temperature stability of the bath was ± 0.01 K. Distilled water was used in the water bath throughout the experiments to avoid any scale deposition in the IFT cell jacket and conduits. The temperature in the cell was measured with a platinum resistance thermometer (same type mentioned in section 4.5.2) connected to a digital multimeter (Philips PM 2534). The temperature stability in the IFT cell was ± 0.05 K.

Similarly, the sample tube in the density meter was thermostated with a water bath (Heto Lab Equipment A/S- thermostat type 01 DBT 623) which circulates water through a stainless steel jacket surrounding the sample tube in a closed system. The temperature was controlled to within ± 0.005 K of the set point. A 2 mm diameter platinum resistance temperature sensor (type as mentioned in section 4.5.2) was placed in the sample tube capillary for continuous temperature monitoring. The Heto thermostat was also connected to an external circulation loop for temperature cooling using tap water.

The reservoir cell was heated by an electrical coil covering the surface of a cylindrical copper jacket surrounding the external surface of the cell. It was controlled by a proportional, integral and derivative (CAL 9000 PID, CAL controls Ltd., U.K.) temperature controller.

The temperature was maintained in the oven housing the Ruska magnetic pump by heating the inside air with a small compact air blowing fan and a thermostat controller (RS Components Ltd., U.K.) set at the desired temperature, with a thermostating accuracy of $\pm$ 1 K.

All the valves and tubing in the rig were thermostated using heating tape (RS product type 379-738) and the temperature controlled with a CAL 9900 autotune PID controller (CAL controls Ltd., U.K.). The temperatures at the GC sampling inlet and inside the Ruska pump oven housing were continuously monitored. The air conditioning unit was operated continuously to maintain a constant laboratory temperature.

4.8 Chemicals and Systems Studied

4.8.1 Chemicals

The components of the model systems studied were high purity hydrocarbons supplied by Fluka (grade > 99.5%) for n-Pentane, n-hexane, n-octane, n-heptane, 2-methylbutane (isopentane), cyclohexane (C_6H_{12}) and toluene (methylbenzene)-(C_7H_8). No additional purification was carried out on these chemicals.

High purity gases and gaseous mixtures were used throughout the experiments. Nitrogen gas of 99.998% purity (oxygen free) was supplied by BOC Ltd. Pure hydrocarbon gases and their mixtures with nitrogen gas were supplied by Linde Gases Ltd. with accurately known mixing ratios of methane/nitrogen (69.99/30.01 mol%), methane/ethane (39.99/60.01 mol%), methane/ethane/nitrogen

(24/36/40 mol%), methane (99.99%) and ethane (99.5%).

The stocktank oil sample was in the liquid phase (light condensate) supplied by Texaco (UK) Ltd. The analysis of the chemical composition of this sample was carried out by Core Laboratories (Aberdeen, U.K.) and is shown in Table 9.

4.8.2 Mixtures

The experiments were performed for different mixtures with fixed mixing ratios of the pure components. For the mixture of n-alkanes: $nC_5+nC_6+nC_7+nC_8$ the components were mixed in equivolume amounts giving molar ratios of n-C_5(0.2932), n-C_6(0.2617), n-C_7(0.2346) and n-C_8(0.2105). For the binary mixture of n-pentane and isopentane they were mixed in equal weight amounts (0.02003 kg $\pm$ 5×10^{-6} kg) of each giving a molar ratio of 0.5 of each compound. The ternary mixture n-pentane+cyclohexane+toluene was also made in equal weight amounts (0.025605 kg $\pm$ 5×10^{-6} kg) of each giving molar ratios of n-C_5H_{12}(0.378741), C_6H_{12}(0.32469) and C_7H_8(0.29657). To investigate the effect of raising or lowering the amount of cyclohexane and toluene in this ternary mixture another two models mixtures were made. In these both models the amount of n-pentane and the total amount of the mixture were kept constant, the same as in the original mixture. The amount of cyclohexane and toluene were varied to give n-C_5 (0.025605 kg), cyclohexane (0.01516 kg) and toluene (0.03605 kg) for the first model; and (0.025605 kg), (0.03605 kg) and (0.01516 kg) respectively for the second model, giving molar ratios of n-C_5 (0.383115), cyclohexane (0.19446) and toluene (0.42243); and (0.37445), (0.45196) and (0.173598) for the first and second model respectively.

4.9 Operation Techniques and Fluid Manipulation

4.9.1 Cleaning

Before introducing a sample into the rig, it was always cleaned by flushing with n -pentane or petroleum ether, dried under vacuum, then purged with nitrogen to ensure the removal of any solvent traces. The next step was to introduce an amount of nitrogen gas and take random GC analyses to check for any left traces of previous fluids in the rig. This process was repeated until the rig was clean.

4.9.2 Operation of the Rig

To carry out an experiment, a sample of hydrocarbon was poured in the IFT cell, closed and then partially evacuated to degas the sample and remove remaining air. The rig was then pressurised with gas to the initial pressure using the gas compressor. The valves connecting the reservoir and IFT cells (V3 and V4, Fig. 4.1) were operated to maintain an appropriate liquid level in the IFT cell with the assistance of the circulating pump. The gas phase was continuously cycled from the vapour region at the upper part of the pressure cells, through tubing and then bubbled through the liquid phase in the reservoir cell to hasten phase equilibria in the liquid phase, x, and vapour phase, x', in the whole system.

Density and composition measurements of the gas phase were taken every ~15 minutes to monitor their values and trend. Equilibrium was reached when stable values of these were obtained two to three times. At this point the values of the density and composition for the vapour phase were recorded at the specified temperature and pressure. The values of density were recorded when the circulating pump was switched off and the system was stable. The composition of the gas phase was determined by injecting a sample in the GC. This measurement was repeated, at the same temperature and pressure, up to four times or until consistent values were obtained.

The circulating valves (V3 and V4, Fig. 4.1) between the IFT and reservoir cells were then adjusted to enable the liquid phase to circulate through the rig. After cycling the liquid to ensure no vapour bubbles were present in the circulating loop tubing, the density and composition were measured for this phase at the same operating conditions. At this stage the IFT was measured.

In order to obtain accurate and stable results during the interfacial tension measurements the following procedure was adopted. When an IFT measurement was made it was required that the temperature and pressure of the rig were stable at the desired values and the system was at equilibrium. It was further required that there was sufficient liquid in the IFT cell to fill the syringe [Fig. 4.2]. The syringe assembly was lowered by its rotating screw so that the tip of the capillary was immersed in the liquid. A small amount of the liquid was drawn into the syringe and then the syringe assembly raised till the capillary tip was positioned at a convenient height in line with the light source and the Tessovar lens through the IFT cell windows. A hanging drop was formed by gently squeezing out a small quantity of the liquid from the capillary with the plunger.

The process of forming a pendant drop was viewed on the monitor screen [Fig. 4.1]. The light source in the background, alignment of the camera, Tessovar and the drop were modified if necessary to achieve optimum video contrast. To avoid any turbulence or disturbance caused by vapour eddies and liquid droplets during digitization of the drop the circulating pump was stopped and the inlet and outlet valves (V3 and V4, Fig. 4.1) on the IFT cell were closed. At this point the appropriate lens magnification for the drop was set, the digitizing program parameters were selected to define the drop frame, namely the video mask lines, the threshold limit and the verticality, together with tessovar alignment, brightness and fine adjustment to obtain a clear sharp focus image of the drop on the monitor. Typically 20 video frames were acquired, using the profile coordinate digitizer, under software control. One of two other programs were then used to compute the IFT from the drop coordinates. Input parameters for these programs include the profile coordinates of each drop, the difference in the phase densities and the number

of pixels per mm. The IFT is computed using Eq.(4.6) utilising the inflexion plane method.

The capillary tip diameters used throughout the experiments were 5.93, 2.43 and 0.61 mm, and their use was dependent on the size of the drop formed, which was a decreasing function of the experimental applied pressure. The most difficult region to form stable hanging drops was near the critical point, where the IFT has very low values and the values of the densities in each phase becomes similar. Under these conditions it was found that fluid in the capillary would not wet the capillary surface and would flow out continuously. It was impossible to form a drop unless the capillary diameter was also very small. It was found that with a capillary diameter of 0.61 mm IFT values as low as 0.0035 mNm^{-1} could be measured.

Care had to be taken at all times to have clean cell windows, free from any traces of liquid droplets, to enable a good level of contrast in the video image, avoiding inadequate thresholding around the drop. Care was also taken to minimise vibrations. This was achieved by mounting the equipment on a levelled, anti-vibration table.

For each drop, the measurement was repeated up to four times or until consistent results were obtained. After completion of all the measurements at the initial pressure step, the pressure was raised to the next pressure and the process was repeated until the desired maximum pressure was reached at constant temperature. The system was then vented, drained, cleaned and then the next samples were added.

As expected it was found that the most stable results were observed at equilibrium conditions. It was also found that it could take from half an hour to several hours to reach equilibrium depending on the complexity of the system and the operating conditions. For multicomponent mixtures and stocktank oil several hours were required to reach equilibrium conditions. Prolonged periods were also required when experimenting near the critical region. More time was thus allowed for the system to reach equilibrium. This is due to the long range molecular forces

becoming dominant and therefore the molecular translational movement is reduced. In this region the molecular properties in the two phases approach each other.

Another observation was that at high pressures near the critical region the fluids became cloudy. This opacity appeared for two or three minutes upon gas addition and then the fluid turned hazy with a slightly yellowish colour when equilibrium was reached. A possible reason for this observation is that near the critical point the individual phases are not homogeneous, there is fluctuation in the phase with slightly different refractive indices which will give rise to light scattering. This may also have been caused by microscopic bubbles of the gas in the liquid phase and small liquid droplets in the gas phase giving the fluids an opaque appearance.

5. RESULTS

In this chapter the results of the experimental and analytical work are presented. Section 5.1 presents the density measurements for pure components and mixtures. Section 5.2 describes the composition results for the gas solute and pseudo-component gaseous solute in the systems studied. Section 5.3 shows the results obtained from the interfacial and surface tension measurements. Finally, section 5.5 presents the results obtained from the application of scaled particle theory to the prediction of IFT, ST and Henry's law constant. Tables of all experimental results can be found in the Appendix.

5.1 Density Measurements

5.1.1 Measured Density of Pure Components

Fig. 5.1 shows the measured values of the density of the pure hydrocarbons: n-pentane, n-hexane, n-heptane, n-octane and isopentane as a function of pressure at a temperature of 313.15 K. The density of the normal hydrocarbons increase in the order of increasing carbon number. Isopentane, however, is less dense than n-pentane. The pressure dependence of density is almost linear for n-octane but becomes increasingly less linear with decreasing chain length.

The measured densities of nitrogen, methane and mixtures of these with ethane as a function of pressure at constant temperature (313.15 K) are shown in Fig. 5.2. Gases, due to their large free volumes between molecules, are highly compressible. The pressure dependence of the density for these gases is positive and non-linear. The magnitude of the density is highest for the mixture with ethane and lowest for pure methane gas.

The phase densities of n-pentane, isopentane and n-hexane as a function of temperature at saturation conditions are given in Fig. 5.3. The temperature

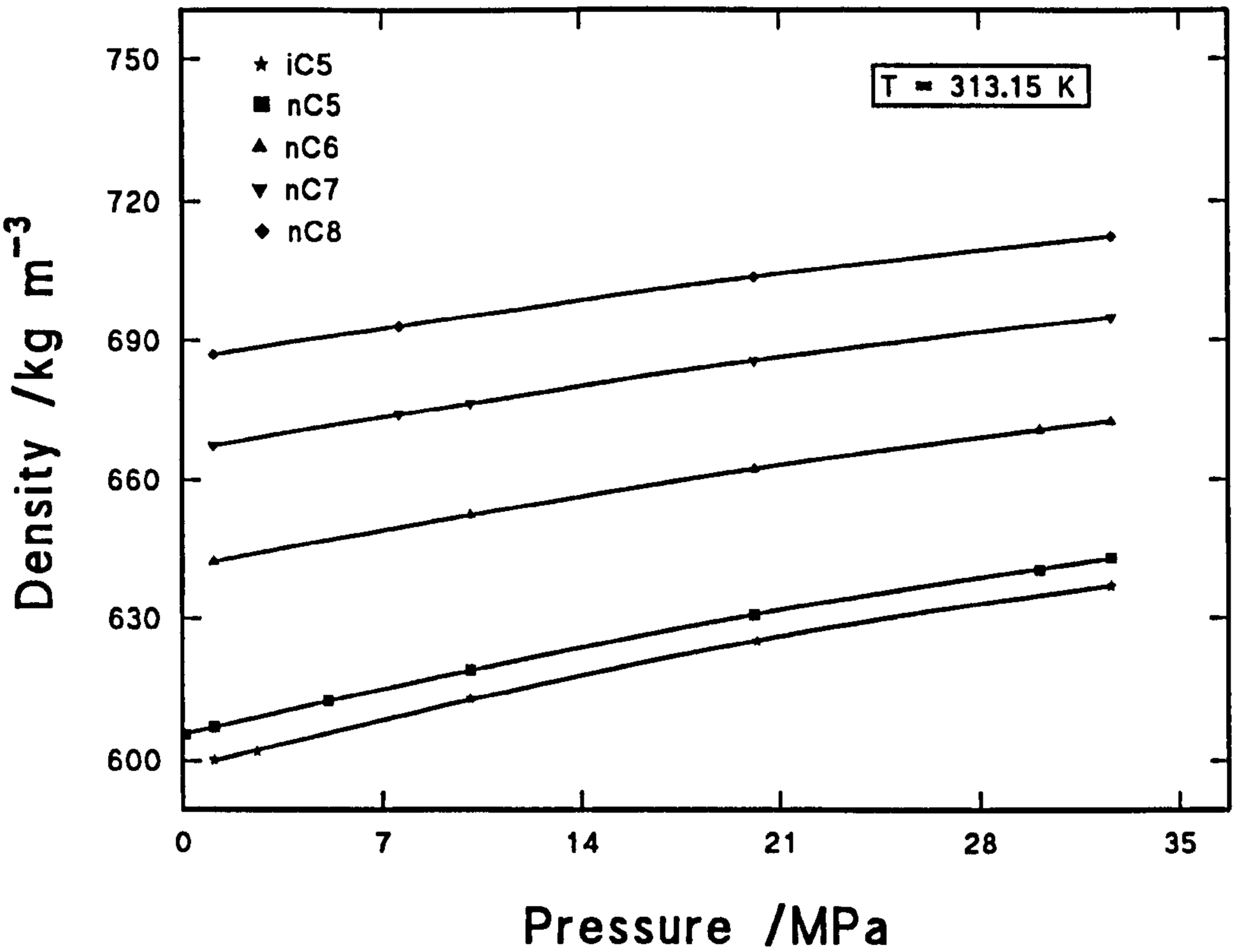

Figure 5.1. Measured phase densities of pure liquids as a function of pressure.

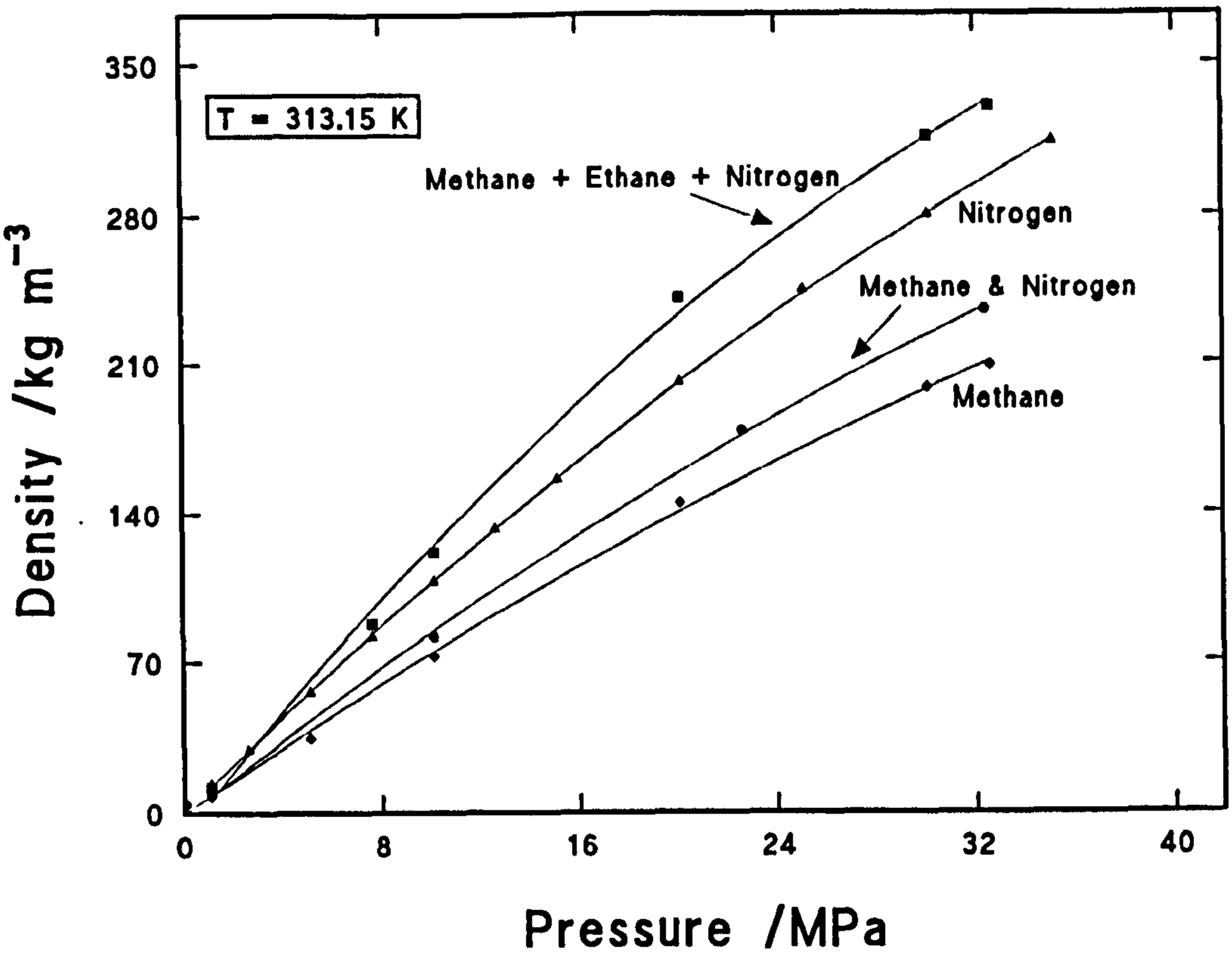

Figure 5.2. Measured gas phase densities as a function of pressure.

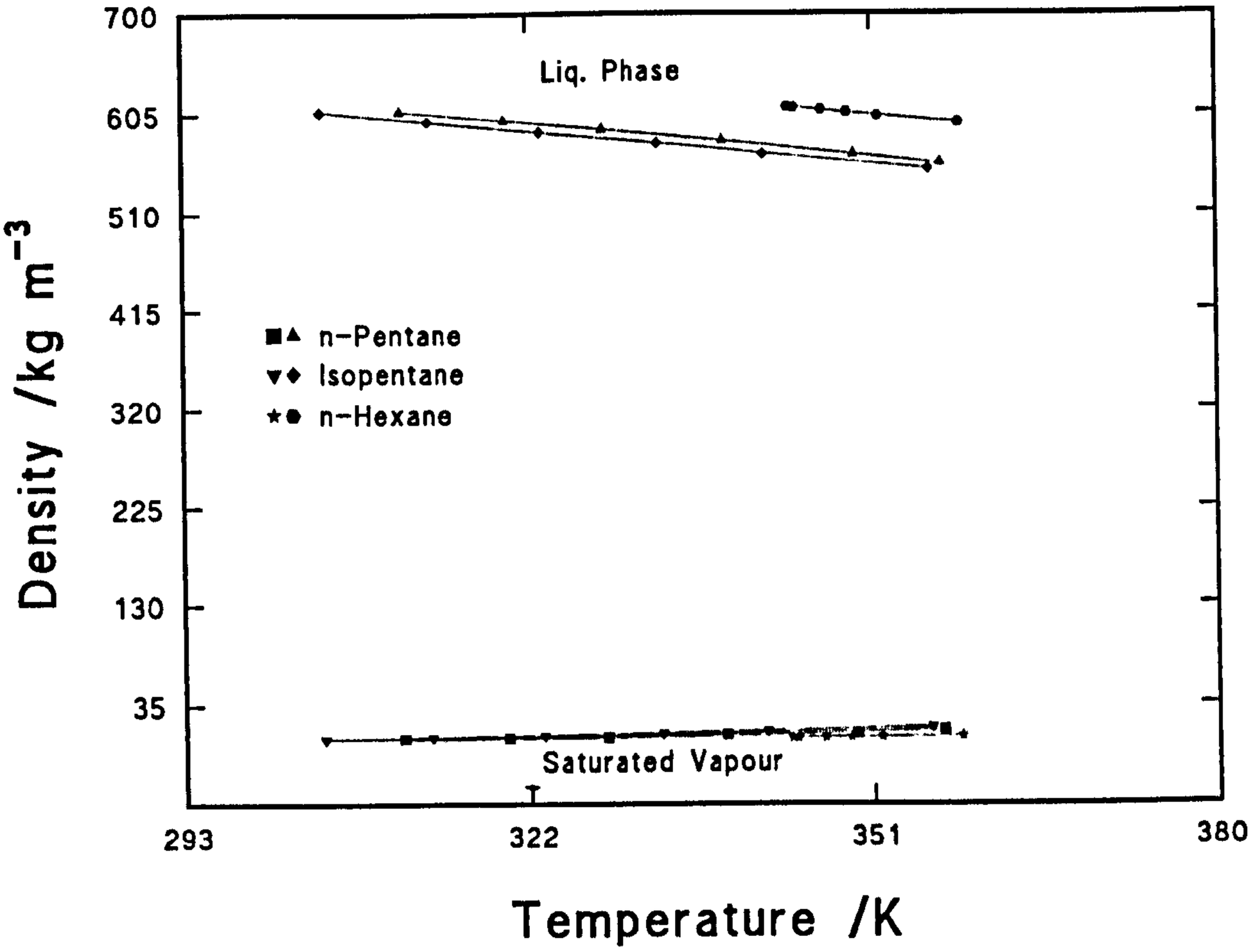

Figure 5.3. Measured phase densities for pure liquids as a function of temperature.

dependence of the density in the liquid and gas phases is approximately linear over the temperature interval 302 to 363 K, which is far from the critical temperature of each of these hydrocarbons (T_c for n-pentane is 469.69 K, for isopentane is 460.43 K and for n-hexane is 507.7 K). In the liquid phase the density decreases with increasing temperature in the order of decreasing carbon number, while in the vapour phase the density increases in the order of decreasing carbon number. The isomer, isopentane, has the lowest liquid phase density.

5.2.2 Density of Mixtures

In this work the effects of adding pure nitrogen gas, or nitrogen with light hydrocarbon gaseous mixtures, to hydrocarbon liquid mixtures were investigated. All the measurements were made as a function of pressure at a constant temperature of 313.15 K, except for the three individual pure liquid components (n-C_5H_{12}, i-C_5H_{12}, n-C_6H_{14}) for which the measurements were made at higher temperatures (chapter 4).

When nitrogen was introduced to a four component mixture of n-alkane (n-pentane+n-hexane+n-heptane+n-octane) the density of the liquid phase as a function of pressure at constant temperature showed a very small positive pressure dependence [Fig. 5.4]. For the system nitrogen-stocktank oil at the same temperature, the liquid phase density increased slightly with increasing pressure but far more than for the previous system [Fig. 5.4].

The effect of nitrogen addition to a three component mixture of a straight chain hydrocarbon, a naphthene and an aromatic compound (n-pentane+cyclohexane+toluene) showed a similar trend for the liquid phase density as that for the four n-alkanes system, but with higher values for the density. Adding an isomer, isopentane, in equal weights to a straight chain compound (n-pentane) lowered the liquid phase density as a function of nitrogen pressure, and thus the critical pressure is expected to be lower than for n-pentane alone [Fig. 5.4].

The gas phase density [Fig. 5.4] as a function of pressure increased rapidly in

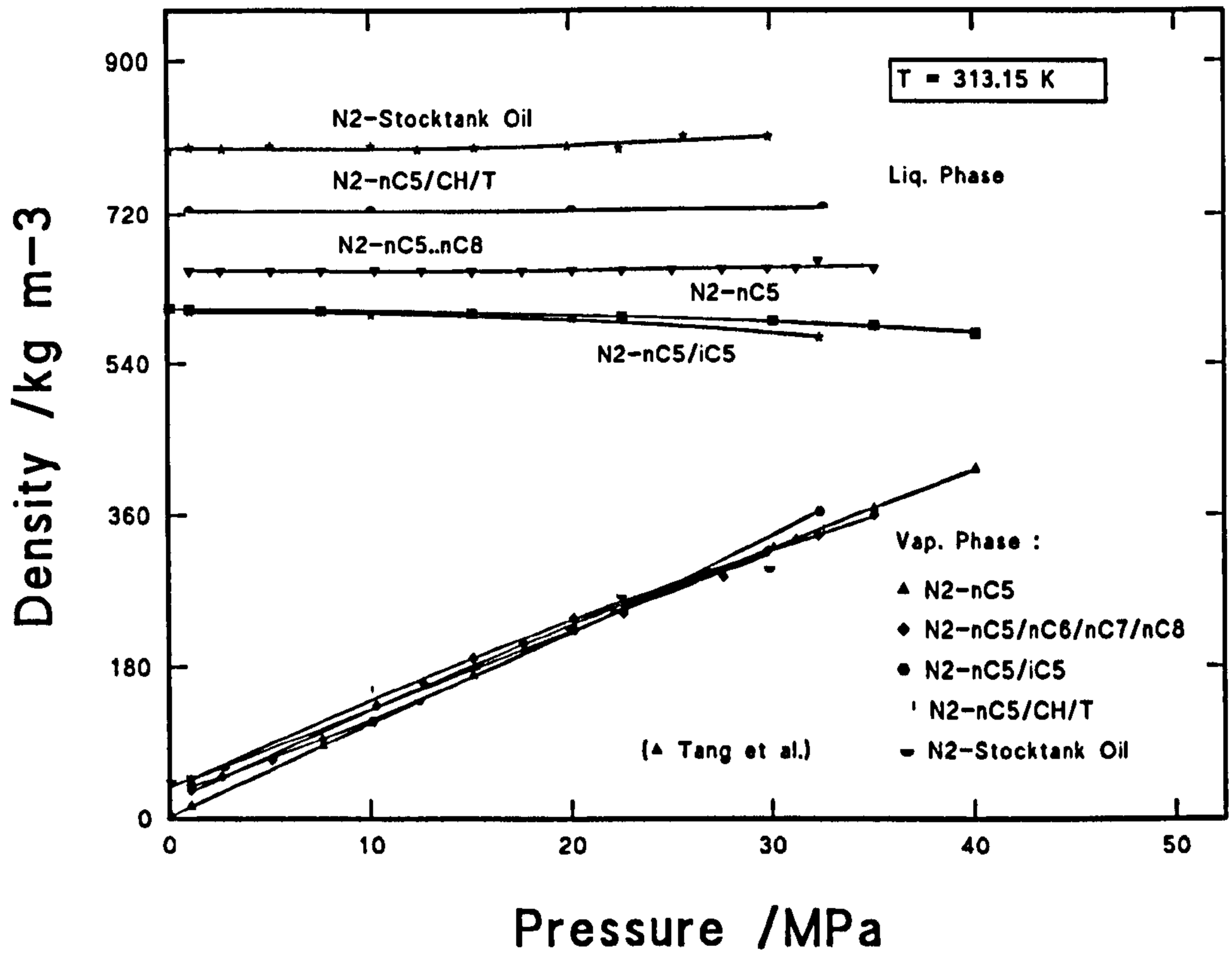

Figure 5.4. Measured phase densities for hydrocarbon systems with nitrogen addition as a function of pressure at 313.15 K.

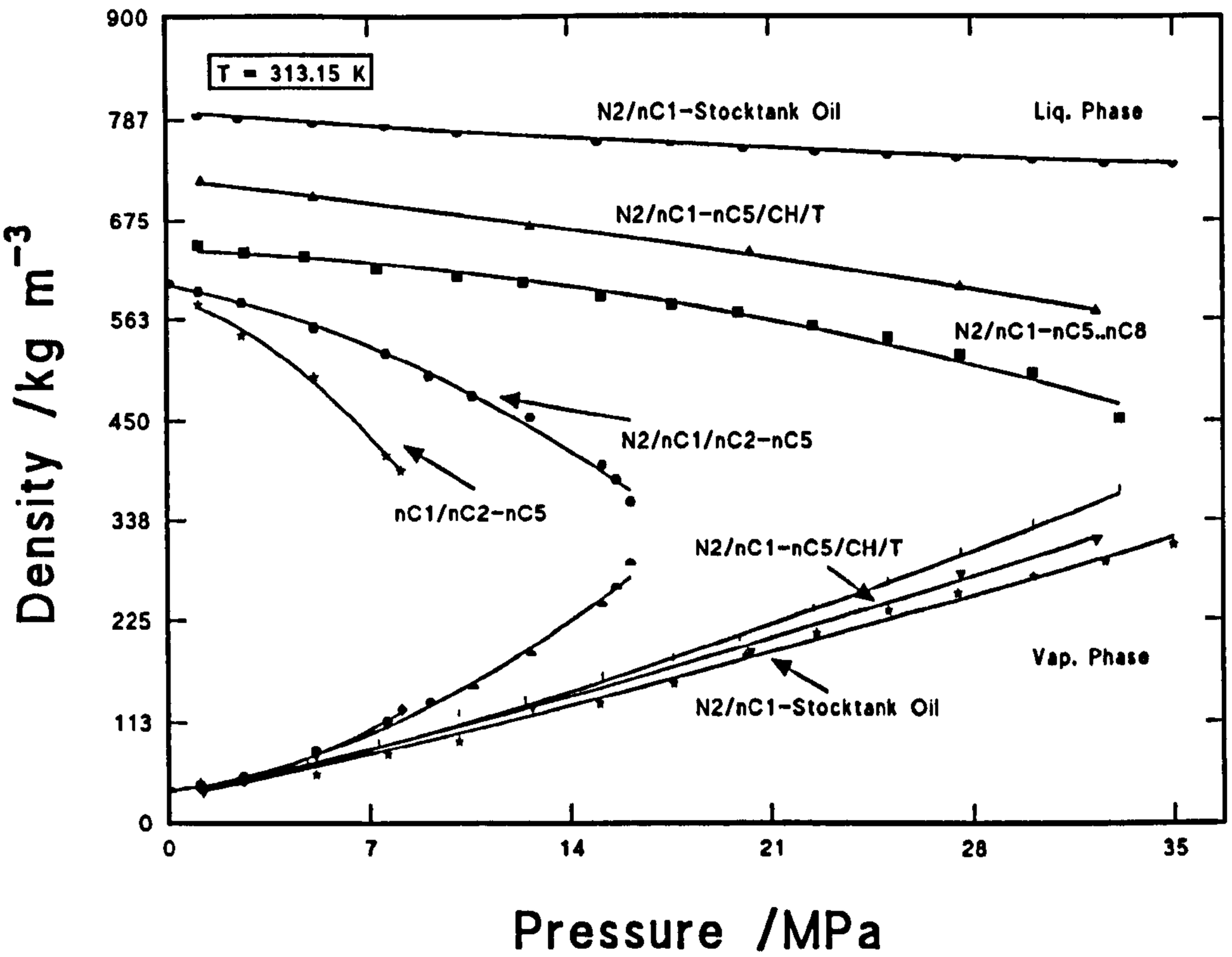

Figure 5.5. Measured phase densities for hydrocarbon systems with gaseous mixtures of nitrogen, methane and ethane as a function of pressure and constant temperature.

all cases in the order of decreasing carbon number. The addition of isopentane to n-pentane showed a small increase in the gas density. The rate of increase for the stocktank oil system is less than that for the (n-pentane+cyclohexane+toluene) system, and for this system it was even less than that for both the four n-alkanes and the n-pentane systems.

The effect of adding gaseous methane (or methane+ethane) at the same constant temperature and increasing pressure to all the mixtures studied, had a substantial influence on reducing the density of the liquid phase and increasing the density in the gas phase and thus on lowering the value of the critical pressure for the system [Fig. 5.5].

When a gaseous (methane/ethane/nitrogen) mixture was added to liquid n-pentane at elevated pressures, with methane/ethane/nitrogen in the ratio of 24/36/40 mol%, the density of the two phases converged more rapidly than for the previous system and the critical pressure decreased to ~17.6 MPa [Fig. 5.6]. When n-pentane was pressurised with methane/ethane in the ratio of ~40/60 mol%, the densities of the liquid and gas phases converged rapidly with a critical pressure ~8 MPa, compared to ~50 MPa when pressurising with pure N_2. Methane also has a similar effect on the binary liquid mixture of n-pentane and its isomer (isopentane) in converging the phase density values and lowering the critical pressure.

When the system composed of pure nitrogen gas and a quaternary liquid mixture of n-alkanes (n-pentane+n-hexane+n-heptane+n-octane) was examined it was found that although the phase densities were approaching each other the critical pressure for this system was substantially higher than 35.1 MPa [Fig. 5.7]. The addition of methane into this system, i.e. CH_4/N_2-$nC_5/nC_6/nC_7/nC_8$, with a methane/nitrogen ratio of ~70/30 mol%, reduced the liquid phase density due to the change in its composition and simultaneously increased the gas phase density. The critical pressure for this system is estimated to be approximately 34 MPa. However, the addition of pure methane gas into this quaternary liquid n-alkane mixture resulted in a critical pressure value of about 23 MPa.

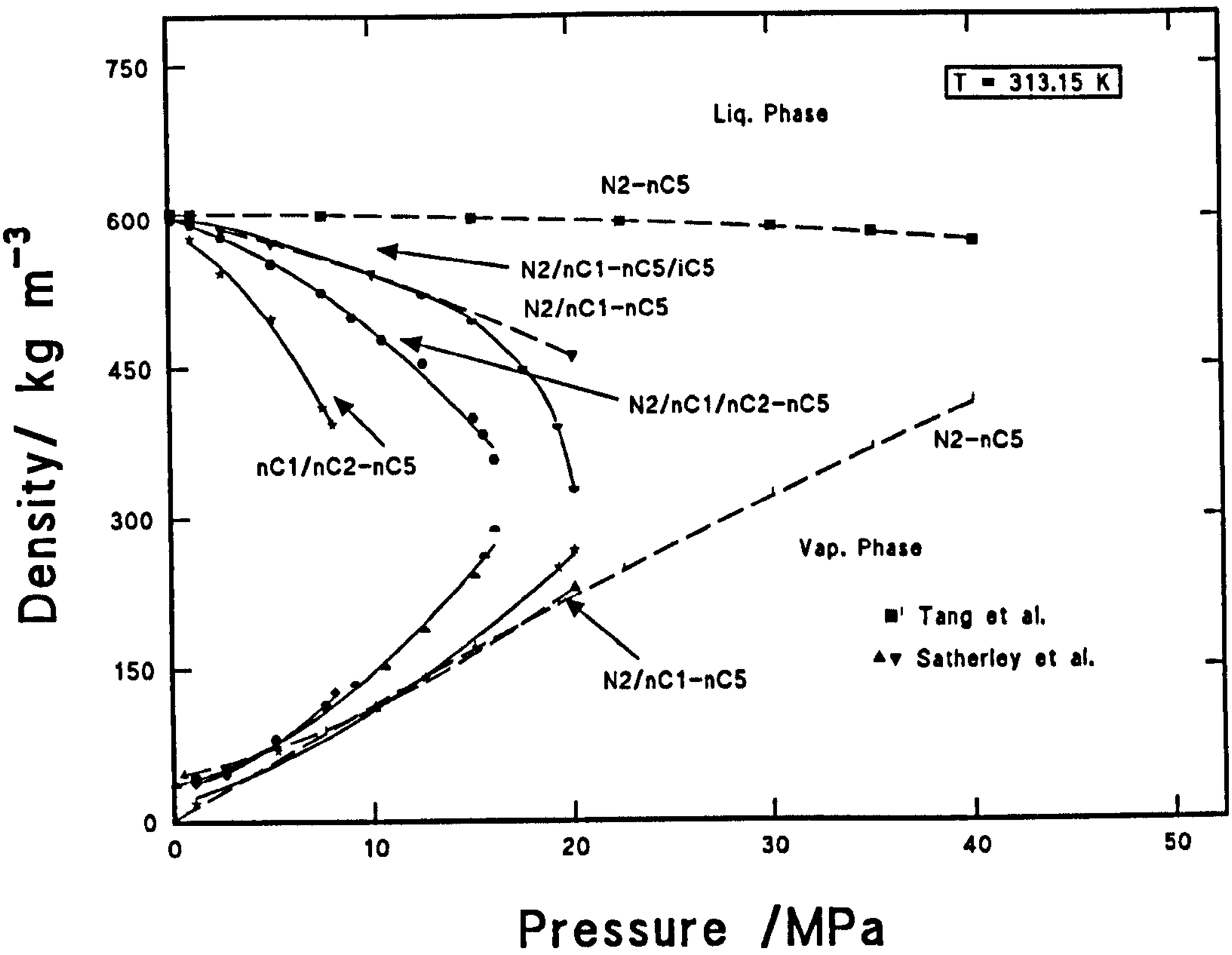

Figure 5.6. Measured phase densities for gaseous mixtures with n-pentane and n-pentane/isopentane with pressure rise.

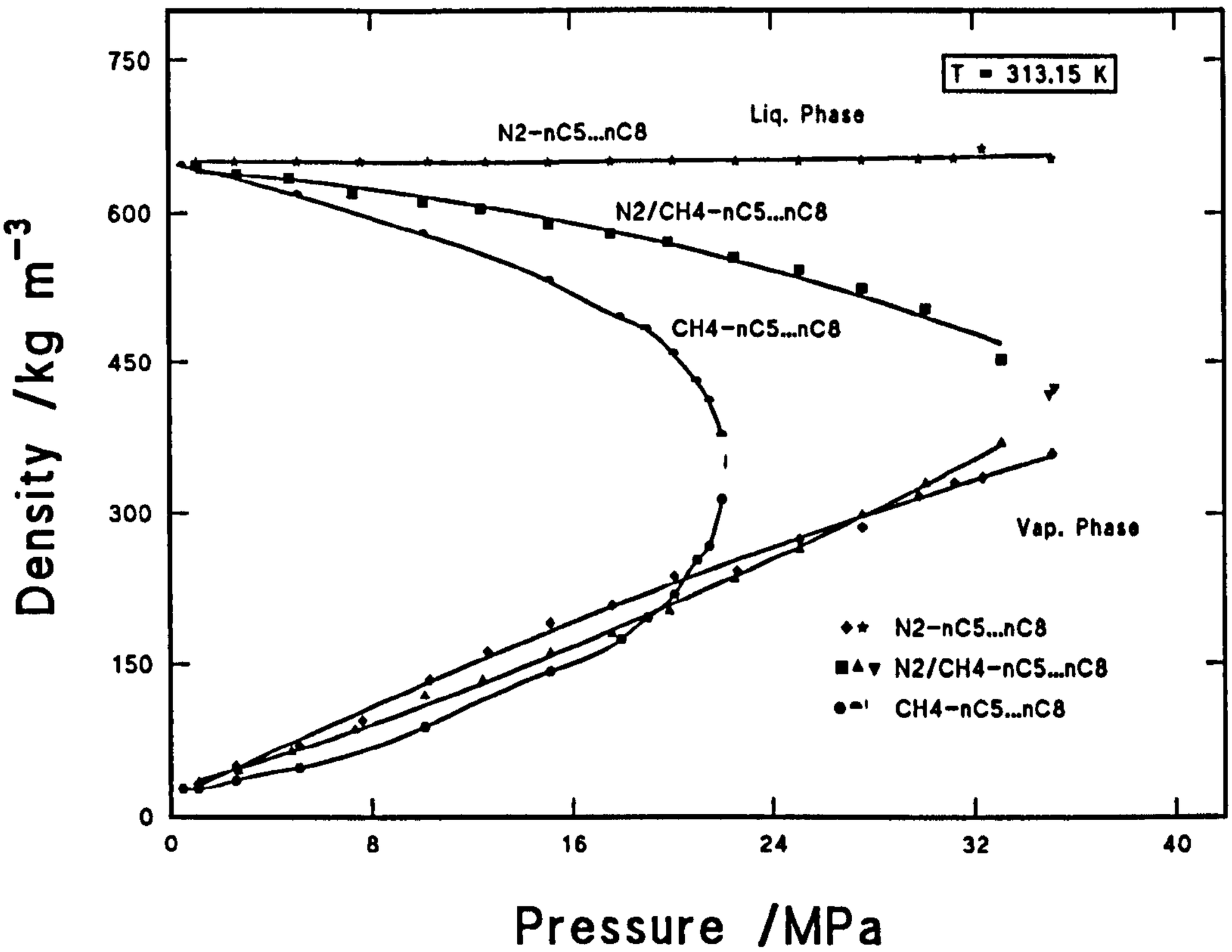

Figure 5.7. Measured phase densities for gaseous mixtures with the quaternary liquid mixture with pressure rise.

The phase density behaviour for the nitrogen/methane (gas mixture ratio of 30/70 mol%) system in the ternary liquid mixture of n-pentane+cyclohexane+toluene is shown in Fig. 5.8 at elevated pressures and constant temperature. The addition of a methane gas component into this system has a significant influence on shifting the liquid phase density to much lower values [Fig. 5.8]. The liquid phase pressure dependence of density for this ternary liquid system pressurised with pure nitrogen but with different cyclohexane/toluene ratios, is almost linear and the density values increase slightly at higher pressures. For these different ratio systems, the density values are highest for the mixture with the highest percentage of toluene, and lowest for the system which has the highest percentage of cyclohexane. The vapour phase pressure dependence of density for these systems increases rapidly and the values differ very slightly for the three ratio systems over the examined pressure range.

The measured density values for the stocktank oil decreased as a function of increasing pressure with the addition of methane/nitrogen gas into the oil mixture but its behaviour was still far from critical region [Fig. 5.5].

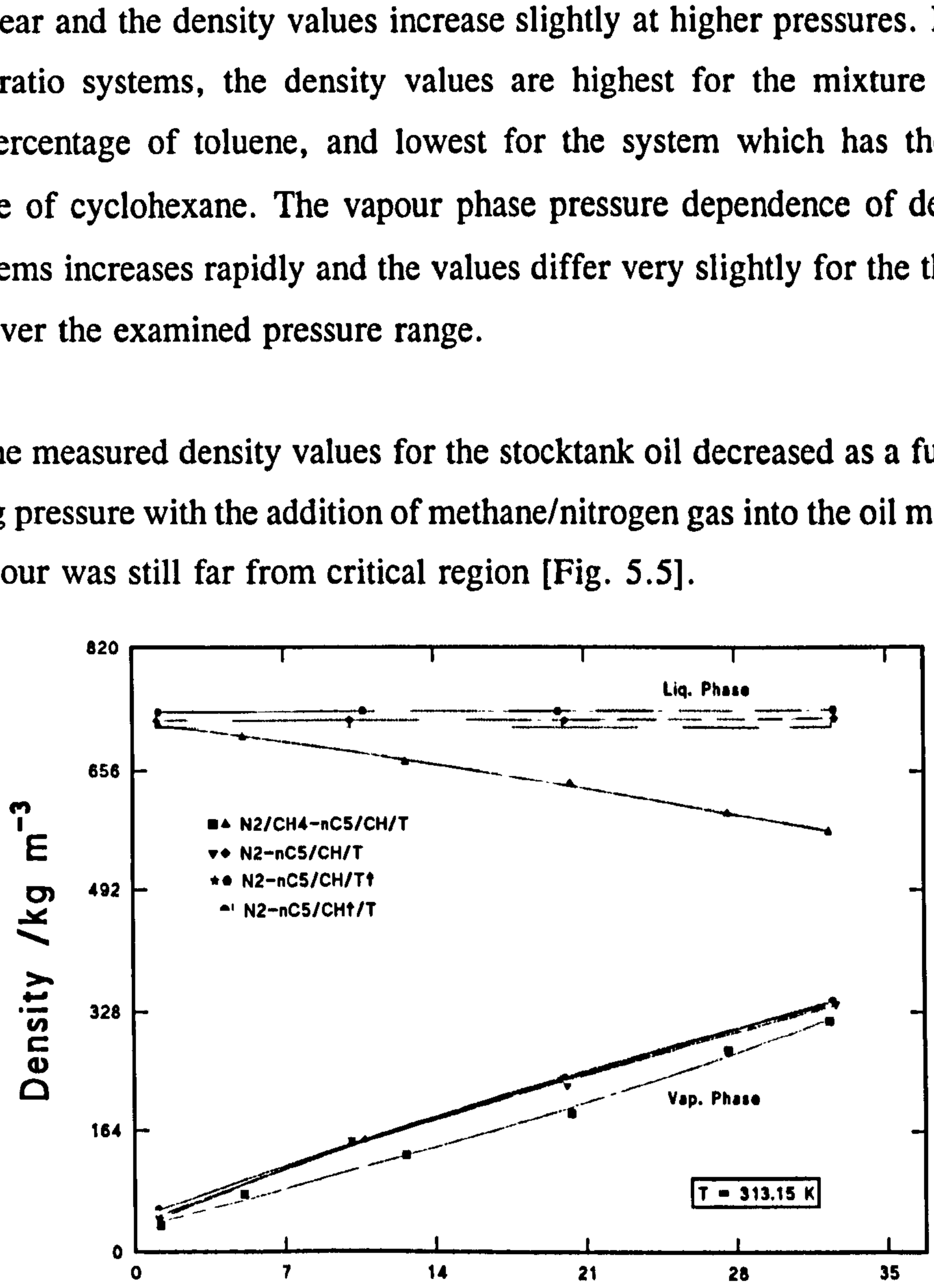

Figure 5.8. Measured phase densities of the ternary liquid mixture with nitrogen and methane addition as a function of pressure.

5.2 Composition Measurements

The measured compositions as a function of pressure and at a constant temperature of 313.15 K [Tables 10 to 14] are plotted as pseudo binaries for the bubble point and dew point curves, as shown in Figs. 5.9 and 5.10. The solubility of nitrogen in the liquid and gas phases is non-linear for all the mixtures examined. It is highest for the lowest carbon chain component and lowest for the n-alkane+aromatic+naphthene liquid phase mixture [Fig. 5.9]. Generally, the rate of increase of the solubility of nitrogen gas in the liquid phase is faster than the rate of hydrocarbon solubility in the gas phase as a function of pressure. In the gas phase, the solubility of the liquid binary mixture (nC5/iC5) increases more than the rest of the liquid mixtures with pressure. In this phase, for this binary mixture, the composition of nitrogen at low pressures increases slightly, then starts to decrease at higher pressures and converges with the liquid phase at the critical point. Although, initially, in the gas phase the solubility values are lower for the mixture $nC_5+nC_6+nC_7+nC_8$ than that for the n-pentane+cyclohexane+toluene mixture, they are almost constant and similar over the examined pressures.

By considering N_2/CH_4, $N_2/CH_4/C_2H_4$ and CH_4/C_2H_4 as one pseudo-component in the liquid and gas phases for the systems studied, the bubble point and dew point curves were plotted as shown in Figs. 5.10 and 5.11. The effect of methane addition in all the systems significantly reduced the critical pressure. Methane was much more soluble in the hydrocarbons than nitrogen. The addition of pure methane into the quaternary mixture $nC_5+nC_6+nC_7+nC_8$ reduced the critical pressure from ~34 MPa to ~23 MPa [Fig. 5.10]. When light hydrocarbons binary gas mixtures of methane and ethane (ratio 40/60 mol%) were added to pure n-pentane, the solubility of the pseudo solute in the two phases converged most rapidly with a critical pressure of ~8 MPa.

The effect of changing the ratios of cyclohexane, toluene and n-pentane in their ternary liquid mixture, on the solubility of nitrogen is shown in Fig. 5.12. Up

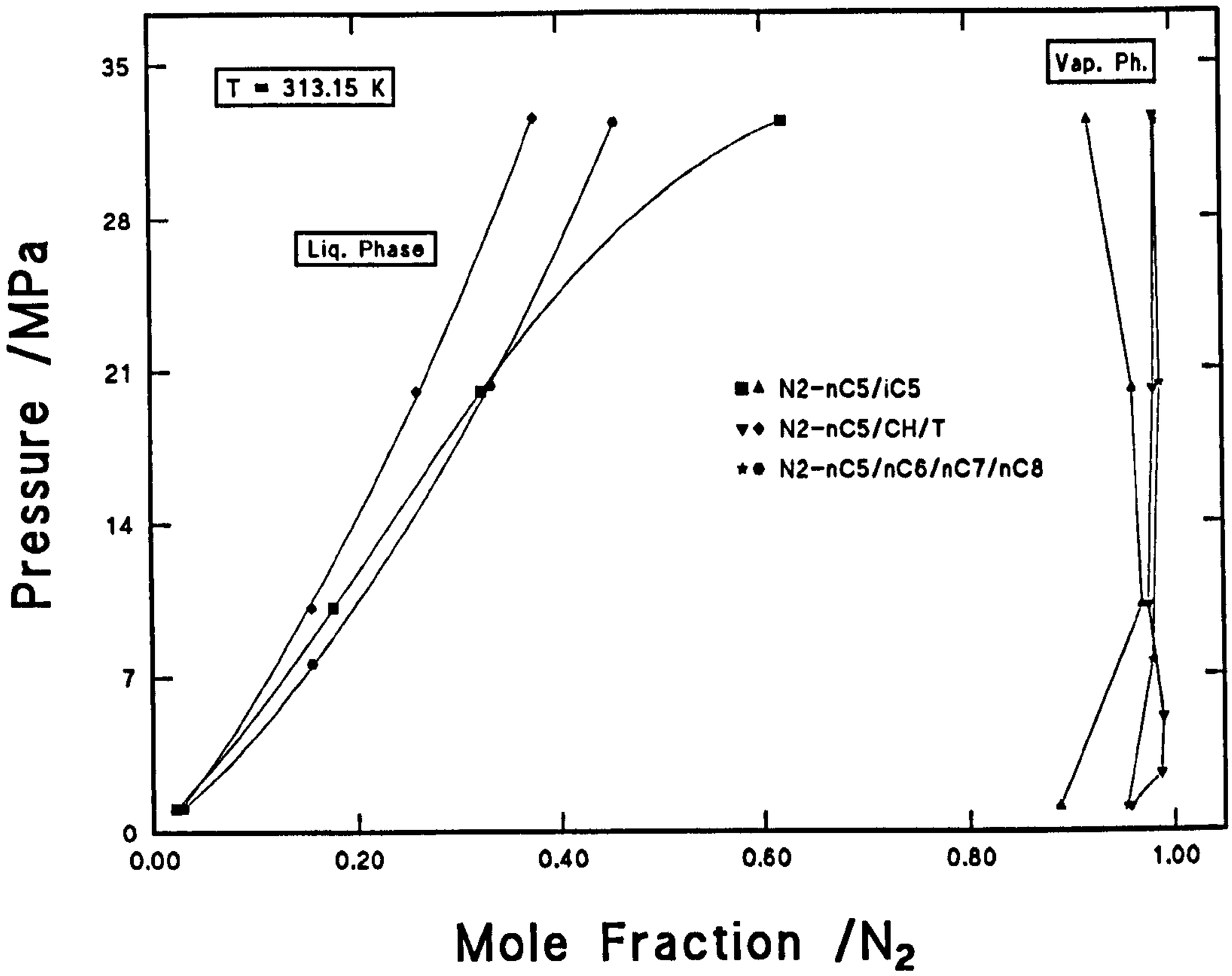

Figure 5.9. Nitrogen phase compositions in the measured systems as a function of pressure at 313.15 K.

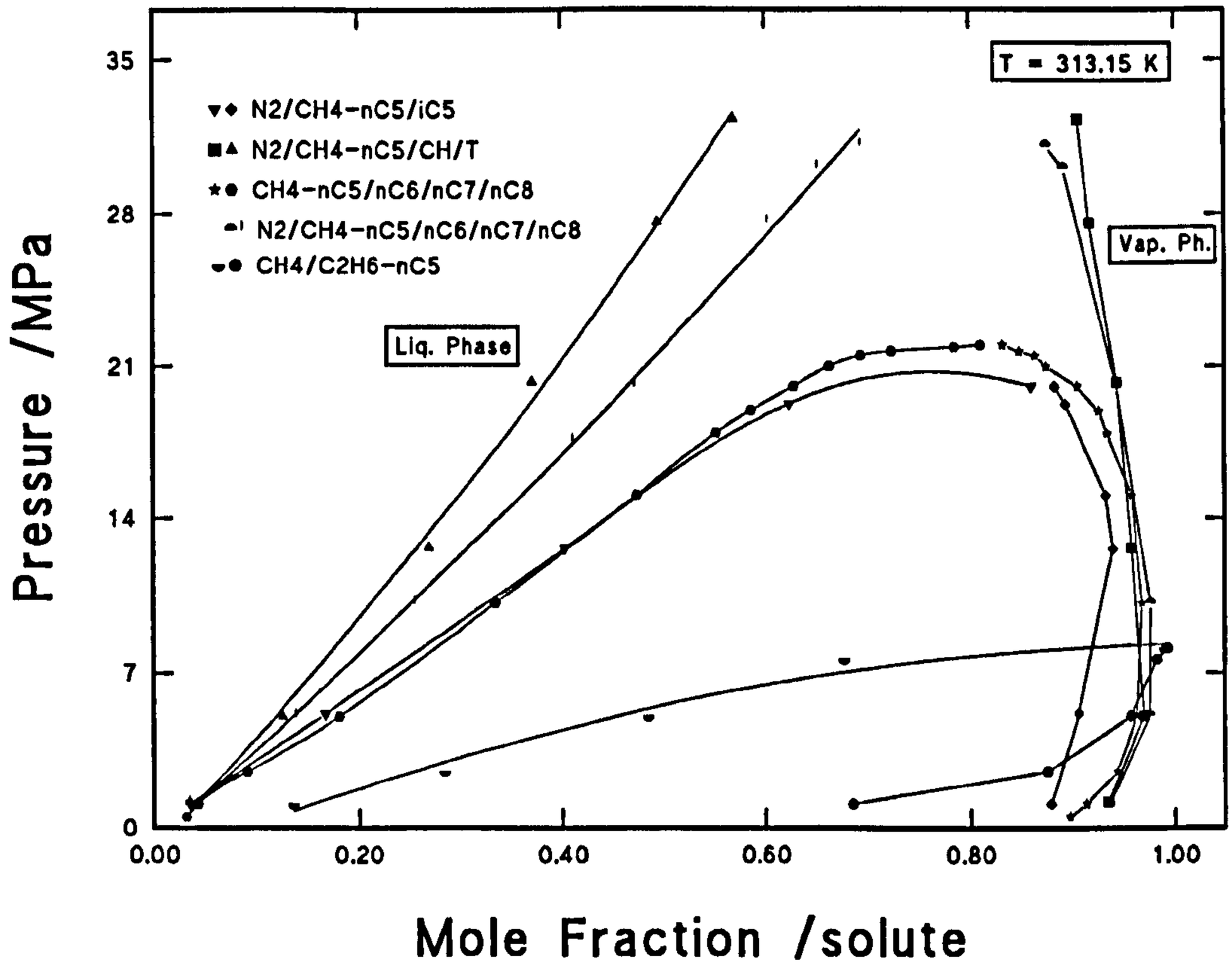

Figure 5.10. Solute and pseudo-solute phase compositions in the measured systems as a function of pressure at 313.15 K.

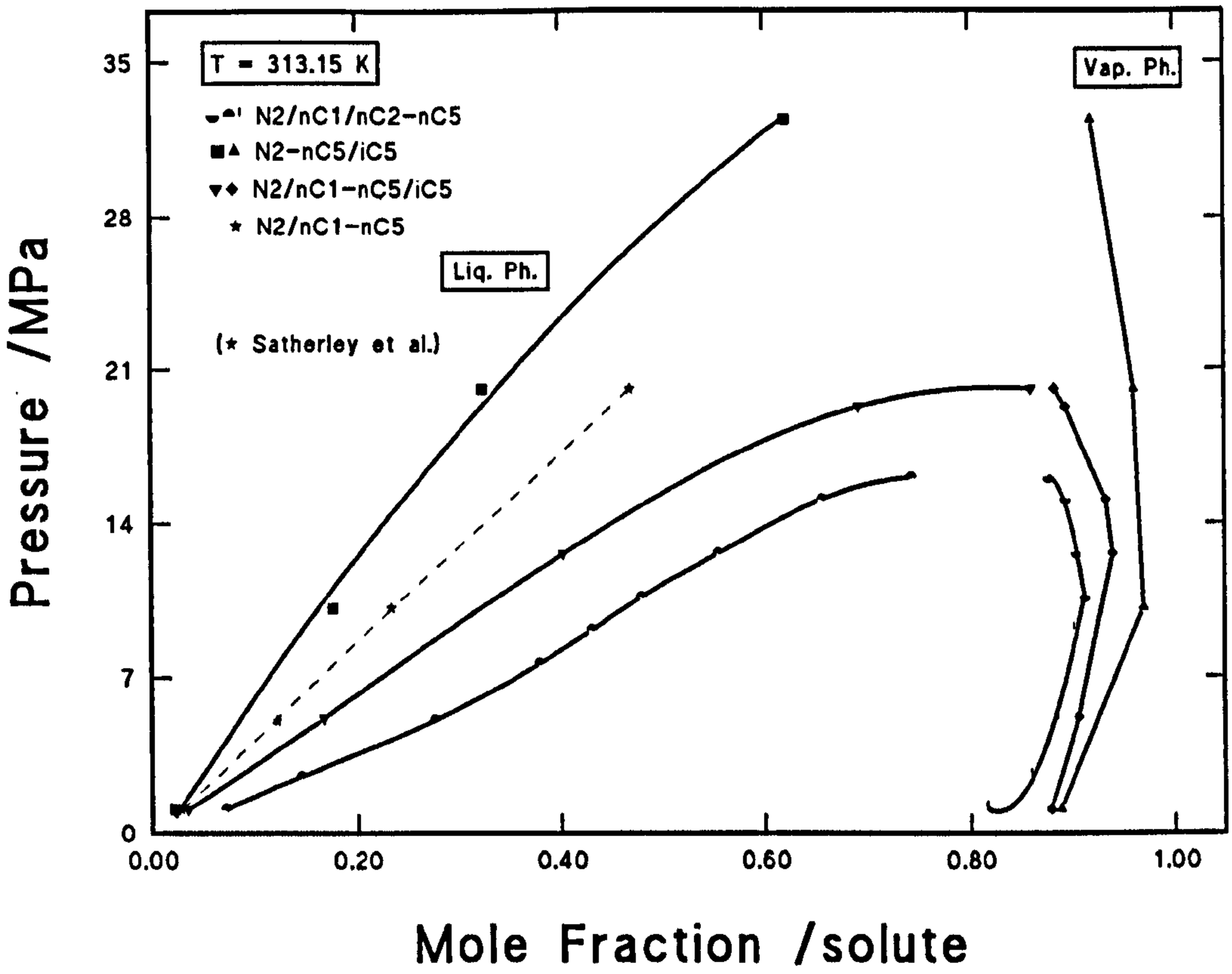

Figure 5.11. Solute and pseudo-solute phase compositions in n-pentane and isopentane as a function of pressure at 313.15 K. Dotted line represents values measured by Satherley et al.

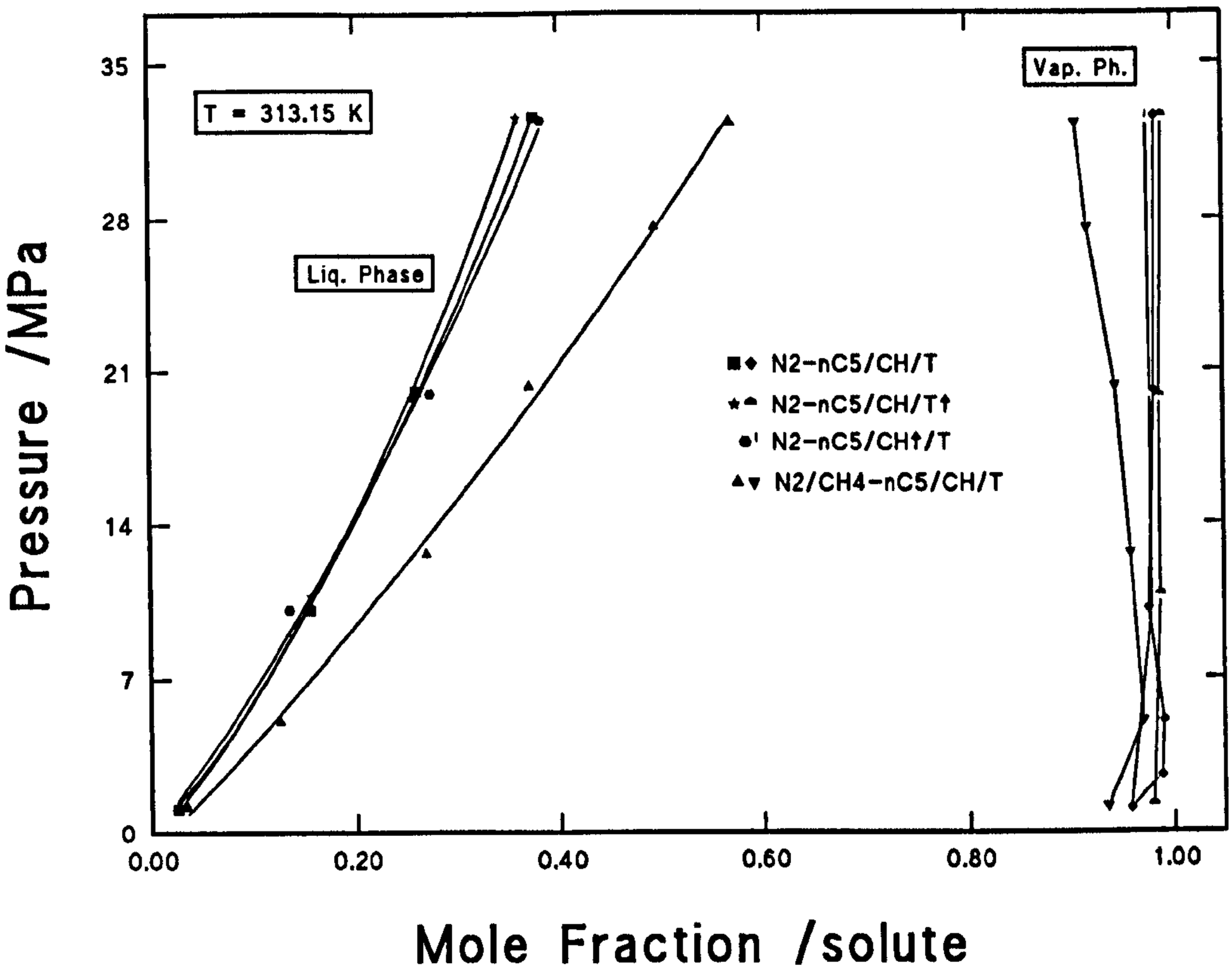

Figure 5.12. Solute and pseudo-solute phase compositions in the ternary liquid mixture as a function of pressure at 313.15 K.

to a pressure of ~16 MPa the three different ratio mixtures were fairly similar and then the solubility increased in the mixture with the higher toluene content and decreased in the mixture with the most cyclohexane [Fig. 5.12]. The solubility in the isopentane+n-pentane mixture in equal weight ratio converged more rapidly for both phases than for pure n-pentane. However, the solubility of methane+nitrogen in this binary mixture and n-pentane is higher than the solubility of pure nitrogen in these systems [Fig. 5.11].

5.3 Interfacial Tension Measurements

The addition of nitrogen, nitrogen+methane, nitrogen+methane+ethane, methane and ethane showed generally a trend of decreasing IFT with increasing gases pressure and with decreasing carbon number at constant temperature [Fig. 5.13]. However, the addition of methane and/or ethane with nitrogen to the liquid mixtures [Fig. 5.14] showed more rapid decline in the IFT as a function of increasing pressure at constant temperature. The plots show a non-linear pressure dependence of the IFT. In the systems examined, nitrogen+stocktank oil gave the highest IFT values and methane/ethane+n-pentane gave the lowest values.

The addition of methane/ethane gas mixture (40/60 mol%) into n-pentane reduced the IFT values by an average of ~2 mNm^{-1} and lowered the critical pressure by half its value (from ~16 MPa down to ~8 MPa) compared with the $N_2/CH_4/C_2H_4$ gas mixture addition to the same pure liquid. Pressurising the liquid mixture of ($nC_5+nC_6+nC_7+nC_8$) with pure methane at elevated pressures [Fig. 5.15] showed a rapid decrease in the IFT values, approaching ultralow values near the critical point at ~23 MPa, compared (at the same pressure, 23 MPa) with a value of IFT of ~2 mNm^{-1} using N_2/CH_4 gas and a value of ~6.4 mNm^{-1} using pure N_2 as a component. For this system it was possible to measure a value of IFT as low as 0.0035 mNm^{-1} at 22.2 MPa (± 0.05 MPa) and 313.15 K. Comparatively, for the system N_2/CH_4-($nC_5+nC_6+nC_7+nC_8$) a measured IFT value of 0.0042 mNm^{-1} was obtained at a pressure of 32.3 MPa, just less than the critical pressure of ~34 MPa.

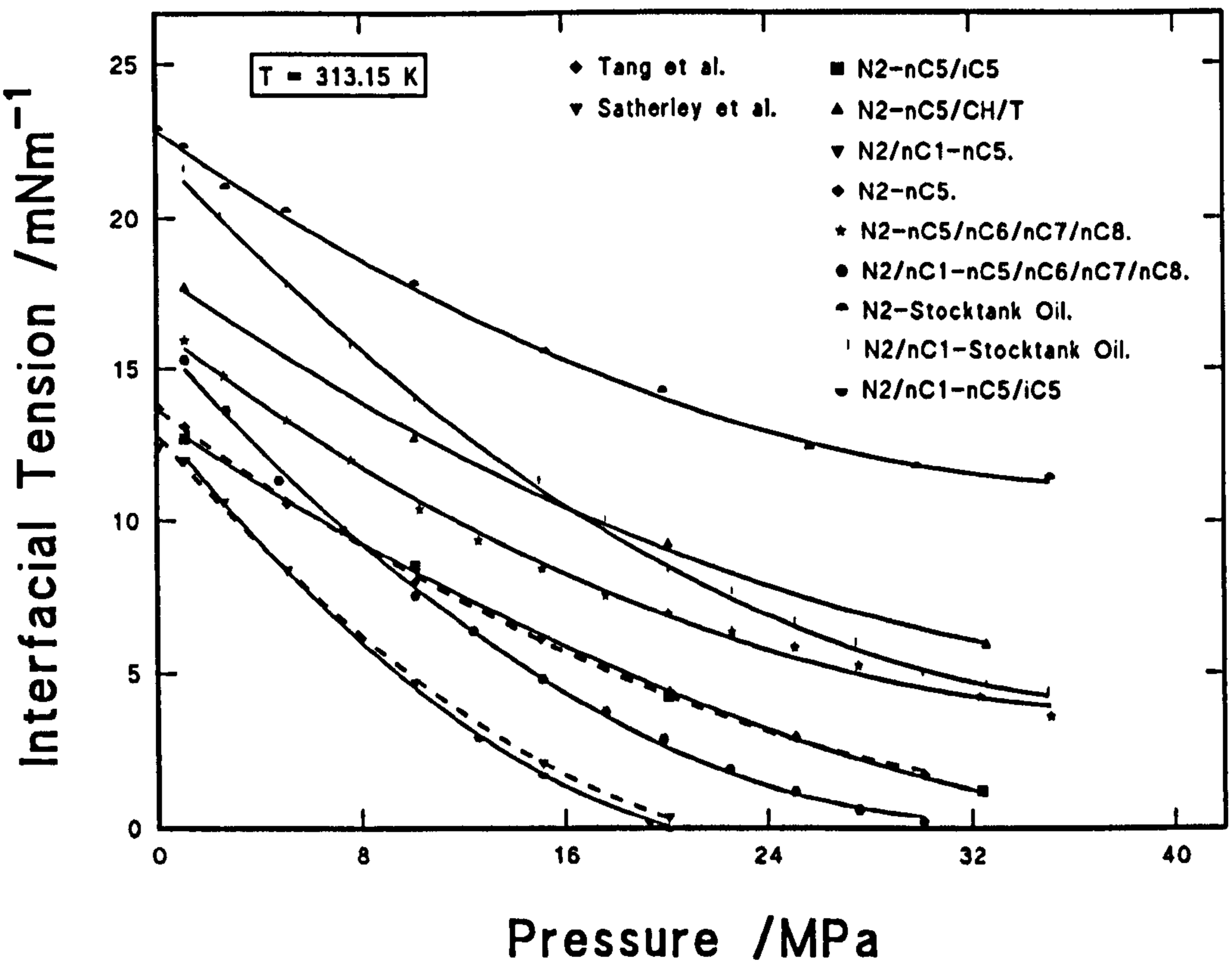

Figure 5.13. Measured IFT for hydrocarbon systems with nitrogen and methane addition as a function of pressure and constant temperature. Dotted lines represent values measured by Satherley et al. and Tang et al.

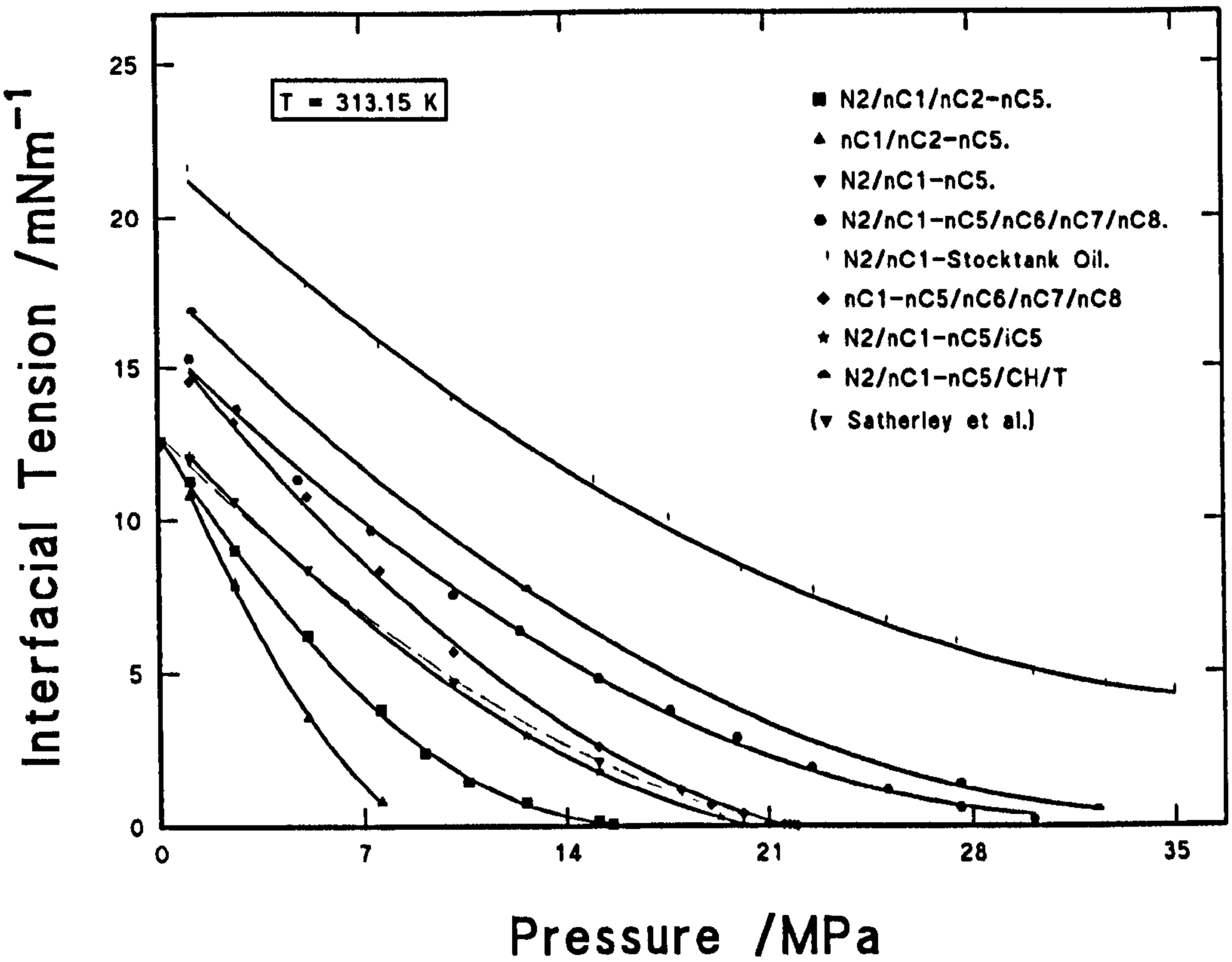

Figure 5.14. Measured IFT for hydrocarbon systems with nitrogen, methane and ethane addition as a function of pressure and constant temperature. Dotted line represents values measured by Satherley et al.

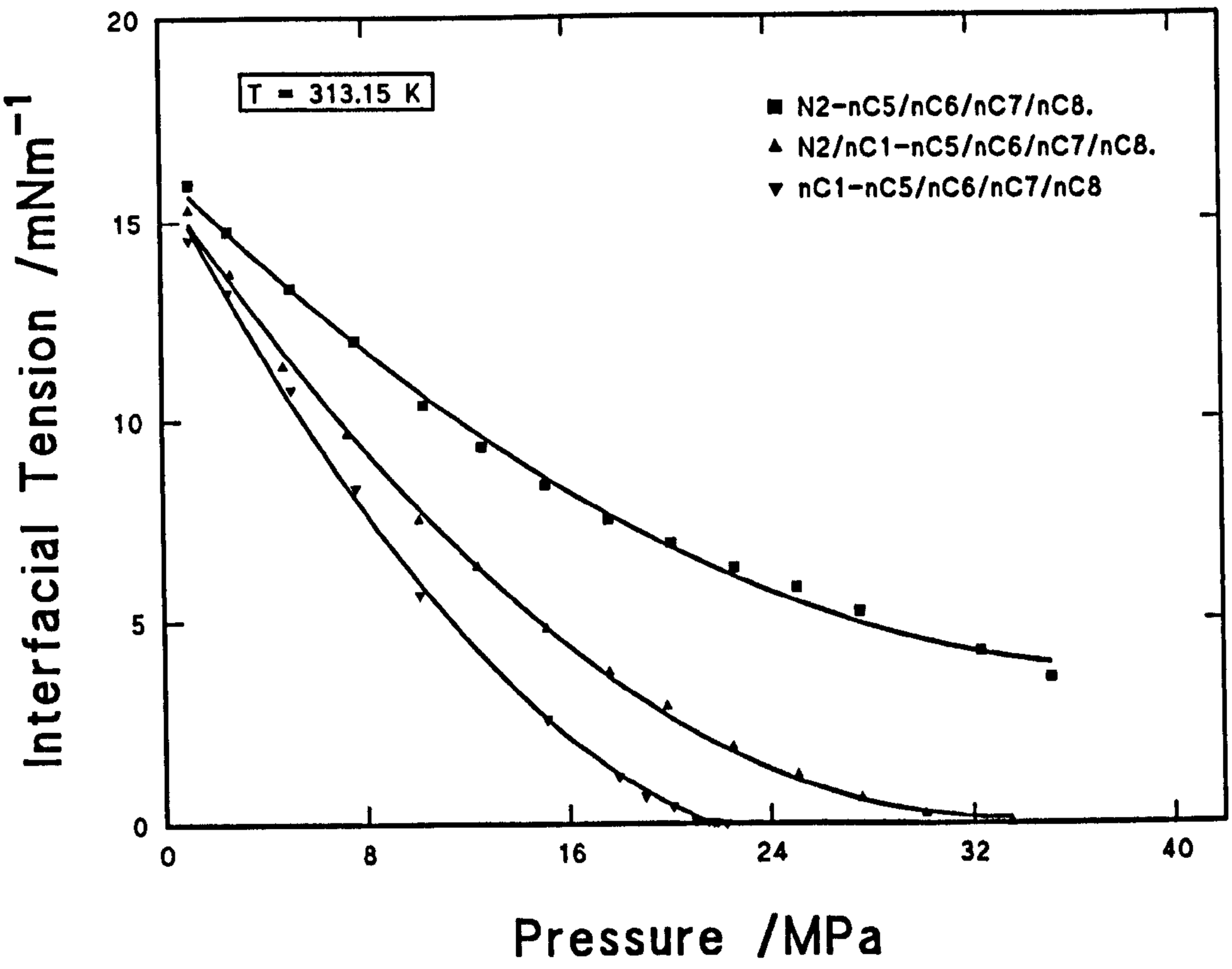

Figure 5.15. Measured IFT for the quaternary liquid mixture with nitrogen and methane addition as a function of pressure and constant temperature.

For the stocktank oil, although it was from a relatively light condensate, only a relatively small reduction in the IFT was observed with nitrogen addition. However, the addition of nitrogen/methane to the oil mixture resulted in a substantial reduction in the IFT, far more than that observed for the model fluids examined [Fig. 5.13].

The effect of the different ratios of n-pentane/cyclohexane/toluene mixtures on IFT is shown in Fig. 5.16. The IFT values are highest for the system which has the highest percentage of toluene and lowest for the system which has highest percentage of cyclohexane. The addition of N_2/CH_4 into the original ratio mixture of n-pentane/cyclohexane/toluene decreased the IFT substantially with increasing pressure but still less than that for the stocktank oil [Fig. 5.17]. The IFT values for the system N_2+n-pentane and isopentane are almost similar to the values for N_2+pure n-pentane [Fig. 5.18]. The addition of N_2/CH_4 into the binary (n-pentane/isopentane) reduces the IFT trend significantly but the values are lower than those for the same gas mixture in contact with pure n-pentane.

Fig. 5.19 shows the effect of the type of solute addition and its composition on the IFT for all the systems studied. The IFT decreases as a function of solute composition. The IFT values generally decrease with alkane carbon number.

The measured values of the surface tension as a function of temperature for the three pure liquids, n-pentane, isopentane and n-hexane are shown in Fig. 5.20. The relation of surface tension with temperature is linear over the temperature range examined (up to ~363 K). The temperature dependence of the surface tension is linear and negative. $d\gamma/dT$ is almost constant for the three liquids: -0.1071, -0.0966, -0.1005 $mNm^{-1}K^{-1}$ for iC_5, nC_5 and nC_6 respectively. The ST values are lowest for isopentane and highest for n-hexane.

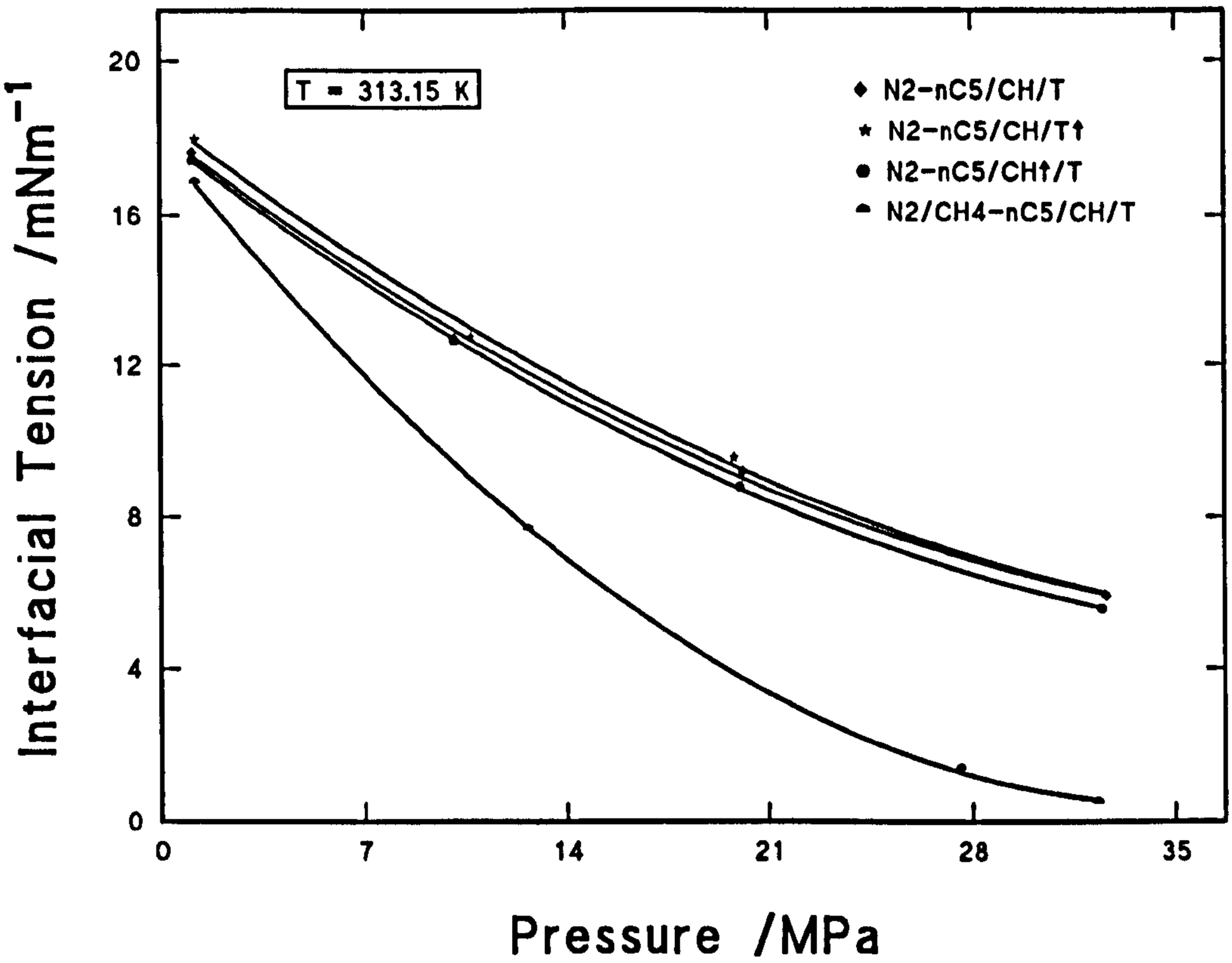

Figure 5.16. Measured IFT for the ternary liquid mixture with nitrogen and methane addition as a function of pressure and constant temperature.

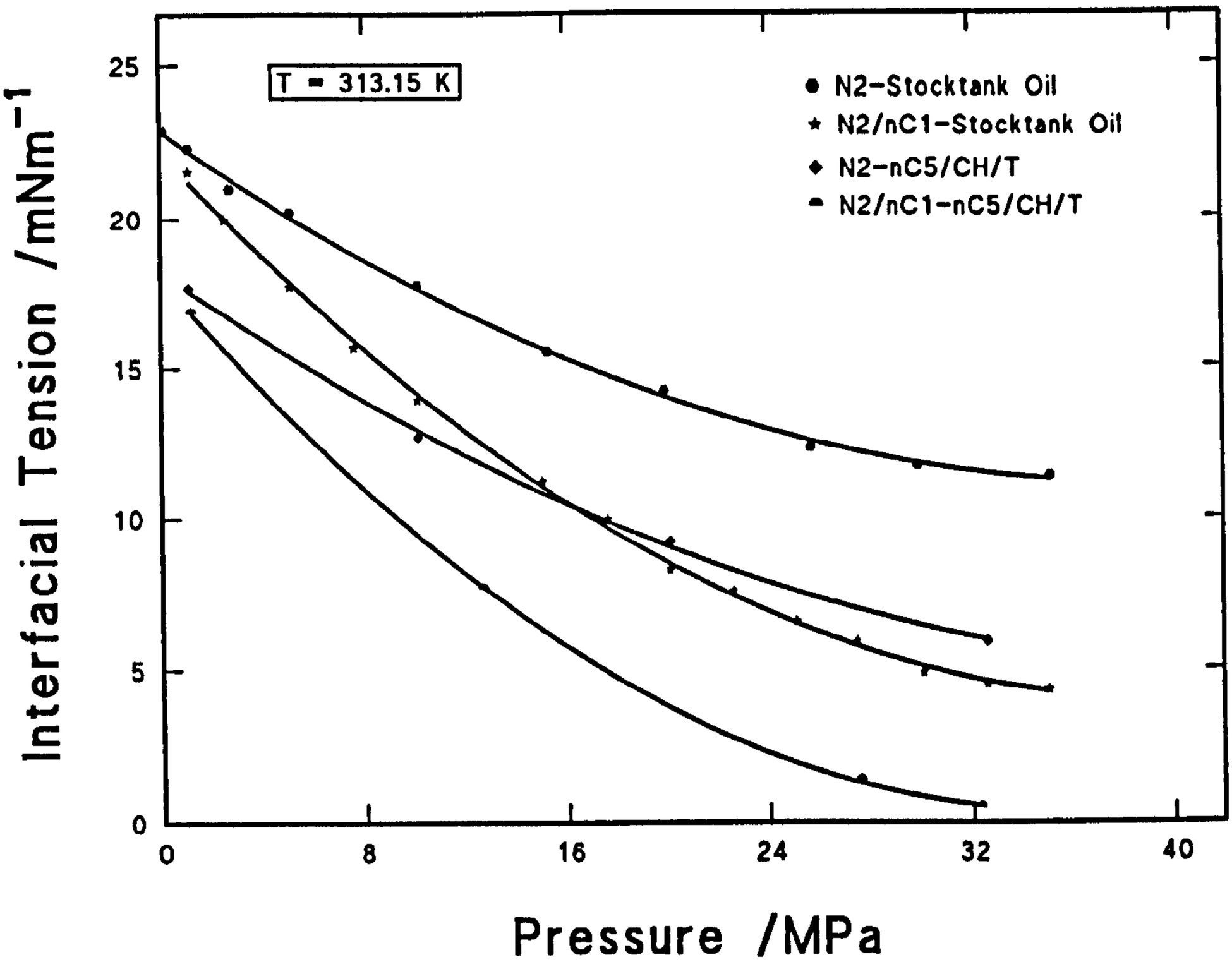

Figure 5.17. Measured IFT for the ternary liquid mixture and stocktank oil with nitrogen and methane addition as a function of pressure and constant temperature.

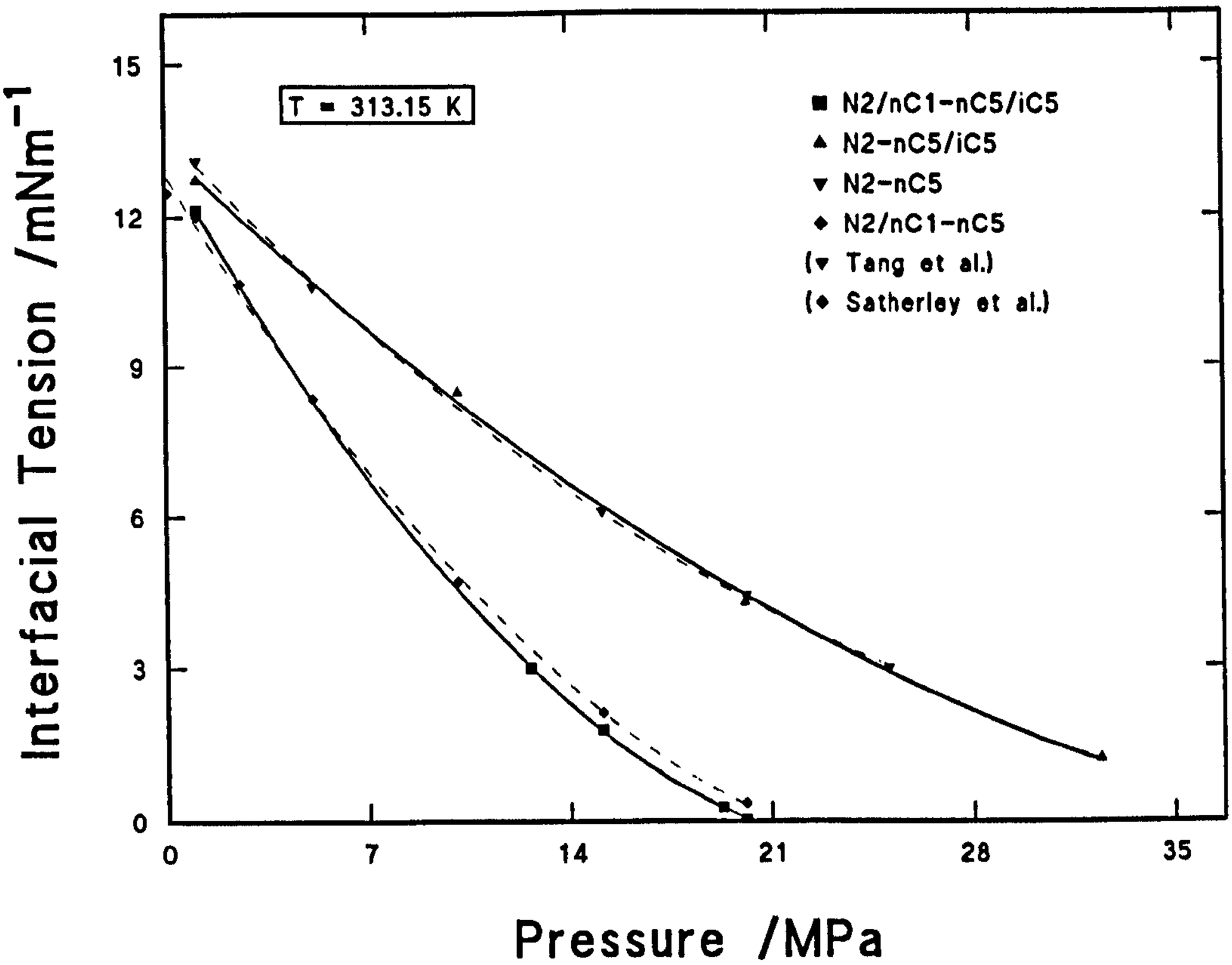

Figure 5.18. Measured IFT for n-pentane/isopentane with nitrogen and methane addition as a function of pressure and constant temperature. Dotted lines represent values measured by Satherley et al. and Tang et al.

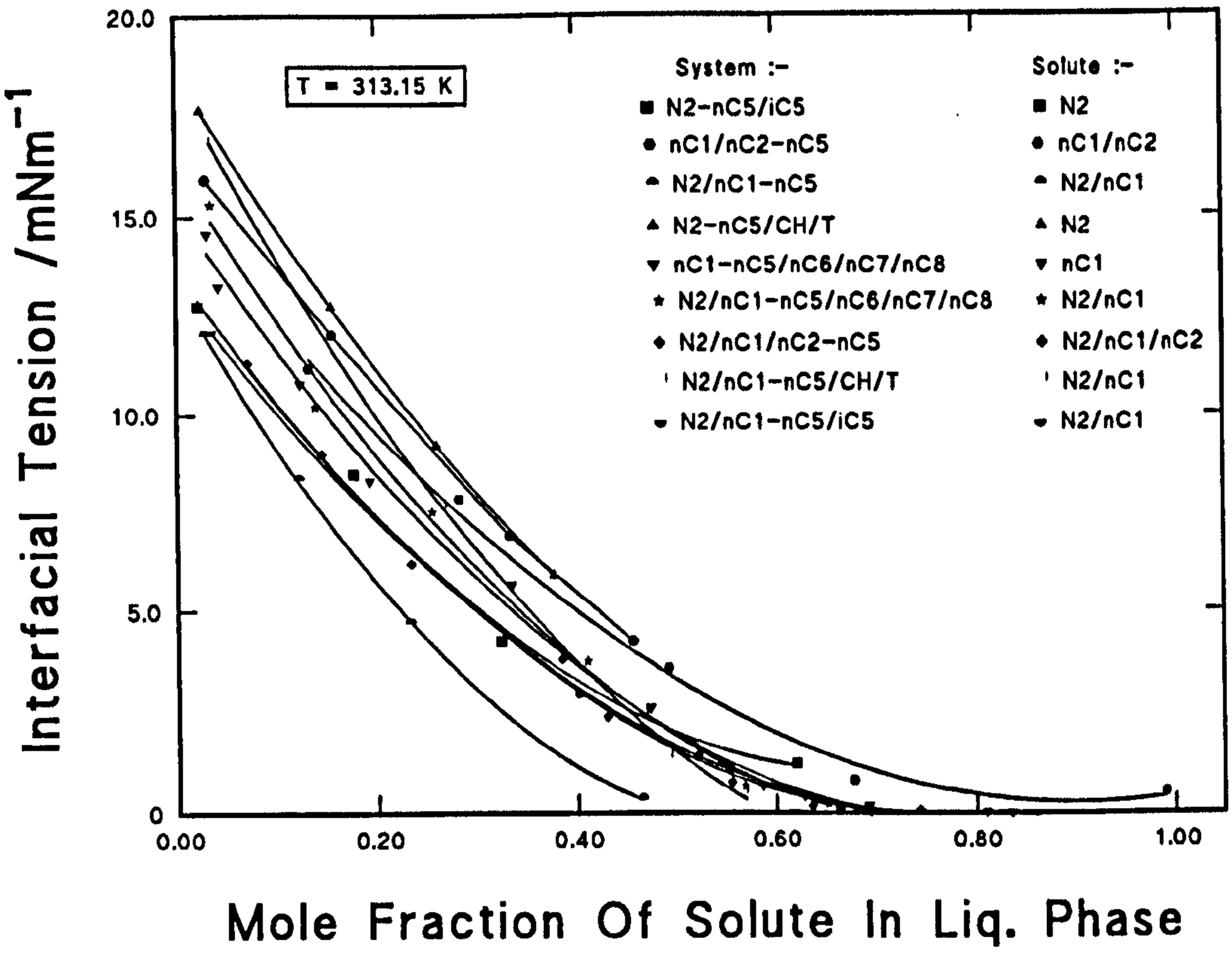

Figure 5.19. Experimental IFT values versus liquid phase compositions of solute and pseudo-solute for hydrocarbon systems.

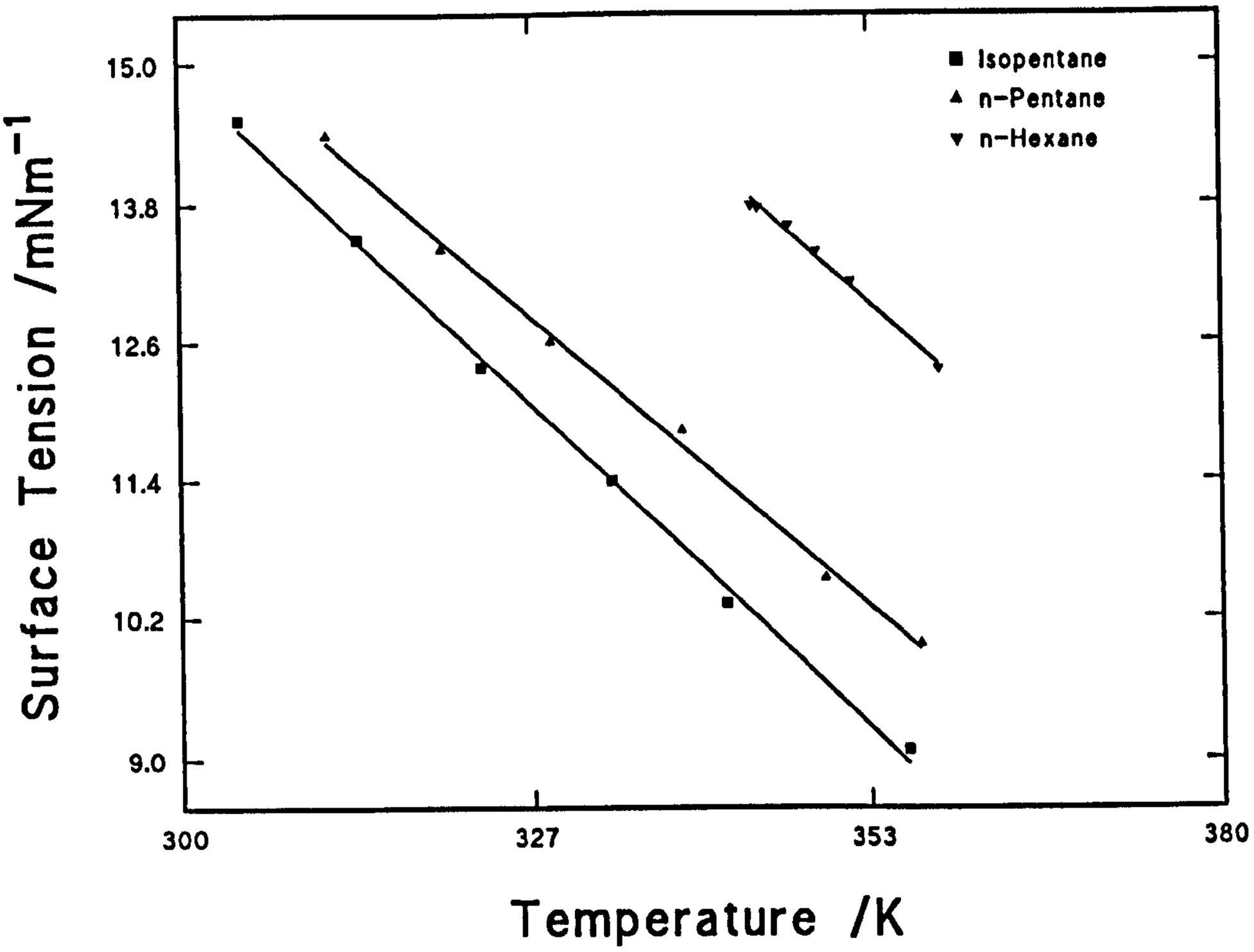

Figure 5.20. Measured surface tension values for pure liquids with temperature rise.

6. DISCUSSION

In this chapter the experimental results are discussed. A comparison of the measured density and composition values with the Extended Corresponding States Correlation (EXCS) and Peng-Robinson equation of state (PR EOS) will be discussed for the systems examined in sections 6.1 and 6.2. Section 6.2 also discusses the prediction of Henrys' Law constant (K_H) from the SPT expression [Eq.(3.7)]. The experimental values of the phase densities and compositions were utilised in predictive correlations (the parachor and corresponding states) to calculate the IFT. In section 6.3 these results are compared with the experimental values. The results of the prediction of ST and IFT from SPT will be discussed in sections 6.3.4 and 6.3.6.

6.1 Density

The measured density of the pure components as a function of pressure at constant temperature [Fig. 6.1], is slightly non-linear for the lighter hydrocarbon components (n-pentane and isopentane) and almost linear for the heavier components. This is due to the larger free volumes of the lighter components. Over a certain range of pressure the effect of compressibility can be noticed for the lighter components more than for the heavier ones depending on their critical pressure, the lower the critical pressure the more non-linearity trend of the density plot is noticed. Isopentane, an isomer, although it has the same carbon number as n-pentane, but due to its molecular shape being more rounded than n-pentane, its molecules are less packed and thus the liquid has a lower density. It also has a lower boiling point than n-pentane since it is branched and its molecular surface area needs less energy to break up the attractive forces between molecules.

Tang et al.[44] measured the density of four individual n-alkanes, using the same experimental rig, in nitrogen as a function of pressure at 313.15 K: n-pentane, n-hexane, n-heptane and n-octane. The density isotherms from these measurements

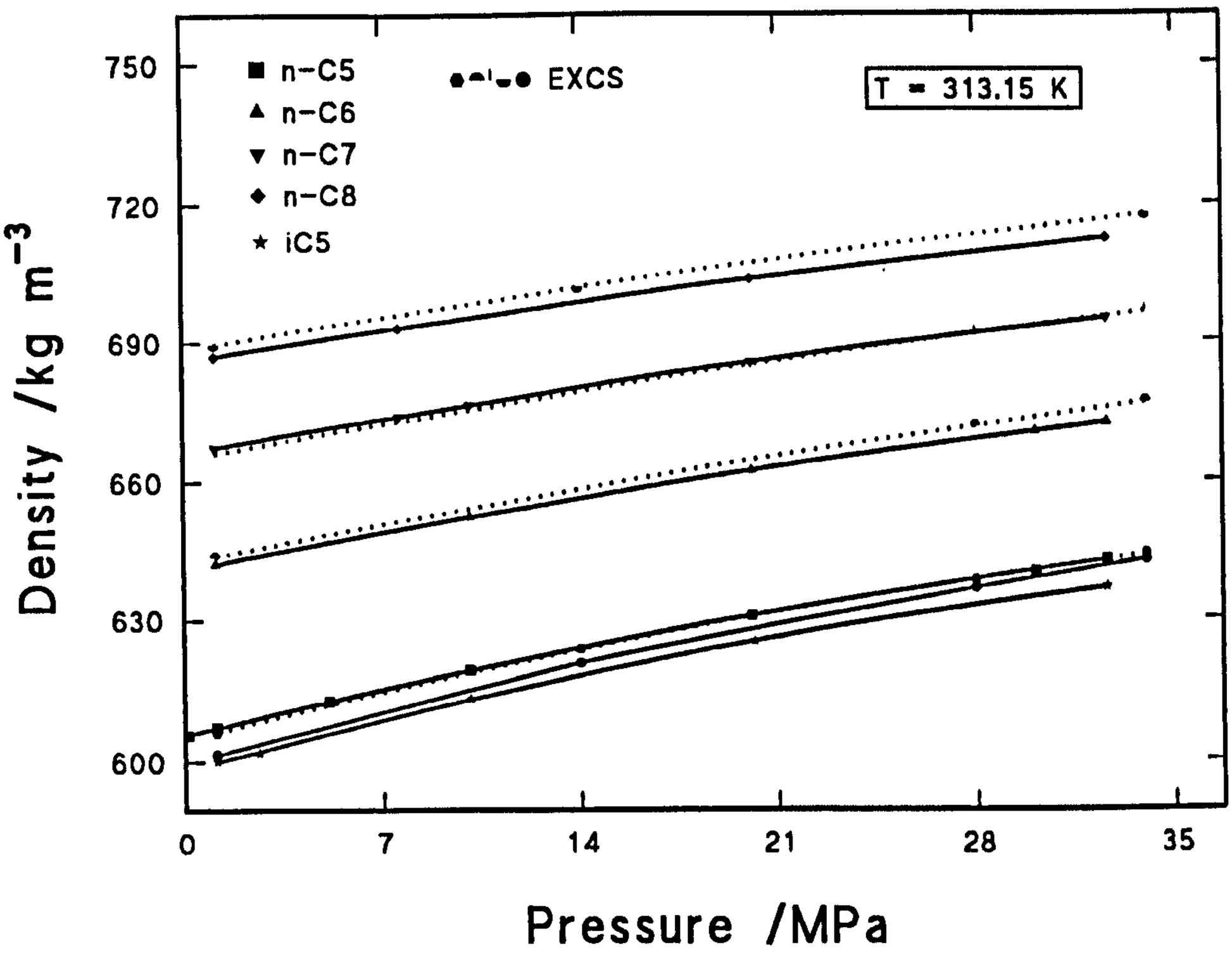

Figure 6.1. Measured densities of pure liquids with pressure rise and constant temperature (solid lines). The densities are compared with calculated values from EXCS (dotted lines, except for iC_5).

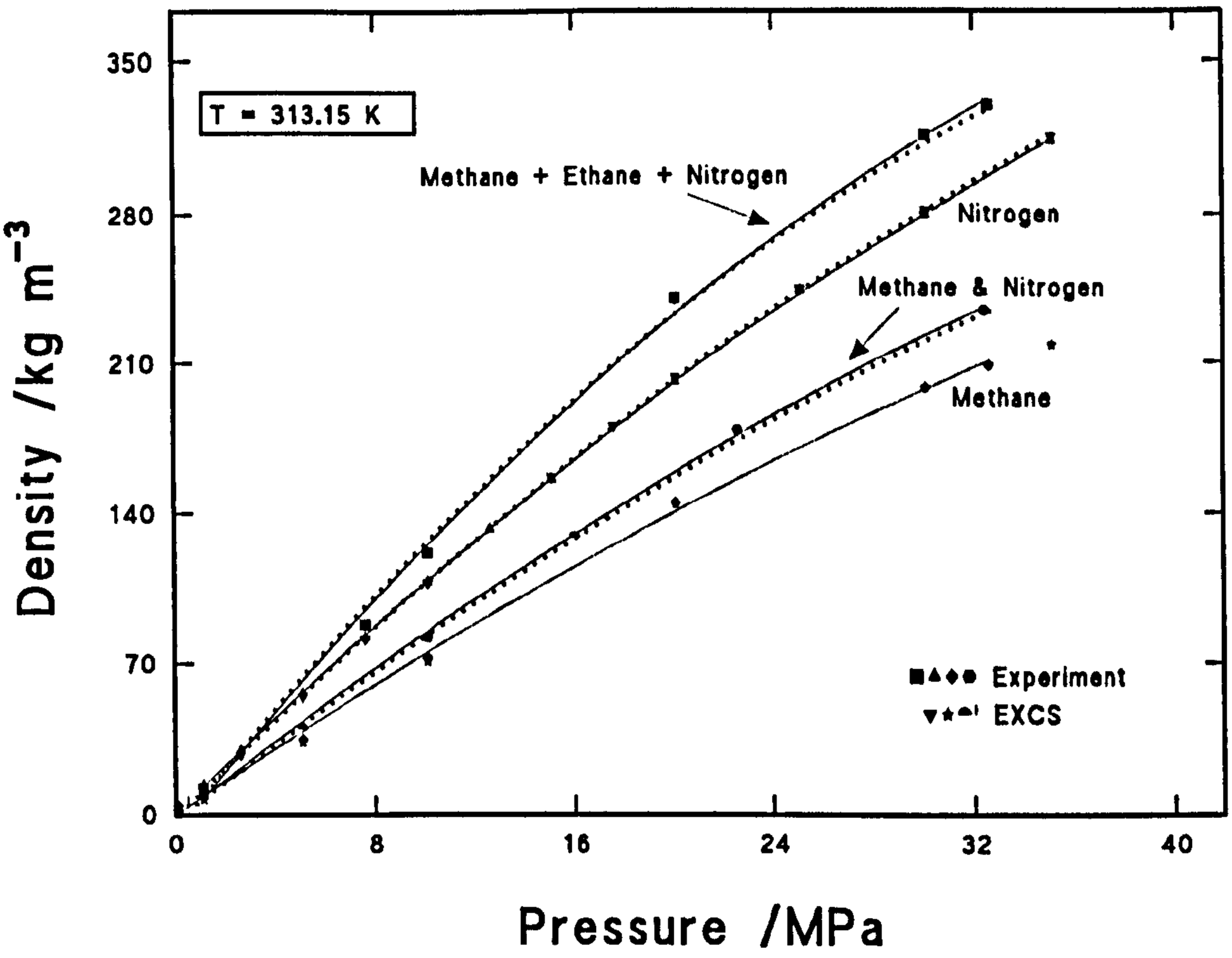

Figure 6.2. Measured densities of nitrogen, methane and ethane with pressure rise and constant temperature (solid lines). The densities are compared with calculated values from EXCS (dotted lines).

show that the pressure dependence is non-linear but approaches linearity with increasing hydrocarbon chain length. The introduction of nitrogen at elevated pressures has the effect of reducing the liquid phase density and increasing the gas phase density in the order of decreasing carbon number. At some pressure of nitrogen the densities of the two phases are expected to converge, i.e. at the critical pressure of the system. Satherley et al.[95] measured the system CH_4/N_2+n-pentane, using the same experimental rig, with a methane/nitrogen ratio of ~70/30 mol%. The densities of the two phases were found to converge significantly [Fig. 5.6].

The measured densities for the liquid components and for nitrogen, methane and ethane were compared with the Extended Corresponding States Correlation (EXCS)[100] as a function of pressure at constant temperature. The agreement is good and the prediction only deviates slightly for n-octane and isopentane [Figs. 6.1 and 6.2].

Figs. 6.3, 6.4 and 6.5 show a comparison between the measured densities of n-pentane, isopentane and n-hexane and predicted values from the EXCS and values taken from Vargaftik[33] as a function of temperature. All the compared values are in very good agreement with experimental results.

Figs. 6.6 and 6.7 show a comparison between the experimental densities and those calculated from the EXCS for the liquid and vapour phases for the systems N_2 or N_2/CH_4 in n-C_5/CH/T at elevated pressures. The agreement is generally good particularly in the liquid phase for the mixtures with different cyclohexane and toluene contents. However, for this system, the EXCS slightly overestimates the liquid phase density and even more so for the mixture with N_2/CH_4. For the gas phase the equation gives lower predictions for the other systems.

For the system N_2, CH_4 or N_2/CH_4 in $nC_5+nC_6+nC_7+nC_8$ [Fig. 6.8], the agreement with the EXCS is generally good, particularly for mixtures with N_2 and CH_4, and the predictions are more accurate at pressures well below the critical pressure.

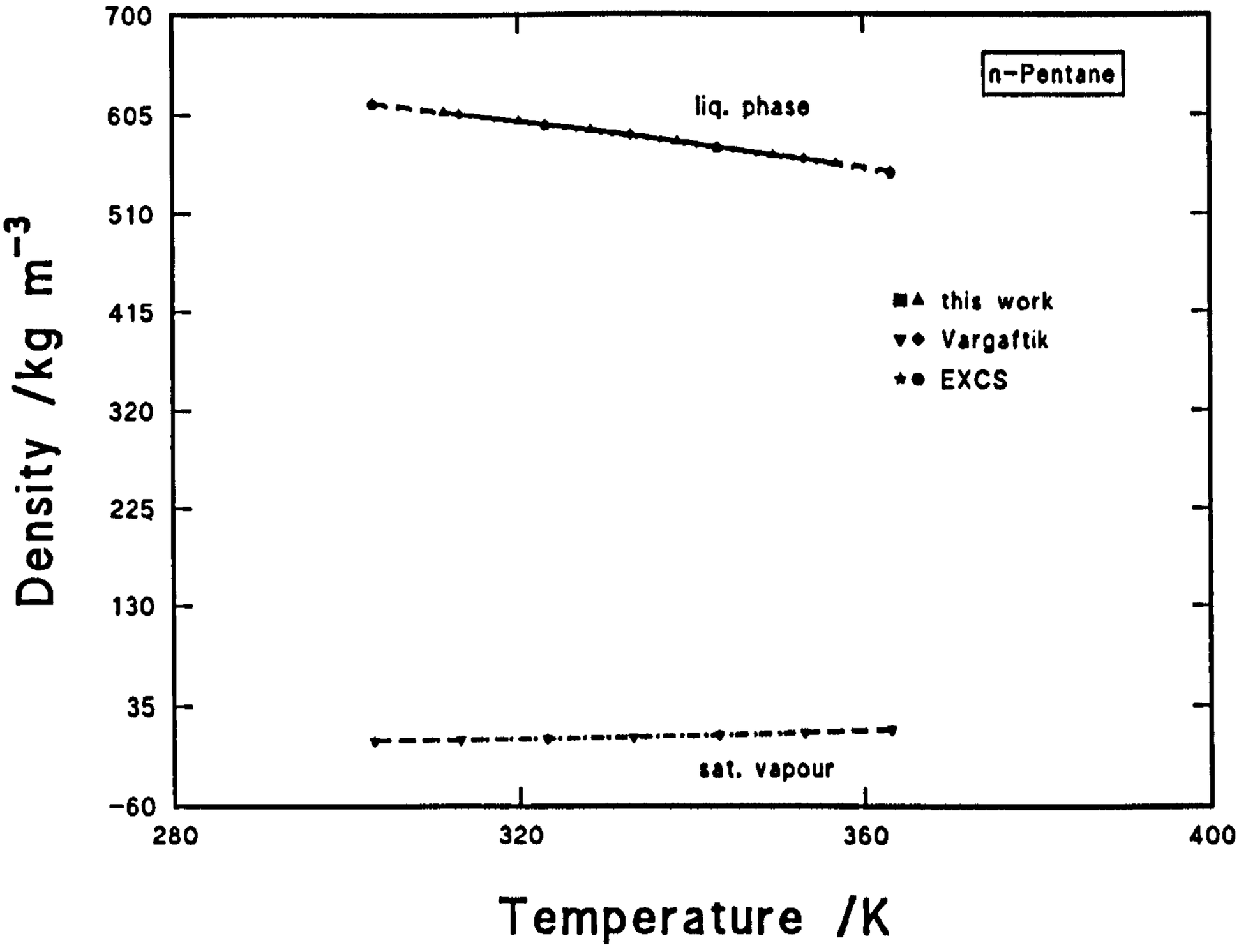

Figure 6.3. Measured phase densities for n-pentane with temperature rise (solid line: liquid phase, dotted line: vapour phase) compared with values taken from Vargaftik (dashed lines) and calculated values from EXCS (dotted lines).

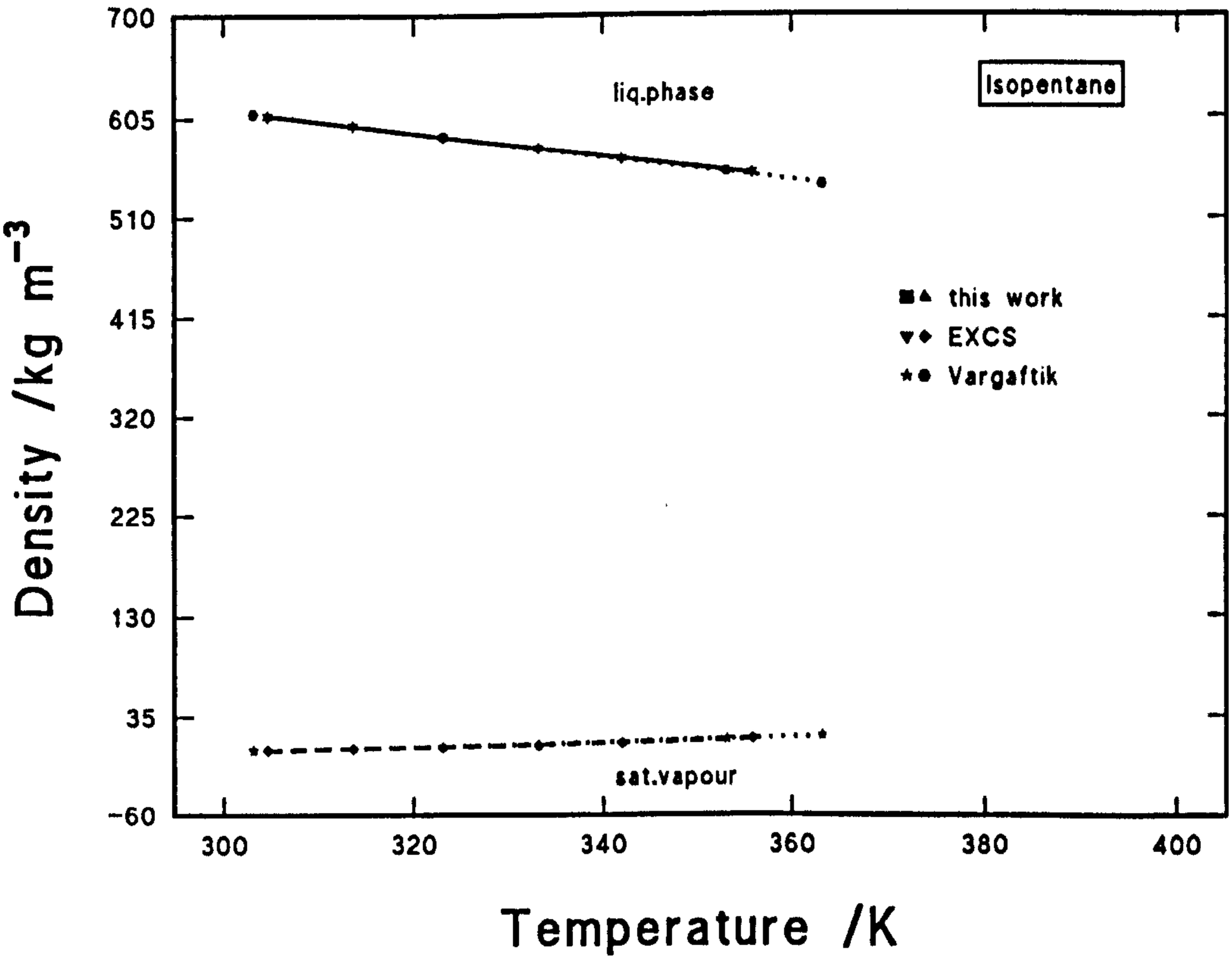

Figure 6.4. Measured phase densities for isopentane with temperature rise (solid line: liquid phase, dashed line: vapour phase) compared with values taken from Vargaftik (dotted lines) and calculated values from EXCS (dashed lines).

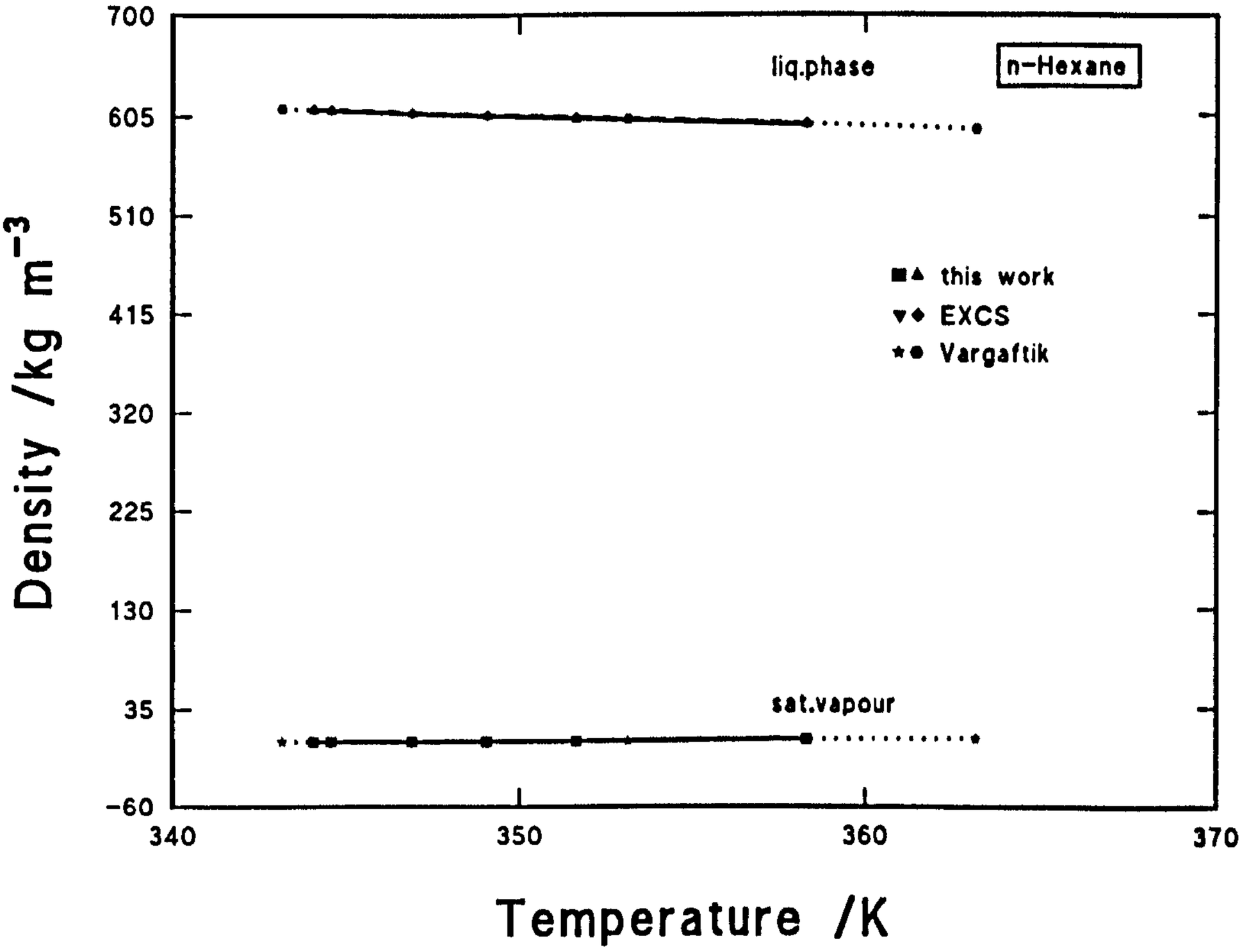

Figure 6.5. Measured phase densities for n-hexane with temperature rise (solid lines) compared with values taken from Vargaftik (dotted lines) and calculated values from EXCS (dashed lines).

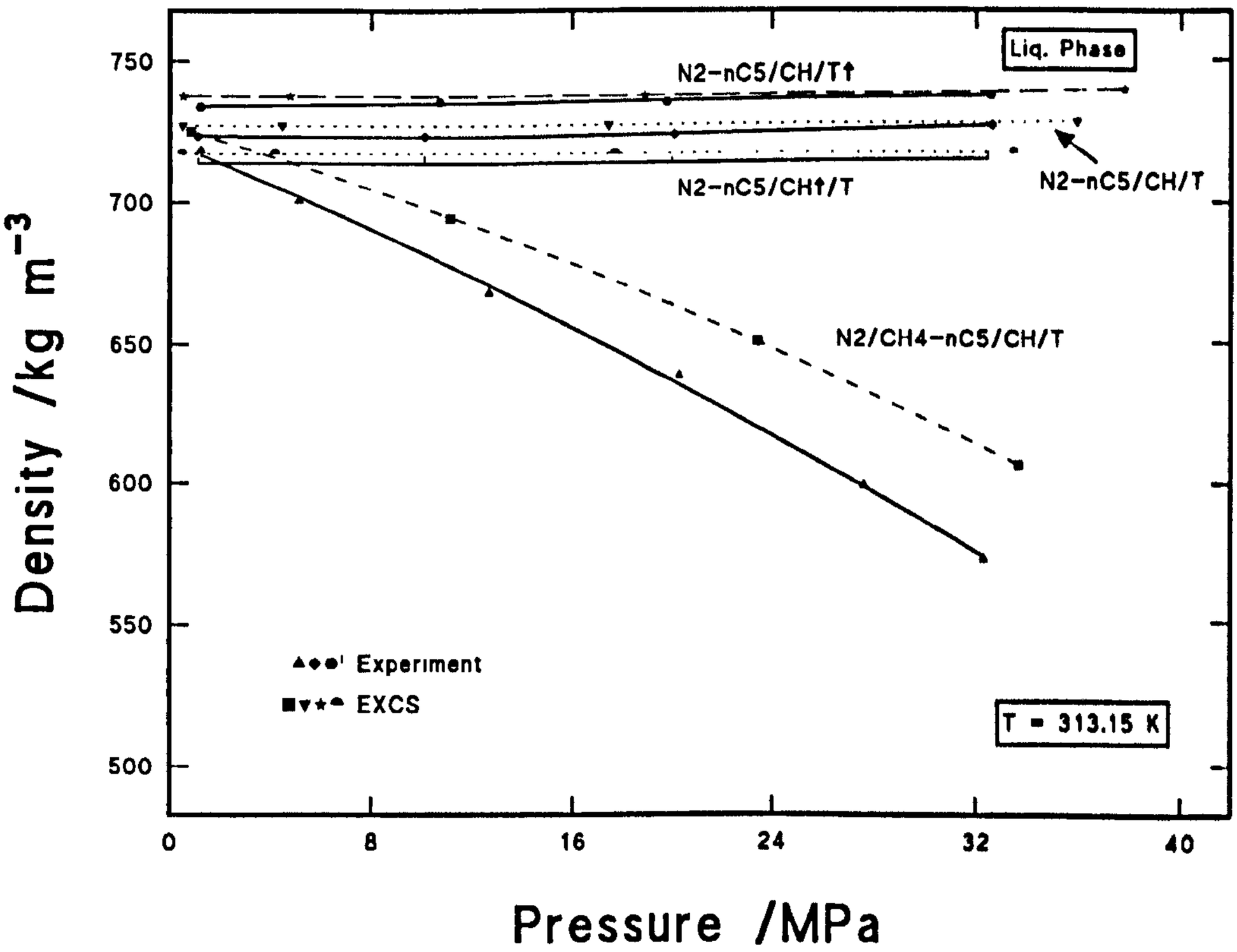

Figure 6.6. Measured liquid phase densities for the ternary liquid mixture with nitrogen and methane addition as a function of pressure (solid lines) compared with calculated values from EXCS (dotted and dashed lines).

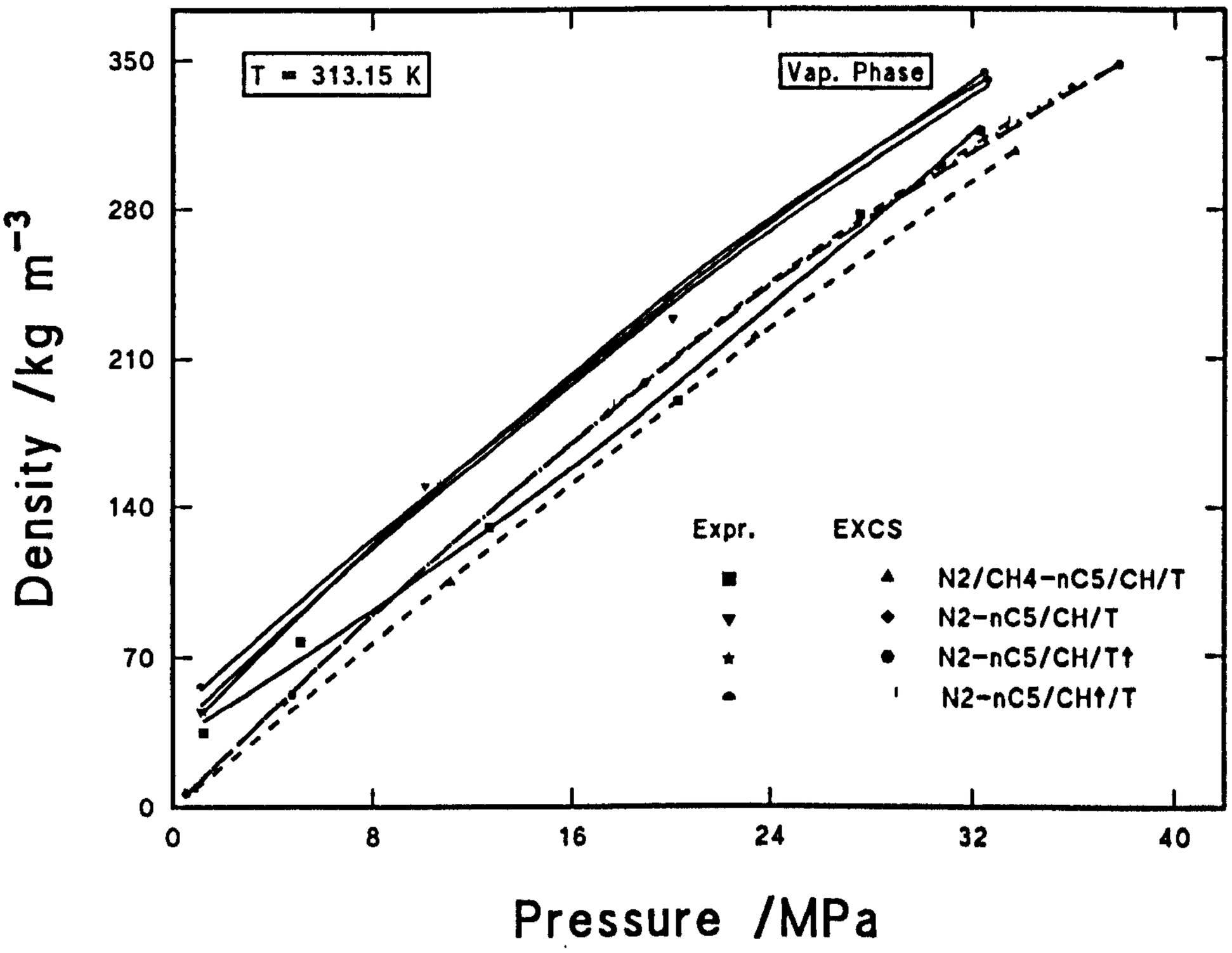

Figure 6.7. Measured vapour phase densities for the ternary liquid mixture with nitrogen and methane addition as a function of pressure (solid lines) compared with calculated values from EXCS (dotted and dashed lines).

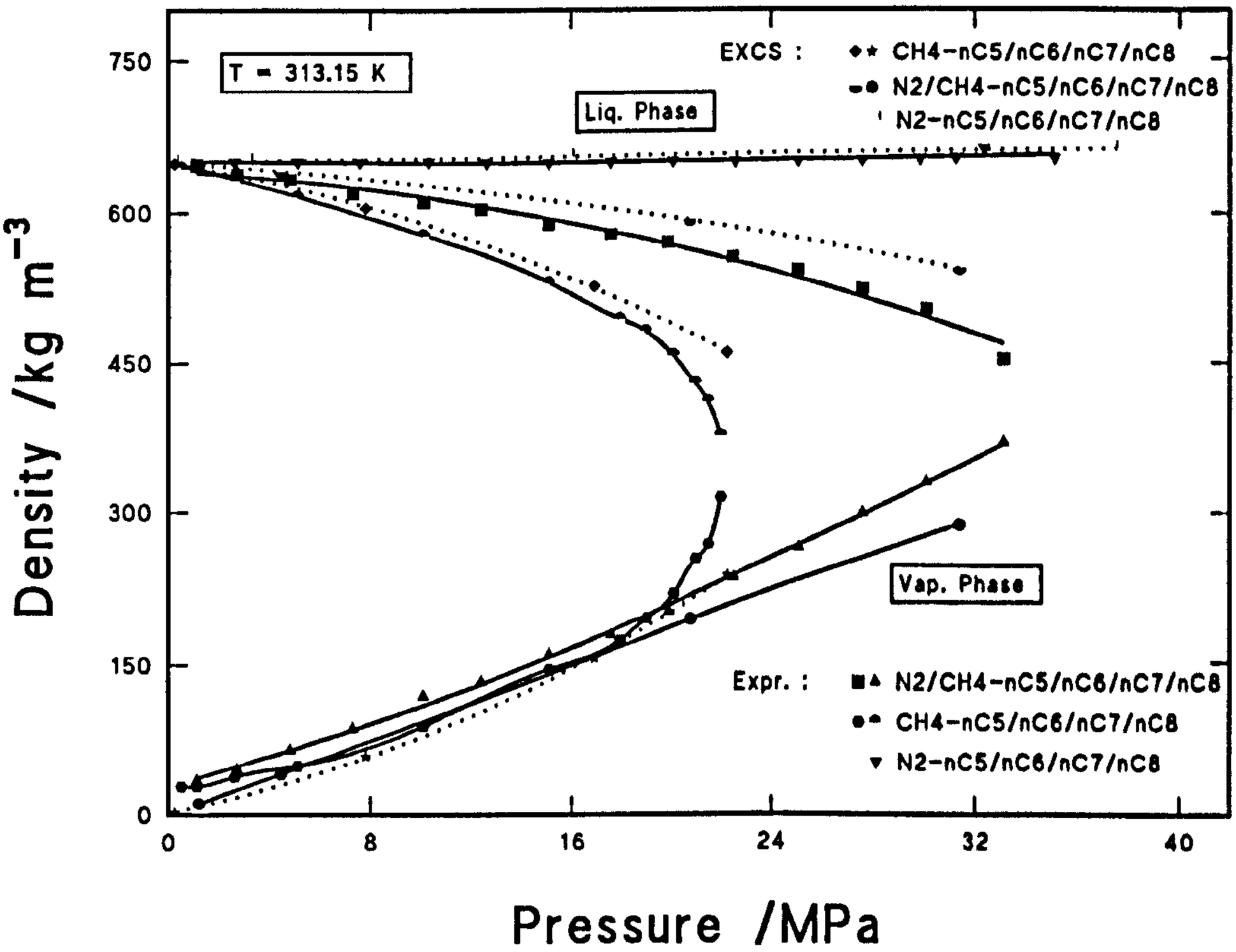

Figure 6.8. Measured phase densities for the quaternary liquid mixture with nitrogen and methane addition as a function of pressure (solid lines) compared with calculated values from EXCS (dotted lines).

The comparison of the density results with the EXCS predictions, for N_2 or N_2/CH_4 in n-C_5/iC_5 is shown in Fig. 6.9. Figs. 6.10 and 6.11 show a comparison in the liquid and gas phases including the methane/ethane and nitrogen/methane/ethane in n-pentane systems. The predictions are fair below the critical pressure for all the systems. However, it overestimates the density values in both phases particularly near the critical point, except for the CH_4/C_2H_6-n-pentane system where the predicted values improve near the critical.

It appears that for most of the above systems the EXCS predicts the phase densities more accurately at pressures below the critical pressure and this is attributed to the fact that the CS theory determines the critical constants T_c and P_c for the mixed system from a mixing rule (chapter 2) which may lead to uncertainty of these values in the critical region. However, the EXCS for these mixed systems and those similar to them, provides useful phase density predictions with small deviations, particularly at pressures below the critical pressure.

The experimental values of the liquid and vapour densities for the systems examined have a non-linear dependency on pressure at constant temperature. The measured density, ρ, results have been fitted to a second-degree polynomial as a function of pressure:

$$\rho = a\,P^2 + b\,P + c \qquad (6.1)$$

The equation applies to both phases as a function of pressure up to 35 MPa and a constant temperature of 313.15 K. The coefficients a, b and c are given in Table 33 for the various systems investigated.

The experimental values of the density for the pure components: n-pentane, isopentane and n-hexane as a function of temperature at saturated vapour pressures, have a linear dependence on temperature between the boiling point and up to 363 K. The data was fitted to a straight line by linear regression:

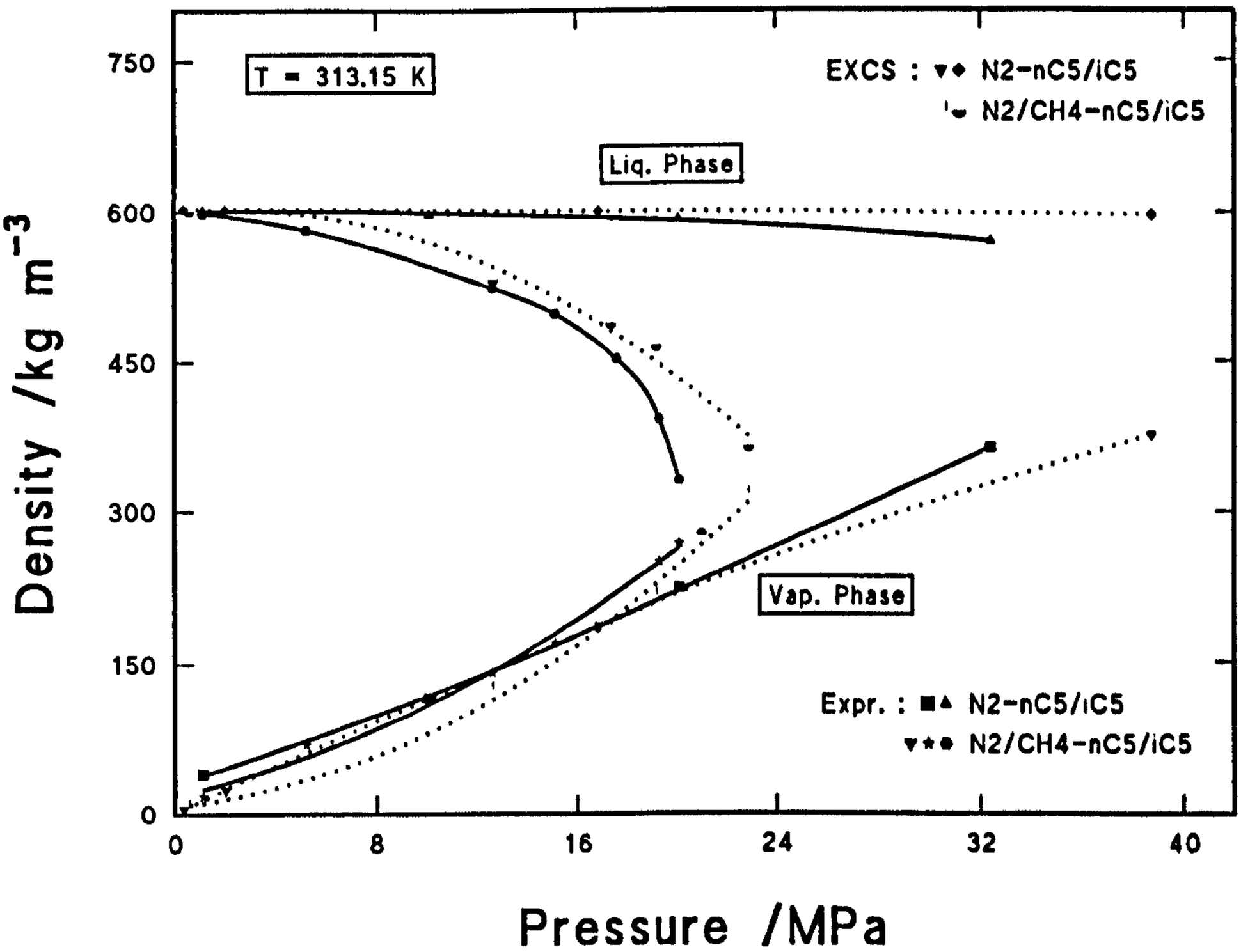

Figure 6.9. Measured phase densities for n-pentane/isopentane with nitrogen and methane addition as a function of pressure (solid lines) compared with calculated values from EXCS (dotted lines).

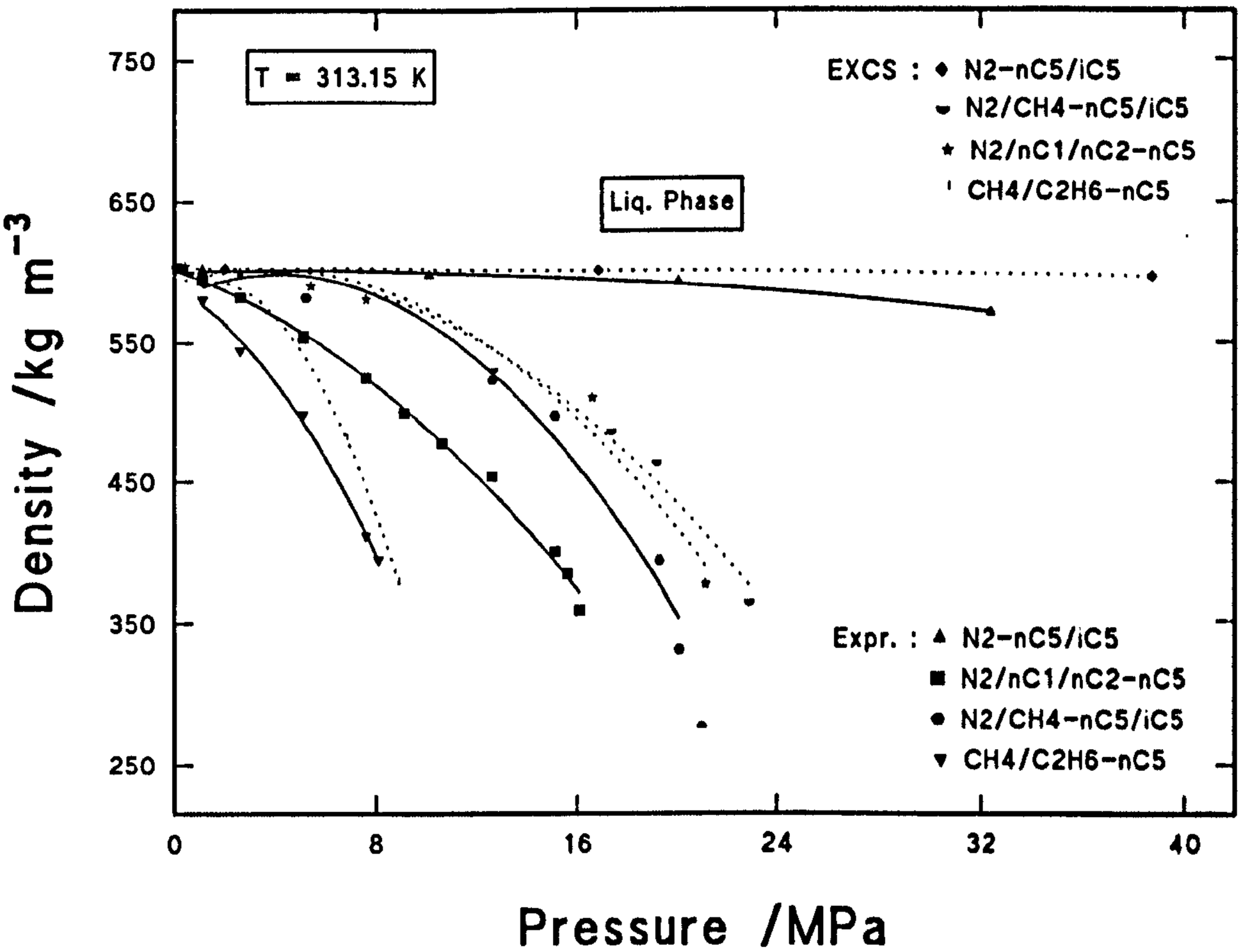

Figure 6.10. Measured liquid phase densities for n-pentane/isopentane with nitrogen and methane addition as a function of pressure (solid lines) compared with calculated values from EXCS (dotted lines).

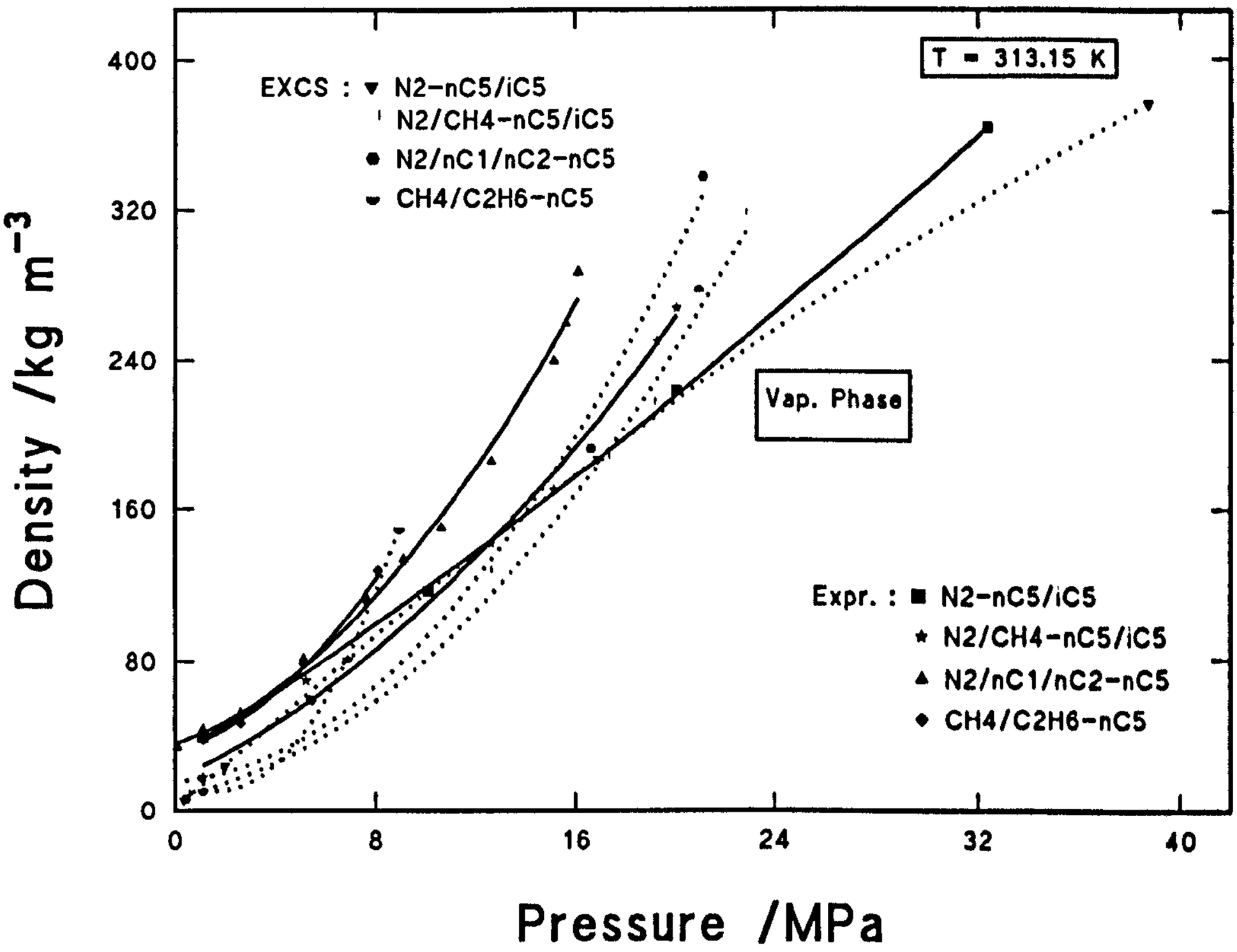

Figure 6.11. Measured vapour phase densities for n-pentane/isopentane with nitrogen and methane addition as a function of pressure (solid lines) compared with calculated values from EXCS (dotted lines).

$$\rho = b\ P + c \tag{6.2}$$

The coefficients b and c are given in Table 34.

6.2 Composition

Tang et al.[44] found that the bubble point curves for four binary n-alkane-N_2 systems, measured on the same experimental rig are approximately linear at low pressures and indicate that nitrogen is relatively soluble in the n-alkanes whereas the gas phase (the dew point curves) contains very little alkane over the pressure range studied (up to 40 MPa) at 313.15 K.

The Henrys' Law constant (K_H) was computed, from the SPT expression [Eq.(3.7)] using the experimental phase densities and the experimentally determined and literature values of the Lennard-Jones parameters[2] [Table 35] for the various components investigated. These parameters have been used for K_H, IFT and ST expressions throughout the calculations. Figs. 6.12, 6.13, and 6.14 show the K_H plots obtained for the systems: N_2-nC_5+cyclohexane+toluene, N_2-nC_5+nC_5 and N_2/CH_4-nC_5+nC_6+nC_7+nC_8. Generally, the predicted K_H from the SPT expression found to be in good agreement with experimental results at low pressures which is expected since the approach is for dilute (ideal) solution.

The composition results obtained in the present work were also compared with predicted values from the Peng-Robinson equation of state (PR EOS) at elevated pressures and constant temperature (313.15 K). Fig. 6.15 shows the experimental and predicted values of the bubble point and dew point curves for the

---

[2] The Lennard-Jones parameters were taken from three sources: Hirschfelder, J.O., Curtiss, C.F., and Bird, R.B., Molecular Theory of Gases and Liquids (Wiley, New York, 1964); Bondi, A., J. Phys. Chem. 68, 411 (1964); and Wilhelm, E. and Battino, R., J. Chem. Thermodynamics, 3, 379-392; 743-751; 761-768 (1971).

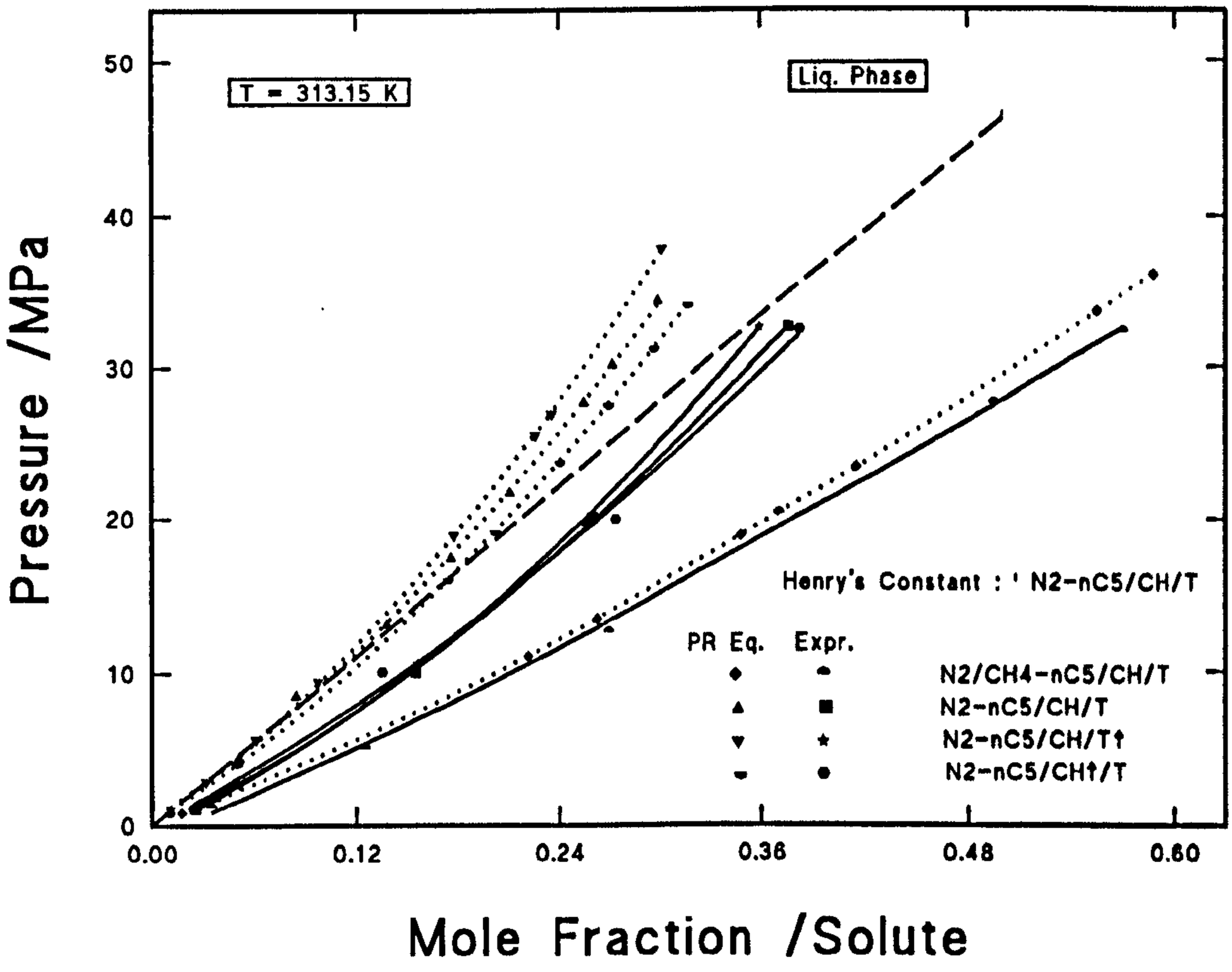

Figure 6.12. Compared measured liquid phase compositions for nitrogen and pseudo-solute in the ternary liquid mixture (solid lines) with PR EOS (dotted lines) and K_H predictions (dashed line).

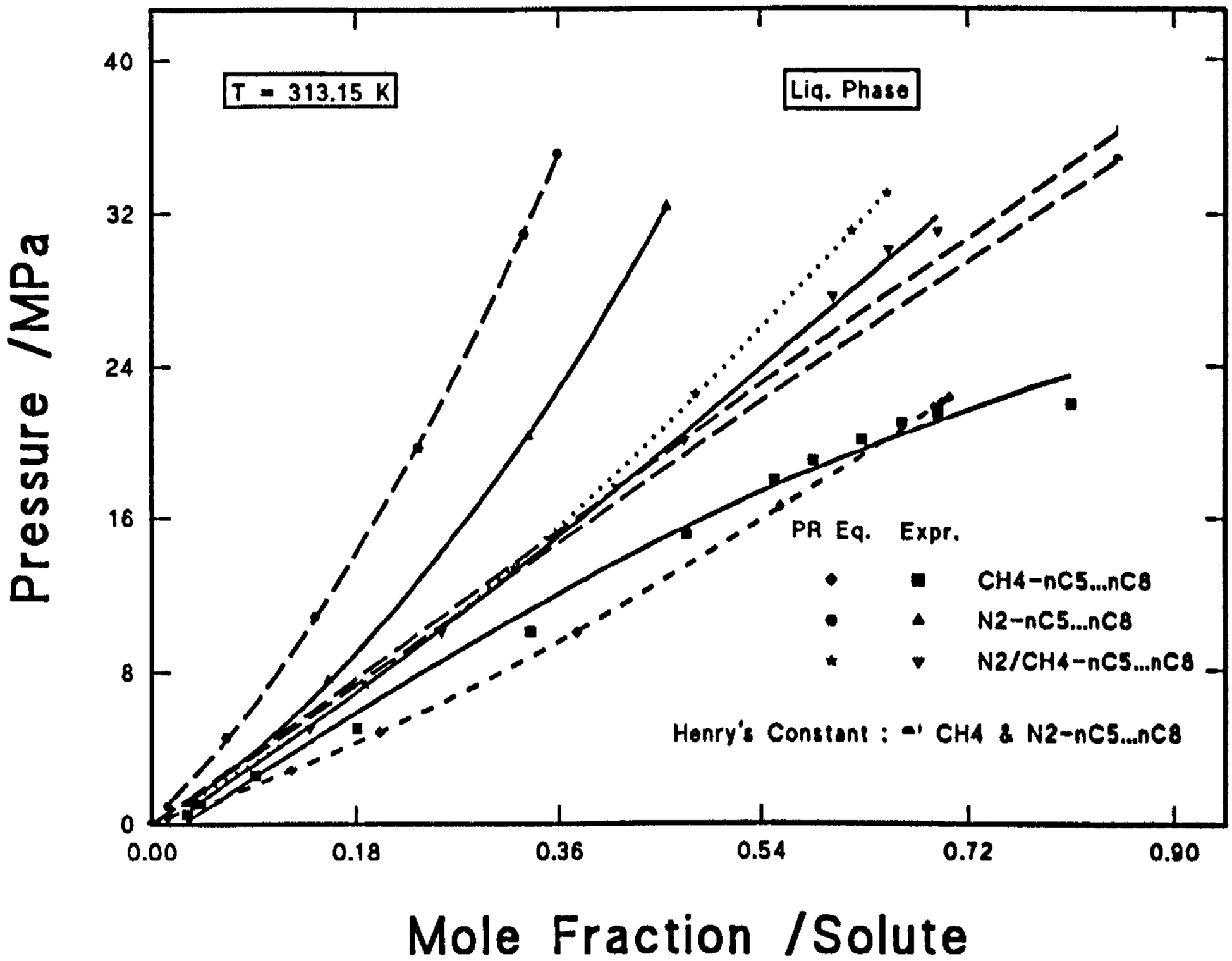

Figure 6.13. Compared measured liquid phase compositions of nitrogen, methane and pseudo-solute in the quaternary liquid mixture (solid lines) with PR EOS (dotted lines) and K_H predictions (dashed lines).

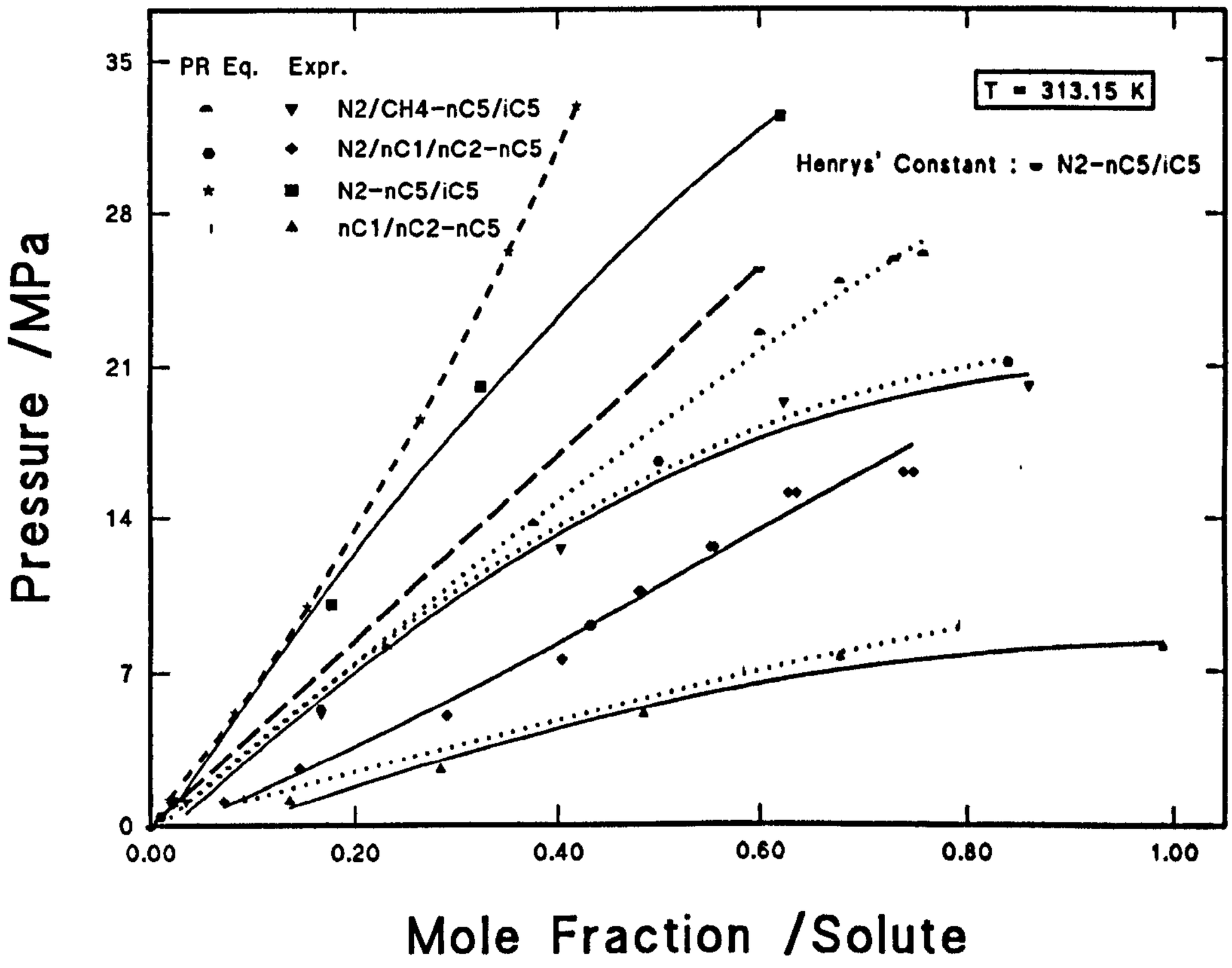

Figure 6.14. Compared measured liquid phase compositions of nitrogen and pseudo-solute in n-pentane and isopentane (solid lines) with PR EOS (dotted lines) and K_H predictions (dashed lines).

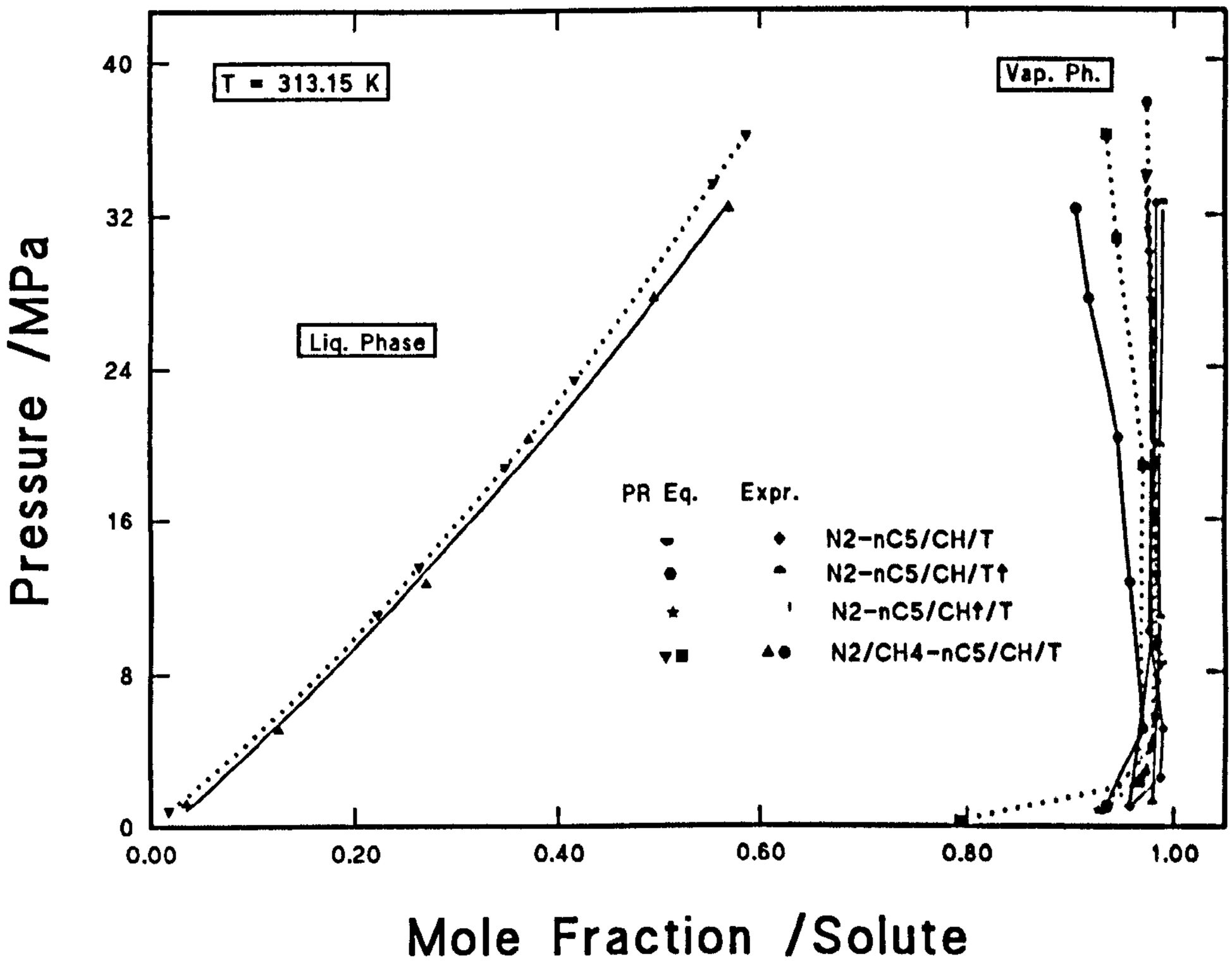

Figure 6.15. Compared measured phase compositions of nitrogen and pseudo-solute in the ternary liquid mixture (solid lines) with PR EOS (dotted lines).

system N_2 and N_2/CH_4 in nC_5+cyclohexane+toluene mixtures with different ratios of cyclohexane and toluene. Fig. 6.12 also shows the comparison in the liquid phase and the plot of Henrys' Law constant, K_H, for the system N_2-nC_5/CH/T. Generally, the PR EOS follows the experimental values and gives good predictions at low pressures, particularly for the mixture with N_2/CH_4 in the liquid phase, and in the vapour phase for all mixtures. However, it overestimates the phase compositions for the other mixtures with nitrogen. The predicted Henrys' constant compares well with experiment at low pressure (~2 MPa), for the above system, and are also in good agreement with the predicted values from the PR EOS.

For the systems of N_2, CH_4 or N_2/CH_4 in $nC_5+nC_6+nC_7+nC_8$, the predicted values from PR EOS [Fig. 6.16] are in fair agreement with experiment data for the systems CH_4-$nC_5+nC_6+nC_7+nC_8$ and N_2-$nC_5+nC_6+nC_7+nC_8$. Fig. 6.13 shows the Henrys' Law constant (K_H) plot in the liquid phase for these above two mixtures with methane and nitrogen. The K_H plots for the two systems are in good agreement with the experimental results and the PR EOS predictions at low pressures, especially for the mixture with nitrogen.

The comparison was also made for the pure nitrogen and the different gaseous mixtures of N_2, CH_4 and C_2H_6 in n-pentane+isopentane and in pure liquid n-pentane [Figs. 6.17 and 6.14]. In general, the PR EOS overestimates the solute solubility particularly near the critical region, but it improves at low pressures and is in good agreement with experimental results in particular for the system of methane/ethane-n-pentane in the liquid phase. The value of K_H predicted from the SPT for the system N_2-nC5/iC5 agrees well with the experimental data at low pressures.

For the binary systems: N_2 in n-pentane, n-hexane, n-heptane and n-octane the values of K_H were calculated from Eq.(3.7) in the liquid phase using the experimental density values from Tang et al.[44] and literature values for the solute and solvents molecular pair potentials [Table 35]. Fig. 6.18 show the results obtained. The predicted K_H plots for these systems are in good agreement with

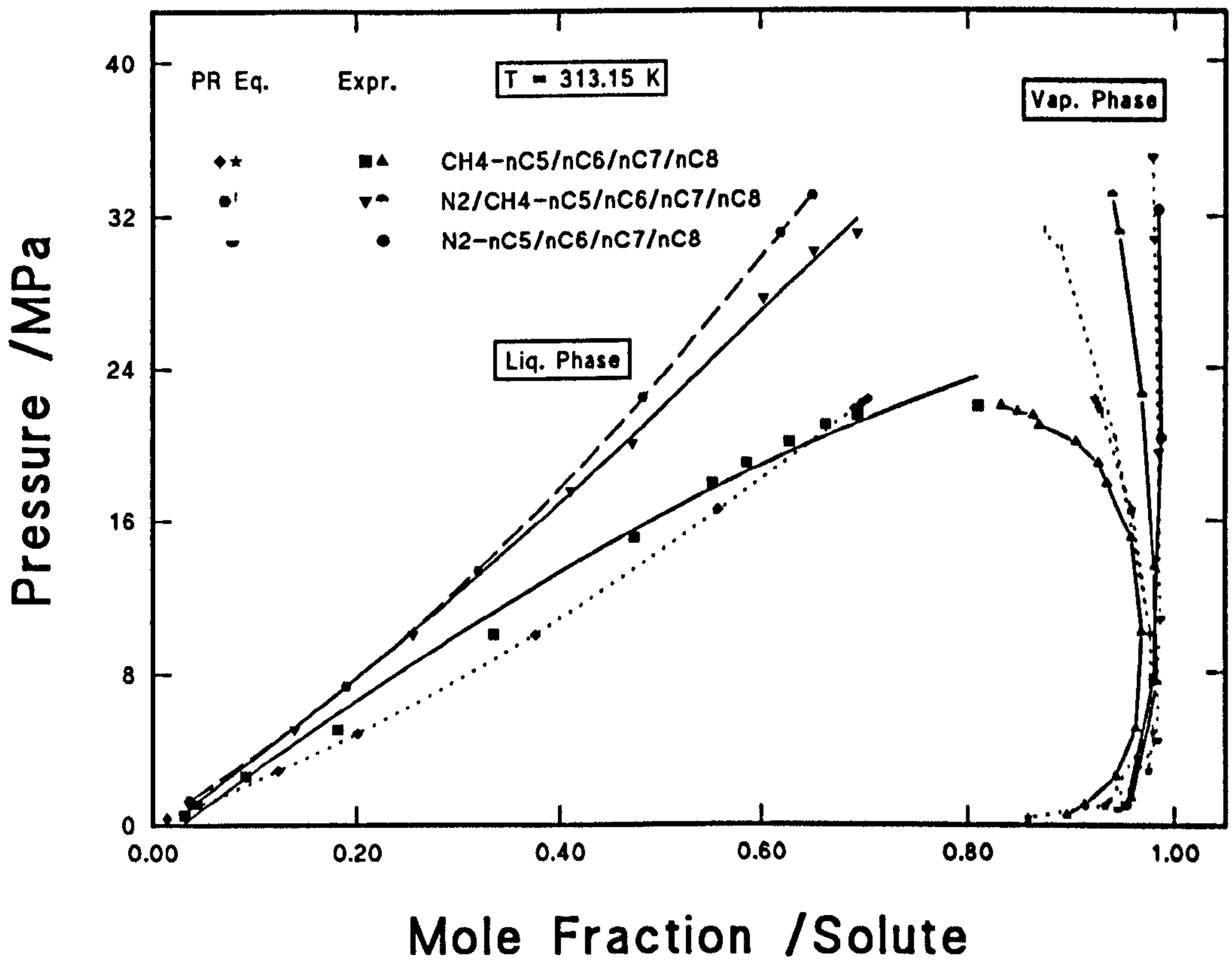

Figure 6.16. Comparison between measured phase compositions of nitrogen and methane in the quaternary liquid mixture (solid lines) and those predicted from the PR EOS (dotted and dashed lines).

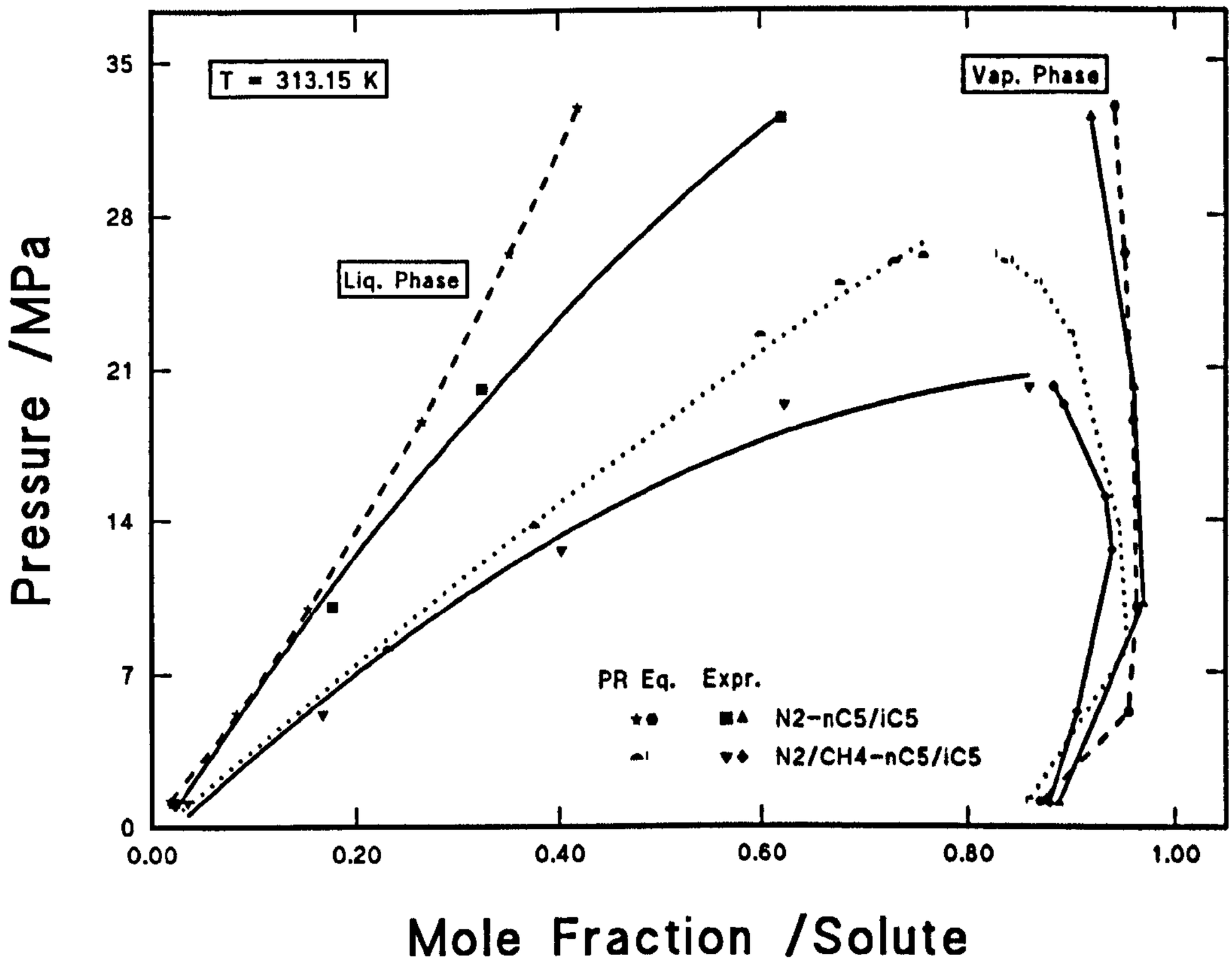

Figure 6.17. Compared measured phase compositions of nitrogen and pseudo-solute in n-pentane/isopentane (solid lines) with PR EOS (dotted and dashed lines).

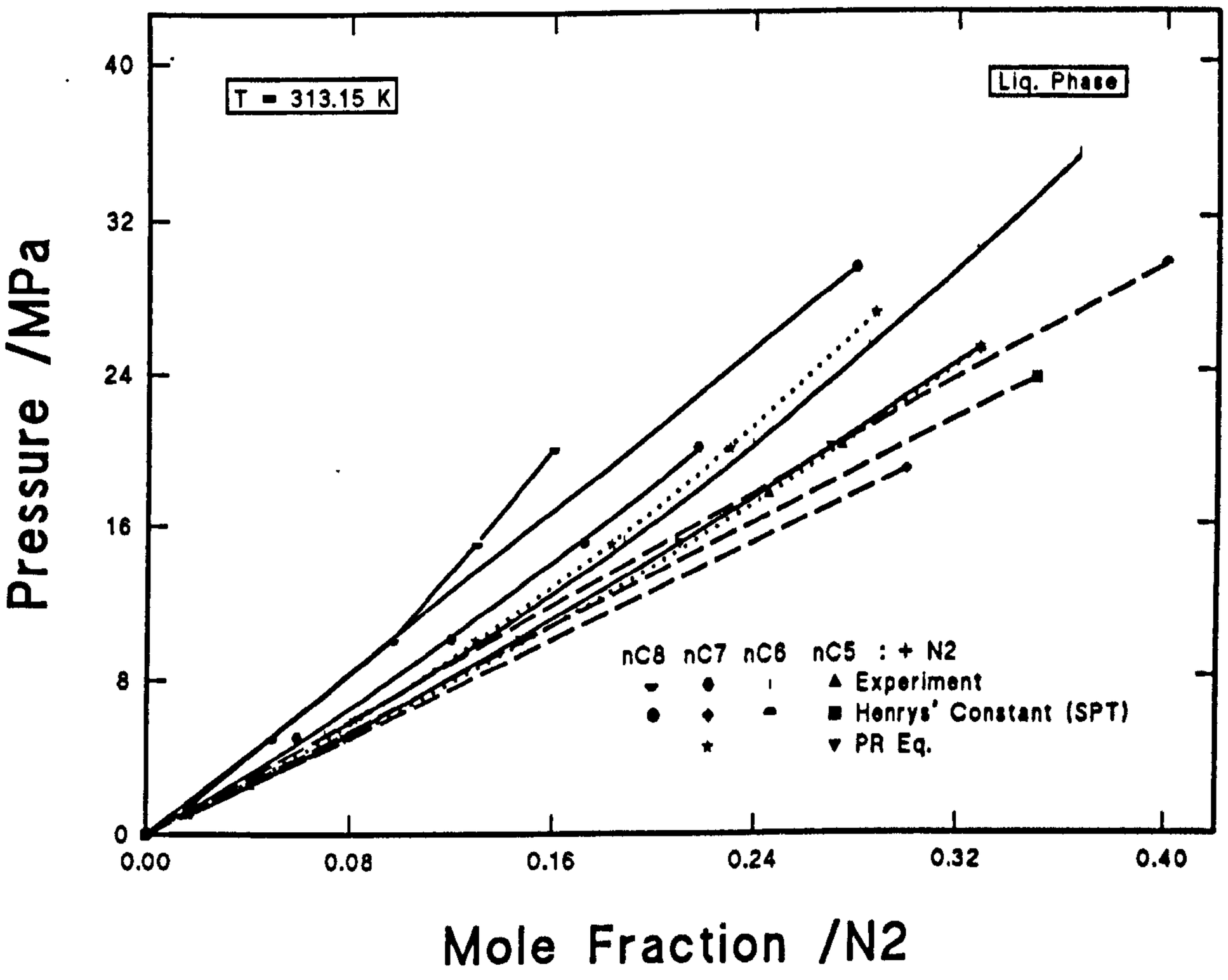

Figure 6.18. Comparison between measured liquid phase compositions of nitrogen in n-pentane, n-hexane, n-heptane and n-octane and K_H plots from SPT.

experiment, particularly for n-pentane and n-octane.

It appears that for most of the above systems the PR EOS predicts vapour-liquid equilibrium (VLE) data more accurately at pressures below the critical pressure. In the equation [Eq.(2.3)], for a mixed system a and b are function of the critical constants T_c and P_c and are determined from a mixing rule using an appropriate binary parameters (chapter 2). Therefore, in the critical region, the uncertainty of the estimated critical constants T_c and P_c and the binary parameters, which the equation uses, leads to inaccuracies in the prediction of compositions for mixed systems. Thus, in this case, the PR EOS provides useful VLE data with small deviations, particularly at pressures well below the critical pressure. However, in the critical region, care has to be taken of the expected overestimation of phase compositions which can be significant. The extent of deviation depends on the number of components and their nature.

It also appears that the SPT expression of Eq.(3.7) for calculating the Henry's Law constant gives good agreement with experimental data. In using this expression, the Lennard-Jones pair potentials were taken from different sources of published literature for the systems studied in order to assess the validity of the theory. The results were found to be sensitive to the chosen molecular-hard sphere diameter of the solute and solvents, rather than to the potential energy values. Thus the appropriate molecular parameter has to be adjusted to obtain better solubility predictions for these systems. As mentioned in chapter 3, SPT is based on assumptions relative to hard sphere simple fluids, and to improve the applicability of this theory improvements in the interactive energy G_i term, particularly for polar mixed systems, can be thought of. However, the SPT provides a useful expression for the prediction of K_H and it can be used for this purpose provided care is taken regarding the possible uncertainty in the results, particularly when accurate molecular properties are not available.

6.3 Interfacial Tension

6.3.1 IFT Variation with Pressure

The experimental IFT for all the measured systems has a non-linear relation dependence on pressure at constant temperature. All the measured IFT values were represented by a second order-polynomial equation as a function of pressure:

$$\gamma = a\,P^2 + b\,P + c \qquad (6.3)$$

The above equation applies to the measured systems to determine the IFT at any required pressure, by gas solute addition, up to 35 MPa and constant temperature of 313.15 K. The coefficients a, b and c are given in Table 31 for the various systems studied.

According to the scaling theory of critical phenomena[101] certain thermodynamic quantities of a fluid system close to the critical point exhibit power-law behaviour and may be characterized by a set of universal quantities. Near-critical region the compositions of the phases are close to the critical composition. IFT between the two phases and phase density differences near the critical point are given by:[43]

$$\gamma = \gamma_o \left[1-\frac{T}{T_c}\right]^{\mu} \qquad (6.4)$$

$$\Delta\rho = \Delta\rho_o \left[1-\frac{T}{T_c}\right]^{\beta} \qquad (6.5)$$

where $\Delta\rho_o$ and γ_o are the scale factors for density difference and IFT respectively. μ and β are universal critical exponents for IFT and density difference respectively, and have values of μ=1.26 and β=0.325. The values of μ and β are constants for all substances and μ/β=3.88. The above two equations result in:

A plot of logγ versus log$\Delta\rho$ should be linear with a slope equal to 3.88. Fig. 6.19 shows a log-log plot of the density difference against the low IFT values near

$$\gamma = \gamma_o \left[\frac{\Delta\rho}{\Delta\rho_o} \right]^{\mu/\beta} \tag{6.6}$$

the critical point giving straight lines for three systems. For the systems N_2 and N_2/CH_4 in $nC_5/nC_6/nC_7/nC_8$ and CH_4 in nC_5/iC_5 the lines slopes are 3.86, 3.87 and 3.12 respectively, which are in good agreement with scaling laws.

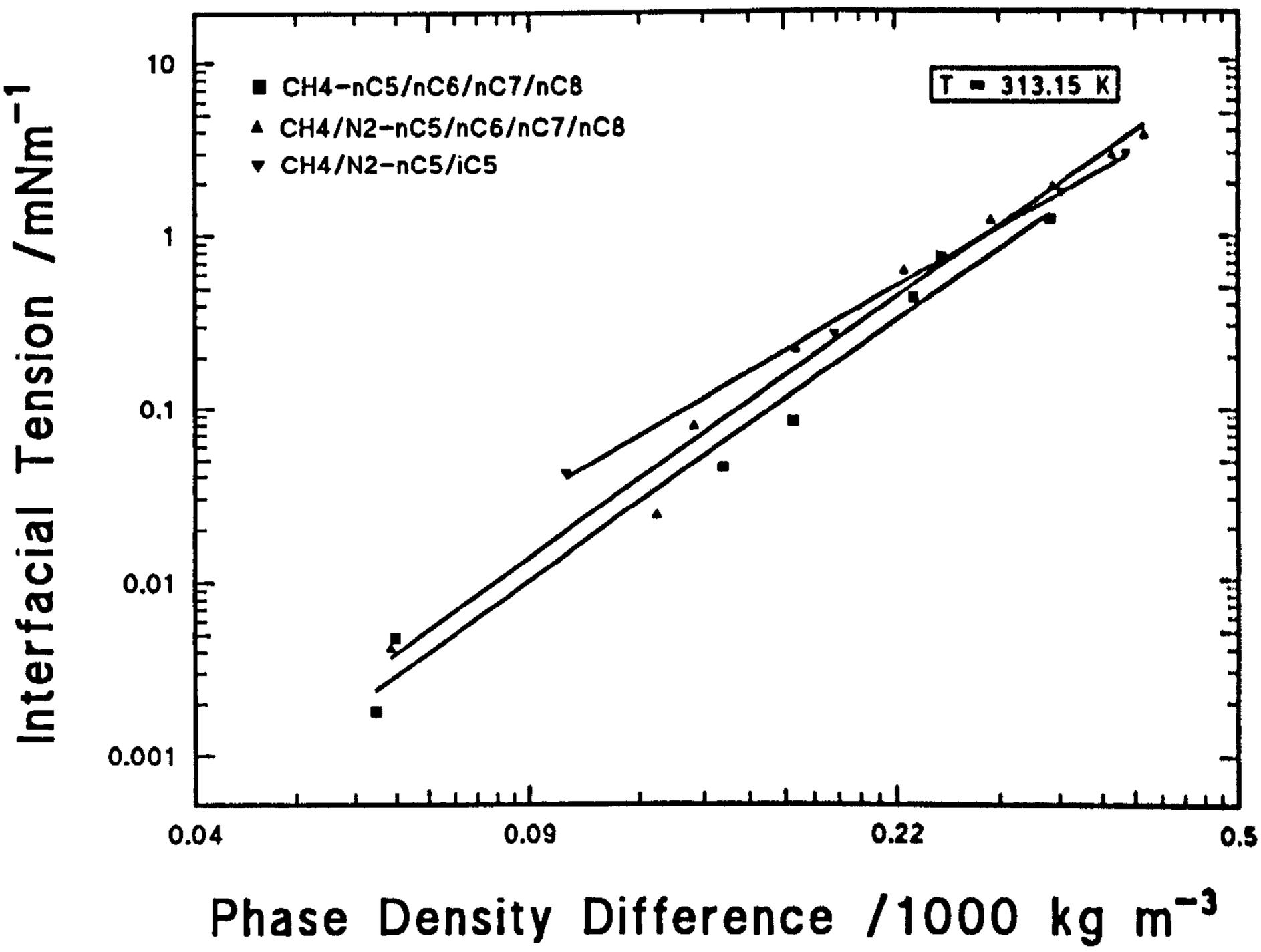

Figure 6.19. Log-log plot for IFT versus phase density difference near the critical region.

6.3.2 ST Variation with Temperature

The measured surface tension of n-pentane, n-hexane and isopentane as a function of temperature follows a linear relationship. The results have been fitted to:

$$\gamma = a\,T + b \qquad (6.7)$$

between the boiling point and 363 K. The coefficients a and b are given in Table 32 for the three liquids.

The rate of change of ST with temperature is almost constant for these liquids over the range examined. This temperature range is only small part of a large temperature span up to T_c which gives the ST-temperature trend a linear relationship rather than a non-linear one within the measured range of T_r between 0.66 to 0.77. This agrees with what Jasper[32] obtained for various liquids within the range of T_r between 0.4 to 0.7.

6.3.3 Predictive Correlations for Mixtures

The measured IFT values for the systems examined as a function of pressure and at constant temperature (313.15 K) were compared with calculations from the Weinaug-Katz parachor correlation (W-K) [Eq.(2.2)] utilising the experimentally determined phase densities and compositions. The parachor values for the various components were taken from literature.[53] Several systems were also compared with predicted values from the Hough-Stegmeier (H-S) (chapter 2) parachor correlation, using the same W-K model but with an exponent of n = 1/3.66. Figs. 6.20, 6.21 and 6.22 show these comparisons for all the examined liquid mixtures with N_2, CH_4, N_2+CH_4, N_2+CH_4+C_2H_6 and CH_4+C_2H_6. Generally, both correlations follow a non-linear trend and under predict the IFT, except for the systems: N_2/nC_1-nC_5/iC_5, nC_1/nC_2-nC_5 and $N_2/nC_1/nC_2$-nC_5 where the W-K correlation is in good agreement

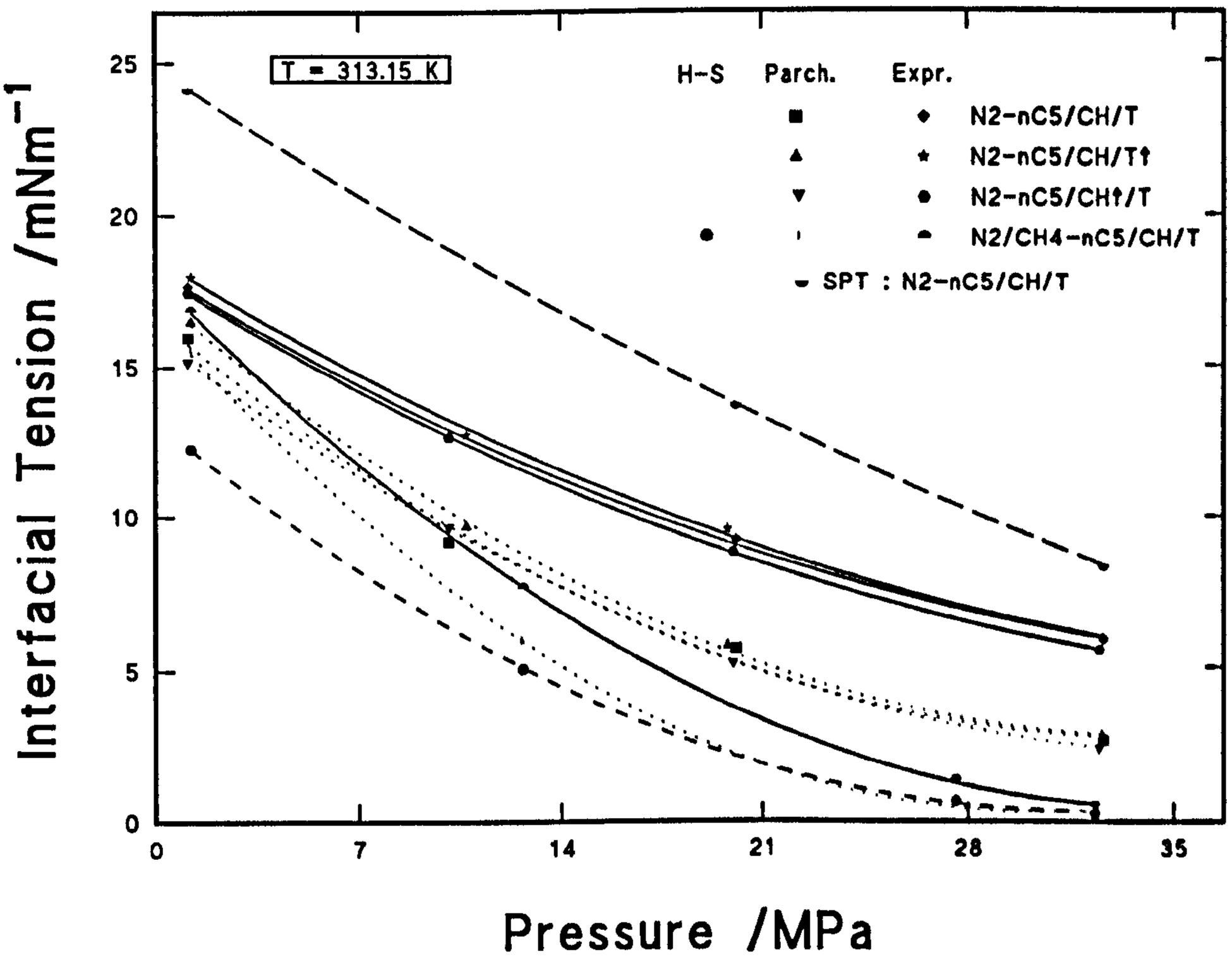

Figure 6.20. Comparison between measured IFT values for the ternary liquid mixture with nitrogen and methane addition as a function of pressure (solid lines) and calculated IFT values from the parachor-dependent correlations (dotted lines) and the SPT (long dashed line).

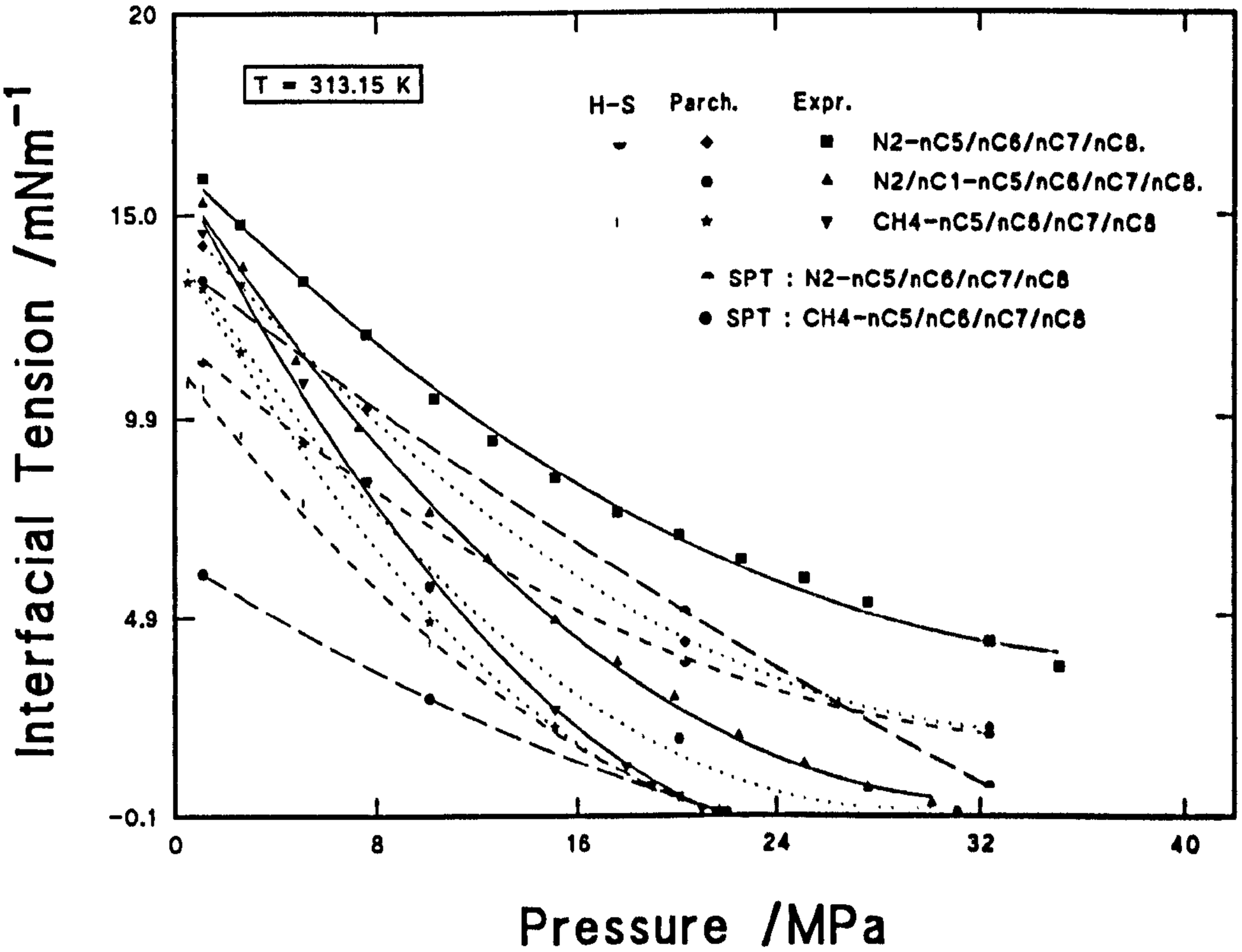

Figure 6.21. Comparison between measured IFT values for the quaternary liquid mixture with nitrogen and methane addition as a function of pressure (solid lines) and calculated IFT values from the parachor-dependent correlations (dotted lines) and the SPT (long dashed lines) .

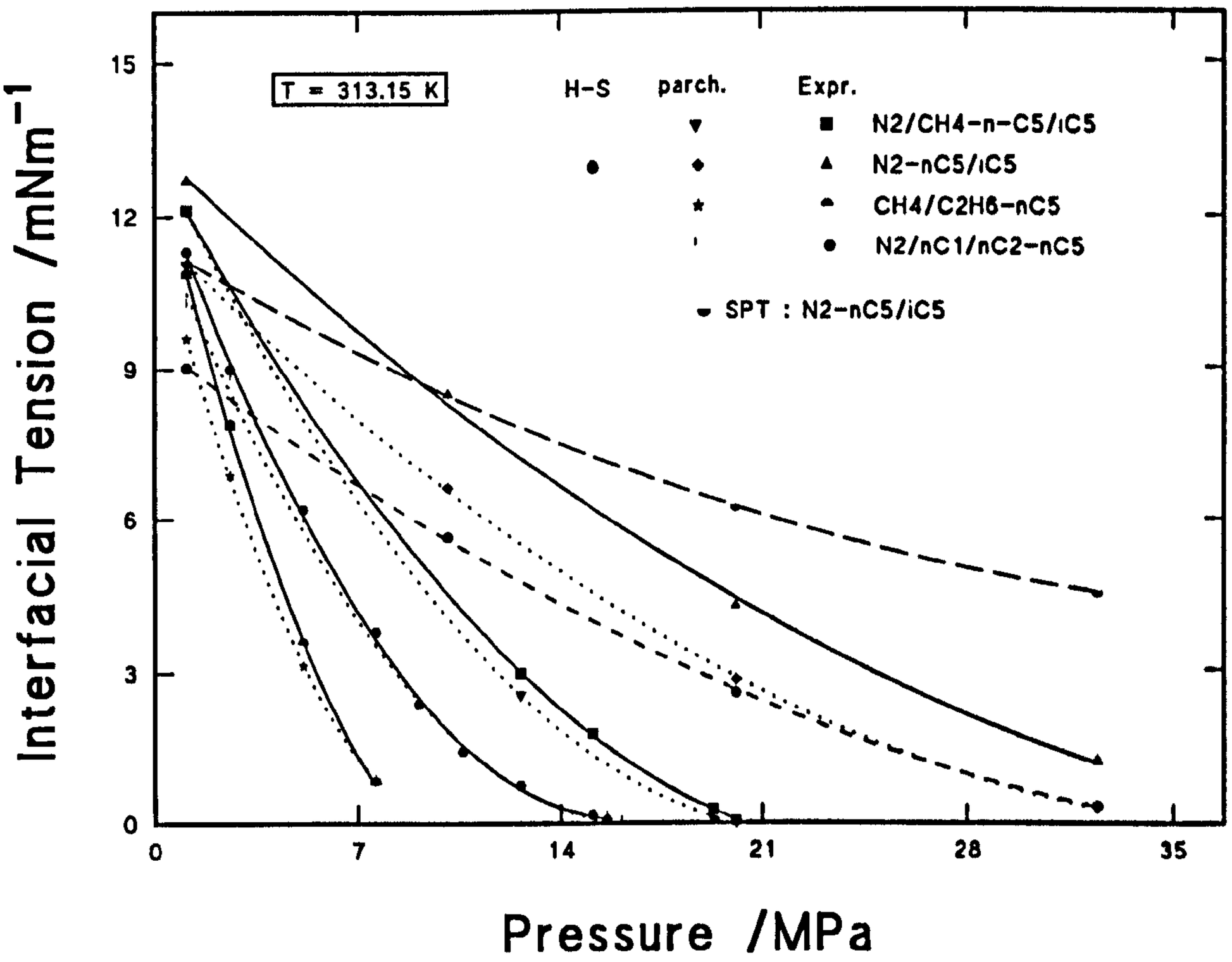

Figure 6.22. Comparison between measured IFT values for n-pentane/isopentane with nitrogen and methane addition as a function of pressure (solid lines) and calculated IFT values from the parachor-dependent correlations (dotted lines) and the SPT (long dashed lines).

with experimental data, particularly near the critical region. It was observed that for mixtures with N_2 the predictions deviate more significantly than with the rest of the gaseous mixtures. The predictions from the H-S correlation are similar to those from W-K except that they give lower values of the IFT at low and intermediate pressures.

The calculated IFT's from the W-K Parachor correlation were also compared with experimental results for the binary systems of N_2 in: n-pentane, n-hexane, n-heptane and n-octane. In the calculation, the experimental phase densities and compositions for these systems were taken from Tang and Satherley.[44] The results are shown in Figs. 6.23 and 6.24. For these systems the correlation is in good agreement with the experiment at low pressures, but deviates at high pressures giving poorer under predictions. The H-S and W-K correlations are similar at high pressures, but the H-S correlation gives even lower IFT predictions at low and intermediate pressures.

It can be concluded from the above that the W-K and H-S correlations have large deviations from the experimental data and give an underestimation of the IFT, with a percentage mean absolute deviation (MAD) between 12 to 36% [Tables 36 to 43]. In evaluating the IFT, these correlations use a mixing rule for the parachors, and therefore in general the deviation increase with number of solvent components and the complexity of the system (e.g. having polar components). The best estimations have been found for the solvent n-pentane in the four systems: N_2/nC_1-nC_5/iC_5, nC_1/nC_2-nC_5, $N_2/nC_1/nC_2$-nC_5 and N_2-nC_5 [Figs. 6.22 and 6.23]. It was also found that the deviations are highest for mixed systems with N_2 more than with the rest of gaseous mixtures [Figs. 6.20, 6.21 and 6.22]. Thus the correlations in some occasions can have a non-system dependency. Therefore, these parachor-dependent correlations, although may be useful in giving guidance to the values of the IFT, they can be unreliable for accurate estimations.

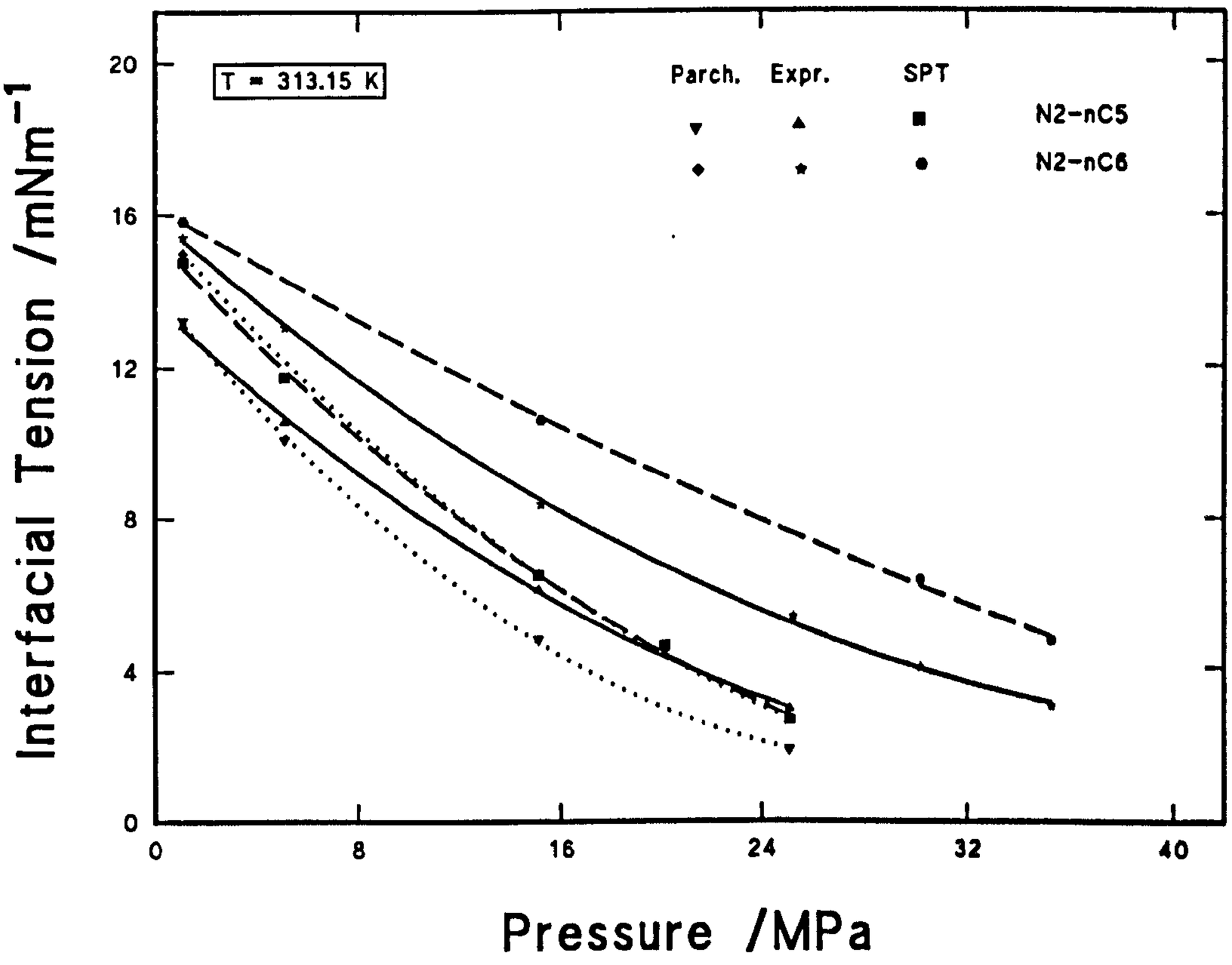

Figure 6.23. Comparison between measured IFT values for the binary systems nitrogen-n-pentane and nitrogen-n-hexane as a function of pressure (solid lines) and calculated IFT values from the parachor-dependent correlations (dotted lines) and the SPT (long dashed line).

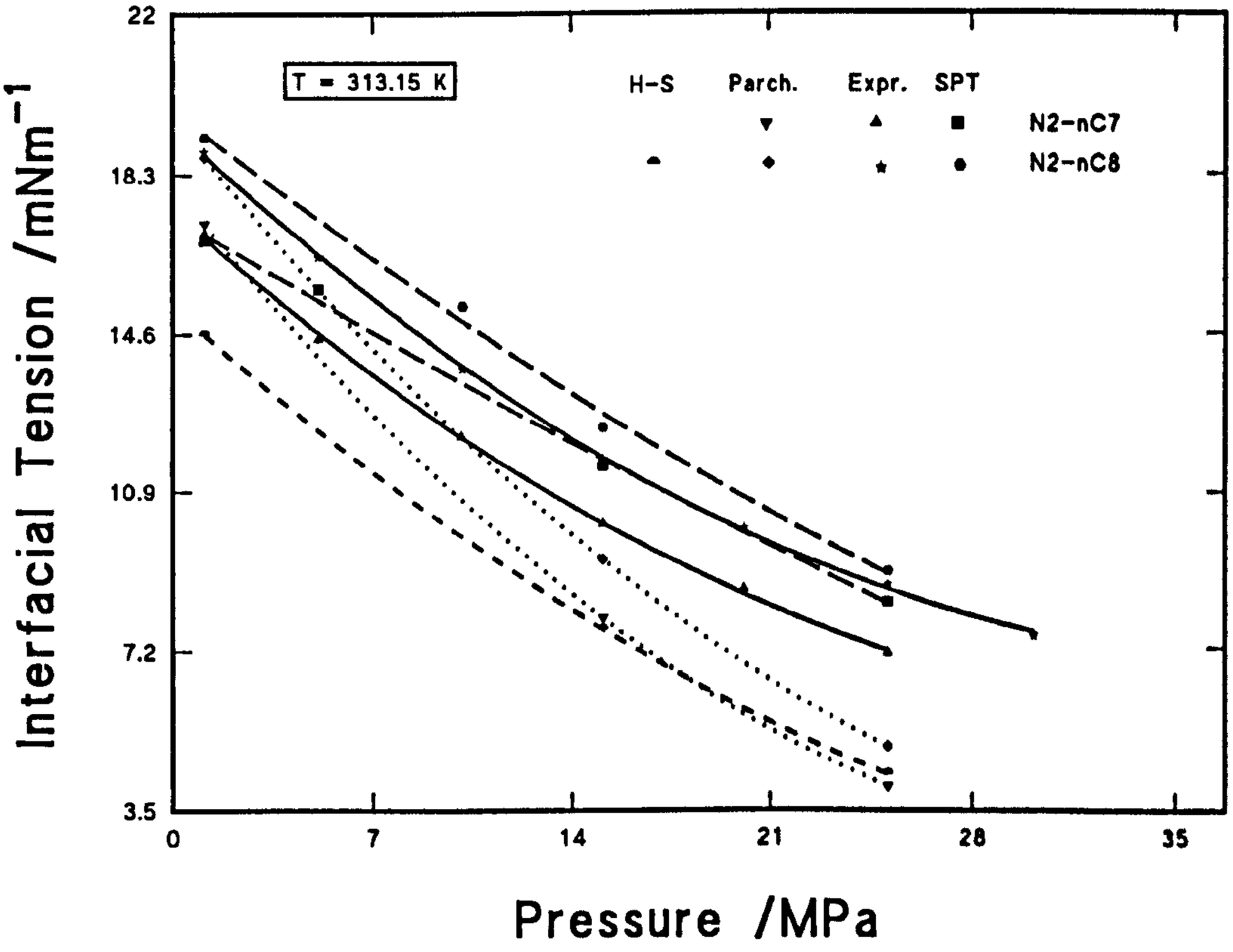

Figure 6.24. Comparison between measured IFT values for the binary systems nitrogen-n-heptane and nitrogen-n-octane as a function of pressure (solid lines) and calculated IFT values from the parachor-dependent correlations (dotted lines) and the SPT (long dashed lines).

6.3.4 IFT from SPT Expression

Figs. 6.20, 6.21 and 6.22 show the calculated values of IFT from the SPT expression [Eq.(3.25)] for N_2 in the ternary liquid mixture of nC_5+cyclohexane+toluene, in the binary liquid nC_5+iC_5 and N_2 and CH_4 in the quaternary mixture nC_5+nC_6+nC_7+nC_8 as a function of pressure. The measured phase compositions and densities were utilised throughout the calculations and the Lennard-Jones pair potentials were taken from literature (section 6.2). The calculated values show a trend of decreasing IFT values with increasing solute pressure and the IFT pressure dependency relation is slightly non-linear. As shown from the plot [Fig. 6.20] for N_2-nC_5+cyclohexane+toluene the prediction is expected to approach the experimental data near the critical point. For the binary liquid mixture nC_5+iC_5 with N_2 [Fig. 6.22] the predicted curve agrees with experimental data at low pressures. For the quaternary liquid mixture with N_2 and CH_4 [Fig. 6.21] the predictions give underestimations in the low pressure region and improves for the mixture with N_2 in the intermediate range while it matches the experiment near the critical point for the mixture with CH_4.

The IFT prediction for the ternary liquid mixture with N_2 [Fig. 6.20] deviates mostly at low pressure and gives a better prediction than the parachor correlations at high pressures. For the binary liquid mixture (nC_5/iC_5) the prediction gives better values than the parachor correlation in the low pressure region. For the quaternary liquid mixture (nC_5/nC_6/nC_7/nC_8) with N_2 the SPT prediction is better than the parachor correlations at intermediate pressures, agrees with them near the critical point for the mixture with CH_4 and deviates significantly at low pressure. For all of the above mixed systems the SPT expression gave a percentage mean absolute deviation (MAD) between 42 to 108% compared to the W-K parachor correlation of 22 to 36% [Tables 36 to 43].

In carrying out the calculations for the IFT predictions from SPT for the above systems, an adjustable molecular parameter was used for evaluating G_c in the

liquid phase [Eq.(3.10)]. An attempt was made to fit an appropriate pseudo-solute molecular diameter, $\sigma_M^v=\sigma_s$, in the liquid phase. Using 1.5 × or 1.8 × of the estimated σ_M from Eq.(3.26) gave underestimation of G_c, and thus a large deviation of IFT. It was found that the best fit is to use approximately twice the size of σ_M, which gave higher (more appropriate) estimations of G_c. This can be understood since G_c should be higher for multicomponent liquid mixtures to overcome the high attractive forces contributed from various components in the mixture, and thus an adjustable molecular parameter was used. The G_c in the vapour phase was found to be reasonably estimated from the G_c expression [Eq.(3.10)] without introducing this adjustable parameter since in this phase the attractive forces are lower than that in the liquid phase .

Looking closely at the above trend of predictions obtained using the SPT expression for IFT for two phase systems shows that for the quaternary liquid mixture the value of the interactive energy (G_i) has lowered the IFT prediction, particularly at low pressure. Another observation is that for the ternary and binary liquid mixtures the effect of G_i was not enough to lower the prediction plot close to the experimental curve. Basically, the G_i effect is expected to have a higher contribution for the ternary (polar) and binary (slightly polar) liquid mixtures than for the quaternary mixture (nonpolar). The attractive forces between nonpolar molecules are weak and the process of separating molecules from one another requires relatively less energy than that for polar molecules. A further improvement on the method of evaluation of G_i and a better understanding of the energy contributions to the process of solution in the vapour phase may lead to better predictions of the proposed expression for fluid mixtures. Another comment, is that this IFT expression from SPT is sensitive to the values of selected molecular diameters for the solute and solvents, and thus more satisfactory predictions can be obtained by manipulating and selecting the appropriate molecular values. The published Lennard-Jones pair potentials, for the various components vary from one source to another. Therefore, in carrying out the above computations, values of these molecular diameters and energy potentials were selected from accepted published values in literature (section 6.2), in order to assess the capability of the expression

regardless of any chosen values.

For the binary systems of N_2 in: n-pentane, n-hexane, n-heptane and n-octane the SPT expression [Eq.(3.25)] was used to predict the IFT values as a function of pressure. The experimental values of phase densities and compositions were taken from Tang and Satherley.[44,95] The plots have a slight non-linear relation except for the n-pentane+N_2 system where the plot shows a clear non-linear relation [Fig. 6.23 and 6.24]. Generally, for these binary systems the SPT expression predicts higher values than the experimental and seems to give good agreement at two points, at low pressure and near the critical point. These IFT predictions give better results than for the above multicomponent mixtures particularly for N_2+nC_5 system. Moreover, these predictions give a much better predictions than the parachor correlations for these systems particularly at high pressures where the parachor correlation noticeably diverges from the experimental plot [Fig. 6.23]. For these binary systems the SPT expression gave a percentage MAD ~8.7, 36.3, 9.8, and 5.5 for the N_2 binaries in nC_5, nC_6, nC_7 and nC_8 respectively, compared to W-K predictions of ~15.8, 24.7, 21.25 and 21.25 for the same systems respectively [Table 36 to 39]. The better prediction from SPT for these binary systems is attributed to the simplicity of the systems and components (being binary and nonpolar) which in turn gives more accurate estimations of G_i and G_c.

The plots of the calculated total Gibbs free energies [$(G/N_A)=(G_c+G_i)/N_A$] in the two phases [Figs. 6.25 and 6.26] approach each other in the critical region where the fluids properties become very similar. At equilibrium the interfacial tension is an energy exerted on surface area resulted from the difference of the Gibbs free energy in each phase. These Gibbs free energies decrease as a function of pressure resulting in a corresponding decrease in IFT's. Thus at the critical point ($P=P_c$ and $V=V_c$), where IFT is zero, the phase Gibbs free energies converge and become equivalent and equal to the phase equilibrium Gibbs free energy.

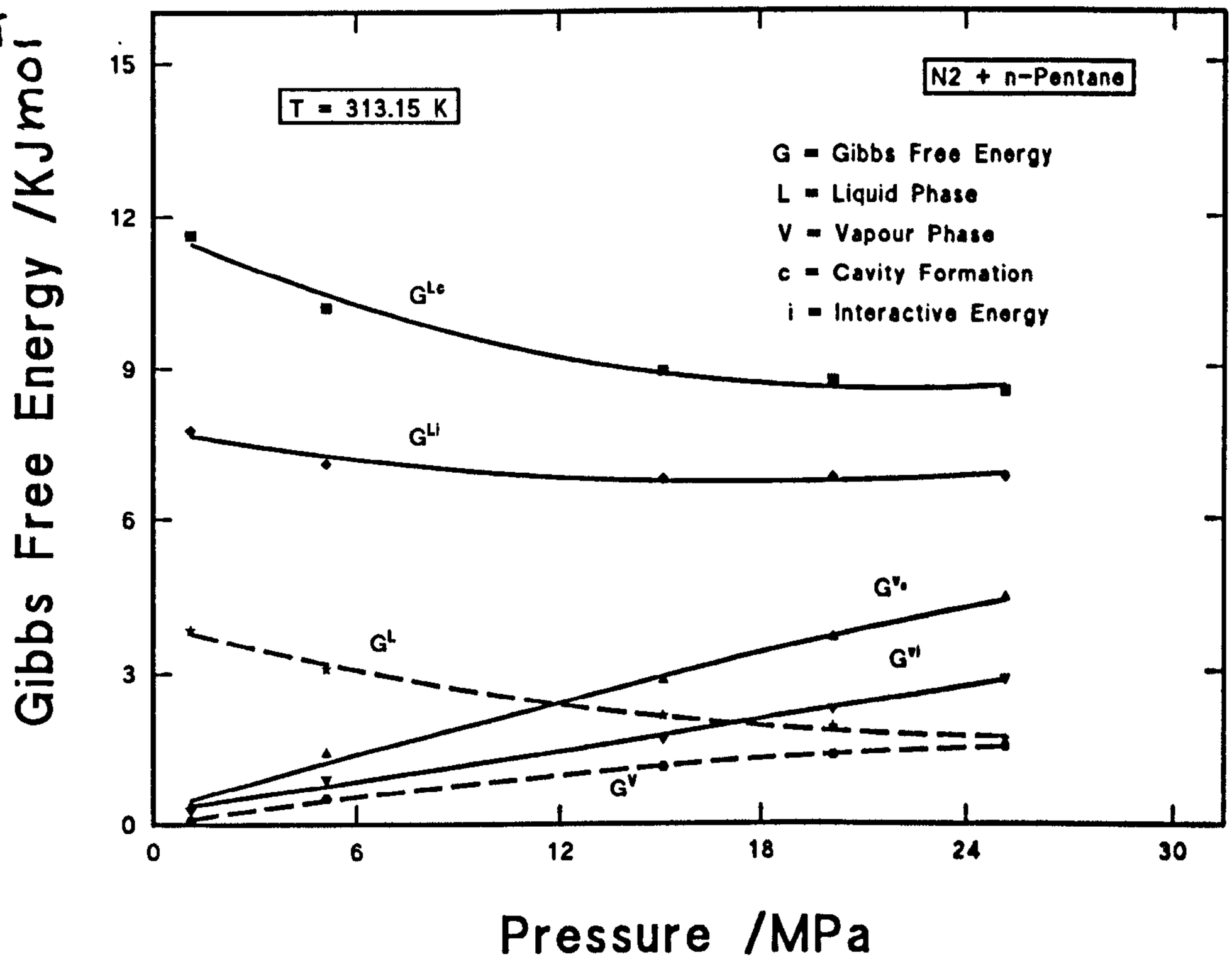

Figure 6.25. Calculated values of Gibbs free energies from SPT versus pressure for the system nitrogen-n-pentane at constant temperature.

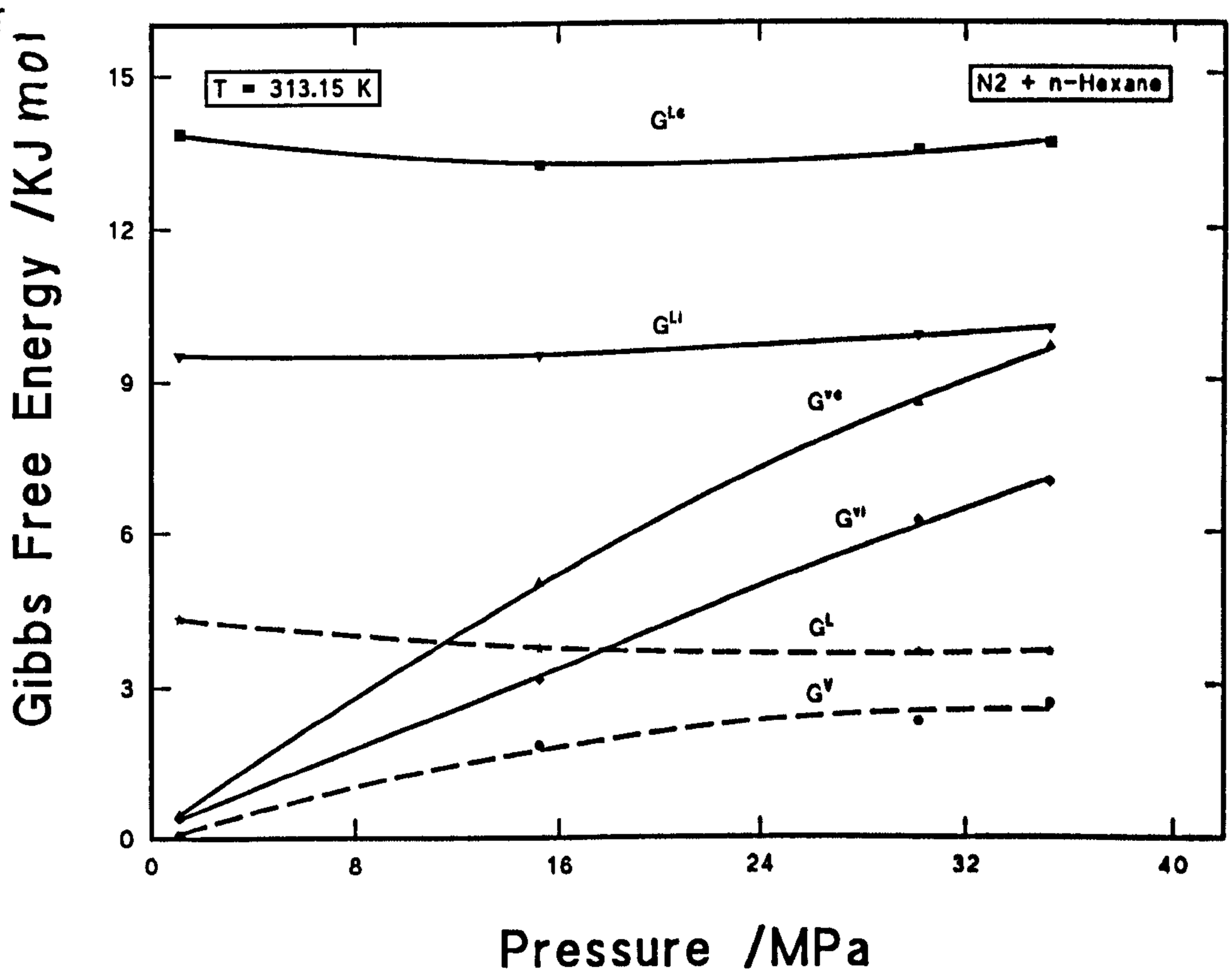

Figure 6.26. Calculated values of Gibbs free energies from SPT versus pressure for the system nitrogen-n-hexane at constant temperature.

6.3.5 Predictive Correlations for Pure Components

The experimental values of the surface tension for the pure liquids: n-pentane, n-hexane and isopentane as a function of temperature, were compared with the Macleod-Sugden expression (M-S) [Eq.(2.1)] using the experimental phase densities and literature values of the parachor (section 6.3.3). Figs. 6.27, 6.28 and 6.29 show plots of the results. The parachor ST values give a linear relation as a function of temperature, which is in good agreement with the experimental values for the three liquids examined. For these liquids the ST values were evaluated from the corresponding states correlation (CSC) [Eq.(2.10)] using critical temperatures and pressures literature.[102] As can be seen from the plots the CSC also gives good prediction with a linear relation trend but its predicted values are slightly lower than the M-S expression [Tables 44 and 45]. Although the M-S expression gives slightly better predicted ST values for these pure liquids than the CSC, the CSC can be more useful and has an advantage over the M-S model in having some theoretical basis by relating the liquid properties to its critical constants.

6.3.6 ST from the SPT

The SPT expression [Eq.(3.22)], for calculating the surface tension for a pure liquid as a function of temperature was used to predict the ST for n-pentane, n-hexane and isopentane over the measured temperature range. The measured densities at elevated temperature were used to determine the molar volumes and number densities throughout the calculations. The hard sphere diameters were taken from literature (section 6.2). Figs. 6.27, 6.28 and 6.29 and Tables 44 and 45 show the results obtained. The prediction is good and the ST values decrease linearly as a function of temperature. The prediction underestimates the ST and improves at higher temperatures particularly for n-pentane and isopentane.

The ST plots [Figs. 6.27, 6.28 and 6.29] give a linear relationship and adjust the estimation from the Reiss's relation [Eq.(3.15)], by adding an interaction energy term which resulted in shifting the prediction close to the experiment with a

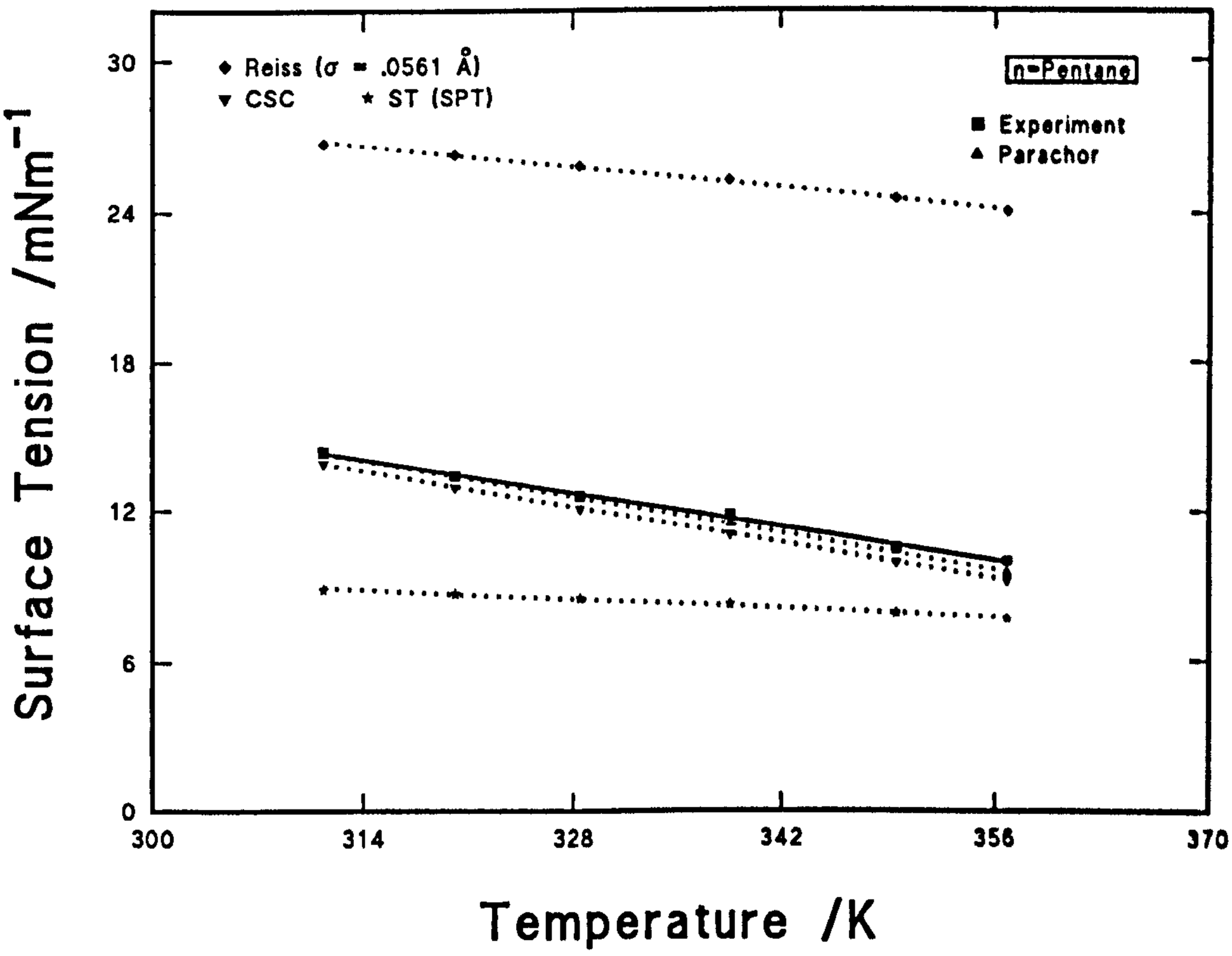

Figure 6.27. Comparison between measured surface tension of n-pentane with temperature rise (solid line) and those calculated from CSC, Reiss's expression, M-S correlation and SPT (dotted lines).

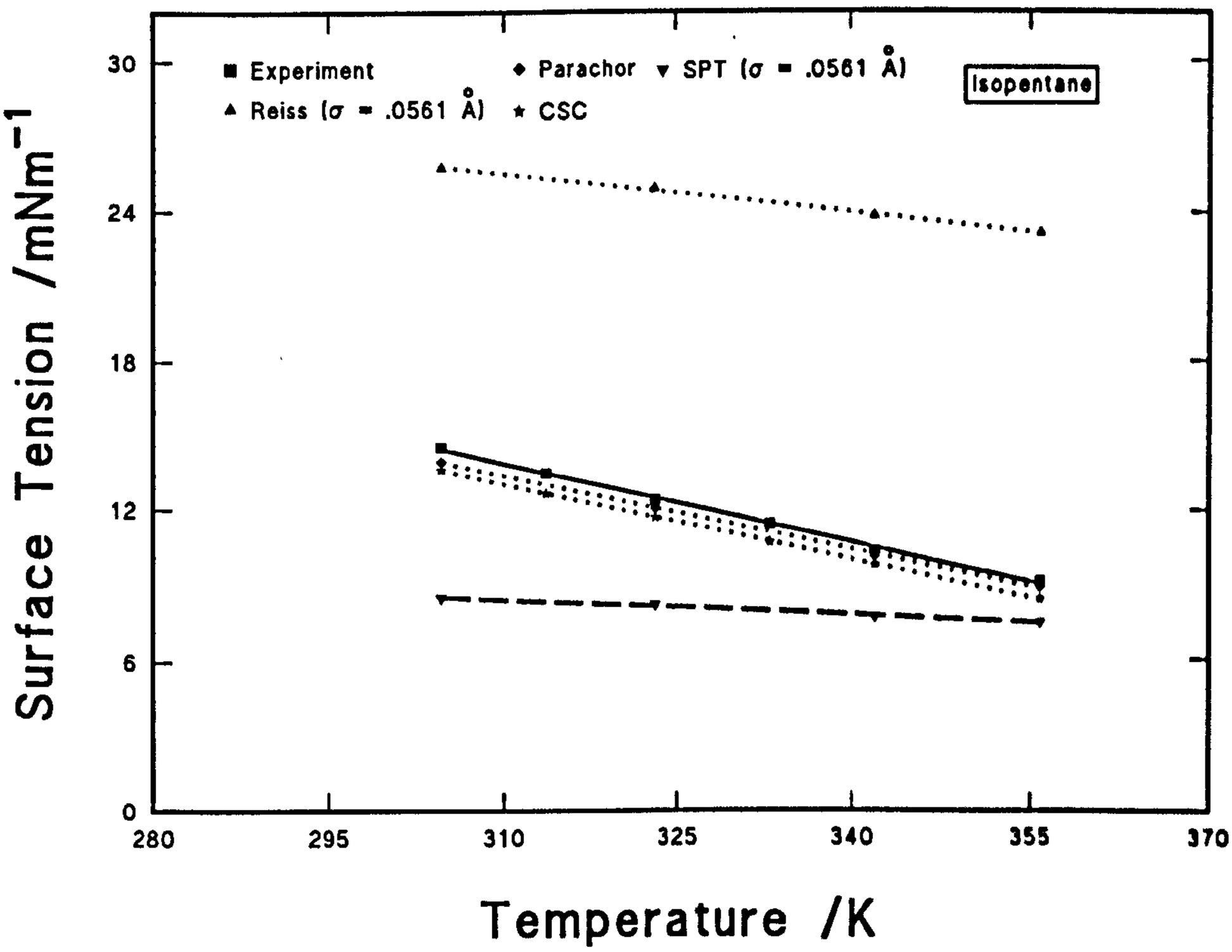

Figure 6.28. Comparison between measured surface tension of isopentane with temperature rise (solid line) and those calculated from CSC, Reiss's expression, M-S correlation (dotted lines) and SPT (dotted and dashed lines).

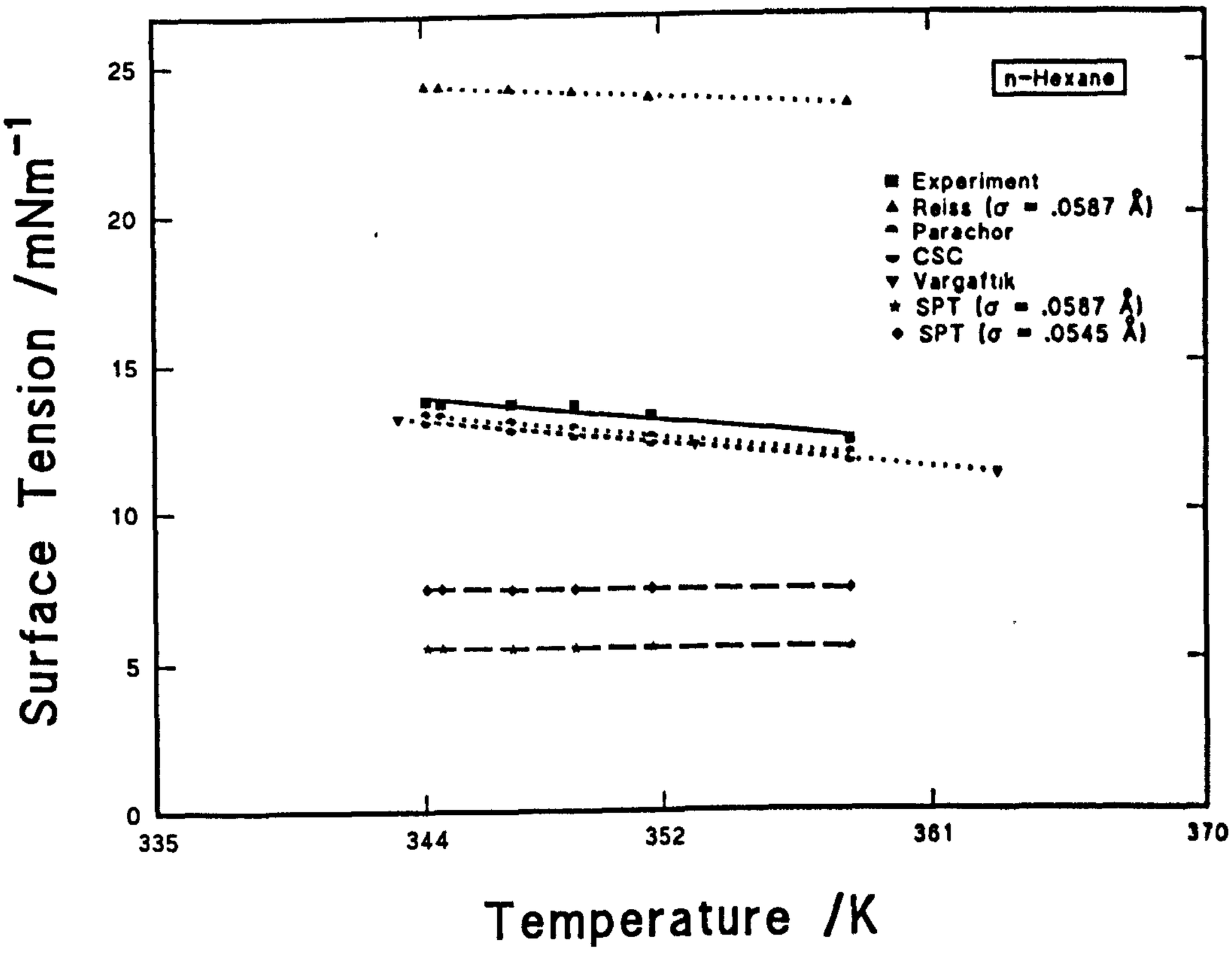

Figure 6.29. Comparison between measured surface tension of n-hexane with temperature rise (solid line) and those calculated from CSC, Reiss's expression, M-S correlation (dotted lines) and SPT (dotted and dashed lines).

percentage MAD between ~29 to 44% compared to ~79 to 116% for the Reiss's expression for these pure liquids.

Reiss expression overestimates the ST considerably for these systems. However, the inclusion of an interaction energy term reduces the predicted ST to values close to the experimental ones. For the systems studied the molecules were non-polar and consequently only the dispersion term was included in the interaction energy. This term is not temperature dependent and for a given system the quantity substracted from the Reiss expression will be a constant. This means that the temperature dependence of ST is still the same as that derived from Reiss expression. Further improvement on the expression can be made by including additional term/s to account accurately for the temperature dependence and to revaluate the G_i as it appears to be overestimated for these systems. Adjusting the appropriate molecular parameters of the liquid may also lead to better estimation of G_i.

7. CONCLUSIONS AND FURTHER WORK

A specially designed high pressure rig has been used to measure the IFT, equilibrium phase densities and phase compositions of selected model hydrocarbon systems and stocktank oil. The main aim has been to study the bulk and interfacial thermodynamic behaviour of these systems and improve the understanding of the miscibility process of nitrogen gas and light hydrocarbon gases in hydrocarbon liquids. Model systems of pure, binary, ternary, quaternary and multicomponent hydrocarbons, as well as a stocktank oil sample, have been examined as a function of pressure up to 35 MPa and temperatures up to 363 K. Compressed nitrogen gas, and mixtures of nitrogen with methane and ethane gases, were introduced into the examined systems to maintain the pressure. The emphasis on using hydrocarbon model systems has enabled the study of fluid properties over a wider range of pressures as possible within the pressure and temperature capabilities of the rig.

A significant amount of new experimental data has been obtained for these systems. The IFT, phase densities and compositions data for these systems represent measurements not previously available in the literature. The data obtained have been fitted to simple polynomial functions for interpolation.

The experimental results of IFT show a non-linear pressure dependence of IFT. In the systems examined, nitrogen+stocktank oil gave the highest IFT values and methane/ethane+n-pentane gave the lowest values.

The IFT results indicate that nitrogen gas reduces the IFT of all the systems studied as a function of pressure. The nitrogen pressure required to drive the systems to low IFT increases with n-alkane chain length and the nature of molecules in the system. The nitrogen pressure increases for the quaternary liquid mixture of n-alkanes, increases more for the ternary liquid mixture composed of n-alkane, toluene and cyclohexane and even more for the stocktank oil.

The addition of methane and/or ethane to the pressurising gas phase reduces the pressure required to reach the critical point. The measured IFT's for stocktank oil decreases with increasing nitrogen pressure, but even at 35 MPa the oil is still far from the critical point. However, by introducing methane+nitrogen to the oil, the IFT falls more sharply. The effect of methane on reducing IFT is more in the oil than in the model systems and more in the ternary liquid mixture, which includes toluene and cyclohexane, than in the other model systems. For some systems like n-pentane pressurised with methane+ethane gaseous mixture, the critical pressure can be as low as ~8 MPa.

A low IFT value of 0.0042 mNm^{-1} (± 0.0005 mNm^{-1}), at the near critical pressure of ~34 MPa, was obtained for the system N_2/CH_4-nC_5+nC_6+nC_7+nC_8 at 313.15 K. However, when the same liquid mixture of nC_5+nC_6+nC_7+nC_8 was pressurised with pure methane an IFT value of 0.0035 mNm^{-1} (± 0.0005 mNm^{-1}) was obtained at a pressure of ~23 MPa at the same temperature.

The measured ST's as a function of temperature for n-pentane, isopentane and n-hexane indicate an almost linear dependence with temperature over the examined temperature range (boiling point to ~363 K). This finding agrees with previous measurements by Jasper[32] at lower temperatures. The ST values are lowest for isopentane and highest for n-hexane.

The phase density of the measured systems increases in the order of carbon number and nature of molecules in the system. In the liquid phase the density for all systems pressurised with nitrogen has a very small positive pressure dependency and the density of the vapour phase has a high positive pressure dependence. However, the effect of adding gaseous methane or methane+ethane to the systems reduces the liquid phase density and increases the vapour phase density substantially. The density difference between the two phases decreases with solute addition until the coexisting phase densities converge near the critical region, at very low IFT values. Near the critical region the density difference is proportional linearly with the IFT with an exponent of ~3.865 and 3.873 for the quaternary n-alkanes mixture with CH_4 and

N_2+CH_4 respectively. This is in good agreement with the scaling laws of the critical theory.

Nitrogen is relatively soluble in the n-alkanes, aromatics, naphthenes and oil phases. At 35 MPa this can be as high as 78 mol% in nC_5/iC_5, 48 mol% in the quaternary n-alkanes, 40 mol% in nC_5/CH/T and 37 mol% in stocktank oil. However, at this pressure the amount of vaporised oil in the gas phase is very low. Much higher pressures are required to increase the solubility of oil in the gas phase. When using N_2/CH_4 and/or CH_4 or $CH_4+C_2H_6$ the solubility of the light components in the oil is increased and the solubility of the liquid in the gas phase is also increased. However, the rate of increase of the solubility of nitrogen gas in the liquid phase boundary is higher than the rate of solubility of the liquid in the gas phase as a function of pressure. The addition of pure methane into the quaternary n-alkanes mixture increased the solubility and reduced the critical pressure substantially from > 35 MPa by using N_2, to ~23 MPa by using CH_4.

The experimental data were compared with predictive correlations of IFT, ST, VLE and phase densities for all the measured systems. The W-K and H-S parachor-dependent correlations for evaluating IFT underestimate the experimental data with large deviations giving a percentage MAD between 12 to 36%. The correlations use a mixing rule for the parachors, and therefore, in general, the deviations increase with number of solvent components and the nature of molecules in the system (e.g. being polar or nonpolar). Moreover, the correlations have non-system dependency. Therefore these parachor-dependent correlations, although they may be useful in giving guidance to the values of IFT, can be unreliable for accurate estimations.

The M-S expression and CSC for ST have given good agreement with experimental data with a percentage MAD of 1.7 to 4.5% and 5 to 6.4% respectively. Although the M-S expression gives slightly better predicted ST values for the three liquids examined than the CSC, the CSC is more useful and has an advantage over the M-S model in having some theoretical basis by relating the liquid

properties to its critical constants. The Reiss expression for ST of pure liquids overestimates the ST considerably for the examined systems over the range of temperature studied with percentage MAD of 79 to 116%. The expression appears to be useful for predicting ST at near ambient condition.

The EXCS and PR EOS for phase densities and phase compositions predictions have shown good comparison with experimental data with slight overestimation of these phase properties for most of the systems. The predictions are most accurate at well below the critical point. The EXCS is in very good agreement with experimental data for pure liquids and gases. For mixtures near the critical point, predictions of phase densities and phase compositions from both correlations always have been found to be higher than the experimental data. This trend agrees with the finding of Prausnitz[2] for other systems. This is attributed to the fact that the EXCS and PR EOS determine the critical constants T_c and P_c for the mixed systems from a mixing rule which may lead to uncertainty of these values in the critical region. These estimated critical constants are also used in the PR EOS to determine its constants and binary parameters [Eq.(2.3)] adding a further uncertainty in prediction. However, as a general recommendation the EXCS and PR EOS for these mixed systems and those similar to them, provide useful phase density and VLE predictions with small deviations particularly at pressures below the critical pressure. This deviation is dependent on the number of components and complexity of the system.

The predicted values of Henry's Law constant (K_H) from the SPT applied to the bubble point curves for the solubility of N_2 and CH_4 in the hydrocarbons have shown good agreement with experimental data for most of the systems studied. For two of the systems: N_2-nC_5+nC_6+nC_7+nC_8 and CH_4-nC_5+nC_6+nC_7+nC_8 the predictions are slightly better than those obtained from PR EOS at low pressure. The result of the assessment of K_H from SPT highlights the capability of this theory even for mixed systems. However, the K_H expression is sensitive to the chosen hard sphere diameter and thus the possible uncertainty of the results must be carefully assessed.

An attempt to develop an IFT and ST expression have been made in this work. Two expressions have been introduced. A ST expression has been extended from the Reiss's expression for the surface tension of pure liquids, and an IFT expression has been derived based on one-fluid theory and SPT for two-phase mixed systems. The calculated values from these two expressions have been compared with the experimental data and a good trend of prediction has been demonstrated particularly for pure and binary systems. For mixed systems the percentage MAD for the IFT expression from experimental data has been between 42 to 108% compared to the W-K parachor correlation of 22 to 36%. For the binary systems the IFT expression from SPT [Eq.(3.25)] has shown much better predictions and comparatively far more accurate than the parachor correlations, particularly at high pressures where the parachor correlation largely diverges from experimental results. The best binary system prediction has given a percentage MAD of ~5.5% compared to 21.25% with the parachor prediction for the same system. The ST expression has allowed the extension of prediction to higher temperatures (up to 363 K) for the systems studied with a percentage MAD between ~29 to 44% compared to ~79 to 116% for the Reiss's expression. However, the above expressions are sensitive to the values of selected hard sphere molecular diameters for the solute and the solvents, and thus the prediction can be adjusted by manipulating and selecting the appropriate values of these hard sphere diameters.

The results of the experimental data indicate that nitrogen can be used in oil production for pressure maintenance, gas flooding, and other improved oil recovery processes as it will add benefits mainly in lowering the oil-gas IFT, the liquid phase density and the critical pressure. However, the critical pressure is still high by reservoir standards. It would be advantageous to use nitrogen in high pressure reservoirs and gaseous mixtures of N_2/CH_4 and/or C_2H_6 in low pressure, high viscosity reservoirs in IOR processes.

Since nitrogen has a relatively high solubility in the oil liquid phase this assists in causing swelling and dislodgement of oil in the capillary pores. Although the required pressures to make an optimum effective use of nitrogen are relatively

high by reservoirs operating conditions, by adding light hydrocarbon gases like methane to the pressurising gas in a flooding process, all the above features are enhanced and the critical pressures are reduced compared with using nitrogen alone. Moreover, the effect would increase the mutual solubility of the gas and oil phases. It would also improve recovery both from the liquid phase due to the high nitrogen solubility causing trapped oil volume swelling and an appreciable reduction of the IFT, and from the gas phase, due to evaporated hydrocarbons being recovered in subsequent stages of production.

Further work is suggested on the experimentation of model hydrocarbon systems including more complicated mixtures of compounds with n-alkanes, such as the isomers, aromatics, cycloaliphatics, alkenes, alkynes in various complex mixtures. In addition to model hydrocarbon systems, measurements can be made on oil samples for comparison, and also on the effect of resins-asphaltenes. Since light hydrocarbons like CH_4, have shown favourable trends as a gas drive, a further study on this application as well as with CO_2 should be carried out. These suggested measurements, in addition to their practical application, have a thermodynamic-theoretical interests.

From the point of view of developing and further assessing SPT for IFT and ST predictions, it is recommended that the proposed theoretical expressions be further tested with experimental data for pure and mixed systems up to and including the critical point. In general, the testing of the ST expression has shown an overestimation of G_i for nonpolar liquids. The IFT expression has also shown inaccuracy for estimating G_i. A further improvement on the method of evaluation of the interaction energy, G_i, and a better understanding of the energy contributions in the process of solution of fluid mixtures to account for polar and nonpolar systems may lead to better predictions in the proposed expressions. For the ST expression an additional term which is temperature dependent should adjust the prediction trend more accurately.

The SPT is based on certain assumptions thermodynamically attributed to

simple fluids. Research on methods of evaluation of these assumptions may lead to extend the applicability of the theory to more complex mixtures. Thus, further studies such as solution molecular dynamics-behaviour, better determination of the pair potential energy parameters, testing the IFT expression by using other than the Lennard-Jones molecular-energy potential models (e.g. square-well model), and molecular shape studies etc. are recommended.

In general, research on developing methods and theories, which are based on physical fundamentals and matching with experimental observations for better understanding and prediction of interfacial tension and related properties are needed.

For optimal oil recovery processes it is advantageous to have the fluid above its critical point. However, in practice this is not an easy task to achieve. In a recovery process it is common that water and/or gas are used for pressure maintenance and flooding processes, hence multi-phase flow behaviour coexist in the reservoir media. Further work on the prediction of two-phase flow behaviour in porous media is an important area of research in this context. Measured values of the gas-liquid two-phase systems can be utilised to investigate the prediction of the flow behaviour in the reservoir capillaries. The measured IFT and equilibrium phase properties can be used to determine the relative permeabilities and capillary pressures.

APPENDIX - TABLES OF EXPERIMENTAL RESULTS

In the following tables the units used are as below:

P	MPa
T	K
γ	mNm^{-1}
ρ	$Kg\ m^{-3}$
ϵ/k	K
σ	Å

Table 1. A and B instrument constants determined from calibration of the Density Meter within a tolerence of ± 0.00005.

P/MPa	A	B
0.10	4.53013	30.51167
1.10	4.52988	30.51348
2.60	4.53027	30.51436
5.10	4.53041	30.51655
7.60	4.53194	30.51742
10.10	4.53251	30.51911
12.60	4.53365	30.52023
15.10	4.53469	30.52144
17.60	4.53511	30.52320
20.10	4.53583	30.52447
22.60	4.53653	30.52646
25.10	4.53696	30.52830
27.60	4.53787	30.52994
30.10	4.53840	30.53109
32.60	4.53979	30.53276
35.10	4.53967	30.53441

Table 2. Calibration of density meter using pure nitrogen as a function of temperature.

(313.55 K)		(323.833 K)	
P /MPa	τ /s	P /MPa	τ /s
0.107032	5.52460	0.105424	5.53657
0.117335	5.52465	0.109440	5.53660
0.139200	5.52474	0.122348	5.53664
0.162800	5.52484	0.143360	5.53674
0.180760	5.52493	0.160860	5.53680
0.208463	5.52506	0.186590	5.53693
0.222190	5.52512	0.211714	5.53704
0.234028	5.52510	0.245361	5.53718
0.255427	5.52525	0.303143	5.53744
0.292717	5.52542	0.351860	5.53764
0.321150	5.52553	0.401030	5.53786
0.353636	5.52570	0.439096	5.53802
0.403855	5.52590	0.497296	5.53827
0.453260	5.52611		
0.497420	5.52631		

Table 3. Calibration of density meter using pure nitrogen as a function of temperature.

(333.718K)		(344.257K)	
P /MPa	τ /s	P /MPa	τ /s
0.106725	5.54821	0.105847	5.56074
0.141256	5.54835	0.123085	5.56080
0.164240	5.54845	0.162915	5.56093
0.185880	5.54854	0.232917	5.56122
0.211058	5.54865	0.315910	5.56155
0.252460	5.54882	0.366330	5.56176
0.289224	5.54895	0.408499	5.56194
0.343640	5.54918	0.440140	5.56204
0.411140	5.54947	0.500607	5.56230
0.459311	5.54966		
0.505000	5.54986		

Table 4. Calibration of density meter using pure nitrogen as a function of temperature.

(353.03K)		(361.89K)		(302.63K)	
P /MPa	τ /s	P /MPa	τ /s	P /MPa	τ /s
0.10685	5.57127	0.10515	5.58201	0.105989	5.51210
0.13342	5.57136	0.11975	5.58205	0.181670	5.51230
0.19764	5.57150	0.14468	5.58212	0.205936	5.51236
0.24956	5.57180	0.17824	5.58226	0.216272	5.51240
0.31790	5.57200	0.29012	5.58268	0.244490	5.51250
0.36277	5.57224	0.37472	5.58300	0.254517	5.51258
0.41451	5.57239	0.41797	5.58314	0.286388	5.51273
0.49778	5.57273	0.49756	5.58346	0.317518	5.51290
				0.336820	5.51300
				0.355138	5.51304
				0.383959	5.51316
				0.414782	5.51331
				0.439004	5.51341
				0.469646	5.51353
				0.499924	5.51367

Table 5. Calibration of density meter using triply distilled water as a function of temperature and pressure.

(303.029 K)		(313.405 K)	
P /MPa	τ /s	P /MPa	τ /s
0.50334	5.90536	0.48759	5.91703
0.43263	5.90535	0.44439	5.91702
0.39222	5.90534	0.38461	5.91700
0.33402	5.90533	0.32554	5.91699
0.27182	5.90532	0.23483	5.91697
0.22843	5.90531	0.16450	5.91696
0.16586	5.90530	0.12470	5.91695
0.12533	5.90530	0.10336	5.91694
0.10382	5.90529		

Table 6. Calibration of density meter using triply distilled water as a function of temperature and pressure.

(324.232 K)		(333.719 K)	
P /MPa	τ /s	P /MPa	τ /s
0.502200	5.92900	0.49833	5.93933
0.402034	5.92899	0.38290	5.93933
0.359275	5.92897	0.31503	5.93932
0.279790	5.92896	0.19883	5.93930
0.168740	5.92893	0.14250	5.93928
0.118500	5.92893	0.11789	5.93928
0.103810	5.92892	0.10381	5.93928

Table 7. Calibration of density meter using triply distilled water as a function of temperature and pressure.

(343.93K)		(353.031K)		(361.72K)	
P /MPa	τ /s	P /MPa	τ /s	P /MPa	τ /s
0.50174	5.95038	0.49610	5.96011	0.49419	5.96938
0.41870	5.95036	0.37995	5.96009	0.40220	5.96936
0.36306	5.95035	0.29053	5.96007	0.33009	5.96935
0.29185	5.95033	0.21636	5.96006	0.24040	5.96932
0.19260	5.95031	0.15551	5.96006	0.17220	5.96930
0.12885	5.95029	0.12863	5.96005	0.12885	5.96929
0.10427	5.95029	0.10598	5.96005	0.10381	5.96929

Table 8. MRF values obtained from GC calibration for different components used in the measured systems.

Component	MRF/10^{11}/(area mol^{-1})
Nitrogen	0.38050*
	0.27703[1]
	0.30840[2]
Methane	0.41030*
	0.54552[1]
	0.32780[2]
Ethane	0.52610*
n-Pentane	1.49200*
	1.03560[1]
Isopentane	0.76021[2]
n-Hexane	1.65130*
	1.17995[1]
	0.80417[2]
n-Heptane	1.78200*
	1.33590[1]
n-Octane	1.84970*
	1.47931[1]
Cyclohexane	1.07708[1]
Toluene	1.12890[1]

* GC injection column temperature (C.T.) 313.15 K.
1 After conditioning the injection valve. GC C.T. 453.15 K.
2 After conditioning the injection valve. GC C.T. 333.15 K.

Table 9. Compositional analysis of stocktank oil sample.

WESTERN ATLAS

Core Laboratories
Advanced Technology Centre

Texaco Limited

File : RFLA 940203

Well : 23/26b-15

Compositional Analysis by Gas Chromatography

Component	Mole%	Weight%
Methane	0.02	0.00
Ethane	0.11	0.02
Propane	0.51	0.13
i-Butane	0.30	0.10
n-Butane	1.25	0.41
Neo-Pentane	0.00	0.00
i-Pentane	1.21	0.49
n-Pentane	1.92	0.77
Hexanes	4.56	2.20
M-C-Pentane	1.43	0.68
Benzene	1.10	0.48
Cyclohexane	1.78	0.84
Heptanes	5.49	3.09
M-C-Hexane	3.32	1.83
Toluene	3.33	1.72
Octanes	6.66	4.28
E-Benzene	0.53	0.31
M/P-Xylene	3.03	1.80
O-Xylene	0.96	0.57
Nonanes	5.65	4.06
T-M-Benzene	0.91	0.62
Decanes	6.60	5.26
Undecanes	5.70	4.69
Dodecanes	4.73	4.26
Tridecanes	4.55	4.46
Tetradecanes	3.67	4.12
Pentadecanes	3.67	4.24
Hexadecanes	2.84	3.54
Heptadecanes	2.49	3.31
Octadecanes	2.36	3.32
Nonadecanes	2.14	3.15
Eicosanes	1.72	2.65
Heneicosanes	1.54	2.51
Docosanes	1.36	2.32
Tricosanes	1.22	2.18
Tetracosanes	1.06	1.96
Pentacosanes	0.96	1.86
Hexacosanes	0.85	1.71
Heptacosanes	0.75	1.58
Octacosanes	0.66	1.43
Nonacosanes	0.58	1.31
Triacontanes Plus	6.28	15.74
Totals	100.00	100.00

Measured Properties		
Whole Sample Density	0.8120	grams/cc @ 60°F
Whole Sample Molecular Weight	178	grams/mole

Calculated Properties		
	Density grams/cc @ 60°F	Mole Weight grams/mole
Heptanes Plus Fraction	0.8220	190
Undecanes Plus Fraction	0.8511	255
Eicosanes Plus Fraction	0.8797	371
Triacontanes Plus Fraction	0.8801	448

Table 10. Measured phase compositions (mole fractions) of methane/ethane as pseudo-component in n-pentane as a function of pressure at 313.15 K.

P/MPa	x	x'
1.1	0.136	0.685
2.6	0.284	0.875
5.1	0.484	0.957
7.6	0.677	0.982
8.1	0.989	0.992

Table 11. Measured phase compositions (mole fractions) for $N_2/CH_4/C_2H_6$ as a pseudo-component in n-pentane as a function of pressure at 313.15 K.

P/MPa	x	x'
1.1	0.072	0.816
1.1	0.071	0.884
2.6	0.146	0.787
2.6	0.145	0.826
2.6	0.145	0.826
5.1	0.289	0.887
5.1	0.291	0.882
7.6	0.403	0.902
7.6	0.403	0.898
7.6	0.404	0.898
9.1	0.432	0.939
9.1	0.429	0.942
9.1	0.429	0.942
10.6	0.479	0.837
10.6	0.482	0.853
10.6	0.479	0.856
12.6	0.551	0.896
12.6	0.555	0.903
15.1	0.629	0.915
15.1	0.636	0.876
15.1	0.629	0.913
15.1	0.636	0.913
16.1	0.739	0.869
16.1	0.748	0.877

Table 12. Measured phase compositions (mole fractions) for nitrogen-n-pentane/n-hexane/n-heptane/n-octane as a function of pressure at 313.15 K.

P/MPa	x	x'
1.10	0.029	0.953
7.60	0.156	0.979
20.35	0.332	0.987
32.35	0.457	0.984

Table 13. Measured phase compositions (mole fractions) for N_2+CH_4 as pseudo-component in n-pentane/n-hexane/n-heptane/n-octane as a function of pressure at 313.15 K.

P/MPa	x	x'
1.1	0.035	0.935
5.1	0.139	0.975
10.1	0.255	0.976
17.6	0.410	0.966
20.1	0.472	0.943
27.6	0.603	0.923
30.1	0.652	0.891
31.1	0.694	0.874

Table 14. Measured phase compositions (mole fractions) for methane-n-pentane/n-hexane/n-heptane/n-octane as a function of pressure at 313.15 K.

P/MPa	x	x'
0.50	0.031	0.896
1.10	0.042	0.913
2.60	0.091	0.943
5.10	0.181	0.962
10.10	0.334	0.968
15.10	0.473	0.958
17.95	0.552	0.934
19.00	0.586	0.926
20.10	0.628	0.905
21.00	0.663	0.869
21.50	0.694	0.863
21.70	0.694	0.848
22.00	0.809	0.832

Table 15. IFT and Phase density measurements for the system methane/ethane-n-pentane as a function of pressure at 313.15 K.

P/MPa	γ/mNm^{-1}	ρ_L/kgm^{-3}	ρ_v/kgm^{-3}
1.1	10.880	580.44	38.80
2.6	7.860	545.00	47.60
5.1	3.590	498.80	79.40
7.6	0.820	411.00	112.00
8.1	0.127	394.30	127.00

Table 16. IFT and phase density measurements for the system nitrogen/methane/ethane-n-pentane as a function of pressure at 313.15 K.

P/MPa	γ/mNm^{-1}	ρ_L/kgm^{-3}	ρ_v/kgm^{-3}
0.1	12.600	603.26	34.70
1.1	11.300	594.60	42.50
2.6	9.000	582.20	53.16
5.1	6.200	554.63	81.43
7.6	3.800	525.00	114.00
9.1	2.400	500.00	133.20
10.6	1.450	478.00	150.00
12.6	0.770	454.00	186.00
15.1	0.170	400.00	240.00
15.6	0.075	384.00	260.00
16.1		358.80	287.00

Table 17. IFT and phase density measurements for the system nitrogen-n-pentane/n-hexane/n-heptane/n-octane as a function of pressure at 313.15 K.

P/MPa	γ/mNm^{-1}	P/MPa	ρ_L/kgm^{-3}	ρ_v/kgm^{-3}
1.1	15.94	1.1	651.00	34.20
2.6	14.77	2.6	650.80	51.60
5.1	13.32	5.1	650.80	70.90
7.6	12.00	7.6	650.90	95.70
10.3	10.40	10.3	651.50	135.00
12.6	9.35	12.6	650.70	162.00
15.1	8.40	15.1	650.30	190.00
17.6	7.52	17.6	650.80	207.40
20.1	6.92	20.1	651.23	236.60
22.6	6.30	22.6	651.05	242.50
25.1	5.80	25.1	651.37	274.00
27.6	5.20	27.6	652.18	286.50
32.35	4.24	29.85	653.40	318.00
35.1	3.60	31.25	654.05	331.40
		32.35	663.12	336.00
		35.1	654.00	360.00

Table 18. IFT and phase density measurements for the system N_2/CH_4-n-pentane/n-hexane/n-heptane/n-octane as a function of pressure at 313.15 K.

P/MPa	γ/mNm^{-1}	ρ_L/kgm^{-3}	ρ_v/kgm^{-3}
1.1	15.31	647.0	34.5
2.7	13.68	639.0	46.0
4.8	11.35	634.0	65.0
7.3	9.67	619.9	87.0
10.1	7.53	611.3	119.0
12.4	6.35	604.4	133.4
15.1	4.81	589.0	160.0
17.6	3.74	579.0	179.0
19.9	2.89	570.0	201.3
22.5	1.90	555.0	234.0
25.1	1.20	542.0	264.0
27.6	0.61	523.0	298.8
30.1	0.22	503.0	330.0
33.5	0.0042	453.0	370.0

Table 19. IFT and phase density measurements for methane-n-pentane/n-hexane/n-heptane/n-octane as a function of pressure at 313.15 K.

P/MPa	γ/mNm^{-1}	P/MPa	ρ_L/kgm^{-3}	ρ_v/kgm^{-3}
1.10	14.57	0.50	646.60	28.66
2.60	13.23	1.10	644.48	28.44
5.10	10.79	2.60	634.66	38.38
7.60	8.34	5.10	617.15	49.30
10.10	5.66	10.10	578.35	89.34
15.10	2.61	15.10	530.71	145.67
17.95	1.18	17.95	493.80	174.14
19.00	0.68	19.00	481.50	194.93
20.10	0.42	20.10	457.05	218.49
21.00	0.081	21.00	429.45	252.80
21.50	0.045	21.50	411.00	267.50
21.70	0.042	22.00	376.60	314.30
21.85	0.025			
22.00	0.0035			

Table 20. IFT and phase density measurements for nitrogen-stocktank oil as a function of pressure at 313.15 K.

P/MPa	γ/mNm^{-1}	P/MPa	ρ_L/kgm^{-3}	ρ_v/kgm^{-3}
0.10	22.89	0.10	795.2	47.40
1.10	22.32	1.10	798.9	52.00
2.70	21.00	2.70	797.5	64.00
5.10	20.20	5.10	800.0	74.70
10.10	17.74	10.10	800.0	118.50
15.25	15.51	12.40	796.2	142.00
19.90	14.21	15.25	798.5	182.00
25.70	12.34	19.90	800.8	227.50
29.90	11.75	22.50	796.6	264.00
35.10	11.40	25.70	811.0	279.70
		29.90	810.8	297.50
		35.10	809.8	326.05

Table 21. IFT and phase density measurements for N_2/CH_4-stocktank oil as a function of pressure at 313.15 K.

P/MPa	γ/mNm^{-1}	ρ_L/kgm^{-3}	ρ_v/kgm^{-3}
1.1	21.55	793.30	46.3
2.5	19.97	789.50	51.0
5.1	17.69	784.70	55.7
7.6	15.67	781.60	77.7
10.1	13.95	773.70	92.1
15.0	11.23	762.90	133.0
17.6	9.95	762.09	155.3
20.1	8.27	755.80	186.0
22.6	7.55	752.20	210.0
25.1	6.54	748.88	235.0
27.5	5.87	746.30	255.0
30.1	4.88	744.30	274.0
32.6	4.51	740.80	290.5
35.0	4.32	739.50	310.0

Table 22. IFT and phase density measurements for nitrogen-n-pentane/isopentane as a function of presssure at 313.15 K.

P/MPa	γ/mNm^{-1}	ρ_L/kgm^{-3}	ρ_v/kgm^{-3}
1.1	12.72	601.64	40.02
10.1	8.49	597.80	116.46
20.1	4.25	592.75	223.45
32.4	1.23	570.94	363.88

Table 23. IFT and phase density measurements for N_2/CH_4-n-pentane/isopentane as a function of pressure at 313.15 K.

P/MPa	γ/mNm^{-1}	P/MPa	ρ_L/kgm^{-3}	ρ_v/kgm^{-3}
1.1	12.13	1.1	598.65	18.00
12.6	2.99	5.2	582.00	70.00
15.1	1.80	12.6	523.79	141.66
19.3	0.27	15.1	498.03	170.57
20.1	0.049	19.3	393.00	249.68
		20.1	331.00	267.40

Table 24. IFT and phase density measurements for N_2-n-pentane/cyclohexane/toluene as a function of pressure at 313.15 K.

P/MPa	γ/mNm^{-1}	ρ_L/kgm^{-3}	ρ_v/kgm^{-3}
1.1	17.66	723.75	44.99
10.1	12.71	723.58	149.80
20.1	9.21	724.08	228.15
32.6	5.89	727.12	339.34

Table 25. IFT and phase density measurements for N_2/CH_4-n-pentane/cyclohexane/toluene as a function of pressure at 313.15 K.

P/MPa	γ/mNm^{-1}	P/MPa	ρ_L/kgm^{-3}	ρ_v/kgm^{-3}
1.20	16.85	1.20	718.72	35.30
12.65	7.65	5.10	700.83	77.30
27.60	1.38	12.65	667.89	130.13
32.30	0.49	20.30	638.46	189.77
		27.60	599.03	276.85
		32.30	572.50	316.28

Table 26. IFT and phase density measurements for N_2-n-pentane/cyclohexane/toluene, with higher amount of cyclohexane, as a function of pressure at 313.15 K.

P/MPa	γ/mNm^{-1}	ρ_L/kgm^{-3}	ρ_v/kgm^{-3}
1.10	17.45	713.91	56.08
10.10	12.65	714.48	143.35
20.00	8.79	713.69	238.60
32.45	5.56	715.34	342.80

Table 27. IFT and phase density measurements for N_2-n-pentane/cyclohexane/toluene, with higher amount of toluene, as a function of pressure at 313.15 K.

P/MPa	γ/mNm^{-1}	ρ_L/kgm^{-3}	ρ_v/kgm^{-3}
1.20	17.98	734.07	44.75
10.70	12.76	735.60	150.85
19.80	9.54	735.38	237.75
32.55	5.95	737.75	340.68

Table 28. Surface tension and phase density measurements for n-pentane as a function of temperature.

T/K	γ/mNm^{-1}	ρ_L/kgm^{-3}	ρ_v/kgm^{-3}
311.336	14.38	607.830	3.282
320.088	13.41	598.880	3.898
328.459	12.61	589.760	4.240
338.588	11.83	578.699	6.368
349.585	10.54	565.930	7.862
356.834	9.97	557.490	11.353

Table 29. Surface tension and phase density measurements for isopentane as a function of temperature.

T/K	γ/mNm^{-1}	ρ_L/kgm^{-3}	ρ_v/kgm^{-3}
304.650	14.52	607.11	3.423
313.650	13.50	598.25	4.532
323.120	12.38	587.99	5.940
333.100	11.39	576.76	7.788
341.970	10.32	566.44	9.769
355.877	9.08	552.31	13.731

Table 30. Surface tension and phase density for n-hexane as a function of temperature.

T/K	γ/mNm^{-1}	ρ_L/kgm^{-3}	ρ_v/kgm^{-3}
344.073	13.78	611.01	3.435
344.566	13.70	610.49	3.479
346.902	13.68	608.42	3.721
349.043	13.61	605.96	3.964
351.649	13.26	602.41	4.266
358.336	12.36	596.07	5.120

Table 31. Coefficients in the equation $\gamma/mNm^{-1} = a\ (P/MPa)^2 + b\ (P/MPa) + c$, valid for IFT values up to 35 MPa at 313.15 K.

System.	a	b	c
$N_2/nC_1/nC_2$-n-pentane.	0.048615	-1.577	12.8558
nC_1/nC_2-n-pentane.	0.102456	-2.444	13.441
N_2/nC_1-n-pentane.	0.017292	-.972053	12.8692
N_2-$nC_5/nC_6/nC_7/nC_8$	0.008073	-.636894	16.3639
CH_4-$nC_5/nC_6/nC_7/nC_8$	0.022937	-1.2461	16.2183
N_2/CH_4- $nC_5/nC_6/nC_7/nC_8$	0.014885	-.968433	16.0501
N_2-nC_5/iC_5	0.005724	-.562307	13.4014
N_2/CH_4-nC_5/iC_5	0.020993	-1.0800	13.2905
N_2-nC_5/CH/T	0.006501	-.588119	18.2122
N_2/CH_4-nC_5/CH/T	0.013941	-.990414	18.0021
N_2-Stocktank Oil	0.007586	-.596982	22.8949
N_2/CH_4-Stocktank Oil	0.011514	-.916181	22.2266

Table 32. Coefficients in the equation $\gamma/mNm^{-1} = a\ (T/K) + b$, valid for ST values up to 363 K.

System	a	b
Isopentane	-0.107114	47.0798
n-Pentane	-0.096588	44.3982
n-Hexane	-0.100526	48.4272

Table 33. Coefficients in the equation $\rho_{v,L}/kgm^{-3} = a\ (P/MPa)^2 + b\ (P/MPa) + c$, valid for $\rho_{v,L}$ values up to the indicated measured pressures in MPa's at 313.15 K.

		ρ_L/kgm^{-3}		
System	P/MP	a	b	c
$N_2/nC_1/nC_2$-n-C_5	16.1	0.50389	-6.20370	601.5430
nC_1/nC_2-n-C_5	8.1	-1.73840	-10.1301	590.2521
N_2-$nC_5/nC_6/nC_7/nC_8$	35.1	0.01199	-0.26878	651.7903
nC_1-$nC_5/nC_6/nC_7/nC_8$	22.0	0.49321	0.14310	639.9240
N_2/nC_1-$nC_5/nC_6/nC_7/nC_8$	33.5	-0.11579	-1.41080	642.3087
N_2-nC_5/iC_5	32.4	-0.35313	0.236172	600.7668
N_2/nC_1-nC_5/iC_5	20.1	-0.96000	7.862500	582.20400
N_2-nC_5/CH/T	32.6	0.00658	-0.117983	723.9342
N_2/nC_1-nC_5/CH/T	32.3	-0.02820	-3.67320	721.5754
N_2-Stock. Oil	35.1	0.02808	-.432782	798.514
N_2/nC_1-Stock. Oil	35.1	0.02388	-2.47510	796.4749

	ρ_v/kgm^{-3}		
System	a	b	c
$N_2/nC_1/nC_2$-nC_5	0.609701	4.8838	36.2170
nC_1/nC_2-nC_5	0.861596	4.4336	32.1208
N_2-$nC_5/nC_6/nC_7/nC_8$	-0.05525	11.5772	19.4664
nC_1-$nC_5/nC_6/nC_7/nC_8$	0.609040	-2.3424	36.1376
N_2/nC_1-$nC_5/nC_6/nC_7/nC_8$	0.097534	7.0140	29.1669
N_2-nC_5/iC_5	0.066484	8.1739	29.9044
N_2/nC_1-nC_5/iC_5	0.300203	6.19650	17.4651
N_2-nC_5/CH/T	-0.053012	10.9718	36.1018
N_2/nC_1-nC_5/CH/T	0.058917	6.97040	32.1406
N_2-Stock. Oil	-0.002377	9.2598	37.8209
N_2/nC_1-Stock. Oil	0.044807	6.711	28.6846

Table 34. Coefficients in the equation $\rho_{v,L}/kgm^{-3} = a\ (T/K) + b$, valid for temperature values up to 363 K.

System	Phase	a	b	c
n-Pentane	v	0.003915	-2.4517	387.259
	L	-0.001950	0.19227	736.663
Isopentane	v	0.002079	-1.1737	168.062
	L	-2.02×10^{-4}	-0.9503	915.763
n-Hexane	v	0.001258	-0.76507	117.764
	L	0.003995	-3.8702	1469.892

v ≡ vapour.
L ≡ liquid.

Table 35. Lennard-Jones parameters used in the calculations of IFT, ST and K_{ij} from SPT.

Component	σ/Å	(ϵ/k)/K
N_2	0.0292	95
	0.0370	
CH_4	0.0382	137
n-C_5H_{12}	0.0561	341
i-C_5H_{12}	0.0561	323
n-C_6H_{14}	0.0587	413
n-C_7H_{16}	0.0591	282
	0.0590	
	0.0610	
n-C_8H_{18}	0.0625	320
	0.0650	
C_7H_8	0.0564	324
	0.0545	
C_6H_{12}	0.0593	377
	0.0563	

Table 36. Comparison of IFT predictions by SPT and W-K parachor-correlation with experiment for the system N_2-n-pentane.

P/MPa	$\gamma^{EXp.}$/mNm^{-1}	γ^{SPT}/mNm^{-1}	$\gamma^{Parch.}$/mNm^{-1}
1.1	13.11	14.745	13.225
5.1	10.59	11.746	10.097
15.1	6.10	6.479	4.825
20.1	4.40	4.605	-
25.1	2.96	2.689	1.921

	% Deviation	
P/MPa	SPT	Parch.
1.1	12.471	0.877
5.1	10.916	-4.655
15.1	6.213	-20.902
20.1	4.659	-
25.1	9.155	-35.101
MAD	8.682	15.822

$$\% \text{ Deviation} = (IFT^{Calc.}-IFT^{Exp.})/IFT^{Exp.} \times 100$$

$$MAD = (1/N)\ \sum | (IFT^{Calc.}-IFT^{Exp.})/IFT^{Exp.} | \times 100$$

where N = number of predictions.

Table 37. Comparison of IFT predictions by SPT and W-K parachor-correlation with experiment for the system N_2-n-hexane.

P/MPa	$\gamma^{Exp.}$/mNm^{-1}	γ^{SPT}/mNm^{-1}	$\gamma^{Parch.}$/mNm^{-1}
1.10	15.41	15.839	14.976
15.20	8.37	10.632	6.513
25.25	5.35	7.435	2.724
30.18	4.03	6.323	-
35.26	3.03	4.724	-

	% Deviation	
P/MPa	SPT	Parch.
1.10	2.789	-2.816
15.20	27.025	-22.187
25.25	38.972	-49.084
30.18	56.898	-
35.26	55.908	-
MAD	36.318	24.696

$$\% \text{ Deviation} = (IFT^{Calc.}-IFT^{Exp.})/IFT^{Exp.} \times 100$$

$$MAD = (1/N) \sum | (IFT^{Calc.}-IFT^{Exp.})/IFT^{Exp.} | \times 100$$

where N = number of predictions.

Table 38. Comparison of IFT predictions by SPT and W-K parachor-correlation with experiment for the system N_2-n-heptane.

P/MPa	$\gamma^{Exp.}$/mNm^{-1}	γ^{SPT}/mNm^{-1}	$\gamma^{Parch.}$/mNm^{-1}
1.1	16.93	16.769	17.161
5.1	14.48	15.621	-
15.1	10.14	11.521	7.944
25.1	7.1	8.289	4.086

	% Deviation	
P/MPa	SPT	Parch.
1.1	-0.950	1.364
5.1	7.879	-
15.1	13.619	-21.657
25.1	16.746	-42.451
MAD	9.799	7.275

$$\% \text{ Deviation} = (IFT^{Calc.}-IFT^{Exp.})/IFT^{Exp.} \times 100$$

$$MAD = (1/N) \sum |(IFT^{Calc.}-IFT^{Exp.})/IFT^{Exp.}| \times 100$$

where N = number of predictions.

Table 39. Comparison of IFT predictions by SPT and W-K parachor-correlation with experiment for the system N_2-n-octane.

P/MPa	$\gamma^{Exp.}$/mNm^{-1}	γ^{SPT}/mNm^{-1}	$\gamma^{Parch.}$/mNm^{-1}
1.10	18.85	19.1826	18.715
10.14	13.80	15.231	-
15.10	11.69	12.431	9.293
25.10	8.68	9.000	4.988

% Deviation		
P/MPa	SPT	Parch.
1.10	1.764	-0.716
10.14	10.369	-
15.10	6.339	-20.505
25.10	3.687	-42.534
MAD	5.539	21.252

$$\% \text{ Deviation} = (IFT^{Calc.}-IFT^{Exp.})/IFT^{Exp.} \times 100$$

$$MAD = (1/N) \sum | (IFT^{Calc.}-IFT^{Exp.})/IFT^{Exp.} | \times 100$$

where N = number of predictions.

Table 40. Comparison of IFT predictions by SPT and W-K parachor-correlation with experiment for the system N_2-n-pentane+n-hexane+n-heptane+n-octane.

P/MPa	$\gamma^{Exp.}$/mNm^{-1}	γ^{SPT}/mNm^{-1}	$\gamma^{Parch.}$/mNm^{-1}
1.10	15.94	13.3210	14.233
7.60	12.00	-	10.154
20.10	6.92	5.2100	4.243
32.35	4.24	0.6328	2.106

	% Deviation	
P/MPa	SPT	Parch.
1.10	-16.404	-10.681
7.60	-	-15.383
20.10	-24.711	-38.685
32.35	-85.075	-50.330
MAD	42.073	28.770

$$\% \text{ Deviation} = (IFT^{Calc.}-IFT^{Exp.})/IFT^{Exp.} \times 100$$

$$MAD = (1/N)\ \sum| (IFT^{Calc.}-IFT^{Exp.})/IFT^{Exp.}| \times 100$$

where N = number of predictions.

Table 41. Comparison of IFT predictions by SPT and W-K parachor-correlation with experiment for the system CH_4-n-pentane+n-hexane+n-heptane+n-octane.

P/MPa	$\gamma^{Exp.}$/mNm^{-1}	γ^{SPT}/mNm^{-1}	$\gamma^{Parch.}$/mNm^{-1}
1.10	14.57	5.985	13.139
10.10	5.66	2.889	4.788
15.10	2.61	-	2.160
22.00	0.0045	0.000311	0.0065

% Deviation

P/MPa	SPT	Parch.
1.10	-58.914	-9.810
10.10	-48.939	-15.380
15.10	-	-17.209
22.00	-93.088	-44.444
MAD	66.9803	21.711

$$\% \text{ Deviation} = (IFT^{Calc.}-IFT^{Exp.})/IFT^{Exp.} \times 100$$

$$MAD = (1/N) \sum | (IFT^{Calc.}-IFT^{Exp.})/IFT^{Exp.} | \times 100$$

where N = number of predictions.

Table 42. Comparison of IFT predictions by SPT and W-K parachor-correlation with experiment for the system N_2-n-pentane+isopentane.

P/MPa	$\gamma^{Exp.}$/mNm^{-1}	γ^{SPT}/mNm^{-1}	$\gamma^{Parch.}$/mNm^{-1}
1.1	12.7212	11.130	11.076
10.1	8.4890	-	6.628
20.1	4.2543	6.231	2.825
32.4	1.2340	4.520	0.305

% Deviation

P/MPa	SPT	Parch.
1.1	-12.508	-12.933
10.1	-	-21.922
20.1	46.463	-33.597
32.4	266.288	-75.284
MAD	108.419	35.934

% Deviation = $(IFT^{Calc.}-IFT^{Exp.})/IFT^{Exp.} \times 100$

MAD = $(1/N)\ \sum|\ (IFT^{Calc.}-IFT^{Exp.})/IFT^{Exp.}| \times 100$

where N = number of predictions.

Table 43. Comparison of IFT predictions by SPT and W-K parachor-correlation with experiment for the system N_2-n-pentane+cyclohexane+toluene.

P/MPa	$\gamma^{Exp.}$/mNm^{-1}	γ^{SPT}/mNm^{-1}	$\gamma^{Parch.}$/mNm^{-1}
1.1	17.658	24.196	15.983
10.1	12.709	-	9.167
20.1	9.210	13.732	5.651
32.6	5.897	8.345	2.657

	% Deviation	
P/MPa	SPT	Parch.
1.1	37.026	-9.486
10.1	-	-27.873
20.1	49.098	-38.643
32.6	41.513	-54.943
MAD	42.546	32.736

$$\% \text{ Deviation} = (IFT^{Calc.}-IFT^{Exp.})/IFT^{Exp.} \times 100$$

$$MAD = (1/N)\ \sum| (IFT^{Calc.}-IFT^{Exp.})/IFT^{Exp.}| \times 100$$

where N = number of predictions.

Table 44. Comparison of ST predictions by SPT, M-S parachor-correlation, CSC and Reiss's relation (RS.) with experiment for n-pentane.

T /K	$\gamma^{Exp.}$/mNm^{-1}	γ^{SPT}/mNm^{-1}	$\gamma^{Parch.}$/mNm^{-1}	γ^{CSC}/mNm^{-1}	$\gamma^{RS.}$/mNm^{-1}
311.336	14.39	8.9155	14.280	13.918	26.782
320.088	13.41	8.7615	13.397	12.984	26.364
328.459	12.61	8.5480	12.565	12.102	25.882
338.588	11.83	8.2765	11.471	11.049	25.291
349.585	10.54	7.9175	10.369	9.928	24.551
356.834	9.97	7.6745	9.511	9.200	24.062

% Deviation

T /K	SPT	Parch.	CSC	RS.
311.336	-38.031	-0.744	-3.259	86.154
320.088	-34.679	-0.116	-3.198	96.555
328.459	-32.186	-0.316	-3.995	105.329
338.588	-30.020	-3.00	-6.572	113.848
349.585	-24.874	-1.607	-5.800	132.958
356.834	-23.031	-4.617	-7.731	141.317
MAD	30.470	1.733	5.093	112.694

$$\% \text{ Deviation} = (ST^{Calc.}-ST^{Exp.})/ST^{Exp.} \times 100$$

$$MAD = (1/N) \sum |(ST^{Calc.}-ST^{Exp.})/ST^{Exp.}| \times 100$$

where N = number of predictions.

Table 45. Comparison of ST predictions by SPT, M-S parachor-correlation, CSC and Reiss's relation (RS.) with experimental data for isopentane.

T /K	$\gamma^{Exp.}$/mNm^{-1}	γ^{SPT}/mNm^{-1}	$\gamma^{Parch.}$/mNm^{-1}	γ^{CSC}/mNm^{-1}	$\gamma^{RS.}$/mNm^{-1}
304.65	14.52	8.528	13.955	13.621	25.79
323.12	12.38	8.228	12.059	11.673	24.95
341.97	10.32	7.699	10.090	9.745	23.81
355.88	9.08	7.447	8.841	8.365	23.16

% Deviation

T /K	SPT	Parch.	CSC	RS.
304.650	-41.269	-3.901	-6.201	77.653
323.120	-33.562	-2.623	-5.747	101.491
341.970	-25.418	-2.266	-5.608	130.652
355.877	-17.983	-2.636	-7.879	155.038
MAD	29.558	2.857	6.359	116.209

$$\% \text{ Deviation} = (ST^{Calc.}-ST^{Exp.})/ST^{Exp.} \times 100$$

$$MAD = (1/N) \sum | (ST^{Calc.}-ST^{Exp.})/ST^{Exp.} | \times 100$$

where N = number of predictions.

Table 46. Comparison of ST predictions by SPT, M-S parachor-correlation, CSC and Reiss's relation (RS.) with experimental data for n-hexane.

T /K	$\gamma^{Exp.}$/mNm^{-1}	γ^{SPT}/mNm^{-1}	$\gamma^{Parch.}$/mNm^{-1}	γ^{CSC}/mNm^{-1}	$\gamma^{RS.}$/mNm^{-1}
344.04	13.78	7.4810	13.324	13.101	24.320
344.53	13.70	7.4805	13.275	13.000	24.295
346.87	13.69	7.4490	13.074	12.824	24.226
349.01	13.61	7.4320	12.842	12.615	24.099
351.61	13.26	7.4220	12.516	12.362	23.884
358.30	12.36	7.3440	11.925	11.716	23.634

% Deviation				
T /K	SPT	Parch.	CSC	RS.
344.038	-45.719	-3.323	-4.941	76.462
344.531	-45.413	-4.289	-5.137	77.285
346.865	-45.540	-4.416	-6.247	77.117
349.008	-45.411	-5.674	-7.342	77.009
351.614	-44.038	-5.629	-6.789	80.087
358.301	-40.597	-3.540	-5.234	91.165
MAD	44.453	4.479	5.948	79.854

$$\% \text{ Deviation} = (ST^{Calc.}-ST^{Exp.})/ST^{Exp.} \times 100$$

$$MAD = (1/N)\ \sum|\ (ST^{Calc.}-ST^{Exp.})/ST^{Exp.}|\ \times 100$$

where N = number of predictions.

REFERENCES

1. Girault, H.H.J., Schiffrin, D.J. and Smith, B.D.V., J. Electroanal. Chem. 137, 207 (1982) and J. Coll. Interf. Sci. 101, No. 1, 257 Sept. (1984).

2. Prausnitz, J.M., Lichtenthaler, R.N., and De Azevedo, E.G., " Molecular Thermodynamics of Fluid - Phase Equilibria ", (Prentice-Hall Inc., N.J., 2nd. Edn., 1986).

3. Weinaug, C.F., and Katz, D.L., Ind. Eng. Chem. 35, pp. 239 and 1091 (1943).

4. Firoozabadi, A., Katz, D.L., Soroosh, H. and Sajjadian, V.A., SPE Resevoir Engineering, Feb. (1988).

5. Taber, J.J., Pure & Appl. Chem., Vol.52, pp.1323-1347 (1980).

6. Hsu, J.C., Nagarajan, N. & Robinson, R.L., Jr., J. Chem. Eng. Data 30, 485-491 (1985).

7. Nagarajan, N. & Robinson, R.L., Jr., J. Chem. Eng. Data 31, 168-171 (1986).

8. Llave, F.M. and Chung, T.H., J. Chem. Eng. Data 33, 123-128 (1988).

9. Legret, D., Richon, D. & Renon, H., ALChE Journal (Vol.27,No.2) March (1981).

10. Naylor, P. and Frorup, M., SPE Annual Conf. 155 (1989). Glaso, O.S., SPE/DOE 4th EOR symposium 641 (1984). Rusting et al., J. Pet. Tech. 1115 (1978). Krock, H.A. and Hutchinson, C.A., Trans. AIME, 213, 7 (1958).

11. Reid, R.C., Prausnitz, J.M. and Poling, B.E., "The properties of gases and liquids", 4th Edn. 1987, McGraw-Hill, Inc.

12. Anderko, A., Fluid Phase Equil. 61, 145 (1990).

13. Asar, H., and Handy, L.L., SPE Reservoir Engineering, Feb. (1988).

14. Bardon, C. & Longeron, D.G., Society of Petroleum Engineering Journal Oct. (1980).

15. Melrose, J.C., & Brandner, C.F., The Journal of Canadian Petroleum technology, Oct.-Dec. (1974).

16. Ali, J.K., Fluid Phase Equil. 95, 383 (1994).

17. Krichevsky, I. and Gamburg, Acta Physicochem. U.R.S.S., 16(5-6), 362 (1942).

18. Michels, A., Skelton, G.F. and Dumoulin, E. Physica, 16(11-12), 831 (1950).

19. Akers, W.W., Kehn, D.M. and Kilgore, C.H., Ind. Eng. Chem., 46, 2536 (1954).

20. Sage, B.H., and Lacey, W.N., Monograph on API Research Project 37, American Petroleum Institute, NY (1950).

21. Reamer, H.H., and Sage, B.H., J. Chem. Eng. Data 8, 508 (1963).

22. Alwani, Z., and Schneider, G.M., Ber. Bunsenges. Physik. Chem. 73 (3), 294 (1969).

23. Lentz, H., Rev. Sci. Instrum., 40 (2), 371 (1969).

24. Engels, P., and Schneider, G.M., Ber. Bunsenges. Physik. Chem. 76 (12), 1239 (1972).

25. Peter, V.S., & Eicke, H.F., Berichte der Bunsen-Gesellschaft Bd.74, No.3 (1970).

26. Legret, D., Richon, D. & Renon, H., ALChE Journal (Vol.27,No.2) March (1981).

27. Wisotzki, K.D., & Schneider, G.M., Ber. Bunsenges. Phys. Chem. 89, 21-25 (1985).

28. Metcalfe, R.s. and Raby, W.J., Fluid Phase Equilibria, 29 563-573 (1986).

29. Darwish, N.A., Gasem, K.A.M., Robinson, R.L., Jr., J. Chem. Eng. Data, 39, 781-784 (1994).

30. Park, J., Yi, X., Gasem, K.A.M., and Robinson, R.L., Jr., J. Chem. Eng. Data 40, 245-247 (1995).

31. Fawcett, M.J., SPE 28611, SPE 69th. Annual Tech. Conference and Exhibition (New Orleans, USA, Sept. (1994).

32. Jasper, J.J., J. Phys. Chem. Ref. Data, 1, 841-1010, (1972).

33. Vargaftik, N.B., "Handbook of physical properties of liquids and gases: pure substances and mixtures", 2nd. Ed. Eng. Trans., Hemisphere Publishing Corp. (1975).

34. Timmermans, J., "Physicochemical Constants of Pure Organic Compounds", Elsevier, Amsterdam, Vols. I and II (1965).

35. "International Critical Tables of Numerical Data, Physics, Chemistry and Technology", Edited by Washburn, E.W., National Research Council of U.S.A., Vol. IV (1928), McGraw-Hill, Inc.

36. MacLeod, D.B., Trans. Faraday, Soc. 19, 38 (1923).

37. Fowler, R.H., Proc. R. Soc., London 159A, 229 (1937).

38. Stegemeier, G.L., Ph.D. Dissertation, University of Texas, Austin, TX, (1959).

39. Hough, E.W. and Stegemeier, G.L., Soc. Pet. Eng. J., Dec. 259-263 (1961).

40. Simon, R., Rosman, A., and Zana, E., Soc. Pet. Eng. J., Feb. 20-26 (1978).

41. Gasem, K.A.M., Dulcamara, P.B., Dickson, K.B. and Robinson, R.L., Fluid Phase Equilibria, 53: 39-50 (1989).

42. Danesh, A., Todd, A.C., Somerville, J. & Dandekar, A., Trans IChemE, Vol.68, Part A, July (1990).

43. Huygens, R.J.M. Ronde H. and Hagoort, J., SPE 26643, 68th Annual Tech. Conf. and Exhibition of the Soc. of Pet. Engrs., Houston, Texas, 3-6 Oct. (1993).

44. Tang Jianhua , Satherley J. and Schiffrin D.J., Chinese J. of Chem. Eng. 1 (4) 223 (1993).

45. Dorshow, R.B., SPE Advanced Technology Series, Vol.3, No.1 (1995).

46. Lee, S.-T. and Chien, M.C.H., SPE/DOE 12643, 4th Symposium on EOR, Tulsa, OK, April 15-18 (1984).

47. Broseta, D. and Ragil, K., SPE Annual Technical Conference and Exhibition held in Dallas, U.S.A., 22-25 Oct. (1995).

48. Sahimi M., Davies, H.T., and Scriven, L.E., SPE 10268, 56th Tech. Conf., San Antonio, Texas (1981).

49. Sahimi, M., and Taylor, B.N., J. Chem. Phys. Vol. 95 (9), PP. 6749 (1991).

50. McCain, William D., Jr., "The properties of Petroleum Fluids" 2nd. Edn., PennWell Publishing Co. (1991).

51. Reiss, H., Frisch, H.L., and Leborvitz, J.L., J. Chem. Phys. 31, 369 (1959).

52. Sugden, S., J. Chem. Soc. 1177 (1924) and (1932).

53. Quayle, O.R., Chem. Revs. 53, 439 (1953).

54. Lennard - Jones, J.E. and Corner, J., Trans. Faraday Soc. 36, 1156 (1940).

55. Hirschfelder, J.O., Curtiss, C.F., and Bird, R.B., "Molecular Theory of Gases and Liquids", Wiley, New York, (1964).

56. Baker, O., and Swerdloff, W., Oil Gas J., 53: 87 (1955).

57. Nokay, R., Chem. Eng., Feb. 23: 147-148 (1959).

58. Fanchi, J.R., J Pet. Tech., Nov.: 2049-2050 (1985).

59. Ahmed, T., Hydrocarbon Phase Behaviour, Gulf, Houston, TX, pp. 226 (1989).

60. Satherley, J., and Schiffrin, D.J., J. Chem. Phys. 97 (3), 1 Aug. (1992).

61. Katz, D.L. and Firoozabadi, A., J. Pet. Tech., Nov.: 1649-1655 (1978).

62. Ohe, S., "Vapour-Liquid Equilibrium Data at High Pressure", Physical Sciences Data 42, Elsevier-Kodansha (1990).

63. NIST Thermophysical properties of Hydrocarbon Mixtures Database (SUPERTRAPP), version 1.04, by James F. Ely and Huber, M.L., National Institute of Standards and Tech., U.S. Dept. of Commerce, Feb. (1990).

64. van der Waals, J.D.: Z. Phys. Chem., 13: 716 (1894).

65. Brock, J.R. and Bird, R.B., AlChE J., 1: 174 (1955).

66. Miller, D.G., Ind. Eng. Chem. Fundam., 2, 78 (1963).

67. Murad, S., Chem. Eng. Commun., 24, 353 (1983).

68. Rice, P. and Teja, A.S., J. Colloid. Interface Sci., 86, 158 (1982).

69. Pierotti, R.A., Chem. Revs. 76, 717 (1976), J. Phys. Chem., 67, 1840 (1963) and J. Phys. Chem., 69, 281 (1965).

70. London, F., Trans. Faraday Soc., 32, 8 (1936).

71. Reiss, H., J. Phys. Chem. 96, 4736 (1992).

72. Lucks, K.D. and Davis, H.T., Ind. Eng. Chem. Fundam. 6, 194 (1967).

73. Thormeier, K., Nucl. Eng. Design, 14, 69 (1970).

74. Sen, U., J. Am. Chem. Soc., 101, 10, May (1979).

75. Lebowitz, J.L., Helfand, E. and Praestgaard, J., J. Chem. Phys. 45, 774 (1965).

76. Pierotti, R.A. and Liabastre, Environmental Res. Centre Report No. 0572, Georgia Institute of Technology (1972).

77. Ben-Naim, A. and Tenne, R., J. Chem. Phys., vol. 67, 2, 627-634 July (1977).

78. Reiss, H., J. Colloid Interface Sci., 53, 61 (1975).

79. Cotter, M., and Stillinger, F.H., J. Chem. Phys. 57, 3356 (1972).

80. Reiss, H. and Casberg, R.V., J. Chem. Phys. 61, 1107 (1974).

81. Liotta, C.L., Purdue, E.M. and Hopkins, H.R., J Am. Chem. Soc., 96, 7981 (1974).

82. Morel-Desrosiers, N. and Morel, J-P., Can. J. Chem. 59, 1 (1981).

83. Abraham, M.H. and Nasehzadeh, A. J. Chem. Soc., Faraday Trans. 1, 77, 321-340 (1981).

84. Leyendekkers, J.V., J. Phys. Chem., 97, 1220-1223 (1993).

85. Geblewicz, G. and Schiffrin, D.J., J. Chem. Soc., Faraday Trans. 1, 84(2), 561-574 (1988).

86. Nandi, N. and Basumallick, I.N., J. Phys. Chem., Vol. 94, 6, 2537-2545 (1990).

87. Gibbons, R. M., Mol. Phys., vol.17, No.1, 81 (1969).

88. Wilhelm, E. and Battino, R., J. Chem. Thermodyn., 3, 379-392; 743-751; 761-768 (1971).

89. Wilhelm, E. and Battino, R., J. Chem. Phys. 58, 9, 3561 and 3558 (1973); 56, 1, 563 (1972).

90. Schulze, G. and Prausnitz, J.M., Ind. Eng. Chem. Fundam., 20, 175 (1981).

91. Mayer, S.W., J. Phys. Chem. 67, 2160 (1963).

92. Atkins, P.W., " Physical Chemistry ", 5th Edn., Oxford University Press (1994).

93. Satherley, J., Girault, H.H.J. and Schiffrin, D.J., J. Coll. Interf. Sci. 136, 574 (1990).

94. Satherley, J., Cleaver, B., and Schiffrin, D.J. " The measurement of interfacial tension in partially miscible liquids at high pressures " a paper to be submitted.

95. Satherley, J. and Schiffrin, D.J., Reports to DoE Conferences, Imperial College, London, (1991-1994).

96. Bashforth, F., and Adams, J.C., "An attempt to test the theories of capillary action." Univ. Press., Cambridge, England, (1883).

97. Andreas, J.M., Hauser, E.A. and Tucker, W.B., J. Phys. Chem. 42, 1001 (1938). Fordham, S., Proc. R. Soc. London A194, 1 (1948). Vos, H., and Los, J.M., J. Colloid Interface Sci. 74, 360 (1980).

98. Haar, L., Gallagher, J.S. and Kell, G.S., NBS/NRC Steam Tables, Hemisphere Pub. Corp.,(1983).

99. EOSPAC, Program distributed by the Imperial College Thermophysical Properties Data Centre (issued October 1993) incorporating the IUPAC Thermodynamic Tables.

100. NIST Thermophysical properties of Hydrocarbon Mixtures Database (SUPERTRAPP), version 1.04, by James F. Ely and Huber, M.L., National Institute of Standards and Tech., U.S. Dept. of Commerce, Feb. (1990).

101. Rowlinson, J.S. and Widom, B., "Molecular Theory of Capillarity", Oxford University Press, N.Y., (1989).

102. Lide, D.R. and Kehiaia, H.V., "CRC Handbook of Thermophysical and Thermochemical Data", CRC press, Inc. (1994).